Quorum Sensing in *Dinoroseobacter shibae* DFL-12^{T}

and its possible role in algae symbiosis

Von der Fakultät für Lebenswissenschaften

der Technischen Universität Carolo-Wilhelmina

zu Braunschweig

zur Erlangung des Grades einer

Doktorin der Naturwissenschaften

(Dr. rer. nat.)

genehmigte

D i s s e r t a t i o n

von Ina Buchholz

aus Wolfenbüttel

1. Referentin: Prof. Dr. Irene Wagner-Döbler
2. Referent: Prof. Dr. Dieter Jahn
eingereicht am: 06.07.2011
mündliche Prüfung (Disputation) am: 19.09.2011

Druckjahr 2011

Vorveröffentlichungen der Dissertation

Teilergebnisse aus dieser Arbeit wurden mit Genehmigung der Fakultät für Lebenswissenschaften, vertreten durch die Mentorin der Arbeit, in folgenden Beiträgen vorab veröffentlicht:

Publikationen

Piekarski T, **Buchholz I**, Drepper T, Schobert M, Wagner-Doebler I, Tielen P, Jahn D. Genetic tools for the investigation of *Roseobacter* clade bacteria. BMC Microbiol. 2009 Dec 18;9:265.

Wagner-Döbler I,…, **Buchholz I**,…, Simon M. The complete genome sequence of the algal symbiont *Dinoroseobacter shibae*: a hitchhiker's guide to life in the sea. ISME J. 2010 Jan;4(1):61-77.

Tagungsbeiträge

Vorträge

Ina Buchholz, Regina Gohl and Irene Wagner-Döbler. The production of autoinducer signals of *D. shibae* DFL-12^T during cocultivation reveals the important role of quorum sensing in algae symbiosis. Kick-off symposium des Transregio 51, 13.-15. Juni 2010, Hanse Wissenschaftskolleg, Delmenhorst, Deutschland.

Poster

Ina Buchholz, Regina Gohl and Irene Wagner-Döbler. The production of autoinducer signals of *D. shibae* DFL-12^T during cocultivation reveals the important role of quorum sensing in algae symbiosis. 3rd Joint Conference German Society for Hygieneand Microbiology (DGHM) Association for General and Applied Microbiology (VAAM) Hannover, 28-31March 2010

Tomasch, J., H. Wang, **I. Buchholz** und I. Wagner-Döbler. Statistische Analyse der morphologischen Heterogenität bakterieller Kulturen. Biostats- Biologie und Statistik in der Praxis, 22.-24. März 2011, Deutsche Stammsammlung für Mikroorganismen und Zellkulturen GmbH, Braunschweig, Deutschland.

IN MEMORY OF MY BELOVED MOTHER

To my family &

to Erik and Nadine

Acknowledgement

I am heartily thankful to my supervisor, Prof. Irene Wagner-Döbler, whose encouragement, guidance and support from the initial to the final level enabled me to develop an understanding of the subject.

Furthermore, I want to thank Prof. Dieter Jahn for being the examiner of my research work and Prof. André Fleißner for being the chairman of my PhD defence.

Thanks to Dr. Thorsten Brinkhoff, Dr. Petra Tielen and PD Dr. Hans-Peter Klenk for their support during my research work, for the fruitful discussions and for their helpful comments to my work.

Lastly, I offer my regards and blessings to all the people of the working group KOM who supported me in any respect during the completion of the project. Particularly, Bettina Elxnat supported and encouraged me during the difficult stages of my life. Thanks a lot to all of you!

Thanks! Vielen Dank! Ina Buchholz

Content

Index of Tables

Index of Figures

Figures

Figures

Abbreviations

α	alpha
β	beta
°C	degree Celsius
µg	microgram
µl	microlitre
µm	micrometer
µM	micromolar
A	ampere
Acc.	accession
acyl-ACP	acylated acyl carrier protein
AHL	acylated homoserine lactone
Amp	ampicillin
ASW	artificial seawater
ATP	adenosine triphosphate
ATPase	enzyme of the ATP synthesis
BChl *a*	bacteriochlorophyll *a*
BLAST	Basic Local Alignment Search Tool
bp	base pair
cfu	colony forming unit
cm	centimeter
Cm	chloramphenicol
DFL	dinoflagellate
DIG	digoxigenin
DNA	deoxyribonucleic acid
dNTP	desoxynucleotidtriphosphat
DSMZ	german Collection of Microorganisms and Cell Cultures
et al.	et alteri
Fig.	figure

g	gram
Gm	gentamicin
h	hour
HAB	Harmful algal bloom
HSL	homoserine lactone
Ka	kanamycin
kb	kilobase
l	liter
lux-Operon	luciferase operon
m	meter
M	molar
mA	milliampere
MB	Marine broth
MCS	multiple cloning site
mg	milligram
min	minute
ml	milliliter
mm	millimeter
mM	millimolar
NCBI	National Center for Biotechnology Information
nm	nanometer
Nr.	number
OA	okaidic acid
OD	optical density
ORF	open reading frame
ORI	origin of replication
p.a.	pro analysis (degree of purity of chemicals)
PBS	phosphate saline buffer
PCR	polymerase chain reaction
R6K	R6K origin of replication
RP4mob	origin of transfer

rpm	rounds per minute
RT	room temperature
SAH	S-adenosyl-homocysteine
SAM	S-adenosyl methionine
sec	second
Sm	streptomycin
sp.	species
SRH	S-ribosyl-homocysteine
TAE	tris-Acetate-EDTA-Buffer
Tc	tetracycline
tra-gene	genes of DNA transfer
U	unit
V	volt
v/v	volume/volume
w/v	weight/volume
wt	wild type

1 Introduction

1.1 Quorum sensing

A bacterium can successfully sustain its species by adapting to a wide range of niches that may already contain a complex consortium of other species. If the bacterium manages to integrate and participate in the effectiveness of the community, it has a better chance to ensure survival. Several bacteria use signals, released into the environment, to respond appropriately to a community. The signaling process is named bacterial communication, also known as quorum sensing (QS). In the last decades, quorum sensing has been discovered to regulate a number of important bacterial features (Bassler 1999;Henke and Bassler 2004). Quorum sensing is a regulatory mechanism of gene expression, which induces bacteria to change their behaviour as the population reaches a certain cell density, the so-called quorum. It functions through a cell-to-cell signaling molecule, also known as autoinducer (AI), which is secreted into the surrounding environment. At low cell-densities the autoinducer is at low concentration. During growth, the concentration increases and is thereby a measure for the bacterial cell density. At a critical threshold concentration, the autoinducer is recognized by the cells and affects gene expression. QS was first discovered in the marine bacterium *Vibrio fischeri*. Its signal synthase LuxI produces acylated homoserine lactones (AHLs), which reach the extracellular environment via diffusion or transport. At a critical signal molecule concentration, the AHLs bind to the receptor LuxR, which can be located in the cytoplasm. The signal–receptor complex activates or inactivates transcription of the target genes (Fuqua *et al.* 2001) (Figure 1A).

A different kind of QS system was found in vibrios. *V. harveyi* uses multichannel QS systems in which different types of signal molecules are produced. One of these channels is mediated by the *V. harveyi* AHL *N*-(3-hydroxybutanoyl)-*L*-homoserine lactone. The signal molecule is detected at the cell surface by a membrane-bound, two-component receptor protein that feeds a common phosphorylation/dephosphorylation signal transduction cascade with the transcriptional response regulator $LuxR_{Vh}$ at the end of the cascade which

activates or inactivates transcription of the target genes (Defoirdt *et al.* 2008) (Figure 1B). 2007, Tu and Bassler proposed that the function of multiple small regulatory RNAs is the translation of increasing autoinducer concentrations into a precise gradient of $LuxR_{Vh}$, resulting in a gradient of expression of quorum sensing-regulated target genes. This is an indication that the three-channel quorum sensing system is independent of a certain quorum of cells, producing AIs, but that different autoinducers are used to fine-tune the global expression of a population (Tu and Bassler 2007).

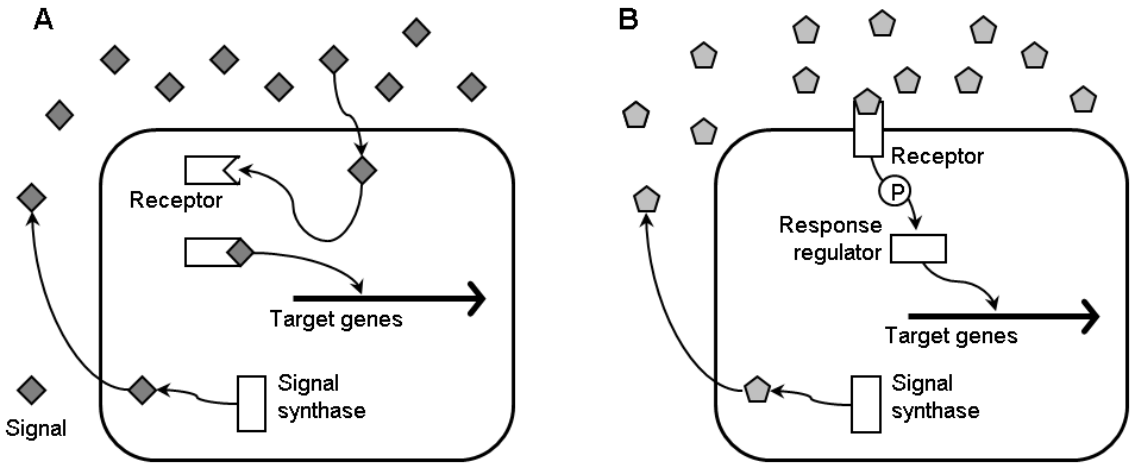

Figure 1 General scheme of quorum sensing systems.

The signal synthase (LuxI in the case of *V. fischeri*) produces signal molecules (AHLs), which reach the extracellular environment either via diffusion or transport. At a critical signal molecule concentration, the signal binds to the receptor (LuxR in the case of *V. fischeri*), which can be located in the cytoplasm. The signal–receptor complex activates or inactivates transcription of the target genes (A). If the receptor is located at the cell surface, target gene transcription is modulated through a phosphorylation/dephosphorylation signal transduction cascade with a transcriptional regulator at the end ($LuxR_{Vh}$ in the case of *V. harveyi*). P denotes phosphotransfer (Defoirdt *et al.* 2010).

1.2 Alternative interpretations

Quorum sensing- the system of self-regulation has been shown to control the expression of different phenotypes with one common feature. They share the necessity of a minimum critical number of bacterial cells and thus a chemical threshold concentration for signal molecules, at which all involved cells would shift to the induction of previously silent phenotypes. This kind of regulation is based on two assumptions:

- a homogeneity of the system, so that signal concentrations could stimulate the entire population and
- an environment in which cells are not allowed to migrate/disperse or aggregate/converge (Alberghini *et al.* 2009).

As a consequence, classical quorum sensing has been a subject of discussion; its current paradigm does not suit the effects of convection (summary of advective and diffusive transfer in fluids), a spatial distribution of cells, the degradation of AIs and the attendence of other bacterial species, which are producing or "scrounging" the same AIs.

Diffusion sensing (DS), an alternative interpretation, has been proposed 2002 (Redfield 2002), in which a single cell would sense an increase in concentration of its own signal when diffusion is hindered by spatial barriers. To avoid high energy costs and the possible loss of costly effectors by diffusion, a cell releases cost-efficient autoinducer signals in order to monitor whether the signal molecules diffuse away or remain in the immediate environment of the cell. Here, an effector is a substance that is produced and released into the environment for its ultimate effect, such as exoenzymes, siderophores, antibiotics, biosurfactants and virulence factors. Diffusion sensing is independent of cell density or spatial distribution. It is based on the view that individual bacteria sense the 'diffusion space' around them by releasing diffusible test molecules (AIs) and, at low diffusion rates, "decide" if they activate their costlier metabolism. DS, which was proposed after QS, is the simpler hypothesis, as it does not invoke social behaviour and group benefits for the evolution of autoinducer sensing.

The concept of **efficiency sensing** (ES), proposed by Hense *et al.*, combines the definitions of quorum sensing and diffusion sensing. The authors suggest that cells sense a combination of cell density, convection and spatial cell distribution as the cell cannot distinguish between each factor, which means they are not coupled and can vary independently. The fact is, that autoinducer and costlier effectors are exposed to the same external factors, meaning that first a cell estimates the cost-benefit analysis of producing AIs regardless of whether the cell density, the convection or the spatial distribution does influence the AI rate. If the combination of all factors indicates the cell an efficient production of AIs, the same applies to the production of costlier effector substances. It is assumed that the theory of ES can only be robust for problems of complexity and cheating cells in situ if the sensing takes place in clonal microcolonies, which can shelter communication within the cluster from cross-talk even in diverse habitats and which can promote the evolution of cooperative behaviour (Hense *et al.* 2007).

Another role for quorum sensing is emerging where quorum signaling pathways converge with stress and starvation circuits to regulate adaption to changing environmental conditions. Quorum signals may even directly signal entry into stationary phase. For the coherence of quorum sensing and stress/starvation pathways the term **starvation sensing** was first coined by Beth A. Lazazzera. She demonstrated that the competence-stimulating-peptide (CSP) of *Bacillus subtilis* is controlled by a sigma factor which becomes active under starvation. As a result, more CSP is produced which then triggers the utilization of alternative energy sources. CSP also controls positively competence, another quorum sensing phenotype (Lazazzera 2000).

Nevertheless, the models of diffusion and efficiency sensing are not consistent with the fact that autoinducer-dependent phenotypes (gene transfer, host invasion, coordinated swarming, change of life-mode) belong to the kind of actions that only apply in an interaction between different cells. In fact, DS and ES do not give a satisfying explanation for group behavior. Because of that and since the term quorum sensing is commonly accepted to describe signaling or cell-to-cell communication in bacteria, it will be used throughout this thesis.

1.3 Quorum sensing regulated phenotypes

Bacterial cell-to-cell communication enables a bacterial population to mount a unified response that is advantageous for its survival by improving access to complex nutrients or environmental niches, collective defence against other competitive microorganisms or eukaryotic host defence mechanisms. Generating and analyzing quorum sensing mutants by transcription profiling (e.g. microarrays), has shown that quorum sensing, in many bacteria, controls gene expression in a global manner (Waters and Bassler 2005). Many phenotypes are considered as QS regulated, such as biofilm formation, motility and swarming, bioluminescence, DNA transfer and the synthesis of extracellular products.

1.3.1 Biofilm formation

Bacteria are able to grow adherend to almost every surface or to each other, forming architecturally complex communities termed biofilms. In biofilms, cells grow in multicellular aggregates that are encased in an extracellular matrix produced by the bacteria themselves. This extracellular matrix confers resistance to many antimicrobials, protection from protozoan grazing, and protection against host defenses.

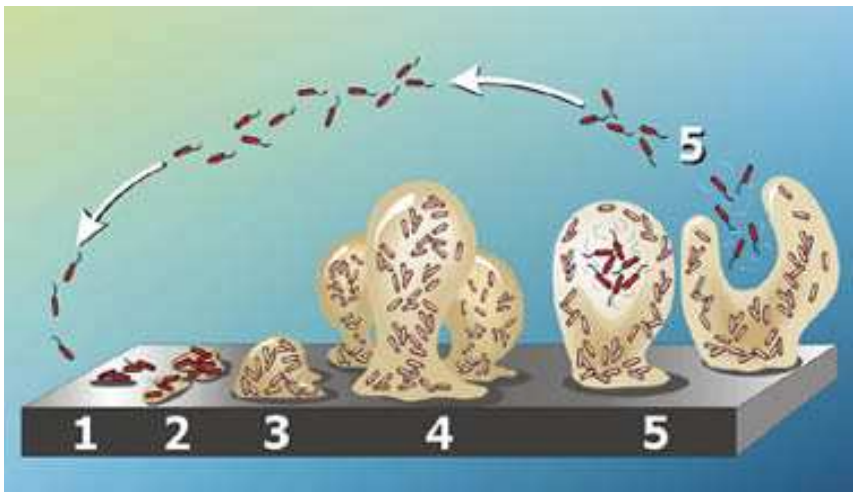

Figure 2 Biofilm development in Gram-negative bacteria.

Biofilm formation can be divided into five stages: 1) reversible adhesion, 2) irreversible adhesion, 3) the appearance of aggregates, 4) the formation of mature structures and 5) the detachment of the cells (http://www.entkent.com/biofilms.html).

Planktonic cells, for example, first localize on a substrate suitable for attachment to begin the growth cycle. Stage 1 is the reversible adhesion which can be activated within seconds and is likely induced by environmental signals. These signals vary from organism to organism but they include e.g. changes in nutrients, nutrients concentrations, pH, temperature, oxygen concentration and osmolality. During this stage, bacterial cells exhibit a logarithmic growth rate. Stage 2 is best described as irreversible adhesion. Through QS signaling the genetic mechanisms underlying exopolysaccharide (EPS) production are activated. During stage 3 cell aggregates are formed and motility is decreased. When the cell aggregates become progressively layered (mushroom-shaped structure), stage 4, known as maturation, is reached. Stage 5 depicts the detachment and dispersal of planktonic cells from the biofilm. It is thought that pieces of the biofilm can break off by mechanical disruption leading to colonization of new surfaces or there may be cues for a program of events, releasing planktonic cells from the biofilm (Costerton *et al.* 1999;Fuqua and Greenberg 2002).

Biofilm formation is the most commonly investigated quorum sensing phenotype. Quorum sensing can affect both the structure and biomass of the biofilm. As in many bacterial species, in *Pseudomonas aeruginosa*, a quorum sensing mutation disrupts the biofilm structure. The cells are still able to form colonies, but due to the loss of EPS production, these tend to be smooth and flat (Branda *et al.* 2005).

1.3.2 Motility and swarming

In general, QS controlled swimming by use of flagella or swarming ensures the dispersal of the species and the tapping of natural resources and new niches. Swarming, also referred to as twitching motility is a flagella-independent form of bacterial translocation on moist surfaces. It occurs by extension, tethering, and then retraction of polar type IV pili. In *P. aeruginosa* flagella are involved in biofilm formation. They are needed for attachment and type IV pili are required for twitching motility on a surface as well as the formation of microcolonies in the attached monolayer that forms on the surface (Costerton *et al.* 1999).

1.3.3 Bioluminescence

The bacterial enzyme luciferase, encoded on the *lux* genes, catalyzes light production in the presence of an aliphatic aldehyde substrate, reduced flavin mononucleotide, and molecular oxygen. Although there has been considerable speculation over a possible biochemical function for luciferase, the only so far demonstrated biological function is as a source of luminescence in animal symbioses. In *V. fischeri*, bioluminescence supports symbiosis with the Hawaiian bobtail squid *Euprymna scolopes*. The bacterial cells colonize the light organ of the squid, where they produce light and thereby aid the camouflage of the squid. In exchange, the squid supplies nutrients to the bacteria (Ruby 1996). The signaling of *Vibrio fischeri* was the first elucidated, quorum sensing system (Eberhard *et al.* 1981;Nealson and Markovitz 1970) and it illustrates, how quorum sensing controls the switch in a species from the free-living into the symbiotic life mode.

1.3.4 DNA transfer

Horizontal gene flow is a driving force for bacterial adaptation. Three distinct mechanisms of gene transfer are common in bacteria: conjugation, transformation and transduction. Both conjugation and transformation are known to be quorum sensing regulated.

Agrobacterium tumefaciens, a plant pathogen, has the unique ability to directly transform plant cells by conjugation of the large tumour-inducing plasmid (Ti plasmid). This conjugation forces the infected plant cells to overproduce phytohormones, which results in the growth of tumours called crown galls. The Ti plasmid carries a functional LuxI-type synthase (TraI), and a LuxR-type signal receptor (TraR). It also encodes genes for the production of opines, which are sources of nutrients for the colonizing bacteria and genes for the production of conjugal proteins (*vir* genes) (White and Winans 2007).

The transformation of bacteria, better known as natural genetic competence, is defined as the ability of a cell to take up free DNA from the surrounding medium. During growth, in several instances under specific conditions, cells develop the

capability to bind and stably incorporate DNA. The ability to take up free DNA from the environment via natural competence is widely distributed among Gram-negative and Gram-positive bacteria, but according to our present knowledge, quorum sensing upregulates competence in all Gram-positive bacteria (Kleerebezem *et al.* 1997;Lorenz and Wackernagel 1994).

1.3.5 Extracellular products

Extracellular products (ECP) regulated by quorum sensing can be enzymes, toxins, antibiotics, siderophores and some pigments, which can aid the pathogenesis of the organism and the establishment in a niche. An exoenzyme, or extracellular enzyme, is secreted by the cell and is usually used for breaking up large molecules and facilitates the uptake of breakdown products that would otherwise not be able to enter the cell. Cellulase, for example, refers to a class of enzymes that catalyze cellulolysis (i.e. the hydrolysis of cellulose). Together with the enzyme cellobiase, the enzyme complex breaks down cellulose to beta-glucose. Most organisms require iron as an essential element in a variety of metabolic and informational cellular pathways. To fulfill their nutritional requirement for iron, bacteria utilize among others low molecular weight iron chelators termed siderophores, which are actively transported across the cytoplasmic membrane by TonB-dependent transporters (Noinaj *et al.* 2010). Toxins, antibiotics and pigments inhibit competitors or weaken the host immune system. In *Pseudomonas aeruginosa* about 6 % of the genome are quorum sensing regulated, enclosing a wide-range of extracellular substances, like exoenzymes such as elastase and alkaline protease, toxins such as exotoxin A, the phenazine pigment, pyocyanin, and the siderophores, pyoverdin and pyochelin (Schuster *et al.* 2003).

1.4 Autoinducer

Bacteria can communicate amongst themselves and with their hosts by producing, sensing and responding to chemical signals. To date a wide range of chemical compounds that function as autoinducers (AIs), are identified. The two best-studied groups of autoinducer are the acylated homoserine lactones (AHL) of Gram-negative bacteria and post-translationally modified peptides in Gram-positive bacteria.

Such compounds possess various characteristics which define them as autoinducer. AIs accumulate in the extracellular milieu during a specific growth stage or under certain physiological conditions, or in response to specific environmental changes. Furthermore the AI has to be recognized by a specific cell surface or cytoplasmic bacterial receptor. The most important feature that separates AI mediated QS from other signal response mechanisms is that autoinducer have the ability to induce a cellular response that extends beyond the physiological changes required to metabolise or detoxify the molecule and that the entire population takes advantage of the opportunities arising from AI induced cell-to-cell signaling (Winzer *et al.* 2002).

1.4.1 AHL mediated quorum sensing in Gram-negative bacteria

Acyl-HSLs have as general structure an acyl chain of variable length and elemental composition conjugated via an amide linkage to a lactonized homoserine moiety. Studies of proteins, belonging to the LuxI family, clearly indicated a role in synthesis of the acyl HL signal, recruiting their substrates from normal metabolic precursors.

In 1981, after the initial discovery that bacteria cells communicate through the production and detection of autoinducers, the structure of the *V. fischeri* signaling molecule was elucidated. The molecule has proved to be *N*-(3-oxohexanoyl)-*L*-homoserine lactone (3OC6-HSL) (Figure 3, left panel) (Eberhard *et al.* 1981). In 1995, a second quorum sensing synthase, *ainS*, was discovered in *V. fischeri*. AinS synthase produces *N*-octanoyl-*L*-homoserine lactone (C8-HSL) that is sensed by AinR, a *V. harveyi* LuxN homologue (Gilson *et al.* 1995). Both AIs, 3OC6-HSL and C8-HSL, control bioluminescence in *Vibrio fischeri* in a sequential manner.

Recently Schaefer *et al.* discovered that the phototrophic soil bacterium *Rhodopseudomonas palustris* and a few other bacterial species utilize an ortholog of *V. fischeri luxI* (*rpaI*) to produce *p*-coumaroyl-AHL (Figure 3, right panel) by using environmental *p*-coumaric acid rather than fatty acids from cellular pools. Several genes, regulated by the *p*-coumaroyl-AHL, are annotated as encoding chemotaxis functions (Schaefer *et al.* 2008). LuxI-type proteins can

synthesize different classes of AHLs, incorporating either fatty acid moieties from the cell metabolism, or external molecules, e.g. lignin fragments.

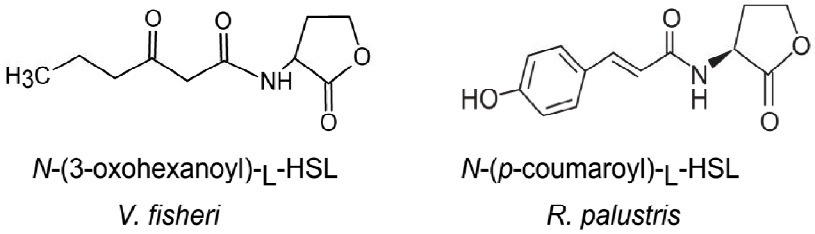

N-(3-oxohexanoyl)-L-HSL
V. fisheri

N-(*p*-coumaroyl)-L-HSL
R. palustris

Figure 3 Examples of homoserine lactone signaling molecules produced by *V. fischeri* and *R. palustris*, respectively (Schaefer *et al.* 2008).

In the past all AIs have been assumed to be freely diffusible in bacterial cells. This assumption is based on the fact that a radiolabeled *Vibrio fischeri* AI, 3OC6-HSL, was shown to freely diffuse into and out of *V. fischeri* and *E. coli* cells (Kaplan and Greenberg 1985). In *P. aeruginosa* it is C4-HSL that freely diffuses into and out of cells. In contrast, 3OC12-HSL is subject to efflux by multidrug efflux pumps (Pearson *et al.* 1999). Thus, it is likely that cell-to-cell communication systems in species other than *P. aeruginosa*, which also rely on *N*-acyl homoserine lactones containing long-chain AIs, also involve multidrug efflux pumps.

1.4.2 The AHL synthesis reaction

AHLs are produced by the LuxI-type synthase from the substrates *S*-adenosyl-*L*-methionine (SAM) and acylated acyl carrier protein (aycl-ACP) in a sequentially ordered reaction. These two substrates adopt roles that differ from their normal cellular functions. SAM usually acts as a methyl donor, whereas acyl-ACPs are components of the fatty acid biosynthetic pathway. Acyl-ACPs had not been implicated in cell-cell communication until their discovery as acyl chain donors in AHL synthesis (Moré *et al.* 1996). Moreover, the internal lactonization of SAM, which demands an unusual cyclic conformation, favors the following synthesis reaction shown in Figure 4. The acyl chain is the substrate for the AHL synthase, which mediates the nucleophilic attack on the γ-carbon of SAM by its own carboxylate oxygen to produce the homoserine lactone product. The *N*-acylation reaction, involving an enzyme-acyl-SAM intermediate (Figure 4, square bracket),

is thought to occur first because butyryl-SAM acts as both a substrate and as inhibitor for the *P. aeruginosa* AHL synthase, RhlI, to produce C4-AHL (Parsek *et al.* 1999). Concomitant byproducts are holo-ACP and 5'-methyl-thioadenosine.

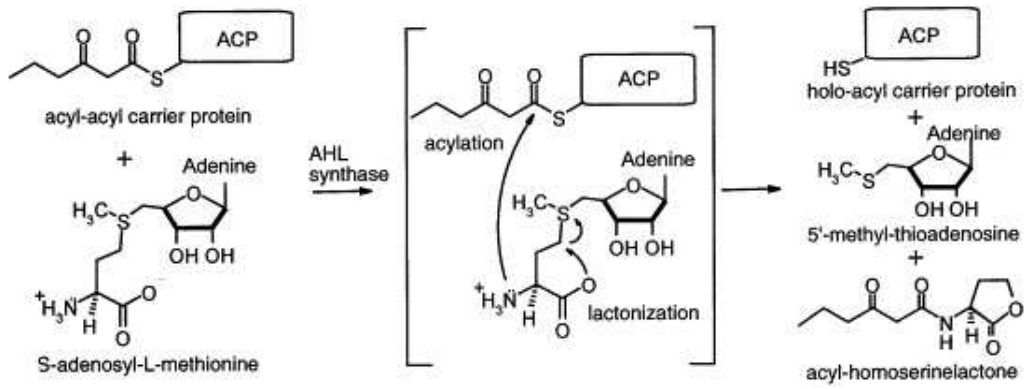

Figure 4 Schematic diagram of the general features of the AHL synthesis reaction.

Acyl-ACP and SAM bind to the synthase and after the acylation and lactonization reactions, the product AHL and byproducts holo-ACP and 5'-methylthioadenosine are released (Watson *et al.* 2002).

1.4.3 Detection of AHLs

AHLs can be detected effectively using AHL-sensitive bioassays. These bioassays are highly sensitive, with the ability to detect sub-picomole amounts of particular AHLs. However, the detection is limited by the specifity of the reporter strain (Gould *et al.* 2006). Reporter strains which were used throughout this thesis recognize a relative wide variety of AHLs.

***E. coli* MT102 pJBA132**

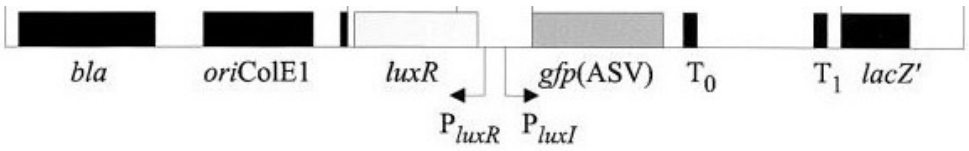

Figure 5 Schematic drawing of the *lux*-based AHL sensor plasmid pJBA132.

pJBA132 contains a *luxI–gfp* (ASV) translational fusion together with the *luxR* gene placed under control of P_{luxR} on the high-copy plasmid pME6031.The genetic components are: P_{luxI}, LuxI synthase promoter fragment of *V. fischeri*; *gfp*(ASV), gene encoding an unstable GFP; *luxR*, gene encoding the transcriptional activator LuxR of *V. fischeri*; T0, transcriptional terminator from phage lambda; T1, transcriptional terminator from *rrnB* operon of *E. coli*; *bla*, gene encoding the ß-lactamase (Amp^R); *ori*ColE1, ori of replication; *lacZ'*, gene encoding the β-galactosidase (Andersen *et al.* 2001).

The pJBA132 construct is used as sensor plasmid in *E. coli* MT102 to detect short-chain AHLs. The product of the *luxR* gene derived from *V. fischeri* encodes the quorum sensor receptor protein. In the presence of exogenous AHLs, LuxR

positively affects the expression of the *luxI* promoter, which then in turn controls expression of an unstable version of the GFP protein. Since expression of *luxI* is controlled by the *lux* quorum sensing system of *V. fischeri*, this sensor is expected to be most sensitive for 3OC6-HSL and related short-chain AHLs (Andersen *et al.* 2001).

P. putida F117 pKR-C12

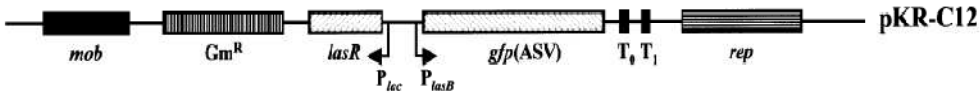

Figure 6 Schematic drawing of the *las*- based AHL sensor plasmid pKR-C12.

pKR-C12 contains a *lasB–gfp* (ASV) translational fusion together with the *lasR* gene placed under control of P_{lac} on the broadhost-range plasmid pBBR1MCS-5. The genetic components are: P_{lasB}, elastase promoter fragment of PAO1; *gfp*(ASV), gene encoding an unstable GFP; *lasR*, gene encoding the transcriptional activator LasR; T0, transcriptional terminator from phage lambda; T1, transcriptional terminator from *rrnB* operon of *E. coli*; Gm^R, gentamicin-resistance marker; *rep*, replication gene; *mob*, mobilization gene (Riedel *et al.* 2001).

The construct of Kathrin Riedel, pKR-C12, is used as sensor plasmid in *P. putida* F117 to detect long-chain AHLs. It contains a translational fusion of the *lasB* elastase gene of *P. aeruginosa* to gfp (ASV), encoding an unstable version of the GFP protein. Furthermore, the sensor contains the *lasR* gene, which encodes the cognate 3OC12-HSL receptor protein under control of a *lac*-type promoter. Since expression of *lasB* is controlled by the *las* quorum sensing system, this sensor is expected to be most sensitive for 3OC12-HSL and related long-chain AHLs (Riedel *et al.* 2001).

Table 1 Detection limit of the sensor strains *P .putida* F117 (pKR-C12) and *E. coli* MT102 (pJBA132) for synthetic AHLs with chain lengths from C4 to C14 (Wagner-Dobler *et al.* 2005).

AHL	*P .putida* (pKR-C12)	*E. coli* (pJBA132)
C4	2.9 mmol	2.9 mmol
3OC6	0.2 mmol	23.5 nmol
C8	2.2 mmol	220 nmol
C12	17.6 nmol	1.76 µmol
Z7-C14-en	161 nmol	160 nmol

The lowest concentration that elicited a response greater than twofold induction of fluorescence is indicated.

Mass spectrometry (MS) and gas chromatography (GC)-MS as well as high performance liquid chromatography (HPLC) coupled to ion trap mass spectrometry (LC-MS) offer alternative methods of AHL detection, which are based on the physical/chemical properties of the compounds, such as the mass/charge ratio of molecular ions, collisionally induced product ions, and chromatographic retention properties (Gould *et al.* 2006).

1.5 Quorum Quenching

The last decades have witnessed a dramatic increase in deaths caused by infections. Treatment with antibiotics eliminates the susceptible microbes and benefits the evolution of multiresistant bacteria. One reason is that antibiotics kill microbes by inhibiting growth-related cellular activities, such as the syntheses of DNA, RNA and proteins (Alekshun and Levy 2007). Futhermore, when applying antibiotics to treat chronic infections which involve metabolically inactive cells, the targets of inhibition are missing. Besides, after several decades of extensive hunting for new antibiotics, most of the natural reservoirs are depleted. The discoveries of quorum sensing and possible quorum sensing inhibitors (QSI) have opened the door to develop new therapeutical strategies.

Unlike antibiotics, QSIs usually do not cause direct inhibition of microbial growth but repress cell-density dependent virulence or pathogen biofilm production. As a consequence, bacteria are not killed directly from the effects of QSIs and therefore exhibit less selective pressure and less likelihood of resistant development. QS relies on a cascade of events like signal production, detection

and gene activation/repression. Interruption of any of these steps could interfere with the signaling system and suppress lethal infections (Pan and Ren 2009). One of the most studied compounds until now are the halogenated furanones produced by the benthic marine macroalga *Delisea pulchra* (Figure 7), which protect the alga from adhesion and fouling by marine bacteria.

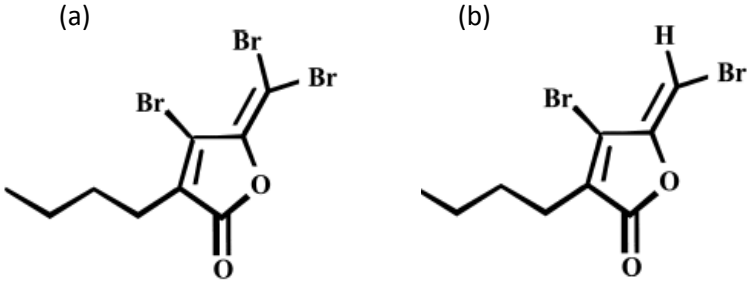

Figure 7 Chemical structures of halogenated furanones produced by the marine alga *Delisea pulchra*.

(a) 4-Bromo-3-butyl-5-(dibromomethylene)-2(5*H*)-furanone and (b) 4-Bromo-5-(bromomethylene)-3-butyl-2(5*H*)-furanone (Rasmussen *et al.* 2000).

In early quorum quenching studies it was assumed that the halogenated furanones bind to the quorum sensing regulator LuxR instead of the corresponding AHL, resulting in inhibition of the QS regulation cascade. Recent studies, however, suggest that halogenated furanones do not compete in the 'classic' way with AHLs for the binding site. In fact, halogenated furanones do not form a stable complex with the LuxR protein but can displace the corresponding AHL from LuxR. The binding of halogenated furanones to LuxR accelerates the proteolytic degradation of the regulatory protein. Consequently, the concentration of LuxR proteins within the bacterial cell is decreased and no quorum response can be activated, regardless of whether the quorum of cells and high AI concentrations are reached (Manefield *et al.* 2002).

For Gram-negative bacteria, it is reported that furanone derivates can inhibit the swarming and biofilm formation at concentrations that are not inhibitory to planktonic growth. In the presence of furanone, the cells in the biofilm are presumably forced to aggregate. Cells die from starvation and accumulation of metabolic waste (Ren *et al.* 2001).

1.6 The Roseobacter Clade

In contrast to terrestrial ecosystems microorganisms of the world's oceans represent the greatest amount of biomass. The most abundant microorganisms of the phytoplankton are divided into nine phylogenetic cluster (Giovannoni and Stingl 2005) including the *Roseobacter* lineage which is a phylogenetically coherent, physiologically heterogeneous group of *Alphaproteobacteria* comprising 10-25% of marine microbial communities, especially in coastal and polar oceans (Brinkhoff *et al.* 2008;Buchan *et al.* 2005;Wagner-Dobler and Biebl 2006). *Roseobacter* bacteria are dwelling in many different marine habitats and ecosystems; in the pelagic zone they are associated with algae, on various biological and abiotic surfaces and sediments.

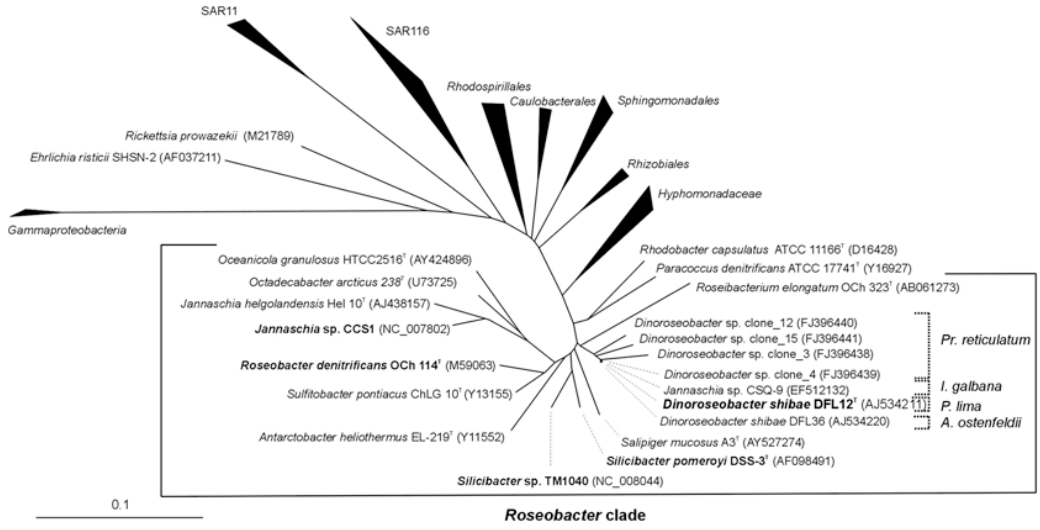

Figure 8 Phylogenetic tree of the *Roseobacter* clade within the *Rhodobacteraceae* (*Alphaproteobacteria*).

The phylogenetic tree was generated using the maximum-likelihood method based on 16S rRNA gene comparison. Members of the *Gammaproteobacteria* were used as outgroup (not shown). Names illustrated in boldface indicate organisms whose complete genome sequences have already been determined. Dotted brackets mark algae hosts from which strains were isolated. *Dinophyceae*: Pr., *Protoceratium*; A., *Alexandrium*; P., *Prorocentrum* and *Haptophyceae*: I., *Isochrysis*. Bar = 0.1 substitutions per nucleotide position (Wagner-Dobler *et al.* 2010).

Due to their physiological heterogeneity such as the ability to reduce organic sulfur compounds like DMSP, the capability of carbon monoxide oxidation, the production of bioactive metabolites, the formation of biofilms, the production of novel autoinducers, the secretion of toxins and the capability of aerobic anoxygenic photosynthesis (AAnP) (Wagner-Dobler *et al.* 2010) the *Roseobacter* clade emerged more and more as one of the most important groups of marine bacteria. Given the importance of Roseobacters in biogeochemical cycles of the ocean, the increasing number of determined genome sequences within a clade, and global abundance, the marine *Roseobacter* clade is ideal for elucidating bacterial diversification and adaptation to changing ocean environments (Kang *et al.* 2010b;Kang *et al.* 2010a;Moran *et al.* 2004;Thrash *et al.* 2010b;Thrash *et al.* 2010a;Wagner-Dobler *et al.* 2010).

1.6.1 AHLs found in *Roseobacter*

In Gram-negative *Alphaproteobacteria*, AHLs represent a group of well-studied autoinducers.

Most of the *Roseobacter* bacteria synthesize numerous kinds of signal molecules. AHLs investigated so far were shown to have side-chain lengths of C8, C10, C13-C15 and C18 whereas long-chain AHLs with side-chain length of C14, C16 and C18 clearly dominated. The shortest AHL found was C8-HSL. The subsequent Table 1 shows a selection of AHLs in marine *Alphaproteobacteria* which were detected by Wagner-Dobler *et al.*, 2005.

Table 2 AHLs identified in marine *Alphaproteobacteria* (Wagner-Dobler *et al.* 2005).

Alphaproteobacteria	**AHL**
Dinoroseobacter shibae	C8-HSL, C18-en-HSL, C18-dien-HSL
Roseovarius mucosus	C14-en-HSL, C18-en-HSL
Roseovarius tolerans	C14-HSL, C14-en-HSL, 3OC14-HSL, C16-HSL, C16-en-HSL
Roseobacter litoralis	C8-HSL
Staleya guttiformis	C16-HSL, C16-en-HSL, C16-dien-HSL
Jannaschia helgolandensis	C14-en-HSL, C16-en-HSL, C16-dien-HSL
Oceanibulbus indolifex	C16-en-HSL
Roseobacter gallaeciencis	3HOC10-HSL, C18-en-HSL

The broad pattern of produced AHLs is common among species of the *Roseobacter* clade. While a great deal has been learned from laboratory studies

concerning well known QS systems, comparatively little is known about *Roseobacter* AHLs. Their physiological functions for the bacteria in their widely different ecological niches still need to be elucidated. Recent studies of *Silicibacter sp*. TM1040 indicate that tropodithietic acid (TDA), a biologically active tropolone compound, acts as autoinducer for its own synthesis and suggests that Roseobacters may use TDA as a quorum signal (Geng and Belas 2010a).

1.7 Physiological roles of AHLs in *Proteobacteria*

Because practically nothing is known about regulated phenotypes regarding *Roseobacter* AHLs, comparisons are drawn in Table 2 with known AHL regulated phenotypes of related *Proteobacteria*. Most of the phenotypes are involved in host invasion or, more generally, in the symbiotic lifestyle of these bacteria.

Table 3 Homoserine lactone regulated phenotypes in diverse *Proteobacteria.*

Species	HSL	Regulated phenotypes	Reference
V. fischeri,	C8-HSL	luminescence	1
V. harveyi		epression of siderophores, metalloproteases, exopolysachharides and repression the type III secretion system	2
Rhizobium sp.	C8-HSL	conjugation and host invasion	3
S. marcescens	C8-HSL	production of the red pigment prodigiosin, the nuclease NucA and biosurfactants	4
R. sphaeroides	C14-en-HSL	biofilm formation and colony morphology	5
R. capsulatus	C16-HSL	Gene transfer agent production	6
S. meliloti	C16-en-HSL	motility, biofilm formation and	7
	C18-HSL	production of exopolysaccharides, host-invasion	8
R. palustris	*p*-coumaroyl-HSL	chemotaxis	9

1, (Schaefer *et al.* 1996); 2, (Tu and Bassler 2007); 3, (He et al. 2003); 4, (Horng et al. 2002); 5, (Puskas et al. 1997); 6, (Schaefer et al. 2002); 7, (Hoang et al. 2008); 8, (Llamas *et al.* 2004;Marketon *et al.* 2002); 9, (Schaefer *et al.* 2008)

1.8 Dinoroseobacter shibae DFL-12^T

1.8.1 Morphology and Physiology

Dinoroseobacter shibae DFL-12^T is a member of the globally important marine *Roseobacter* clade. Cells of *D. shibae* are Gram-negative cocci or ovoid rods. They are motile by a single, polarly or subpolarly inserted flagellum. Liquid cultures are pink to light red if grown in the dark. Dark-grown colonies are wine-red (Figure 9a). *D. shibae* is able to grow in complex medium like Marine Broth (MB, Difco 2216) or in pure artificial, mineral medium (SWM) containing the carbon source only, as it requires addition of biotin, nicotinic acid and 4-aminobenzoic acid. The strain is strictly salt-dependent and requires at least 1 % salinity, but usually concentrations of normal sea water (3.5 %) are used in SWM. *D. shibae* grows between 15 and 38 °C. Optimum grow temperature is at 33 °C and optimum pH range was found between 6.5 to 8.8.It utilizes a wide spectrum of organic compounds, like acetate, succinate, fumarate, lactate, citrate, glutamate, pyruvate, fructose and glycerol. Ethanol, methanol and butyrate are not metabolized (Biebl *et al.* 2005)

D. shibae DFL-12 was isolated from *Prorocentrum lima*, a benthic dinoflagellate, which can produce toxic okadaic acid during harmful algal blooms (Allgaier *et al.* 2003).

D. shibae DFL-12 was chosen as a model organism because of its metabolic versatility. It is postulated to live planktonically or associated with algae and combines many physiological abilities which are shared with other members of the *Roseobacter* clade and therefore enable this cluster to adapt successfully to numerous niches in the marine realm. *D. shibaes* physiological versatility includes, for example, the capability to perform light-driven ATP synthesis using bacteriochlorophyll *a* in the presence of oxygen, a large number of extrachromosomal replicons, the biosynthesis of vitamin B12, the degradation of DMSP, the possible reversible oxidation of CO to CO_2 and the discovery of novel acylated homoserine lactone (AHL) compounds. Furthermore the fully sequenced and annotated genome sequence of *D. shibae* DFL-12 revealed traits that presumably are highly adaptive in the habitat of bloom-forming algae. The

bacteria provides the grow-limiting vitamins B1 and B12 to its dinoflagellate host, but at present, it is not known if and how the exchange of metabolites between bacteria and algae in the phycosphere is achieved (Wagner-Dobler *et al.* 2010).

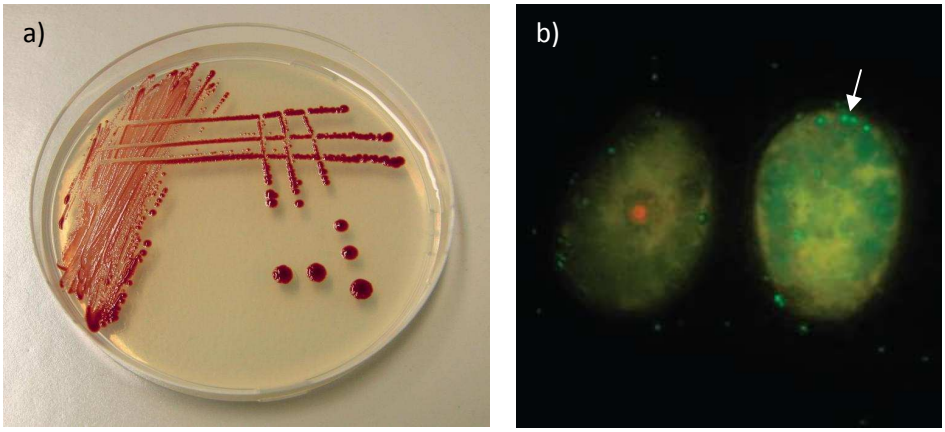

Figure 9 *D. shibae* DFL-12^T.

The figure depicts (a) a streak plate of *D. shibae* DFL-12 on Marine Agar (DSMZ/Wozniczka) and (b) *D. shibae* DFL-12 (white arrows, green dots) closely associated to its dinoflagellate host, *Prorocentrum lima*. Cells of *D. shibae* DFL-12 are visualized by catalyzed reporter deposition fluorescent in situ hybridization (CARD-FISH) with *Dinoroseobacter*-specific 16S rRNA probes (Wagner-Dobler *et al.* 2010).

1.8.2 Genomic features

D. shibae DFL-12 has a genome size of ~ 4.4 Mbp. The genome is composed of one circular chromosome and five plasmids and contains 4.219 protein-encoding genes of which 2.538 are predicted with known function and 1.681 without. The five plasmids represent examples for conjugation-based horizontal gene transfer (*cox* gene cluster of 47 kb, *vir* gene cluster) and vertical recruitment of chromosomal genes (*thiC*). Many genes were identified to promote the adaption to this symbiotic lifestyle. Apart from some genes, responsible for the attachment on the dinoflagellate host, like fascicline (*fas* genes) and alginate (*alg* genes), sets of flagella and conjugal type IV secretion system genes (*vir* genes, sex pili formation) were found. Furthermore the genome data suggest that *D. shibae* is able to synthesize two nutrients, vitamin B12 (cobalamin) and vitamin B1 (thiamine) that are essential and potentially growth limiting for their hosts. Two different biosynthetic routes for vitamin B12 synthesis are known in bacteria: an oxygen-independent (anaerobic) and an oxygen-dependent (aerobic) pathway. *D. shibae* harbors all genes required for vitamin B12 synthesis for both pathways, except for *cobG*, which is regarded as a signature gene for the

aerobic route. In addition, *D. shibae* DFL-12 possesses a complex viral defense system (Wagner-Dobler *et al.* 2010). Responsible for the antiviral resistance are CRISPRs (clustered regularly interspaced small palindromic repeats) which are small, transcribed DNA spacers separated by short palindromic repeats adjacent to *cas* (CRISPR associated) genes. Due to the fact that the majority of CRISPRs originated from bacteriophages, one assumes that CRISPRs are involved in RNAi-like mechanisms such as cleaving invading DNA (Garneau *et al.* 2010).

1.8.3 Quorum sensing in *D. shibae* DFL-12^T

The genome analysis of *D. shibae* DFL-12 revealed three autoinducer synthases (LuxI type) and five LuxR type genes for AHL-controlled transcriptional regulators. $LuxI_1$ (Dshi_0312) and $LuxI_2$ (Dshi_2851) are located on the chromosome adjacent to a LuxR regulator ($LuxR_1$ Dshi_0311, $LuxR_5$ Dshi_2852) with an intergenic region of approximately 100 bp. $LuxI_3$ (Dshi_4152) is located on the 86 kb plasmid (pDS86) without an adjacent LuxR type regulator. Furthermore *D. shibae* DFL-12 harbors three orphan LuxR regulators which are located on the chromosome without adjacent LuxI synthase: $LuxR_2$ (Dshi_1550), $LuxR_3$ (Dshi_1815) and $LuxR_4$ (Dshi_1819).

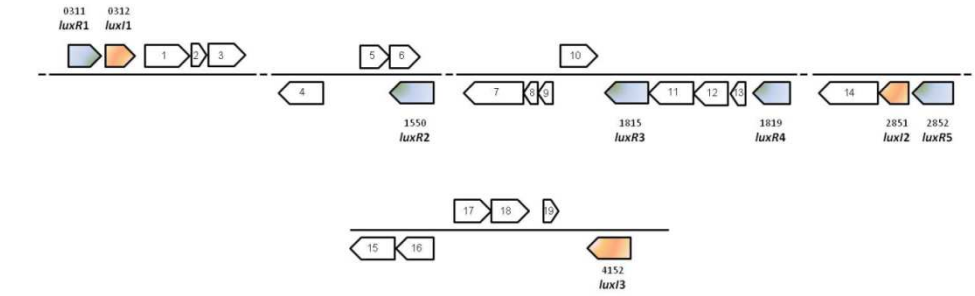

1 ATPase central domain protein
2 Camphor resistance CrcB protein
3 pseudouridine synthase, RluA family
4 PfkB domain protein
5 ribosomal protein S2
6 translation elongation factor Ts
7 hypothetical protein, transporter activity
8 tRNA-Asp
9 tRNA-Asp
10 hypothetical protein [unknown function]
11 MscS Mechanosensitive ion channel
12 Pirin domain protein [unknown function]
13 hypothetical protein [unknown function]
14 ATPase RecD-like DNA helicase
15 glycosyl transferase family
16 ABC-2 type transporter
17 Acetyltransferase (isoleucine patch superfamily)
18 hypothetical protein [unknown function]
19 hypothetical protein [unknown function]

Figure 10 Neighborhood of the *lux* genes.

The genes of the five LuxR type regulators are depicted in blue. The genes of the three LuxI synthases are presented in red. Adjacent genes are numbered consecutively and corresponding product names are listed in the legend. Numbers written above the gene names match with the Dshi locus Tags.

D. shibae DFL-12 produces three different AHLs: C8-HSL, C18-en-HSL with the C-C double bond located at C11 and C18-dien-HSL, whereas the double bonds are

located at C2 and C11. The C-C double bonds found in the C18 side chain are novel and may confer signal specifity. Due to the fact that C18-HSL is known to control the regulation of symbiosis relevant genes in *S. meliloti*, it has been suggested that C18-en-AHL and C18-dien-AHL of *D. shibae* also play a role in symbiotic gene control.

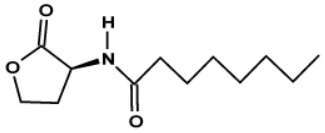

N-octanoyl-L-homoserine lactone (C8-HSL)

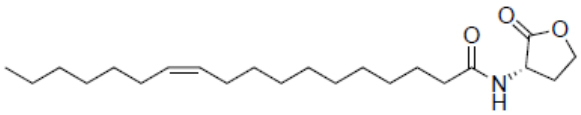

N-(3*R*, 11*Z*)-octadec-11-enoyl-L-homoserine lactone (C18-en-HSL)

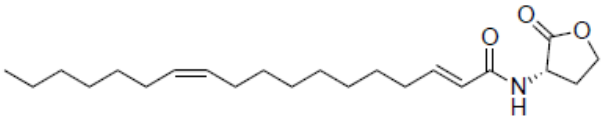

N-(3*R*,2*E*,11*Z*)-octadec-11-enoyl-L-homoserine lactone (C18-dien-HSL)

Figure 11 C8-HSL, C18-en-HSL and C18-dien-HSL produced by *D. shibae* DFL-12^T.

1.9 Algae

Algae are a diverse group of mainly unicellular photosynthetic organisms. Algae play an important role in marine, freshwater and some terrestrial ecosystems. They grow unicellular, multicellular or colonial. Some algae, like the diatoms, are microscopically small. Other algae, like the kelp, are as big as trees. Algae inhabit various kinds of biospheres, like the phytoplankton, drifting in the pelagic zone. Epiphytic or benthic algae grow attached to rocks, docks, plants and other solid objects (Raven *et al.* 1999).

1.9.1 Classification

The major groups of eukaryotic algae are the green algae, red algae, brown algae, diatoms and dinoflagellates. Blue-green algae, also known as *cyanobacteria*, are another group, but they class among the prokaryotes.

1.9.2 Economic and ecological importance

Algae are the base of the aquatic food chain and have found their way into human diet. The marine algae nori and kelp, for example, have been harvested in China for over two thousand years (Lembi 1988). *Spirulina*, a microscopic blue-green alga in the shape of a spiral coil, which is rich in protein and vitamin B, lives both, in sea and fresh water. It is used as a human dietary supplement, as well as a main food component, and is available in tablet, flake, and powder form. It is also used as a feed supplement in the aquaculture, aquarium, and poultry industries (Vonshak 1997). Some types of algae can cause environmental problems such as red tides and fishy-tasting water. These problems are usually caused by excessive release of nutrients from farms, sewage and other human activities. The outbreak of the nerve-toxin-producing *Pfiesteria* (a dinoflagellate) on the Atlantic coast, for example, has been linked to overflowing sewage lagoons (Faith and Miller 2000).

1.9.3 Algal blooms

Algal blooms occur in freshwater as well as marine environments and are defined as a rapid increase or accumulation in the population of algae in an aquatic system. Typically, only one or a small number of phytoplankton species are involved. Blooms are often green, yellow-brown or red, depending on the

density of species-specific pigmented cells. Harmful algal blooms (HABs) are of special interest. A harmful algal bloom is a bloom that causes negative economic and health impacts to other organisms as a consequence of the production of neurotoxins which can cause mass mortalities in fish, seabirds, sea turtles and marine mammals. Consuming seafood contaminated with such neurotoxins can result in human illness or even death (Silbergeld *et al.* 2000). The term “red tide” is colloquially used to describe HABs in coastal areas, as the dinoflagellate species involved in HABs are often red or brown and tint the water to a reddish color. But this is not entirely accurate as firstly harmful algal blooms are not associated with tides, secondly not all HABs cause reddish discoloration of the water and thirdly, not all algal blooms are harmful, even those involving red discoloration (Cortes-Altamirano *et al.* 1995).

1.9.4 Dinoflagellates and haptophyte algae

Dinoflagellates are organisms found in all types of aquatic ecosystems and are best known as causers of HABs. They are unicellular algae with armor made of cellulose and flagella which cause them to spin as they swim (Greek dinos "whirling" and Latin flagellum "whip, scourge"). Roughly half of the species in the group are photosynthetic (Gaines and Elbrächter 1987), the other half is exclusively heterotrophic and lives via osmotrophy and phagotrophy. Dinoflagellates, together with diatoms, are marine primary producers. As phagotrophic organisms they are also components of the microbial loop in oceans and make a contribution to channel significant amounts of energy into planktonic food webs. As a consequence, they are prominent members of the phytoplankton and the zooplankton, but they are also common in benthic environments and sea ice. Until 2008 more than two thousand extant species have been described, more than 1.700 are marine and about 220 are from freshwater (Taylor *et al.* 2008). Genetically, dinoflagellates are unique. Most dinoflagellates contain a singular nucleus, the dinokaryon. *Dinokarya* lack histones and nucleosomes, but the chromosome contains a small amount of basic protein that has been termed “histone-like”. They contain very high amounts of DNA per cell: 3.000-215.000 Mbp and the chromosomes appear

fibrillar because they remain continuously condensed during both interphase and mitosis (Rizzo 2003).

The ***Prorocentrales*** are a small order of dinoflagellates, which are distinguished from other groups by having their two flagella inserted apically, not associated with grooves, rather than ventrally and groove-associated as in other groups. The transverse flagellum is a wavy ribbon in which only the outer edge undulates from base to tip, due to the action of axoneme which runs along it. This flagellar movement produces forward propulsion and the main turning force. The longitudinal flagellum is relatively conventional in appearance. It beats with only one or two periods to its wave and works like a "rudder", directing the propulsive force into helical swimming (Miyasaka *et al.* 2004). Marine dinoflagellates of the genus *Prorocentrum* are famous for the production of okadaic acid (OA) which is produced during HABs causing diarrhetic shellfish poisoning (DSP) (Heredia-Tapia *et al.* 2002).

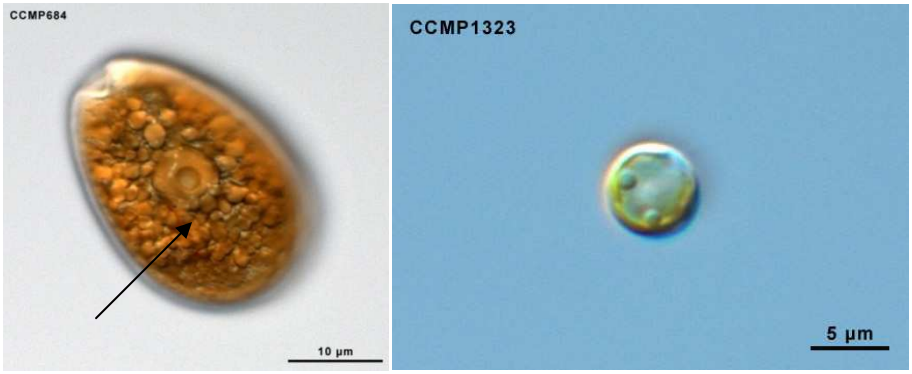

Figure 12 Light microscopy of *Prorocentrum lima* CCMP 684 and *Isochrysis galbana* CCMP 1323.

The left panel depicts *P. lima*, which has a central peridinin-containing plastid (pyrenoid) with a starch sheath (the ring-like structure, black arrow) Peridin is a light-harvesting carotenoid, a pigment associated with chlorophyll. The right panel shows a single cell of the haptophyt *I. galbana* (CCMP database).

Haptophyte algae are a monophyletic group that includes all photosynthetic organisms with a haptonema, as well as some nonphotosynthetic relatives, and some that have secondarily lost the haptonema. The haptonema, from which the group derives its name, is a microtubule-supported appendage that extends forward between two approximately equal flagella (flagella completely lack tripartite tubular hairs). The function of the unique haptonema includes the

capture of prey particles in mixotrophic and heterotrophic species and attachment to surfaces. Some of the haptophyte algae possess one flagellum with an autofluorescent substance (flavin) that plays a role in phototaxis. All haptophyte algae have chlorophyll a and one or more types of chlorophyll *c*. Furthermore these algae are rich in carotenoids, giving them a golden or brown color (Andersen 2004).

Isochrysis is a well known genus of the haptophyte algae. It is an important primary producer in aquatic habitats. *Isochrysis* serves as food for various bivalve larvae. The haptophyte algal is nowadays widely cultured for use in the aquaculture industry, because it is rich in long chain polyunsaturated fatty acids such as docosahexaenoic acid (DHA), which is one of the main omega-3 essential fatty acids (Qi *et al.* 2002).

1.10 Symbiosis

Symbiosis is ubiquitous in terrestrial, freshwater and marine communities. In general the word symbiosis broadly describes the living together of biological species. In mutualistic symbiosis the symbiont as well as the host benefits from the association. Eukaryote-associated microbes act as metabolic partners for accessing limiting nutrients and also as protector, producing toxins that ward off herbivores or pathogens (Moran 2006). There are two types of mutualism: obligate mutualism and facultative mutualism.

Obligate: The species involved are in close proximity and interdependent with one another in a way that one cannot survive without the other.

Facultative: The interacting species derive benefit from each other but not being fully dependent that each cannot survive without the symbiotic partner.

Mutualistic relationships may be either obligate for both species, obligate for one but facultative for the other, or facultative for both. Some symbiosis, such as the highly specific association between *V. fischeri* and its squid host *E. scolopes* appear to be facultative for both partners. The relationship indeed entails a life cycle stage in which the symbiont replicates outside of the host, but when the juvenile, bacteria-free squid once had obtain an inoculum of the naturally

occurring *V. fischeri* from ambient seawater, the symbiont population is maintained a lifetime in the squids light organ (Visick and Ruby 2006). *Silicibacter sp*. TM1040, a member of the *Roseobacter* lineage, forms biofilms on the surface of the dinoflagellate *Pfiesteria piscicida*. The dinoflagellate has an obligate requirement for *Silicibacter sp*.. Bacteria-free (axenic) dinoflagellate cultures fail to grow and ultimately die. Adding back *Silicibacter sp.* to axenic dinoflagellates restores growth to normal levels.

While the symbiosis is obligate for the dinoflagellates, it is facultative for *Silicibacter sp.*, which can be grown in both complex and defined minimal media without phytoplankton (Belas *et al.* 2009).

2 Aim of Work

Quorum sensing, density dependent regulation of gene expression, enables bacteria to establish in a niche, switch between different modes of life (planktonic or associated with eukaryotic hosts) and synchronize gene expression of the whole population. QS is mediated by signal molecules which are called autoinducers. In *Roseobacter*, most known autoinducers belong to the group of acylated homoserine lactones (AHLs) and regulated traits are not known so far.

It is the aim of this work to unravel the quorum sensing system of the *Roseobacter* model organism *Dinoroseobacter shibae* DFL-12 and its regulatory role in algae symbiosis. To elucidate all sides of this question, the work was divided into two parts.

The first part concentrates on the investigation of the functionality and specifity of the three *luxI* synthases, present in *D. shibae* DFL-12, by use of heterologous expression in *E. coli*. The genes $luxI_1$- $luxI_3$ will be separately knocked-out by a gene replacement vector and phenotypes of the mutants will be characterized. QS regulated traits will be identified by transcriptome profiling using a whole genome microarray.

The second part elucidates the regulatory role of QS during cocultivation with the dinoflagellate *P. minimum* and the haptophyt *I. galbana*, respectively. To this end, the effect of cultivation parameters on the synthesis of AHLs will be studied. For detection of AHL synthesis *in vivo*, a GFP-based reporter construct will be introduced into *D. shibae* DFL-12.

3 Material and Methods

3.1 Strains

Table 4 *Dinoroseobacter shibae* DFL-12 wild type and genetically modified strains.

Strain	Name	Relevant genotype and characteristics	Source or reference
D. shibae DFL-12	wild type	Isolated from the dinoflagellate *Prorocentrum lima*, type strain	1, 2, 3
D. shibae DFL-12	$LuxI_{1\text{-}3}$ OE	Overexpression of $luxI_{1\text{-}3}$ pBBR1MCS2::(P_{Gm}-$luxI_{1\text{-}3}$)	This study
D. shibae DFL-12	Δ$luxI_1$	Δ$luxI_1$, Gm^R	This study
D. shibae DFL-12	Δ$luxI_2$	Δ$luxI_2$, Gm^R	This study
D. shibae DFL-12	Δ$luxI_3$	Δ$luxI_3$, Gm^R	This study
D. shibae Δ$luxI_1$	Comp1	pBBR1MCS2::(P_{Gm}-$luxI_1$)	This study
D. shibae Δ$luxI_1$	Comp0	pBBR1MCS2 ,vector control	This study
D. shibae DFL-12	FACS6	pKR-C12, FACS selected clone.	This study

1,(Allgaier *et al.* 2003); 2,(Biebl *et al.* 2005); 3,(Wagner-Dobler *et al.* 2010)

Table 5 *Escherichia coli* strains

Strain	Relevant genotype and characteristics	Source or reference
E. coli CC118 α pir	D(*ara±leu*) *araD* D*lacX74 galE galK phoA20 thi-1 rps-1 rpoB argE*(Amp) *recA thi pro hsdRM*+ RP4-2-Tc: :Mu-Km: :Tn7 *kpir*	4
E. coli BL21 DE3	Protein expression F⁻ *ompT hsdSB*(r_B^- m_B^-) *gal dcm*	Novagen
E. coli Tuner™ DE3	Protein expression F⁻ *ompT hsdSB* (r_B^- m_B^-) *gal dcm lacY1*	Novagen
E. coli DH5α	General cloning strain *endA1 hsdR1*[r_K – m_K +] *glnV44 thi- recA1 gyrA relA* [*lacZYA-argF*)*U169 deoR* [80*dlac* [*lacZ*]M15)	4
E. coli DH10B	General cloning strain F⁻ *mcrA* Δ(*mrr-hsd*RMS-*mcrBC*) Φ80d*lacZ*ΔM15 Δ*lacX*74 *endA1 recA1 deoR* Δ(*ara,leu*)7697 *araD*139 *galU galK nupG rpsL* λ⁻	5
E. coli TOP 10	General cloning strain F⁻ *mcrA* Δ(*mrr-hsd*RMS-*mcr*BC) ϕ80l*acZ*ΔM15 Δ*lac*X74 *rec*A1 *ara*D139 Δ(*ara-leu*) 7697 *gal*U *gal*K *rps*L (Str^R) *end*A1	Invitrogen
E. coli TOP 10 F’	General cloning strain F´{*lac*Iq Tn10 (TetR)} *mcr*A Δ(*mrr-hsd*RMS-*mcr*BC) Φ80*lac*ZΔM15 Δ*lac*X74 *rec*A1 *ara*D139 Δ(*ara-leu*)7697 *gal*U *gal*K *rps*L *end*A1 *nup*G	Invitrogen
E. coli ST18	Biparental mating S17-1Δ*hemA thi pro hsdR-M*- with chromosomal integrated [RP4-2 Tc::Mu:Kmr::Tn7, Tra+ Trir Strr]	6

4, (Herrero *et al.* 1990); 5,(Grant *et al.* 1990); 6 (Thoma and Schobert 2009)

Table 6 Sensor strains for AHL detection

Strain	Relevant genotype and characteristics	Source or reference
E. coli MT102	Detection of short-chain AHLs. Contains the sensor plasmid pJBA132. F– *thi araD139 ara±leu*D*7679* D(*lacIOPZY*) *galU gal*«K r^{-} m^{+} Sm^{R}	7
P. putida F117	Detection of long-chain AHLs. Contains the sensor plasmid pKR-C12	8

7, (Andersen *et al.* 2001); 8, (Riedel *et al.* 2001)

3.2 Plasmids

Table 7 Plasmids

Plasmid	Relevant genotype and characteristics	Source or reference
pBBR1MCS2	Source of complementation construct Ka^R; broad-host-range vector	9
pBBR1MCS5	Source for amplifying the Gm^R cassette Gm^R; broad-host-range vector	9
pKR-C12	Sensor plasmid Gm^R; pBBR1MCS-5 carrying P_{lasB}-*gfp*(ASV) P_{lac}-*lasR*	8
pJBA132	Sensor plasmid Tc^R; pME6031-*luxR*-P_{luxI}-RBSII-*gfp*(ASV)-T0-T1	7
pJP5603	Source plasmid for the Knock-out construct Ka^R; oriR6K cloned to Tn5 kan mobRP4	10
pJP5603KO1	pJP5603 + Φ (819 bp 5'Dshi_0312-Gm^R- 654 bp 3' Dshi_0312), Ka^R	This study
pJP5603KO2	pJP5603 + Φ (800 bp 5' Dshi_2851-Gm^R- 900 bp 3' Dshi_2851), Ka^R	This study
pJP5603KO3	pJP5603 + Φ (818 bp 5' Dshi_4152-Gm^R- 919 bp 3' Dshi_4152), Ka^R	This study
MCS2 Comp1-3	Complementation/Overexpression pBBR1MCS-2::P_{Gm}-*luxI*$_{1-3}$, Ka^R	This study
pTrcHis-TOPO TA®	Protein expression control vector	Invitrogen
pCR4 TOPO TA®	Insertion of Taq polymerase-amplified PCR products for sequencing.	Invitrogen
PCR2.1 TOPO TA®	Insertion of Taq polymerase-amplified PCR products for sequencing.	Invitrogen

7, (Andersen *et al.* 2001); 8, (Riedel *et al.* 2001); 9,(Kovach *et al.* 1995); 10,(Penfold and Pemberton 1992)

3.3 Primer

All primers were used with an annealing temperature of 60°C.

Table 8 Primers used for characterization of the *luxI* synthases
Nucleotides in bold indicate the built-in restriction sites.

Primer	Sequence (5' → 3')	Purpose
luxI1_F_NdeI	AAA **CAT ATG** CAA ACC ACC ACG CTT	Expression of *luxI*
luxI1_R	TGC GCG CGG CGC CTA	Expression of *luxI*
luxI1_R_NdeI	AAA AA**C ATA TG**T GCG CGC GGC GCC TA	Complementation
luxI2_F_NdeI	AAA **CAT ATG** ATC CGT TTC GTC TAT GCC	Expression of *luxI*
luxI2_R	TCA GGC CGC CAA GCT	Expression of *luxI*
luxI2_R_NdeI	**CAT ATG** TCA GGC CGC CAA GCT	Complementation
luxI3_F_NdeI	AAA **CAT ATG** ATT ACA ATA GCA CGT GG	Expression of *luxI*
luxI3_R	CTA GGC TGC CTT TGG	Expression of *luxI*
luxI3_R_NdeI	AAA AA**C ATA TG**C TAG GCT GCC TTT GG	Complementation
1ups_F_SacI	AAA **GAG CTC** CGG CTG GAC GTC TAA TTC TG	Knock-out
1ups_R_SalI	AAA **GTC GAC** CAG TCT CCA GTT TGT GGT GGT	Knock-out
2ups_F_EcoRI	AAA **GAA TTC** TGG AAT CGT TTC TGG	Knock-out
2ups_R_SalI	AAA **GTC GAC** GGG GGC GGC CCT CTT	Knock-out
3ups_F_EcoRI	AAA **GAA TTC** CCC ACA TCT GAC GCG	Knock-out
3ups_R_SalI	AAA **GTC GAC** GCT GCA GTC CTT CTT	Knock-out
1dos_F_NheI	AAA **AGC TAG** CCT GAT CAG CGA GAT GAC CAA GG	Knock-out
1dos_R_NheI	AAA **AGC TAG** CCC GAT ATC CTC CAC	Knock-out
2dos_F_NheI	AAA **AGC TAG** CCG TCG GTC TGT GGT C	Knock-out
2dos_R_NheI	AAA **AGC TAG** CGC TGC CGC TCC GCG G	Knock-out
3dos_F_NheI	AAA **AGC TAG** CCT CTG GCC TGT TCA A	Knock-out
3dos_R_NheI	AAA **AGC TAG** CGA CTC TAA AGC TTC C	Knock-out
Amp_NheI/SalI_R	AAA AAA **GTC GAC** AAA **GCT AGC** GCG GAA CCC CTA TTT GTT TA	Amp cassette (pCR4)
Amp_SalI_F	AAA AAA **GTC GAC** GCT GAA GCC AGT TAC CTT CG	Amp cassette (pCR4)
Gm_F	GGA AAC GGA TGA AGG CAC GAA	Gm cassette
Gm_R	GCC CAG CGC CAG CAG GAA C	Gm cassette
Gm PromF	ACG GCA TGA TGA ACC TGA AT	Complementation
Gm PromR_ndeI	**CAT ATG** CGT TGC TGC TCC ATA ACA TC	Complementation

Characterization primers were used with *Pfu* proofreading polymerase.

Table 9 Primers used for verification

Primer	Sequence (5' → 3')	Purpose
16S rRNA F27	AGA GTT TGA TCC TGG CTC AG	Colony PCR
16S rRNA R1492	GGT TAC CTT GTT ACG ACT T	Colony PCR
pJP5603_MCS_F	AAC AGC TAT GAC CAT G	Verification
pJP5603_MCS_R	GTA AAA CGA CGG CCA GT	Verification
Gm_SF	TTT CGG GGA AAT GTG CGC G	Sequencing
Amp_SR	TTC CAC TGA GCG TCA GAC CC	Sequencing
Amp_SF	AAC TGT CAG ACC AAG TTT AC	Sequencing
I1_SF	CAT CCG CCC CAA GGA GAG CG	*luxI* replacement
I1_SR	GCG CGG CTT GTC AAC TCT GC	*luxI* replacement
I2_SF	GCA TGG TGG TGA TCT GTG CC	*luxI* replacement
I2_SR	CGC CCA CCA CAT GCA GCT TG	*luxI* replacement
I3_SF	GAG TTG AGC AGG GAA CCG GG	*luxI* replacement
I3_SR	ACG GGA CCG GGT CTT GGA TG	*luxI* replacement

Verification primers were used with *Taq* polymerase.

Table 10 Primers used for qRT-PCR and verification

Primer	Sequence (5' → 3')	Purpose
GyrA_F	AGC TCC TAT CTC GAT TAC GC	Reference QPCR
GyrA_R	GTA CTT GCC CAT CAC ATC G	Reference QPCR
I1 P1 F	ATG TCC ATA AAG CTA GGC ATC G	*luxI* replacement/ QPCR
I1 P3 R	AGG ATG CCG AAC GGA TC	*luxI* replacement/ QPCR
RT luxI1 F	AAA CAT ATG CAA ACC ACC ACG CTT	QPCR
RT luxI1 R	CGCAGGCCCATAGAGCA	QPCR
RT luxI2 F	TCG ATA CCT ATC CCC GTC TC	*luxI* replacement/ QPCR
RT luxI2 R	TCA CGT AGA TCG GGT TTT CC (	*luxI* replacement/ QPCR
RT luxI3 F	GTG GAT CAA TGC GGA TAC TTC	*luxI* replacement/ QPCR
RT luxI3 R	AGA AAC ACA GAA GCG TGT GC	*luxI* replacement/ QPCR
RT luxR1 F	AAA GCT AGG CAT CGA ACT GG	QPCR
RT luxR1 R	TAG CGA TCC TTC CAC TCT TG	QPCR
RT luxR5 F	GTG TTC TCG GTC AAC AAT CG	QPCR
RT luxR5 R	GCC GTC GGA TTT ATG TCT TC	QPCR
RT_thiC_F	CTG ATC GAA CAG GCT GAA CA	QPCR
RT_thiC_R	GAA ACT TTC GCG GTG ATG AT	QPCR
RT_alg_F	GGA GAT CAA CTT CCG GGT CT	QPCR
RT_alg_R	TCA AGC GTC TCG ACA TTC AG	QPCR
RT_cobN_F	ATC CAT TTC GGG TTG ACC AC	QPCR
RT_cobN_R	AAC GGC CGA TCT ATC ACA AC	QPCR
RT_cbiX_F	TGC CCT ATT TCC TGT TCA CC	QPCR
RT_cbiX_R	GCC TTG ACG AAC TGG ATC TC	QPCR
RT_fas_F Dshi_0412	GTG CAG GGA CTG AAG GAC AT	QPCR
RT_fas_R Dshi_0412	CGA GAC GTG ATA GAG CAG CA	QPCR
RT_fas_F Dshi_0621	CCA TCC TGA CCT ACC ACG TC	QPCR
RT_fas_R Dshi_0621	AGG GCA GCA GAA CCT TGT C	QPCR

3.4 Bacterial cultivation

3.4.1 Media

All media were solidified with 15 g/l agar and sterilized by autoclaving at 121 °C for 20 min.

Luria-Bertani Medium (LB)

LB Miller (Sigma) and 40 g LB agar (Roth) were dissolved in 1 L deionised water for liquid and for solid LB, respectively. These ready-to-use media consisted of the following components: 10 g/l tryptone, 5 g/l yeast extract, 10 g/l NaCl and in case of agar plates 15 g/l bacto agar.

Marine broth (MB)

37.4 g/l ready-to-use MB broth (Difco 2216) was dissolved in 1 L deionised water. Before autoclaving, the medium was heated with frequent agitation and boiled for 1 minute to completely dissolve the powder.

Half-concentrated Marine broth (hMB)

Several antibiotics can be affected in their chemistry by high salt concentrations, as found in MB. Half-concentrated MB (hMB) allows growth of *D. shibae*, albeit with partly decreased growth rates compared to MB and required antibiotics remain active during cultivation (Piekarski *et al.* 2009).

18.7 g/l ready-to-use MB broth (Difco 2216) was dissolved in 1 L deionised water. Before autoclaving, the medium was heated with frequent agitation and boiled for 1 minute to completely dissolve the powder.

SWM – artificial seawater medium

SWM-Basis 5x:

100 g	NaCl
20 g	Na_2SO_4
15 g	$MgCl_2$*6 H_2O
2.5 g	KCl
1.25 g	NH_4Cl

Dissolve in 1 litre H_2O and autoclave for 20 min at 121°C.

Stock solution 100x:

1.9 g $NaHCO_3$

Dissolve in 100 ml dest. H_2O and autoclave for 20 min at 121°C.

Stock solution 1000x:

20.0 g KH_2PO_4

15.0 g $CaCl_2$ x 2 H_2O

Dissolve in 100 ml dest. H_2O and autoclave for 20 min at 121°C, respectively.

Succinate stock solution 0.5 M:

Dissolve 29.52 g succinic acid (M = 118.09 g/mol) in 400 ml dest. H2O. Adjust pH value with NaOH to pH 7.5. Bring to the volume of 500 ml with dest. H_2O and autoclave for 20 min at 121°C.

Trace element solution (1000x)		
	1000ml	500ml
H_2O	50 ml	25 ml
$FeSO_4$ x $7H_2O$	2.1 g	1.05 g
25%ige HCL	13 ml	6.5 ml
Titriplex III (Na_2EDTA)	5.2 g	2.6 g
Titriplex III may form clumps. Adjust pH value to 6.0 - 6.5; Titriplex III gets solved.		
H_3BO_3	30 mg	15 mg
$MnCl_2$ x 4 H_2O	100 mg	50 mg
$CoCl_2$ x 6 H_2O	190 mg	95 mg
$NiCl_2$ x 6 H_2O	24 mg	12 mg
$CuCl_2$·x 2 H_2O	2 mg	1 mg
$ZnSO_4$ x 7 H_2O	144 mg	72 mg
Na_2MoO_4 x 2 H_2O	36 mg	18 mg
Autoclave for 15 min at 121°C		

Vitamin stock solution (100x)	
Biotin	2 mg
nicotinic acid	20 mg
4-aminobenzoic acid	8 mg
Dissolve in 100 ml dest. H_2O and filter-sterilize.	

To obtain 100 ml SWM 5 mM succinate, combine the stock solutions as follows:

76.7 ml autoclaved dest. H_2O, 20 ml SWM-Basis 5 x, 1 ml succinate (0.5 M), 1 ml $NaHCO_3$ (100x), 100 µl KH_2PO_4 (1000x), 100 µl $CaCl_2$ x 2 H_2O (1000x), 100 µl trace element solution (1000x) and 1 ml vitamin stock solution (100x).

SOC medium (Sambrook and Maniatis 1989)

This medium was used to recover the *E. coli* cells after transformation. It is mixed from SOB medium and glucose.

SOB medium

20 g	Tryptone (Difco)
5 g	Yeast Extract (Difco)
0.5 g	NaCl (Roth)
10 ml	0.25 M KCl
5 ml	2 M $MgCl_2$

The components were dissolved in 980 ml deionised water, and the pH was adjusted to 7. For one litre SOC medium, 20 ml 1 M sterile D-glucose (Sigma) was added to SOB medium.

Additives

Additives, like antibiotic stock solutions or aminolevulinic acid (ALA) were dissolved in their respective solvent, filter sterilzed, stored at –20°C and diluted prior to use in the growth media.

Table 11 Additives used in this study

Additive	Solvent	Stock conc. mg/ml	Working conc. µg/ml *E. coli*	Working conc. µg/ml *D. shibae* DFL-12
Ampicillin	water	100	50-100	100
Gentamicin	water	500	25-50	50-200
Kanamycin	water	1000	50	50-500
Tetracycline	methanol	25	25	-
Aminolevulinic acid	water	50	50	-

3.4.2 Cultivation conditions

All bacteria were cultivated aerobically using standard microbiological techniques. They were streaked onto an agar plate from a glycerol stock. Single colonies were inoculated into 20 ml liquid medium in a 100 ml Erlenmeyer flask or a 50 ml polypropylene tube. This preculture grew overnight. Main cultures of *E. coli* or *P. putida* were routinely cultivated in LB media at 37°C and 30°C with agitation (180 rpm), respectively. *D. shibae* DFL-12 was routinely cultivated in MB, hMB or SWM media (choice of media depends on experiment) with agitation (160 rpm) in the dark. Growth was monitored by measuring the optical density at 600 nm (OD_{600nm}) with a Pharmacia Biotech spectrophotometer.

3.4.3 Glycerol stock cultures

For preparation of glycerol stock cultures, cells were grown in the respective media supplemented with the appropriate antibiotic. In the mid-log phase 850 µl cells were mixed with 150 µl 87% (v/v) glycerol, aliquoted and stored at – 70°C.

3.5 Algae cultivation

Axenic (bacteria-free) algae strains used in this study were ordered at the Provasoli-Guillard National Center for Culture of Marine Phytoplankton (CCMP).

3.5.1 Media

L1 medium for algae cultivation

This enriched seawater medium is based upon f/2 medium (Guillard and RYTHER 1962) but has additional trace metals and Na_2SiO_3 is omitted. It is a general purpose marine medium for growing coastal algae.

Prepare the stock solutions (g/l) of the first two components as indicated below and autoclave them.

Component	Stock Solution
$NaNO_3$	75.0 g/l (8.82 x 10^{-1} M)
$NaH_2PO_4 \cdot x\ H_2O$	5.0 g/l (3.62 x 10^{-2} M)

L1 Trace Element Stock Solution

Prepare the primary stock solution of each trace element (except for Na_2EDTA x 2 H_2O and $FeCl_3$ x 6 H_2O). To obtain 1 litre of the L1 Trace Element Stock solution dilute each of the primary stock solution 1:1000 (1ml of each primary stock solution, except for Na_2EDTA x 2 H_2O and $FeCl_3$ x 6 H_2O) and bring the final volume to 1 litre with dest. H_2O. Autoclave.

Component	Primary Stock Solution	Stock solution	Final Concentration in 1 liter L1.
Na_2EDTA x 2 H_2O	---	4.36 g/L	1.17 x 10^{-5} M
$FeCl_3$ x 6 H_2O	---	3.15 g/l	1.17 x 10^{-5} M
$MnCl_2$·x 4 H_2O	178.10 g/l	178.10 mg/l	9.09 x 10-^{7} M
$ZnSO_4$ x 7 H_2O	23.00 g/l	23.00 mg/l	8.00 x 10^{-8} M
$CoCl_2$ x 6 H_2O	11.90 g/l	11.90 mg/l	5.00 x 10^{-8} M
$CuSO_4$ x 5 H_2O	2.50 g/l	2.50 mg/l	1.00 x 10^{-8} M
Na_2MoO_4 x 2 H_2O	19.9 g/l	19.9 mg/l	8.22 x 10^{-8} M
H_2SeO_3	1.29 g/l	1.29 mg/l	1.00 x 10^{-8} M
$NiSO_4$ x 6 H_2O	2.63 g/l	2.63 mg/l	1.00 x 10^{-8} M
Na_3VO_4	1.84 g/l	1.84 mg/l	1.00 x 10^{-8} M
K_2CrO_4	1.94 g/l	1.94 mg/l	1.00 x 10^{-8} M

f/2 Vitamin Stock Solution

First prepare the primary stock solutions of biotin and cyanocobalamin. To prepare the vitamin stock solution, begin with 950 ml of dest. H_2O and dissolve the thiamine. The primary stock solution of biotin is diluted 1:100 to obtain a stock solution with 1.0 mg/l. The primary stock solution of cyanocobalamin is diluted 1:1000, to obtain a stock solution with 1 mg/l. Filter sterilize the vitamin stock solutions and store in refrigerator or freezer.

Component	Primary Stock Solution	Stock solution	Molar mass
thiamine (vit. B1)	---	200 mg/l (5.93×10^{-4} M)	337.3 g/mol
biotin (vit. H)	0.1g/l (4.09×10^{-4} M)	1.0 mg/l (4.09×10^{-6} M)	244.3 g/mol
cyanocobalamin (vit. B12)	1.0 g/l (7.38×10^{-4} M)	1.0 mg/l (7.38×10^{-7} M)	1355.4 g/mol

To prepare 1litre of L1 begin with 950 ml of filtered natural seawater. Add 1ml of the stock solutions of the first two components as indicated below, and then bring the final volume to 997.5 ml with filtered natural seawater. Autoclave. Final pH should be 8.0 to 8.2.

After autoclaving and cooling of the L1 medium, add 1ml of the trace element stock solution and 0.5 ml of each vitamin stock solution to the medium.

Component	Stock Solution	Final molar conc./L
$NaNO_3$	1 ml	8.82×10^{-4} M
$NaH_2PO_4 \cdot x\ H_2O$	1 ml	3.62×10^{-5} M
Autoclave.		
trace element solution	1ml	See trace element stock solution recipe
thiamine	0.5 ml	2.96×10^{-7} M
biotin	0.5 ml	2.05×10^{-9} M
cyanocobalamin	0.5 ml	3.69×10^{-10} M

L1 medium for *D. shibae* DFL-12 cultivation

To cultivate *D. shibae* DFL-12 separately in L1 medium, the L1 medium is combined with the stock solution of the SWM trace element solution and the SWM vitamin solution. Succinate is used as carbon source.

To prepare 1litre of L1 5 mM succinate for *D. shibae* DFL-12 cultivation begin with 950 ml of filtered natural seawater. Add 1ml of the stock solutions of the first two components as indicated below, and then bring the final volume to 979 ml with filtered natural seawater. Autoclave. Final pH should be 8.0 to 8.2.

After autoclaving and cooling of the L1 medium, add 1 ml of the SWM trace element stock solution and 10 ml of the SWM vitamin stock solution to the medium.

Finally add 10 ml of the SWM succinate stock solution (0.5 M) to the medium.

Component	Stock Solution
L1 $NaNO_3$	1 ml
L1 $NaH_2PO_4 \cdot x\ H_2O$	1 ml
Autoclave.	
SWM trace element solution	1 ml
SWM vitamin solution	10 ml
SWM succinate	10 ml

3.5.2 Cultivation conditions

Both axenic algae (*P. minimum* CCMP1329, *I. galbana* CCMP1323) were cultivated as permanent cultures using L1 medium. It is impossible to prepare glycerol stock solutions, therefore every algae was monthly inoculated in 90 ml fresh L1 medium with 10 ml of the previous culture. For experiments, additional working cultures were inoculated with 10 or 5 ml of the latest permanent culture. Routinely 250 ml Erlenmeyer flasks were used, capped with a plug made of cotton besides the metal over-cap. *P. minimum* was grown statically, at room temperature on a light/dark-cycle with a light intensity of 24 µmol photons m^{-2} s^{-1}. *I. galbana* was cultivated statically, at 13°C on a 12 h light/dark-cycle with a light intensity of 24 µmol photons m^{-2} s^{-1}.

3.5.3 Chlorophyll extraction

(Biebl *et al.* 2005)

The growth of algae was calculated as the amount of chlorophyll *a.* Therefore, 2 ml of the alga culture were harvested and centrifuged at 13.000 rpm for 10 minutes. The supernatant was discarded and the pellet was resuspended in 1 ml of a mixture of acetone/methanol (7:2). The suspension was incubated 1 h at room temperature in the dark, vortexed and centrifuged again for 1 minute at 10.000 rpm. The supernatant was used to determine the chlorophyll *a* content and the absorbance was measured at 664 nm (abs_{664nm}) with a Pharmacia Biotech spectrophotometer.

3.5.4 Coculture conditions

Cobalamin (vitamin B12) was omitted from the L1 coculture medium to grow the algae under vitamin B12 limitation which forced the exchange of metabolites and, if required, the attachment of *D. shibae* DFL-12 to the algae host. At that time at which lacking of cobalamin became growth limiting (20-30 days of cultivation, depending on the algae), one set of three biological replicas were inoculated with *D. shibae* DFL-12 (strain FACS6, Table 3). A second set of three biological replicas were provided with 0.5 ml of the cobalamin stock solution and a third set of three biological replicas remained untreated (negative control). Three biological replica of the algae culture with complete medium and without inoculation of *D. shibae* DFL-12 were used as positive control to monitor normal algae growth. As positive control for bacterial growth, three biological replica of L1 enriched with the SWM vitamins and 5 mM succinate were also inoculated with *D. shibae* DFL-12 (strain FACS6, Table 3). Positive and negative controls were incubated at the same conditions as their cocultures.

3.6 Extraction and anlaysis of AHLs produced by marine bacteria

3.6.1 Preparation of AHL extracts

Methanol extracts:

Marine bacteria were grown in marine broth 2216 (Difco) or SWM with 5 mM succinate. Medium was inoculated from fresh plates and incubated always at 30°C with agitation in 50 ml polypropylen tubes overnight, in the dark, until an OD_{600nm} of 0.5-1.0 had been reached. The preculture was added to fresh medium (100 ml) in a 500 ml Erlenmeyer flask. The neutral adsorber resin Amberlite XAD-16 (2 mL, Rohm & Haas) was added, and the culture was incubated for 36 hours with shaking until an OD_{600nm} above 1.0 had been reached. The culture supernatant was discarded. Methanol (50 ml) was added to the resin, and the mixture was left without shaking overnight. The resin was removed by filtering through a paper filter. The methanol extract was concentrated to several ml in an evaporator and stored at -20°C.

Dichloromethane extracts:

Dichloromethane extracts were prepared with the same experimental setup as for methanol extracts, except for the treatment of the adsorber resin. The culture supernatant was discarded through an analytic sieve. The resin was collected and transferred into a separating funnel. 25 ml dichloromethane and 200 ml dest. water were added and the resin was shaked out. Dichloromethaneous phase was collected in round-bottom flask. The extraction of the resin with dichloromethane and water was repeated for four times, in order that in total 100 ml dichloromethane were used for extraction and finally concentrated to several ml in an evaporator and stored at -20°C.

3.7 AHL- Bioassay

Sensor strains were grown on LB medium and incubated at 37 °C (*E. coli* MT102) or 30°C (*P. putida* F117) on a shaking platform for 12–20 h until an OD_{600nm} of 1.0 had been reached. The respective strains were inoculated from plates into preculture (3 mL), which was then transferred to fresh medium (100 mL) and incubated for an additional hour. The methanol or dichloromethane extracts (10 µl-50 µl) were pipetted into 96-well microtiter plates and evaporated under the fume cupboard. Afterwards 100 µl of LB medium were transferred into the wells and the sensor strains (100 µl) were added. Each methanol or dichloromethane extract was measured in triplicates. Microtiter plates were incubated at 30°C with agitation. After 0, 2, 4, 8 and 24 h, fluorescence was determined in a Victor1420 Multilabel Counter (Perkin–Elmer) at an excitation wavelength of 485 nm and a detection wavelength of 535 nm. OD_{620nm} was also measured. Methanol or dichloromethane (10 µl) was used as a negative control, and synthetic homoserine lactones were used as a positive control. Fold induction of fluorescence was calculated by dividing the specific fluorescence (gfp535/OD620) of the test sample by the specific fluorescence of the negative control.

3.8 GC-MS analyses

The analyses of the AHL extracts were carried out on a GC System Typ 7890A connected to a Mass Selective Detector Typ 5975C from Agilent Technologies with split/splitless-Injector. The device was fitted with a Fused-Silica-Capillary column (HP-5ms, 30m * 0.25 mm i.d., 0.25 µm film thickness, Agilent Technologie). The carrier gas was helium at 1.2 ml per minute. The GC was programmed as follows: 5 min at 50°C, increasing with 5°C per minute to 320°C and operated in splettless mode. The injection volume was 1µl and the front inlet temperature 250°C. Analyses were prepared by Alexander Neumann from the Technical University in Braunschweig.

3.9 Standard RNA techniques

3.9.1 Preparing planktonic cells for RNA extraction

An appropriate volume of planktonically grown cells (2-10 ml for *D. shibae* DFL-12 and 10-50 ml for *D. shibae* DFL-12 cocultured with *I. galbana* or *P. minimum*) was centrifuged for 2 min. at 13.000 rpm. The supernatant was discarded and the pellet resuspended in the Stop solution (1/5 volume of the source culture volume). Subsequent the sample was frozen in liquid nitrogen for 10-20 seconds or stored at – 70°C until RNA extraction. For immediate extraction samples were thawed on ice and centrifuged for 2 min. at 13.000 rpm (4°C). The supernatant was discarded and the pellet was used for RNA isolation.

Stop solution : 5 % phenole, 95 % EtOH (pure)

3.9.2 RNA isolation

For isolation and purification the RNeasy-kit (Qiagen) was used according to the manufacturer's manual. Some modifications are listed below. Cell lysis was performed for at least 25 minutes at room temperature enzymatically using 15 mg/mL lysozyme in tris-EDTA-buffer (pH 8.0) and mechanically by vortexing for 3 min with acid washed glass beads (diameter 106 µm). A first digestion of genomic DNA was performed on the column, using RNase-free DNase I (Qiagen) according to the manufacturer's protocol. Total RNA was eluted in 88 µL RNase-free H_2O and a second DNase I-digestion of genomic DNA was performed in solution, followed by a second RNeasy purification step. In this second

purification an additional washing step with 80 % ethanol was performed prior to elution with 30µl RNase-free water.

The quality of the total RNA was controlled on a denaturating formaldehyde agarose gel and the absence of gDNA with a standard PCR.

3.9.3 Denaturating gel electrophoresis for RNA

For RNA gel electrophoresis, 0.6 g agarose was dissolved in 5 ml 10x FA buffer and 45 ml autoclaved Milli-Q water by heating in a microwave. 0.9 ml 37% formaldehyde and 1 µl ethidium bromide (10 mg/ml) were added to the chilled agarose and the gel was casted. RNA samples were mixed with 5x loading buffer, incubated at 65°C for 5 minutes and put on ice prior to loading onto the gel. Electrophoresis was started with 50 V until the samples entered the gel matrix and continued at 70 V until visualization using UV light.

10 x FA gel buffer

200 mM 3-[*N*-morpholino]propanesulfonic acid (MOPS) (free acid)
50 mM sodium acetate
10 mM EDTA
pH to 7.0 with NaOH

3.10 Microarray

3.10.1 Design of the microarray

A customized whole genome microarray was designed using the Agilent eArray platform (https://earray.chem.agilent.com/earray/). For 96% of the genes antisense probes (60 bp in length) could be designed. Where it was possible three probes were designed per gene. Two plasmids of *D. shibae* contain highly homologous regions (Wagner-Dobler *et al.* 2010). Probes were designed but it is not possible to trace back the signal to the plasmid it originates from. Randomly selected probes were spotted scattered on the array in 10 replicates in order to determine the quality of the hybridisation. Positive and negative controls as well as spike in controls from Agilent have been included.

3.10.2 RNA labeling

Labeling of RNA was carried out with the ULS labeling kit (Kreatech, Germany), using

Cy3/Cy5 as fluorescence dyes, according to the manufacturer's instructions. The reaction mixture contained 2 µl of 10 x labeling solution, 2 µl of Cy-ULS dye and 2 µg of total RNA. The reaction was filled up with RNase free water to 20 µl. Reference RNA was labelled using Cy3 and sample RNA was labelled using Cy5. The reaction was incubated for 15 minutes at 85°C and kept on ice until removal of unbound dye.

Dye removal of labeled RNA

1. Re-suspend column material by vortexing
2. Loosen cap ¼ turn and snap off the bottom closure
3. Place the column in a 2 ml collection tube
4. Pre-centrifuge the column for 1 minute at 20.800 x g
5. Discard the flow-through and column cap
6. Add 300 µl of water to the column and centrifuge for 1 min at 20.800 x g
7. Discard flow-through and collection tube
8. Place column into a 1.5 ml collection tube
9. Add labelling solution onto the centre of the column bed
10. Centrifuge for 1 min at 20.800 x g
11. Flow-through contains the purified labelled DNA

Determination of the degree of labeling (DoL)

To ensure that the RNA was properly labelled and could be used for microarray hybridisation, the degree of labelling (DoL) was determined. Therefore, 2 µl of labelled RNA was measured with the NanoDrop (Thermofischer Scientific) (program: microarray). The DoL was calculated using a web form on the manufacturer's homepage.

(http://www.kreatech.com/Portals/kreatech/downloads/labeling/27_DoL%20calculator_28082007.xls)

3.10.3 RNA fragmentation

For the fragmentation 700 ng of each RNA sample (Cy3 and Cy5 labelled RNA) was mixed, 5 µl of 10 x blocking agent (Agilent) and 1 µl 25 x frag. Buffer (Agilent) were added and the reaction was filled up to 25 µl with water. The reaction was incubated for 30 min at 60°C until 25 µl of 2x GE hybridization buffer (Agilent) was added. The reaction was stored on ice until hybridisation.

3.10.4 RNA hybridisation and scanning

Hybridisation was carried out at 65°C for 17 hours using the Agilent hybridisation chamber. Scanning was achieved using the Agilent DNA microarray scanner.

3.10.5 Data analysis

Background correction and loess normalization were performed using the Agilent scanner algorithms and raw data were extracted using the agilent feature extraction software. Data processing was carried out with the Bioconducter – Linear Models for Microarray analysis (LIMMA) package (Wettenhall and Smyth 2004) using the R language (http://www.r-project.org). The p-values for differential expression were adjusted for false-discovery rate using the method by Benjamini and Hochberg (BH) (Benjamini and Hochberg 1995). Genes with a BH-adjusted p-value higher than 0.01 and a log2 fold change = 2 were filtered out from subsequent analysis. The quality of the experiment was determined by principal component analysis and regulated genes were analysed using K-Means clustering and Gene Set Enrichment Analysis (GSEA) (Subramanian *et al.* 2005) for KEGG pathways.

3.11 Reverse transcription

Synthesis of cDNA was carried out using the Quantitect reverse transcription kit (Qiagen) according to the manufacturer's instructions.

<u>Protocol for the Quantitect reverse transcription kit</u>

Step 1

- RNA up to 1 µg
- gDNA wipeout 2 µl
- water up to14 µl

Incubate for 2 min at 42°C, place on ice.

Step 2

- Primer mix 1 µl
- 5x buffer 4 µl
- RNA mix from step 1 (14 µl)
- RT enzyme 1 µl

Incubate at 42°C for 15-30 minutes, heat to 95°C for 3 min.

3.12 Standard DNA techniques

All reactions were performed in 0.2 ml PCR soft tubes in an Eppendorf thermocycler. The DNA was separated routinely on 1% (w/v) TAE agarose gels (NEED ultra-quality agarose, Roth). DNA was visualized by staining in an ethidium bromide (2 µg/ml) bath for 15-30 min.

3.13 Isolation of genomic and plasmid DNA

Preparation of genomic DNA and plasmid DNA was carried out using the Nucleospin Tissue kit (Macherey & Nagel) and by plasmid miniprep kits (Eppendorf, Macherey Nagel), respectively, according to the instructions of the manufacturer. The culture volume for plasmid DNA isolation ranged from 3 ml to 20 ml depending on the required concentration.

For high throughput verification of clones containing modifications in the genomic DNA or at the plasmid DNA, lysates of single colonies were applied instead of pure DNA solutions. For this, a colony was picked out and dissolved in 20 µl MilliQ water in an Eppendorf tube. The tube was heated at 98 °C for 15 minutes in a Thermoblock, to disrupt the cells. Then the lysed cells were centrifuged at 17.000 x g for 1 minutes and the supernatant was applied in PCR reactions.

3.14 Standard PCR

All standard PCRs were routinely carried out using Taq polymerase from Qiagen. Primers were dissolved in water to a concentration of 10 µM. The reaction mixture was assembled according to the manufacturer's instruction, containing 3 mM $MgCl_2$, 200 µM of dNTPs, 200 nM of each primer and 0.25 U/µl *Taq* polymerase.

For high troughput standard PCRs the HotMasterMix from 5 PRIME was used according to the manufacturer's instruction. The program consists of a 1 min pre-denaturating step at 98°C, followed by 30-35 cycles of denaturation for 15 sec at 98°C, annealing for 45 sec at 60°C and elongation for x min at 73°C. The program was finished by a 5 min post elongation step at 73°C. Because of the GC-rich target sequences the temperature for template denaturation was increased from 94°C to 98°C.

3.15 Amplification of GC-rich targets

When PCR products could not be obtained by standard PCR, the PCR reaction parameters, especially for GC-rich targets, required some modification. The dNTP concentration was increased from 200 µM to 300-500 µM and for extremely GC-rich targets (>70%) GC-destabilizing co-solvents like 5% DMSO were used. The temperature for template denaturation was already increased to 98°C in the standard PCR protocol.

3.16 High fidelity PCR

High fidelity PCRs were carried out using *Pfu* polymerase (Promega). All conditions were similar to the standard PCR techniques using *Taq* polymerase, except that $MgCl_2$ was replaced by $MgSO_4$ and that 0.025 U/µl *Pfu* polymerase were used.

3.17 Quantitative RT-PCR

Quantitative RT-PCR was performed using the LightCycler 480 system (Roche, Mannheim, Germany) and the reaction mixtures were prepared using the Quantitect SYBR Green PCR Kit (Qiagen). Changes in the level of gene expression were calculated automatically by the LightCylcer 480 software using the $\Delta\Delta C_T$ method. The gyraseA gene (Dshi_1476) was used as the housekeeping reference gene. For each reaction, 5 µl primer mix (1 µM of each primer), 5 µl of diluted cDNA and 10 µl of the Quantitect SYBR Green Solution were mixed and transferred into a well of a 96 well LightCycler standard plate. All subsequent PCR steps were performed according to the manufacturer's protocols. All measurements were done in triplicates.

3.18 Purification of DNA

For removal of nucleotides, proteins, salts, etc., the PCR purification kit from Qiagen was used. For extraction of single bands from agarose gels, the gel extraction kit (Qiagen) was used.

3.19 Addition of 3´ A-Overhangs Post-Amplification

Direct cloning of DNA amplified by proofreading polymerases (*Pfu* polymerase) into TOPO TA Cloning® vectors is often difficult because of very low cloning efficiencies. This is because proofreading polymerases remove the 3´ A-overhangs necessary for TA Cloning®. Invitrogen has developed a simple method to clone these blunt-ended fragments.

After amplification with the proofreading polymerase, place vials on ice and add 0.7-1 unit of *Taq* polymerase per tube. Mix well. It is not necessary to change the buffer. A sufficient number of PCR products will retain the 3´ A-overhangs. Incubate at 72°C for 8-10 minutes in the Thermo Cycler. Place on ice and use immediately in the cloning reaction.

If the sample has to be stored overnight before proceeding with cloning, the sample has to be purified with the PCR purification kit from Qiagen to remove the polymerases.

3.20 Restriction digestion

Restriction enzymes were purchased from New England Biolab (NEB) or Fermentas and reactions were carried out using the corresponding buffers. For analytical purposes, reactions were carried out in a volume of 20 µl using routinely 500-1000 ng DNA and 1-5 units of restriction enzyme. For preparative digestions the volume was scaled up to 50 µl and up to 5 µg of DNA was used. Reactions were carried out at 37°C (25°C in the case of SmaI) for 3-4 hours, followed by heat inactivation at 65/80°C (dependent on the enzyme) for 20 minutes.

3.21 Dephosphorylation of DNA

Before the ligation of inserts, digested plasmids were dephosporylated using shrimp alkaline phosphatase (SAP, Fermentas). 1 µl of SAP was added directly to the heat inactivated restriction digestion reaction and incubated at 37°C for 30

minutes. After dephosphorylation the products were purified using the PCR purification kit from Qiagen.

3.22 Blunting of 5'- or 3' overhangs

For blunting of 5'-or 3' overhangs prepare the following reaction mixture according to Fermentas.

5 x reaction buffer	4 µl
Linear DNA or PCR product	1 µg
dNTP Mix, 2 mM each	1 µl (0.1 mM final concentration)
T4 DNA Polymerase	0.2 µl
Water, nuclease free	to 20 µl

Mix thoroughly, spin briefly and incubate at room temperature for 5 minutes.

Stop the reaction by heating at 75°C for 10 minutes.

3.23 Ligation

Routinely, ligation reactions were performed in a volume of 20 µl, using 1 Weiss unit of T4-Ligase (Fermentas) and were incubated overnight at 16°C. For the ligation of inserts into plasmids, 100 ng of plasmid (vector) and x ng of insert in a ratio of 1:3 were used. The required ng of insert was calculated with the following formular:

$$\text{ng Insert} = \frac{\text{100 ng Vector x kb Insert}}{\text{kb Vector}} \text{ x } \frac{3}{1}$$

For facilitating blunt end ligations 10% (w/v) PEG 4000 was added.

To perform restriction and ligation simultaneously, the reaction was carried out in the designated restriction enzyme buffer, supplemented with 1 mM ATP and 10% (w/v) PEG 4000. Restriction enzyme and ligase were added to a concentration of 1 (weiss) Unit. The mixture was incubated at 25°C for 3 hours, followed by overnight incubation at 4°C.

Ligation reactions that contained no PEG were heat inactivated at 65°C for 15 minutes prior to transformation.

3.24 Transformation

TSS-transformation of DNA into *E. coli*

An overnight culture was diluted 1:100 in 10 ml of fresh LB media and incubated for two hours. Subsequently 1 ml was shortly pelleted, the supernatant discarded and the pellet resuspended in 100 µl ice-cold TSS buffer. Up to 10% (v/v) of DNA was added to the cells and gently mixed. The mixture was put on ice for 30 minutes, followed by 45 sec incubation at 42°C in a water bath. Afterwards cells were chilled on ice for 1 min and 250 µl SOC media was added. Cells were incubated at 37°C for one hour, prior to plating on selective agar plates.

TSS medium

For preparation of TSS medium LB media was supplemented with:

- 10% (w/v) PEG 8000
- 30 mM $MgCl_2$
- 5% (v/v) DMSO.

The medium was autoclaved at 121°C for 15 minutes.

Transformation of DNA into chemically competent *E. coli* (Rubidium-chloride methode)

- Prepare overnight culture: 5-20 ml of LB in polypropylene tube (maybe additives are required, e.g. ALA 50 µg/ml).
- Prepare 250 ml Erlenmeyerflask with 50 ml LB 20 mM MgSO4 and inoculate with overnight preculture (1:100).
- Grow until OD_{600nm} 0.4-0.7 (approx. 2-4 h).
- Centrifuge 5 min at 4000-6000 rpm, 4°C.
- Discard supernatant and resuspend pellet carefully in 20 ml icecold (-20°C) TFB1 buffer.
- Incubate 5-10 min on ice.
- Centrifuge 5 min at 4000-6000 rpm, 4°C.
- Discard supernatant and resuspend pellet carefully in 2 ml icecold (-20°C) TFB2 buffer.

- Incubate 15-60 min on ice.
- Prepare 50 µl aliquots (use chilled Eppendorf tubes) and freeze immediately in liquid nitrogen.

Store competent cells for 3 month at longest at – 70°C or thaw them on ice for direct transformation.

Up to 10% (v/v) of DNA was added to the cells and gently mixed. The mixture was put on ice for 30 minutes, followed by 45 sec. incubation at 42°C in a water bath. Afterwards cells were chilled on ice for 1 min and 250 µl SOC media was added. Cells were incubated at 37°C for one hour, prior plating on selective agar plates.

1L TFB1: 100 ml

30 mM	KAc (M=98.45 g/mol)	2.95 g/l	0.295 g/100 ml
10 mM	$CaCl_2$ x 2 H_2O (M=147.02 g/mol)	1.47 g/l	0.147 g/100 ml
50 mM	$MnCl_2$ x 2 H_2O (M=197.9 g/mol)	9.9 g/l	0.99 g/100 ml
100 mM	RbCl (M=120.9 g/mol)	12.1 g/l	1.21 g/100 ml
15%	Glycerine (86%)	148.5 ml	14.9 ml

Adjust pH value with 1M acetic acid to 5.8 and sterilize by filtration.
(Buffer is stable for weeks when stored at 4°C.)

1L TFB2: 10 ml

10 mM	MOPS (M=209.3 g/mol)	2.1 g/l	0.021 g/10 ml
75 mM	$CaCl_2$ (M=147.02 g/mol)	11.0 g/l	0.11 g/10 ml
10 mM	RbCl (M=120.9 g/mol)	1.21 g/l	0.0121 g/10 ml
15%	Glycerin (86%)	148.5 ml	1.49 ml

Adjust pH value with 1M KOH to 6.5 and sterilize by filtration.

Buffer is less stable because of the MOPS. Buffer is stable for 1-2 weeks when stored light-protected and at 4°C.

3.25 Biparental mating

(Piekarski *et al.* 2009)

The recipient, *D. shibae* DFL-12, was cultivated overnight in MB medium. The donor *E. coli* strain ST18 was grown in LB medium supplemented with 50 µg/ml aminolevulinic acid (ALA) up to the logarithmic phase (OD_{600nm}= 0.5 - 0.6). *E. coli* ST18 is a *hemA* mutant of *E. coli* S17 λ-pir. This strain is not able to synthesize the general tetrapyrrole precursor aminolevulinic acid (ALA). Hence, to complement the lethal mutation, ALA has to be added to the growth medium for normal growth. Both cultures were mixed vigorously in a donor:recipient ratio of 10:1 according to the optical density (OD_{600nm}) of the cultures. The cells were sedimented by centrifugation for 2 min at 8.000 x g at 20 °C, resuspended in the residual liquid and used to inoculate hMB agar supplemented with 50 mg/ml ALA, in form of a spot. The plates were further incubated for 48 h. Subsequently, the cells were scraped from the plate and resuspended in 1 ml hMB by pipetting. A dilution series in hMB solution was made and plated on hMB with the appropriate antibiotic concentration. Since the plates did not contain ALA the auxotrophic donor *E. coli* strain was not able to grow.

3.26 Protein techniques

3.26.1 Expression and purification of LuxI

For expression, *E. coli* (TOP10, BL21 or Tuner) carrying pTrc-His::*luxI* 1-3 was grown in an 250 ml LB culture to an OD_{600nm} of 0.6 and expression was induced by adding different final concentrations of IPTG (usually 1 mM). The cells were grown for additional two to four hours, harvested (4.000 x g, 20 min, 4°C) and resuspended in 50 mM NaH_2PO_4, pH 7.0, 300 mM NaCl, 25 mM imidazole and 5 mg/ml lysozyme and incubated on ice for 30 min. Subsequently, the cells were further lysed by sonification (4x 1 min pulse, 1 min break, MS72 probe with 25% power; Bandelin Sonoplus HD2200, Berlin, Germany) and the soluble 6His-LuxI extract was separated from insoluble cell material by centrifugation (25.000 x g, 30 min, 4°C). The 6His-LuxI protein was directly analysed by SDS page or, referring to $LuxI_1$, purified by IMAC affinity chromatography using Talon resin (Clontech, Saint-Germain-en-Laye, France) or Protino®Ni-IDA resin (Macherey-

Nagel). Bound protein was washed with 8 bed volumes 50 mM NaH_2PO_4, pH 7.0, 300 mM NaCl, 25 mM imidazole and eluted with 50 mM NaH_2PO_4, pH 7.0, 300 mM NaCl, 300 mM imidazole. Additionally the eluted 6His-$LuxI_1$

protein (purity >90% on an SDS-PAGE) was concentrated by chloroform-methanol precipitation (see below) and afterwards always stored on ice until it was verified by SDS-PAGE and Western Blot (Anti His-tag antibody, Novagen).

Chloroform-methanol-precipitation (Wessel and Flngge 1984)

An aliquot (800 µl) of methanol was added to 200 µl of protein sample and the samples were vortexed and centrifuged (10 s at 9.000g) for total collection of the sample. Then chloroform (200 µl) was added and the samples were vortexed and centrifuged again (10 s at 9.000g). For phase separation 600 µl of water was added, and the samples were vortexed vigorously and centrifuged for 1 min at 9.000g. The upper phase was carefully removed and discarded. A further 600 µl methanol was added to the rest of the lower chloroform phase and the interphase with the precipitated protein. The samples were mixed and centrifuged again for 2 min at 9.000g to pellet the protein. The supernatant was removed and the protein pellet was dried under a stream of air. For SDS-PAGE the pellets were dissolved in 20-50 µl electrophoresis loading buffer containing 10% SDS.

3.26.2 SDS-PAGE

SDS-PAGE was carried out according to standard procedures using a biometra gel electrophoresis system (Laemmli, 1970, Sambrook & Gething, 1989). Proteins were separated using a 15% running gel that was overlayed with a 4% stacking gel. Protein samples were mixed with loading buffer and boiled at 85°C for 5 minutes. The samples were briefly centrifuged and loaded onto the gel. Electrophoresis was carried out in SDS running buffer at 10V/cm at ambient temperature and the gel was stained using the PageBlue protein staining solution (Coomassie) from Fermentas.

Running gel

Water	3.6 ml
1.5 M Tris/HCl pH 8.8	3.8 ml
Acrylamide/bisacrylamide (37.5: 1)	7.8 ml
10% (w/v) SDS	150 µl
TEMED	20 µl
25% (w/v) APS	20 µl

Stacking gel

Water	2.9 ml
0.5 M Tris/HCl pH 6.8	1.26 ml
Acrylamide/bisacrylamide (37.5: 1)	0.85 ml
10% (w/v) SDS	50 µl
TEMED	10 µl
25% (w/v) APS	15 µl

Loading buffer

Tris base	1.52 g
Glycerol	20 g
SDS	4.6 g
Bromphenolblue	0.05 g
Beta-mercaptoethanol	10 ml
Water ad.	0.05 L

Adjust pH with HCl to pH 6.8

SDS running buffer

Glycine	14.4 g
Tris base	3.03 g
SDS	1 g
Water ad.	1 L

3.26.3 Western-Blot

For detection of His-tagged proteins, proteins from the SDS-PAGE were blotted onto a PVDF membrane using a semi-dry blotting system from NOVEX. The membrane was equilibrated with methanol. The whatman papers (Schleicher & Schuell, Germany) and the transfer chamber were equilibrated with blotting buffer. Afterwards, two whatman papers (3 mm), the gel, the membrane and two whatman papers (3 mm) were assembled within the transfer chamber. Blotting was carried out for one hour at 120 mV. After transfer the membrane was washed two times for 10 min in 20 ml 1x TBS buffer. Afterwards the membrane was incubated for 20 minutes in 20 ml blocking solution and washed two times for 10 min in 20 ml 1x TBSTT and again 10 min with 20 ml 1x TBS. The membrane was incubated overnight in 20 ml blocking solution containing the 1:1000 diluted anti-his-tag monoclonal antibody (Novagen). The membrane was washed twice for 10 minutes with 20 ml 1x TBSTT buffer and once again with 20 ml 1x TBS for 10 minutes. The membrane was incubated for 1 hour with the secondary goat anti-mouse antibody which was diluted 1:5000 in 8 ml blocking solution. The membrane was washed five times for 10 minutes with 20 ml 1x TBSTT and drained afterwards. The membrane was covered with CDP-Star AP substrate (Novagen) and afterwards visualised using a phosphoimager (Biorad).

Blotting buffer

Tris base	25 mM
Glycine	192 mM
Methanol	20% (v/v)

1x TBS

20x TBS (Novagen)	dilute 1:20 in water

1x TBSTT

20x TBSTT (Novagen)	dilute 1:20 in water

Blocking solution

5% (w/v) alkali soluble casein (Novagen) dilute 1:5 in water

3.27 Bacterial cell analysis

3.27.1 How to count marine bacteria

(Lunau *et al.* 2005)

To determine the current cell number during an experiment, cells were stained directly on a black Nuclepore filter. Staining and mounting the samples with the moviol-SybrGreen I solution allowed an accurate and highly reproduceable enumeration of bacteria. 1 ml of a planktonic cell culture was fixed with glutaraldehyde (2% final conc.) for 5-10 min. Usually, at low cell densities, the 1ml fixed culture was diluted with 9 ml 1 x PBS pH 7.5 (10-1) and the whole 10 ml were filtered through a black polycarbonate membrane (Whatman, ∅ 25 mm, 0.2 µm) using a vacuum filtration system. To stabilize the black polycarbonate membrane and to ensure a homogenous distribution of cells, a white nitrocellulose membrane (Whatman, ∅ 25 mm, 10 µm) was placed below the black one. At increasing cell densities a dilution series was made, to obtain 10 ml of a 10-2 and 10-3 dilution. After filtration of the appropriate dilution, the filter was washed 3 x with 1 ml of 1 x PBS buffer and transferred to a microscope slide. 35 µl of the staining solution were dropped in the middle of a cover slip, which was then put upside down on the filter. Finally, the cover slip was pressed carefully onto the slide by tweezers to dispense the staining solution equally over the filter.

Cells can be inspected by fluorescence microscopy immediately, but storing the sample for at least 15–30 min at 4°C before counting, allows an equal dispersion of the mounting medium under the cover slip. Staining is fine for several hours if slides are kept at room temperature. Storage at –20°C keeps a bright fluorescence signal for at least several months.

Preparation of the moviol solution

2.4 g Moviol 4-88 (polyvinylalcohol 4-88, Fluka) were added to 6 ml of AF1 and vigorously mixed at room temperature for 30 min. Moviol did not dissolve completely. Thereafter, 6 ml of distilled water was added and the solution was stirred for two more hours. Some of the moviol still remained undissolved. The addition of 14 ml of PBS (1x, pH 7.4) and mixing for another 2 h at 50°C dissolved moviol completely and turned the solution clear. Finally, the solution was filtered through a 0.2 µm filter and aliquots of 200–1000 µl were stored frozen at –20°C.

Freshly prepared 1M ascorbic acid solution (M = 176.12 g/mol)

1.76 g ascorbic acid were dissolved in 10 ml 1x PBS pH 7.4 and filtered through a 0.2 µm filter.

Composition of the staining solution (for glutaraldehyde-fixed samples (2% final concentration)

moviol solution	989 µl	
SybrGreen I (10.000 x conc. in DMSO)	1 µl	1 ml
1M ascorbic acid solution	10 µl	

For imaging an Olympus BX60 fluorescence microscope, equipped with a colorview II camera and a 100/1.3 oil immersion objective was used. The filter U-MWIBA3 (excitation 460-495 nm, emission 510-550 nm, dichromatic filter 505 nm) from Olympus (Seelze, Germany) was used to visualize SybrGreen I with an exposure time of 5 sec. Images were recorded under the same condition, using the cellB software from Olympus. For better visualizations on print-outs, brightness and contrast were modified equally for all images using Adobe Photoshop.

For each filter 10 randomly pictures were taken. To calculate the cells per picture, the freeware tool “CountThem”, developed by Heribert Cypionka (ICBM, Carl von Ossietzky University of Oldenburg), was used.

The final cell number (cells/ml) for each picture was calculated using the formular:

$$K = \frac{Z \cdot Fa}{n \cdot V \cdot Fg \cdot D}$$

K = cells/ml

Z = cells per picture

Fa = filter area (μm^2) (2.8×10^8 μm^2)

n = number of pictures, n = 1

V = filtered sample volume (ml)

Fg = area of fluorescence picture (μm^2) (Pictures taken with the 100x oil objective have a area size of 3822.6 μm^2.)

D = dilution (10^{-1} = 0.1 or 10^{-2} = 0.01)

3.27.2 Fluorescence-activated cell sorting (FACS)

FACS is a specialized type of flow cytometry that provides a method for sorting a heterogeneous mixture of cells into different containers, one cell at a time, based upon light scattering and fluorescent characteristics of each cell.

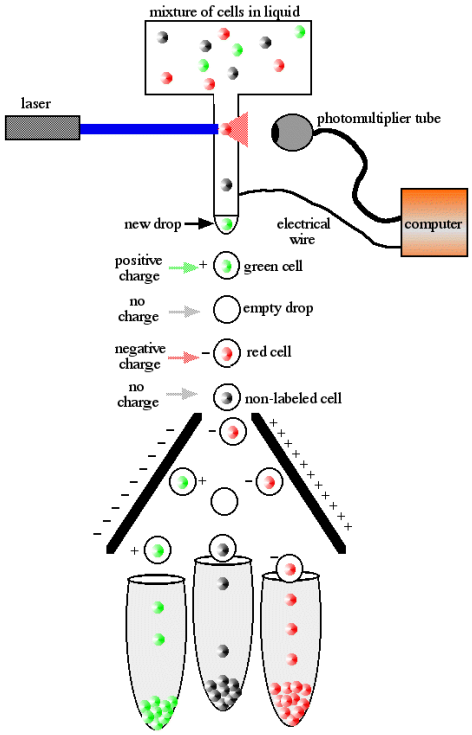

Figure 13 Diagram of FACS machine. Cells have been fluorescently tagged with either red or green fluorescent stainings.

The process begins by placing the cells into a flask and forcing the cells to enter a small nozzle one at a time. The cells travel down the nozzle which is vibrated at an optimal frequency to produce drops at fixed distance from the nozzle. As the cells flow down the stream of liquid, they are scanned by a beam of laser light of a single wavelength (blue light in Figure 13). Some of the laser light is scattered (red cone emanating from the red cell) by the cells and this is used to analyze the cells. A number of detectors (photomultiplier tube, Figure 13) are aimed at the point where the stream passes through the light beam: one in line with the light beam (Forward Scatter or FSC) and several perpendicular to it (Side Scatter (SSC) and one or more fluorescent detectors). Each suspended particle from 0.2 to 150 micrometers passing through the beam scatters the ray, and fluorescent chemicals found in the particle or attached to the particle may be excited into emitting light at a longer wavelength than the light source. This combination of scattered and fluorescent light is picked up by the photomultiplier tube, and, by brightness at each detector (one for each fluorescent emission peak), it is then possible to derive various types of information about the physical and chemical structure of each individual particle. FSC correlates with the cell volume and SSC depends on the inner complexity of the particle (shape of the nucleus, the amount and type of cytoplasmic granules or the membrane roughness). The final step is sorting the cells, which is accomplished by electrical charge. The computer determines how the cells will be sorted before the drop forms at the end of the stream. As the drop forms, an electrical charge is applied to the stream and the newly formed drop will form with a charge. This charged drop is then deflected left or right by charged electrodes and into waiting sample tubes. Drops that contain no cells are sent into the waste tube. The end result is three tubes with pure subpopulations of cells. The number of cells is each tube is known and the level of fluorescence is also recorded for each cell. In this study FACS was performed on a FACSAriaTM II Cell Sorter System (Becton Dickinson). Filtered PBS was used as the sheath fluid. Cells were kept at 25°C during sorting and were collected directly in hMB Gm 50 µg/ml or single cells were spotted directly on hMB Gm 50µg/ml agar. Forward and side scatter were set to log with a threshold of 100 on both parameters. Detection of GFP fluorescence was through a 585/42

nm (PE) and a 530/30 nm (FITC) bandpass filter. PMT Voltage was 370 for FSC, 205 for SSC, and 467 for GFP. The GFP intensity of cells was partitioned into five gates (R3-R7), whereas cells with the highest GFP intensity were counted among gate R6.

3.27.3 Scanning Electron Microscopy (SEM) and Transmission Electron microscopy (TEM)

SEM

The fixation of bacterial and coculture suspensions were usually performed by incubation with 2% glutaraldehyde. 20 µl of the suspension were spread on polylysine coated cover slips (provided by H. Lünsdorf) and incubated for 5 minutes at room temperature. Samples were washed twice with TE buffer (pH7). The fixed specimens were then dehydrated in an aqueous acetone series (10, 50, 70, 90 and 100%) on ice, by transferring the cover slips from one vessel to the next, with 10 minutes in each vessel. Cells were then transferred to the pressure chamber of a critical point drying unit (CPD030, Bal-Tec, Lichtenstein) filled with acetone at 10°C to replace the organic solvent in turn with a transitional fluid such as liquid carbon dioxide at high pressure. The dry specimen was mounted on aluminum stubs and sputter coated with gold (SCU040; Balzer Union, Lichtenstein). Samples were examined with a scanning electron microscope, such as a Zeiss DSM 982 Gemini (LEO) equipped with a field emission gun, in a magnification range from x 500 to x 10.000 at 5 kV and 8 mm working distance. Images were recorded either digitally or on type 120 roll film.

TEM (Lunsdorf *et al.* 2001)

The sample preparations were carried out by Ingeborg Kristen (Scanning electron microscopy laboratory, department vaccinolgy, HZI) according to Lunsdorf *et al.*, 2001. Samples were examined by Dr. Heinrich Lünsdorf with an energy-filtered transmission electron microscope, such as Zeiss Libra 120 Plus at 120 kV under elastic bright-field settings (energy slit, 20 eV; objective aperture, 60 µm; condenser aperture, 300 µm/600 µm). Images were recorded digitally with a Tröndle CCD Camera TRS sharp-eye (2x2 K).

3.27.4 Nile red staining

K. N. Timmis (ed.), Handbook of Hydrocarbon and Lipid Microbiology, DOI 10.1007/978-3-540-77587-4_292, © Springer-Verlag Berlin Heidelberg, 2010.

Nile red presents an orange-red fluorescence with an excitation and emission wavelength at 542 nm and 598 nm respectively. Nile red staining allows the direct observation of the lipidic inclusions which appear as intensive red spot inside the cell, visualized by fluorescence microscoping. Nile red only determines the existence of storage depots like lipidic inclusions. It is not specific for polyhydroxyalkanoates (PHAs). Samples were prepared as described below:

- Add 50 µl Nile red (Fluka) solution (0.25 mg/l in DMSO) to 1 ml culture sample.
- After agitation, centrifuge at 14.000 rpm, at room temperature for 5 minutes.
- Discard supernatant and add 2 ml MgCl2 (10 mM) to eliminate the excess of Nile red.
- Wash a second time with 2 ml MgCl2 (10 mM).

5 µl of the sample is disposed on a microscope slide and covered with a cover slip. The sample is ready for fluorescence microscopy.

4 Results Chapter A

Changing light regimes have a great impact on the transcriptional response of the photoheterotrophic bacterium *D. shibae* DFL-12 (Tomasch *et al.* 2011).

Therefore, incubation of the bacterial cultures was performed consistently in the dark except for the cocultivation.

4.1 Lux gene expression and AHL synthesis in *D. shibae* DFL-12

Before elucidating the functionality and specifity of every single LuxI synthase independently, the expression of the Lux genes and the AHL production of *D. shibae* DFL-12 were investigated.

Figure 14 depicts a representative growth curve of *D. shibae* DFL-12 in SWM supplemented with 5 mM succinate. The stationary phase was reached after 13 hours at OD_{600nm} 0.9.

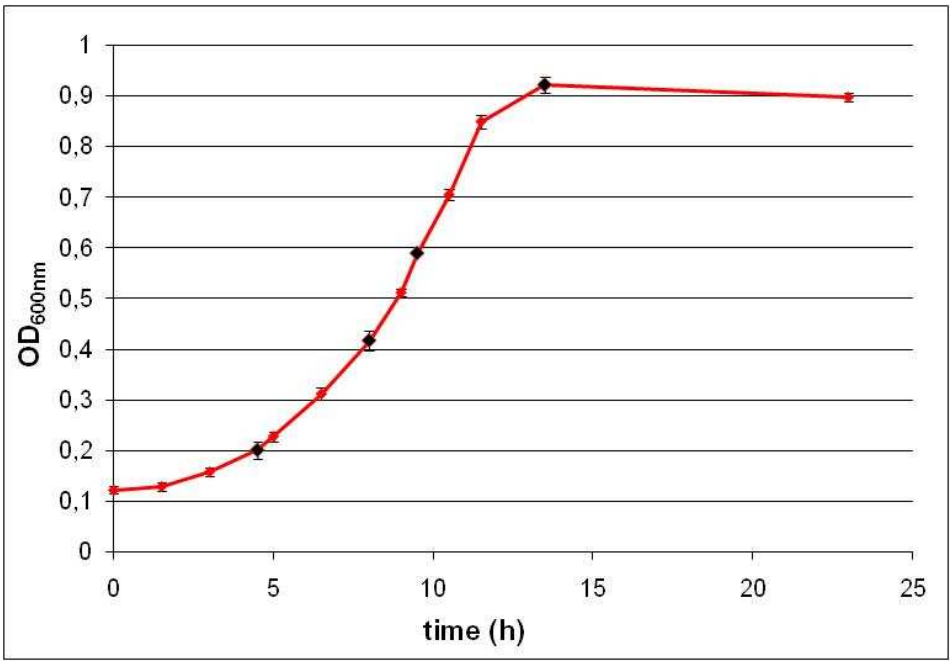

Figure 14 Representative growth curve of *D. shibae* DFL-12 in SWM with 5 mM succinate.

Presented values are the mean of two biological replicates. At OD_{600nm} 0.2; 0.4; 0.6 and 0.9 (black marked data points) an appropriate volume of cells was harvested to extract the RNA.

After RNA extraction according to the protocol, the following RNA concentrations were obtained:

Table 12 RNA concentrations calculated with the NanoDrop (Thermofischer Scientific).

OD_{600nm}	Sample volume	RNA concentration
0.2	8 ml	267.1 ng/µl
0.4	4 ml	853.2 ng/µl
0.6	4 ml	733.0 ng/µl
0.9	2 ml	652.0 ng/µl

4.1.1 QRT-PCR of *lux* genes present in *D. shibae* DFL-12

QRT primers of the *lux* genes (Table 10) were used to determine their expression. The gyraseA gene (Dshi_1476) was used as the housekeeping reference gene. Amplified fragments had a size of $LuxI_1$:146 bp, $LuxI_2$: 141 bp, $LuxI_3$: 125 bp, $LuxR_1$: 135 bp, $LuxR_5$: 137 bp, GyrA: 177 bp.

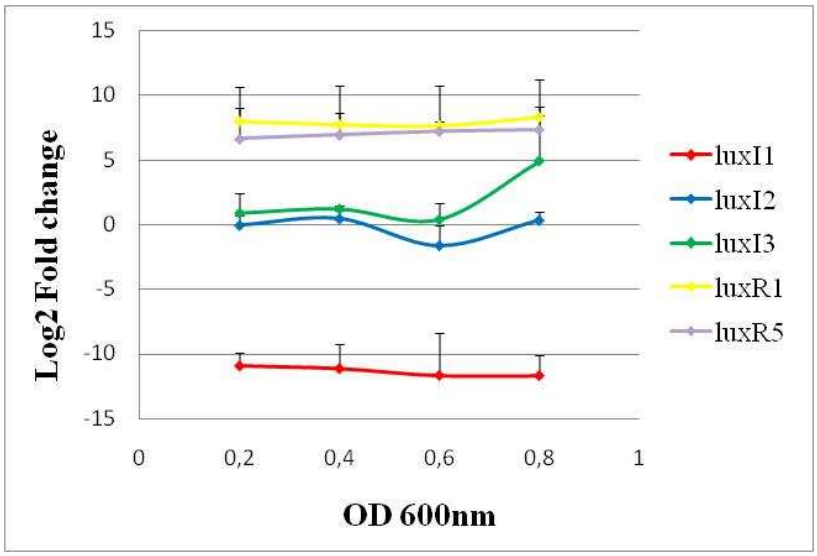

Figure 15 Expression of the *lux* genes of *D. shibae* DFL-12 at four different optical densities in SWM 5 mM succinate.

Expression of the *lux* genes $luxI_1$, $luxR_1$, $luxI_2$, $luxR_5$ and $luxI_3$ present in *D. shibae* DFL-12 was determined by qRT-PCR. Mean values of three technical replicates from each of two biological replicates are presented as Log2 fold change relative to the housekeeping gene *gyrA* at four different optical densities.

All *lux* genes were expressed during cultivation in SWM with 5 mM succinate. The two LuxR regulators (yellow and grey line in Figure 15) were constitutively and 32-fold higher expressed than the reference gene *gyrA*. The three *luxI* synthases differed. $LuxI_1$ was transcribed 1000-fold lower than the gyraseA with downward tendency. $LuxI_2$ and $luxI_3$ were fluctuating at the gyraseA transcription level. At stationary phase the expression of $luxI_2$ and $luxI_3$ started to increase. In theory, at high cell densities, the regulator LuxR binds its corresponding autoinducer signal, becomes active and induces expression of its own and of the adjacent LuxI synthase. Although it is assumed that $LuxR_1$ and $LuxI_1$ are cotranscribed, the regulation of both seems to be varying. $LuxI_1$ was repressed during cultivation whereas the transcriptional rate of $LuxR_1$ was continuously high. Moreover, the expression of the *lux* genes in SWM medium did not occur in a QS dependent manner, because increasing of the transcription rate in the mid logarithmic phase was lacking.

4.1.2 AHL production of *D. shibae* DFL-12

In previous bioassay analyses short-chain AHLs were not detectable when *D. shibae* DFL-12 was grown in SWM with 5 mM succinat. Therefore, *D. shibae* DFL-12 was grown in SWM 50 mM succinate to avoid carbon source limitation during 36 hours of cultivation and to increase the absolute cell density (50 mM succinate corresponds to the carbon concentration of complex MB).

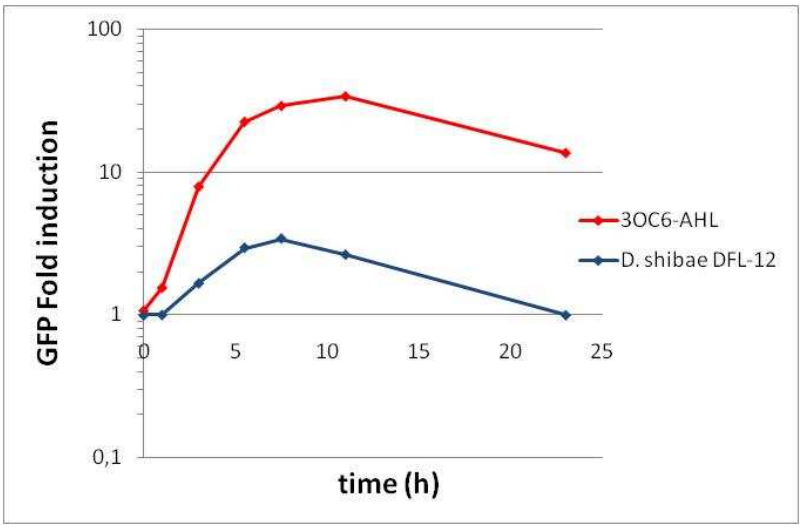

Figure 16 Detection of short-chain AHLs produced by *D. shibae* DFL-12.

Detection of short-chain AHLs by use of the sensor strain *E. coli* pJBA132. In red, the positive control (3OC6-AHL, 2.4 µM) is depicted while the blue line displays the AHL extract of *D. shibae* DFL-12 which was obtained during cultivation in SWM 50 mM succinate. Represented are the mean values of three technical replicas.

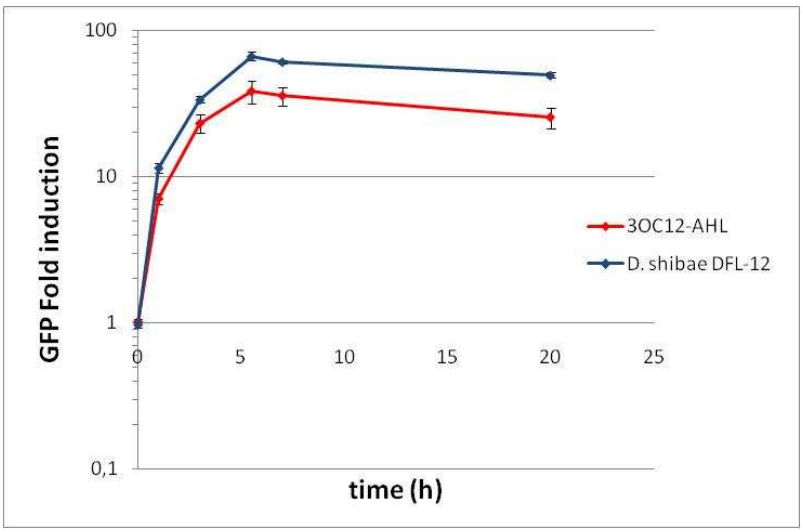

Figure 17 Detection of long-chain AHLs produced by *D. shibae* DFL-12.

Detection of long-chain AHLs by use of the sensor strain *P. putida* pKR-C12. In red, the positive control (3OC12-AHL, 2.4 µM) is depicted while the blue line displays the AHL extract of *D. shibae* DFL-12 which was obtained during cultivation in SWM 50 mM succinate. Represented are the mean values of three technical replicas.

D. shibae DFL-12 produced low amounts of short-chain AHLs and high concentrations of long-chain AHLs during cultivation in SWM 50 mM succinate.

GC-MS analyses of the wild type extract identified the long-chain AHLs to be C18-en-HSL and C18-dien-HSL. Although short-chain AHLs were detected in the bioassay, no predicted C8-HSL was identified via GC-MS. The sensor strain *E. coli* pJBA132 is known to be sensitive to high amounts of long-chain AHLs such as 3OC12-AHL and C14-en-AHL. The GFP fold induction of the short-chain AHLs was relatively low. Thus, the short-chain signal detected by *E. coli* pJBA132 could not be due to short-chain AHLs, but rather a background signal of high concentrated long-chain AHLs present in the extract.

4.2 Heterologous expression of the LuxI synthases in *E. coli* (pTrcHis)

To investigate the functionality of every single LuxI synthase, the coding sequence (CDS) of each synthase was amplified with the *Pfu* polymerase, 3´ A-overhangs post-amplification were added and the purified product was cloned into the pTrcHis-TOPO TA® vector from Invitrogen and transformed into *E. coli* TOP10 according to the manufacturer's protocol.

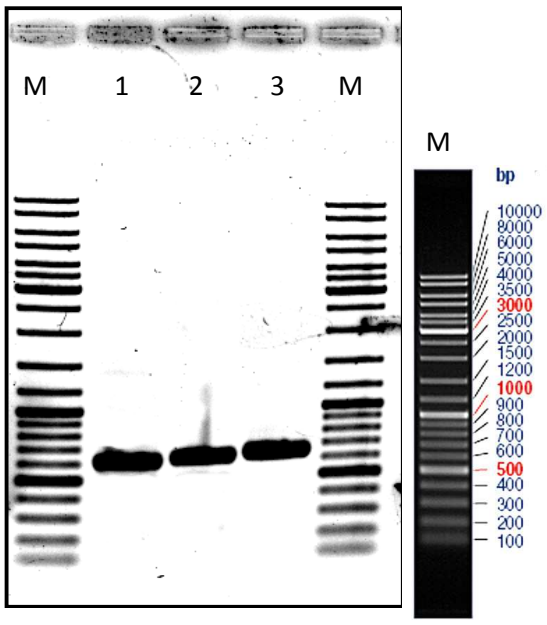

1: Primer pair: 37/38 *luxI* 1
Template: *D. shibae* DFL-12 WT
Product size: 606 bp
Product conc.: 500. 9 ng/µl

2: Primer pair: 39/40 *luxI* 2
Template: *D. shibae* DFL-12 WT
Product size: 627 bp
Product conc.: 350.8 ng/µl

3: Primer pair: 41/42 *luxI* 3
Template: *D. shibae* DFL-12 WT
Product size: 642 bp
Product conc.: 455.8 ng/µl

Figure 18 Purified PCR products of the *luxI*$_{1-3}$ CDS after *Pfu* Polymerase and 3´ A-overhangs post-amplification.

4 µl of the purified PCR products were mixed with 2 µl 6 x Loading dye (Fermentas) and transferred to a 1% agarose gel. M: 4 µl of the GeneRuler DNA Ladder Mix (Fermentas) were used for sizing of PCR products.

4.2.1 AHL production of *E. coli* TOP10 pTrc-His::*luxI*$_{1-3}$

E. coli TOP10 carrying the protein expression vector pTrcHis::*luxI*$_1$, pTrc-His::*luxI*$_2$ and pTrc-His::*luxI*$_3$ respectively, was grown in 500 ml LB Amp 50 µg/ml with addition of 0.5 mM IPTG to induce expression of the inserted gene. 2% XADs were added and the culture was cultivated for 36 hours, shaking (120 rpm). Methanol extracts were made as described and 10 µl of the extracts were used for bioassay studies according to the protocol.

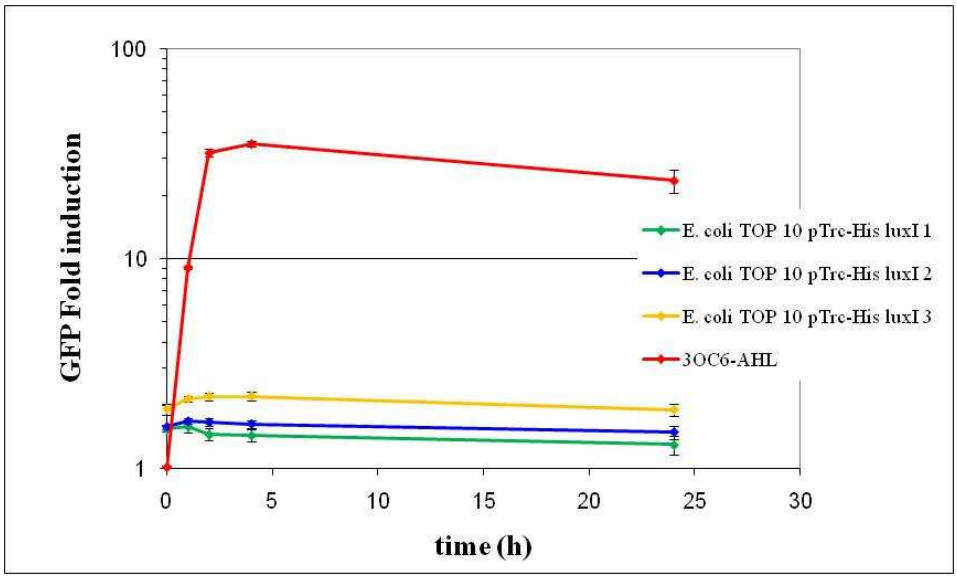

Figure 19 Detection of short-chain AHLs produced by *E. coli* TOP10 pTrc-His::*luxI*$_{1-3}$ cultivated in LB Ka 50 µg/ml.

Detection of short-chain AHLs by use of the sensor strain *E. coli* pJBA132. In red, the positive control (3OC6-AHL, 0.24 µM) is depicted. The blue line displays the AHL extract of *E. coli* TOP10 pTrc-His::*luxI*$_1$, the green line corresponds to the AHL extract of *E. coli* TOP10 pTrc-His::*luxI*$_2$ while the black line depicts the AHL extract of *E. coli* TOP10 pTrc-His::*luxI*$_3$. Presented are the mean values of three technical replicas.

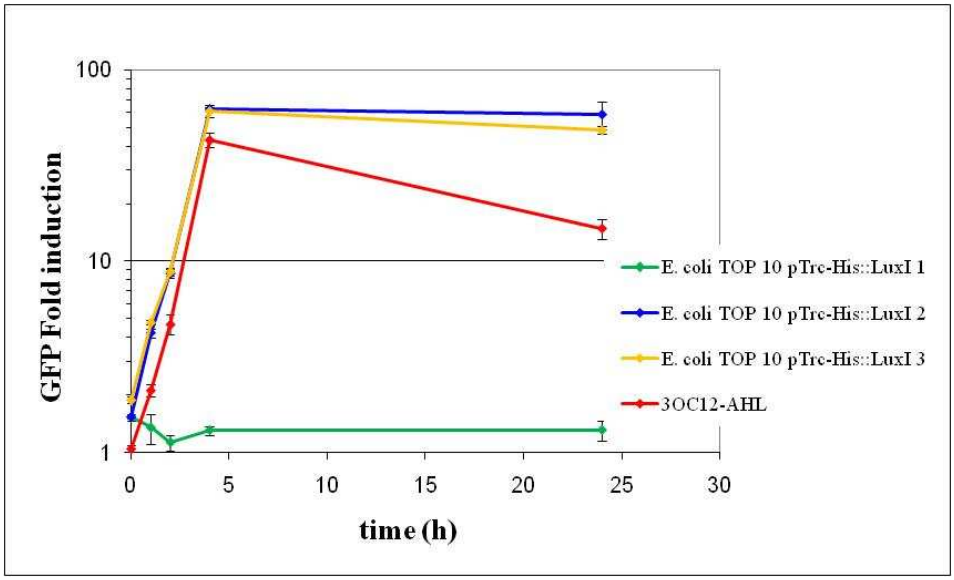

Figure 20 Detection of long-chain AHLs produced by *E. coli* TOP10 pTrc-His::*luxI*$_{1-3}$ cultivated in LB Ka 50 µg/ml.

Detection of long-chain AHLs by use of the sensor strain *P. putida* pKR-C12. In red, the positive control (3OC12 AHL, 2.4 µM) is depicted. The blue line displays the AHL extract of *E. coli* TOP10 pTrc-His::*luxI*$_1$, the green line corresponds to the AHL extract of *E. coli* TOP10 pTrc-His::*luxI*$_2$ while the black line depicts the AHL extract of *E. coli* TOP10 pTrc-His::*luxI*$_3$. Presented are the mean values of three technical replicas.

E coli TOP10 pTrc-His::*luxI*$_1$ was shown to produce neither short-chain nor long-chain AHLs in detectable amounts. *E. coli* TOP10 carrying pTrc-His::*luxI*$_2$ and pTrc-His::*luxI*$_3$, respectively was able to produce high concentrations of long-chain AHLs.

The GC-MS analyses of the extracts produced by *E. coli* TOP10 carrying pTrcHis::*luxI*$_1$, pTrc-His::*luxI*$_2$ and pTrc-His::*luxI*$_3$ respectively, plus *E. coli* TOP10 without vector resulted in the following table:

Table 13 GC-MS analyses of the AHL extracts obtained by the heterologous expression of *luxI*$_{1-3}$

Strain /Extract	GC-MS analyses
E. coli TOP10	no AHLs detected
E. coli TOP10 pTrc-His::*luxI*$_1$	no AHLs detected
E. coli TOP10 pTrc-His::*luxI*$_2$	3-oxo-C12-HSL, C13-HSL, 3-oxo-C13-HSL, C14-HSL, 3-oxo-C14-HSL, C14-en-HSL, C15-HSL and C16-en-HSL
E. coli TOP10 pTrc-His::*luxI*$_3$	C14-HSL, 3-oxo-C14-HSL

The results of the GC-MS analyses are comparable with the bioassay results. *E. coli* cells without expression vector were not able to synthesize any AHLs. AHLs were not detected in the extract of *E. coli* TOP10 pTrc-His::*luxI*$_1$. LuxI$_2$ und LuxI$_3$ heterologous expressed, synthesized a broad pattern of different long-chain AHLs. The manifold production of long-chain AHLs which differed from the wild type could be due to the specific *E. coli* metabolism. The lacking AHL synthesis of LuxI$_1$, controlled by an inducible promoter, needed further investigations.

4.2.2 Investigation of the functionality of LuxI$_1$

The correct insertion of the complete *luxI*$_1$ CDS into the protein expression vector pTrc-His was confirmed via sequencing by use of the commercial available primers

pTrcHis Forward (5´-GAGGTATATATTAATGTATCG-3´) and

pTrcHis Reverse (5´-GATTTAATCTGTATCAGG-3´) from Invitrogen.

The *luxI*$_1$ gene was inserted completely, without any gaps, generated Stop-codons or frame shifts into the expression vector (Sequence in Appendix).

4.2.3 Transcription of *luxI*$_1$ in *E. coli* pTrcHis::*luxI*$_1$

To confirm whether the *luxI*$_1$ gene was completely transcribed in *E. coli* pTrcHis::*luxI*$_1$, the expression strain was cultivated in LB Amp 50 µg/ml at two different temperatures (30°C and 37°C). The RNA was extracted and used as template for a standard PCR with the primer pair P37F/P38R (*luxI*$_1$, 606 bp), to exclude DNA contaminations in the RNA extract. As positive control, genomic DNA of *D. shibae* DFL-12 served as template and water as negative control (Figure 21, lanes 1-4). Use of genomic DFL-12 DNA generated the expected PCR product of 606 bp (Figure 21, lane 1). DNA contaminations of the RNA extracts could be excluded because of lacking PCR products in lane 2 and 3 (Figure 21). Thus, the RNA was used in a RT-PCR reaction to amplify the cDNA of *luxI*$_1$. In Figure 21, lanes 5 and 6 depict the successfully amplified cDNA of *luxI*$_1$ obtained from the RNA extract of *E. coli* pTrcHis::*luxI*$_1$ (30°C and 37°C). LuxI$_1$ was transcribed as full-length transcript in the expression strain *E. coli* pTrcHis::*luxI*$_1$ at 30°C and 37°C.

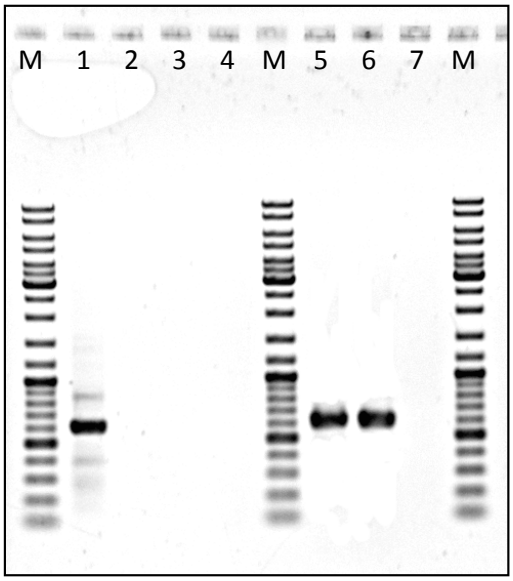

Primer pair: 37/38 *luxI* 1 (606 bp)

Standard PCR

1: DNA *D. shibae* DFL-12

2: RNA *E. coli* pTrcHis::LuxI 1 (30°C)

3: RNA *E. coli* pTrcHis::LuxI 1 (37°C)

4: water

RT-PCR

5: RNA *E. coli* pTrcHis::LuxI 1 (30°C)

6: RNA *E. coli* pTrcHis::LuxI 1 (37°C)

7: water

Figure 21 PCR and RT-PCR products of *luxI*$_1$.

Lanes 1-4 depict the *luxI*$_1$ product (primers P37F/P38R, 606 bp) of a standard PCR.. Lanes 5-7 display the *luxI*$_1$ product (cDNA) of the RT-PCR. 4 µl of the PCR/RT-PCR products were mixed with 2 µl 6 x Loading dye (Fermentas) and transferred to a 1% agarose gel. M: 4 µl of the GeneRuler DNA Ladder Mix (Fermentas) were used for sizing of PCR/RT-PCR products.

4.2.4 Translation of *luxI*$_1$ in *E. coli* pTrcHis::*luxI*$_1$

To confirm whether the mRNA of *luxI*$_1$ is translated, the protein was expressed in *E. coli* TOP10 carrying pTrcHis::*luxI*$_1$ and analysed by SDS-Page. Furthermore the protein expression of *luxI*$_{2\text{-}3}$ in *E. coli* TOP10 was additionally investigated serving as positive control. The expression of genes was induced by addition of 0.25 mM, 0.5 mM and 1 mM IPTG, respectively. 10 ml LB Amp 50 µg/ml were inoculated with an overnight preculture (1:100) and grown to OD_{600nm} 0.6. IPTG was added and cultures cultivated for additional four hours at 37°C, shaking. Afterwards 1 ml of the cultures was prepared according the protocol and 20 µl of the total protein were transferred to the SDS-Page. For determination of the molecular weight, 20 µl of the SigmaMarkerTM wide range (mol wt, 6.5-66 kDa) from Sigma-Aldrich were used.

Expected molecular weights are:

luxI$_1$ 22.20 kDa + 6xHis-tag (3.87 kDa) = 26.07 kDa

luxI$_2$ 23.03 kDa + 6xHis-tag (3.87 kDa) = 26.90 kDa

luxI$_3$ 24.41 kDa + 6xHis-tag (3.87 kDa) = 28.28 kDa

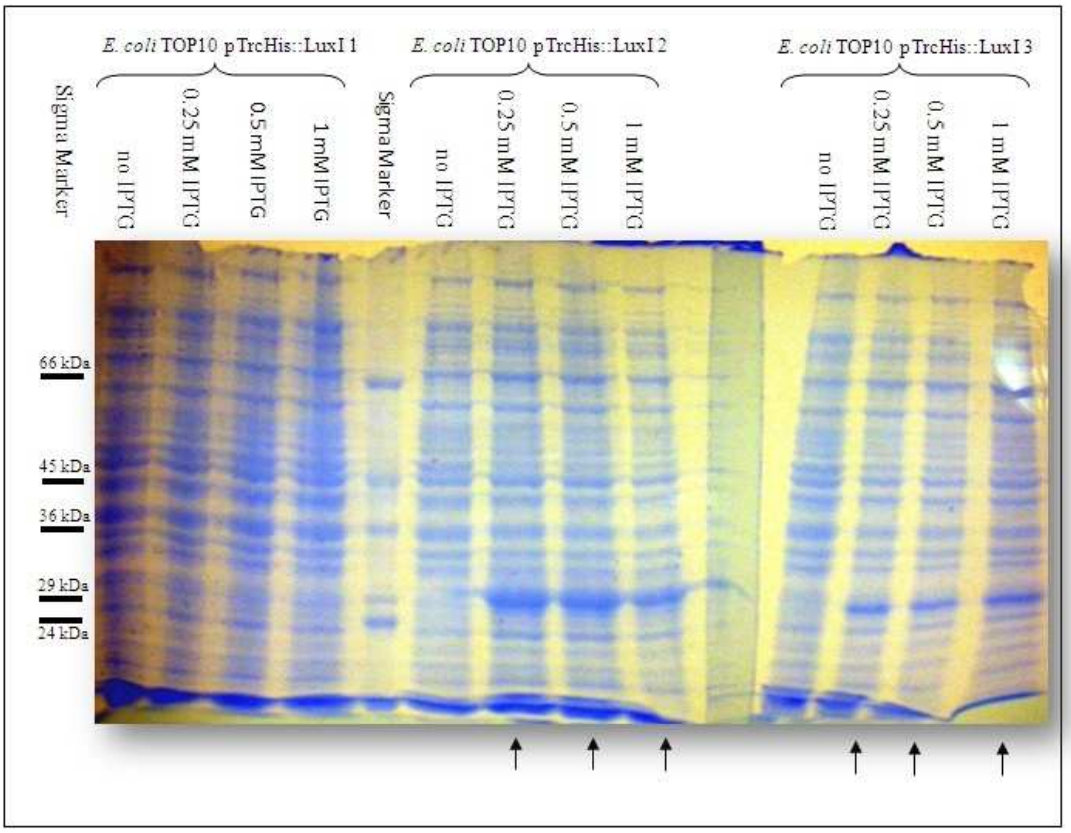

Figure 22 SDS-PAGE of the total protein extracted from *E. coli* TOP10 pTrc-His::*luxI*$_1$, pTrc-His::*luxI*$_2$ and pTrc-His::*luxI*$_3$, respectively.

The expression of genes was induced by addition of 0 mM (no IPTG); 0.25 mM; 0.5 mM and 1 mM IPTG, respectively. For determination of the molecular weight, SigmaMarkerTM wide range (mol wt, 6.5-66 kDa) from Sigma-Aldrich was used. The black bars on the left-hand-side indicate the molecular weight standards of the SigmaMarker. Lanes marked with black arrows depict the total protein sample including overexpression of the *luxI* protein.

Figure 22 depicts the total protein of *E. coli* TOP10 carrying pTrcHis::*luxI*$_1$, pTrcHis::*luxI*$_2$ and pTrcHis::*luxI*$_3$, respectively, analysed by SDS-PAGE. Overexpression of *luxI*$_2$ and *luxI*$_3$ was induced by addition of 0.25 mM – 1 mM IPTG (Figure 22, lanes marked with black arrows) and became visible by increasing concentrations of the protein (enhanced protein bands). Without

IPTG, expression of *luxI*$_2$ and *luxI*$_3$ was repressed. Expression of *luxI*$_1$ was not visibly induced by addition of IPTG. pTrcHis::*luxI*$_1$ was additionally transformed into *E. coli* TunerTM and BL21, but the expression was also not detectable (data not shown).

Note: BL21 is the most widely used host background for protein expression and has the advantage of being deficient in the *lon* and *ompT* proteases. Tuner™ strains are lacZY deletion mutants of BL21, which enable adjustable levels of protein expression throughout all cells in a culture. The *lac* permease (*lacY*) mutation allows uniform entry of IPTG into all cells in the population.

4.2.5 Purification and Western-Blot of LuxI$_1$

Low concentration of LuxI$_1$ could be covered by remaining protein bands of the proteom. Therefore the crude lysate of an *E. coli* BL21 pTrcHis::*luxI*$_1$ culture (250 ml, 2 h IPTG 1 mM induction, room temperatur) was subdivided into two parts and purified by IMAC affinity chromatography using Talon resin (Clontech, Saint-Germain-en-Laye, France) and Protino®Ni-IDA resin (Macherey-Nagel). Both eluats were concentrated by Chloroform-methanol-precipitation. 20 µl of the concentrated eluats and of the unpurified crude lysate were mixed with loading buffer and boiled at 85°C for 5 minutes, briefly centrifuged and loaded onto the SDS gel. The SDS gel was afterwards used for Western-Blot analyses to detect the purified and concentrated his-tagged LuxI$_1$ protein eluates.

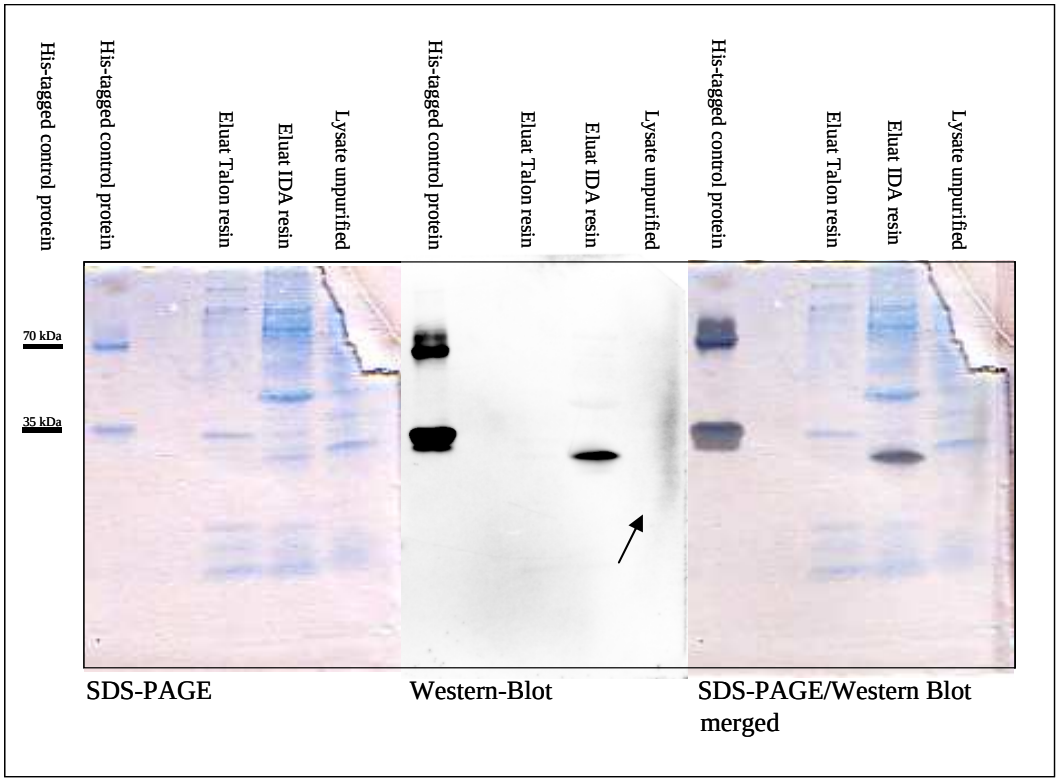

Figure 23 Western-Blot analysis of the concentrated *luxI* protein separated by SDS-PAGE.

The crude lysate and purified eluats were separated by SDS-PAGE (left panel). The SDS-PAGE was afterwards used for Western-Blot analyses to detect the purified and concentrated $LuxI_1$ protein (black arrow, mid panel). To highlight the matching his-tagged protein, images of SDS-PAGE and Western-Blot were merged by Adobe Photoshop (right panel). Black bars on the left-hand-side indicate the molecular weight standards in kDa. A his-tagged control protein with known molecular weight (35 and dimerized 70 kDa) was used as standard.

SDS-Page of the crude lysate and the purified, concentrated $LuxI_1$ protein using Talon and IDA resins resulted in a different protein pattern Figure 23 shows that the Talon resin was not suitable to purify and concentrate the requested protein. Also in the unpurified crude lysate the concentration of $LuxI_1$ was beneath the detection limit and could not be identified via Western-Blot. Using the IDA resin, detectable concentrations of $LuxI_1$ were obtained and could be visualized in the Western-Blot, Western-Blot, black arrow), indicating that very low concentrations of the $LuxI_1$ protein are present in the heterologous expression strain.

4.3 Heterologous expression of the LuxI synthases in *E. coli* (pBBR1MCS2::P_{Gm}-*luxI*$_{1-3}$)

4.3.1 Construction of the vector pBBR1MCS2::P_{Gm}-*luxI*$_{1-3}$

The heterologous expression of $LuxI_1$ in *E. coli* using the expression vector pTrcHis was less successful. Therefore, new LuxI expression vectors were constructed for heterologous expression in *E. coli* as well as the genetic complementation of *D. shibae* DFL-12 Δ*luxI*.

Because it is just possible to transmit DNA into *D. shibae* DFL-12 via biparental mating, a conjugative plasmid was required. Furthermore, nothing is known about the structure and location of promoter regions which regulate *luxI* expression. Therefore, the constitutive gentamicin promoter known to be functional in *D. shibae* DFL-12 was used to activate *luxI* expression.

The new expression/complementation vectors pBBR1MCS2::(P_{Gm}-*luxI*$_1$), pBBR1MCS2::(P_{Gm}-*luxI*$_2$) and pBBR1MCS2::(P_{Gm}-*luxI*$_3$), hereafter named Comp1, Comp2 and Comp3 were constructed as follows.

The CDS of all three *luxI* genes using primer pairs P37F/P38R, P39F/P40R and P41F/P42R and the promoter of the gentamicin cassette derived from pBBR1MCS5 using primers P115F/P116R were *Pfu* amplified. Afterwards PCR products were digested using the restriction enzyme NdeI which is cutting once at the end of the promoter sequence and once at the start codon of *luxI*. After PCR purification, products were ligated in a ratio 1:1 with a total amount of 100 ng DNA per 20 µl.

Three possible ligation combinations revealed in the mixture:

P_{Gm} – P_{Gm} (648 bp)

luxI – *luxI* (1.212bp *luxI*$_1$, 1.254 bp *luxI*$_2$ and 1.284 bp *luxI*$_3$)

P_{Gm} – *luxI* (930 bp *luxI*$_1$, 951 bp *luxI*$_2$ and 966 bp *luxI*$_3$)

1 µl of each ligation mixture was used as template for a *Pfu* PCR using the primer combinations P115F/P38R, P115F/P40R and P115F/P42R to amplify the gentamicin promoter-*luxI* product.

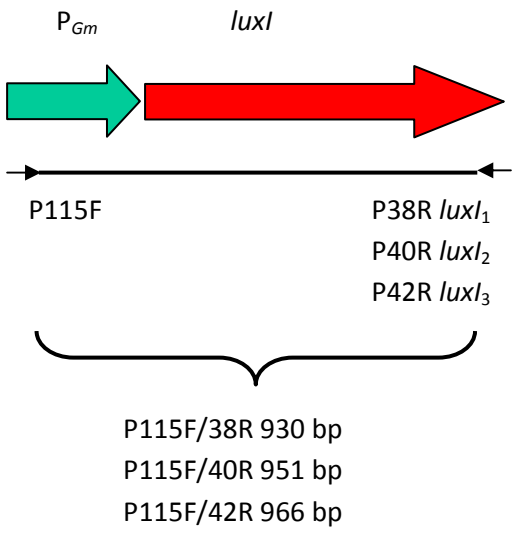

Figure 24 Scheme of the P$_{Gm}$-*luxI* amplification product.

Primers P115F/P38R, P115F/P40R and P115F/P42R were used to amplify the *luxI* genes, now controlled by the constitutive gentamicin promoter.

Expected PCR products of approx. 950 bp were gel purified and reused as template for a second *Pfu* PCR with the same primers. PCR products were afterwards purified and cloned through blunt-end ligation into pBBR1MCS-2 using the EcoRV and EcoICRI site.

1.1.1 Verification and functionality of vector Comp1-3

The functionality of vector Comp1-3 was tested in *E. coli* DH10B cells. The vector comprises a kanamycin resistance cassette and kanamycin resistant clones were investigated via plasmid preparation and standard PCR techniques.

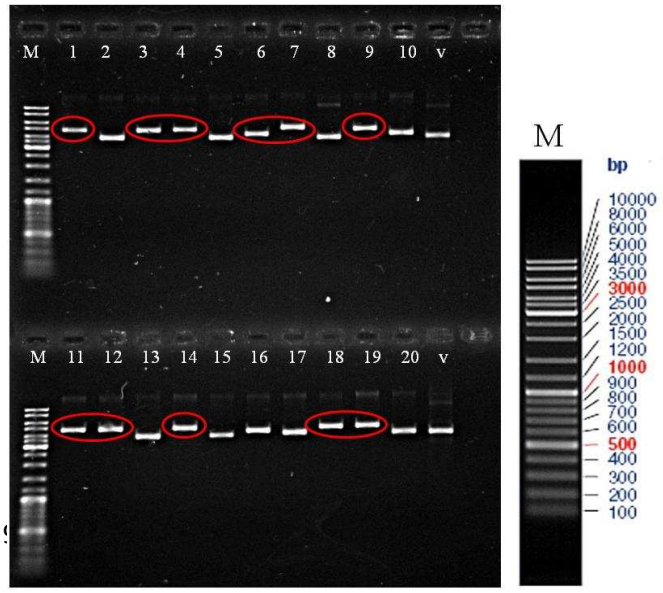

Figure 25 Plasmid preparation of twenty *E. coli* pBBR1MCS2 Comp1 clones.

Clones with increased plasmid size (red circles) compared to the empty vector pBBR1MCS2 (v) were chosen for PCR verification. 4 µl of the plasmid were mixed with 2 µl 6 x Loading dye (Fermentas) and transferred to a 1% agarose gel. M: 4 µl of the GeneRuler DNA Ladder Mix (Fermentas) were used for sizing of plasmids.

Clones 1, 3, 4, 6, 7, 9, 11, 12, 14, 18 and 19 with increased plasmid size compared to the empty pBBR1MCS2 vector were chosen as template for a standard PCR using the primer combination P115F/P73R.

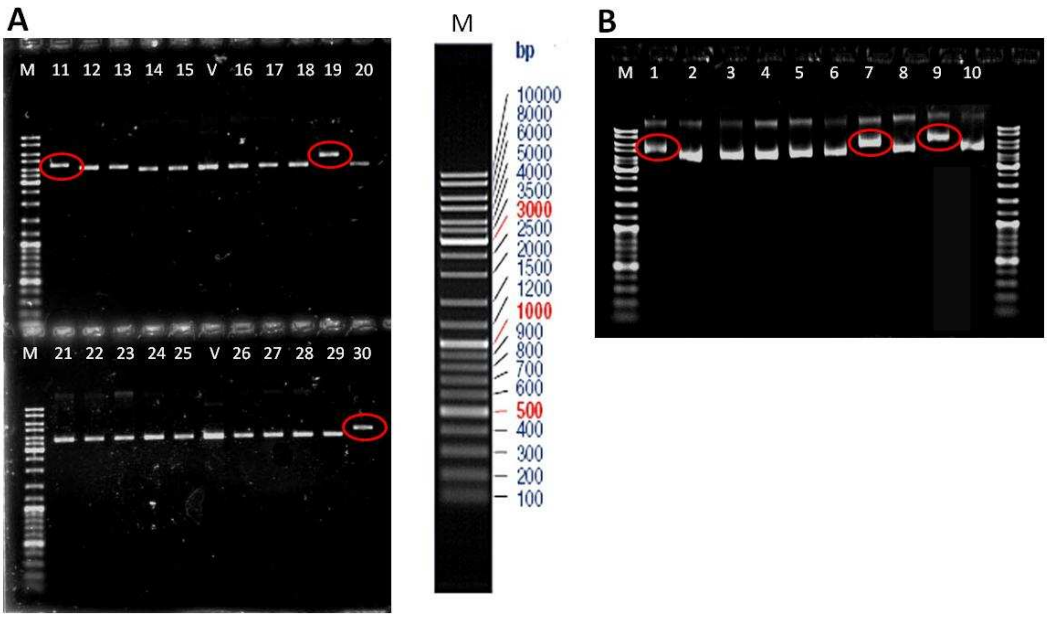

Figure 26 Plasmid preparation of *E. coli* pBBR1MCS2 A) Comp2 and B) Comp3 clones.

Clones with increased plasmid size (red circles) compared to the empty vector pBBR1MCS2 (v) were chosen for PCR verification. 4 µl of the plasmid were mixed with 2 µl 6 x Loading dye (Fermentas) and transferred to a 1% agarose gel. M: 4 µl of the GeneRuler DNA Ladder Mix (Fermentas) were used for sizing of plasmids.

The first ten *E. coli* pBBR1MCS2 Comp2 kanamycin resistant clones were religated without insertion of the P_{Gm}-*luxI*$_2$ fragment. Clones 11, 19 and 30 of *E. coli* Comp2 with increased plasmid size compared to the empty pBBR1MCS2 vector as well as clones 1, 7 and 9 of *E. coli* Comp3 were chosen as template for a standard PCR using the primer combination P115F/P73R.

The PCR is confirming the insertion of the *luxI* gene into the complementation vector as well as the orientation of the gene.

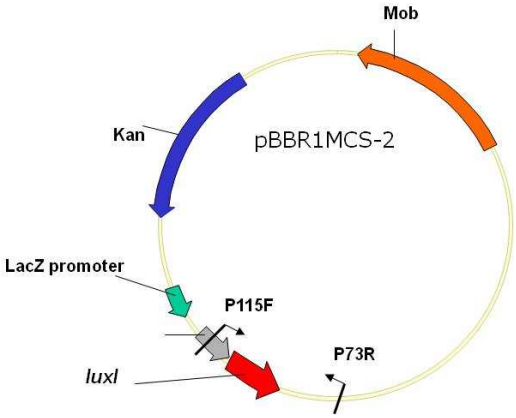

Standard PCR
Primer 115F/73R (1.046 bp)

plasmid DNA of Comp1 clones:
1, 3, 4, 6, 7, 9, 11, 12, 14, 18, 19

plasmid DNA of Comp2 clones:
11, 19, 30

plasmid DNA of Comp3 clones:
1, 7, 9

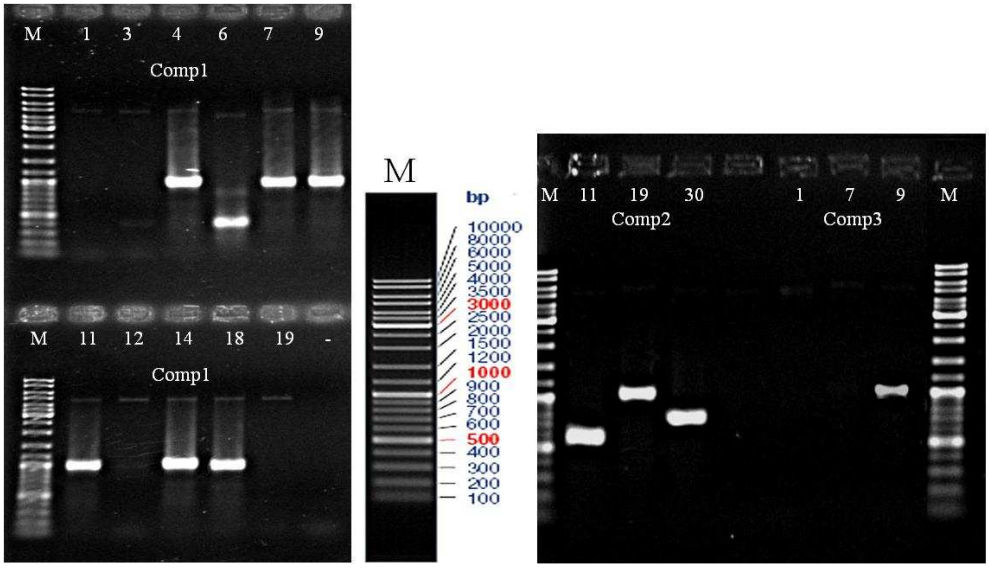

Figure 27 Verification of the pBBR1MCS2 Comp1-3 constructs.

The map of the complementation vector depicts the integration site of the gentamicin promoter controlled *luxI* gene. It is inserted into the MCS of the vector adjacent to an additional *lacZ* promoter. Amplification of the PCR product using primers P115F and P73R ensures a correct orientation of *luxI* which should not be located contrarily to the *lacZ* promoter. Gel electrophoresis shows the P115F/P73R PCR product using selected subclone DNA. Comp1 clones 4, 7, 9, 11, 14 and 18 are carrying the accurate orientated complementation construct as well as Comp2 clone 19 and Comp3 clone 9. 4 µl of the PCR products were mixed with 2 µl 6 x Loading dye (Fermentas) and transferred to a 1% agarose gel. M: 4 µl of the GeneRuler DNA Ladder Mix (Fermentas) were used for sizing of PCR products.

Six *E. coli* pBR1MCS2 Comp1 as well as one Comp2 and one Comp3 subclone were identified, carrying the accurate inserted $luxI_{1\text{-}3}$ complementation vector. LuxI expression is controlled directly through the constitutive gentamicin promoter, supported by the adjacent *lacZ* promoter. *E. coli* DH10B carrying pBBR1MCS2 Comp1 clone 14, pBBR1MCS2 Comp2 clone19 and pBBR1MCS Comp3 clone 9 and pBBR1MCS2 without modification, hereafter named Comp0,

were cultivated in LB 50 µg/ml kanamycin with addition of 2% XADs. Methanol AHL extracts were prepared and bioassay analyses should clarify whether the functionality of pBBR1MCS2 Comp0-3 in *E. coli* cells was fulfilled.

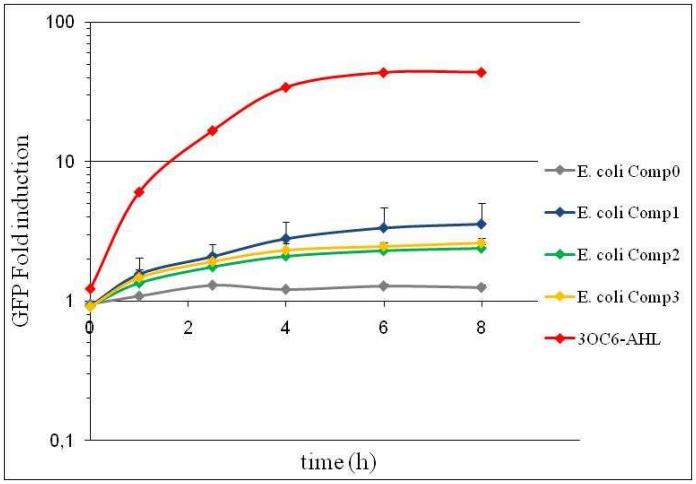

Figure 28 Detection of short-chain AHLs produced by *E. coli* ST18λpir carrying pBBR1MCS2 Comp1, Comp2, Comp3 and Comp0, respectively.

Detection of short-chain AHLs by use of the sensor strain *E. coli* pJBA132. In red, the positive control (3OC6-AHL, 2.35 µM) is depicted. The blue line displays the AHL extract of *E. coli* pBBR1MCS Comp1, the green line corresponds to the AHL extract of *E. coli* pBBR1MCS2 Comp2, the yellow line is the extract of *E. coli* pBBR1MCS2 Comp3 and the grey line depicts the AHL extract of *E. coli* pBBR1MCS2 Comp0. Presented are the mean values of three technical replicates from each of two biological replicates.

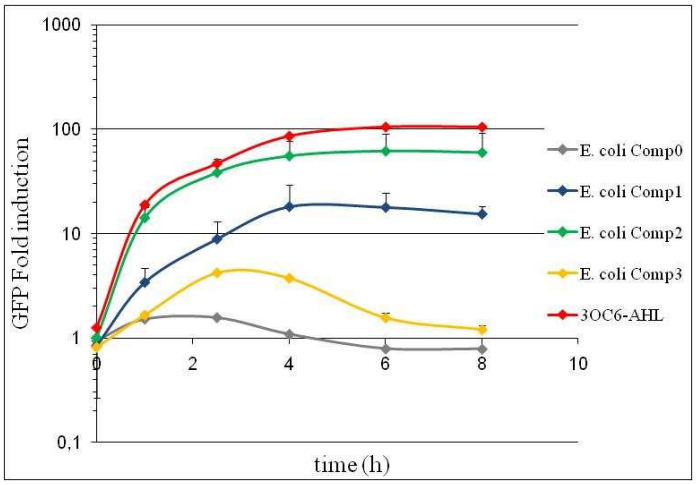

Figure 29 Detection of long-chain AHLs produced by *E. coli* ST18λpir carrying pBBR1MCS2 Comp1, Comp2, Comp3 and Comp0, respectively.

Detection of long-chain AHLs by use of the sensor strain *P. putida* pKR-C12. In red, the positive control (3OC12-AHL, 2.35 µM) is depicted. The blue line displays the AHL extract of *E. coli* pBBR1MCS Comp1, the green line corresponds to the AHL extract of *E. coli* pBBR1MCS2 Comp2, the yellow line is the extract of *E. coli* pBBR1MCS2 Comp3 and the grey line depicts the AHL extract of *E. coli* pBBR1MCS2 Comp0. Presented are the mean values of three technical replicates from each of two biological replicates.

All three complementation constructs were functional in *E. coli* ST18λpir which partly reconfirmed the results of the heterologous expression of the *luxI* genes

using the pTrcHis vector. The Comp vectors in which *luxI*$_{1\text{-}3}$ are controlled by the constitutive gentamicin promoter, supported by the *lacZ* promoter, are not only complementation vectors. Moreover, they seem to be a *luxI*$_{1\text{-}3}$ overexpression construct. Due to the twofold intensified and constitutive expression, it was in fact possible to induce *luxI*$_1$ expression and to obtain low concentrations of short-chain and moderate amounts of long-chain AHLs produced by *E. coli*. Furthermore, *E. coli* Comp2 was shown to produce low amounts of short-chain AHLs and high concentrations of long-chain AHLs while *E. coli* Comp3 produced low amounts of short-chain AHLs and low concentrations of long-chain AHLs. *E. coli* ST18λpir carrying the unmodified vector Comp0 was not able to synthesize AHLs. Also for these bioassay results were true that the GFP fold induction of the short-chain AHLs were relatively low and the sensor strain *E. coli* pJBA132 is known to be sensitive to high amounts of long-chain AHLs such as 3OC12-AHL. Thus, the short-chain signals detected by *E. coli* pJBA132 could not be due to short-chain AHLs, but rather a background signal of high concentrated long-chain AHLs present in the extracts.

The extracts were supplied for GC-MS analyses, but AHLs could not be identified.

4.4 Overexpression of a single LuxI synthase in *D. shibae* DFL-12

pBBR1MCS2::(P_{Gm}-*luxI*$_{1-3}$) (Comp1-3) which has been designated for genetic complementation of the LuxI mutants was used to increase the specific autoinducer signal of especially one single LuxI synthase in the wild type background. Each of the three complementation plasmids was transformed into *D. shibae* DFL-12 by biparental mating. Dichloromethane extracts of these "overexpression" strains were prepared during cultivation in MB and used for bioassay analyses.

As shown in Figure 30 and Figure 31, overexpression of LuxI$_1$ in *D. shibae DFL*-12 resulted in an enhanced synthesis of short-chain AHLs while the long-chain AHL production was repressed compared to the wild type. Overexpression of LuxI$_2$ and LuxI$_3$ in the wild type background decreased the production of short-chain AHLs while the long-chain AHL synthesis remained equal to the wild type.

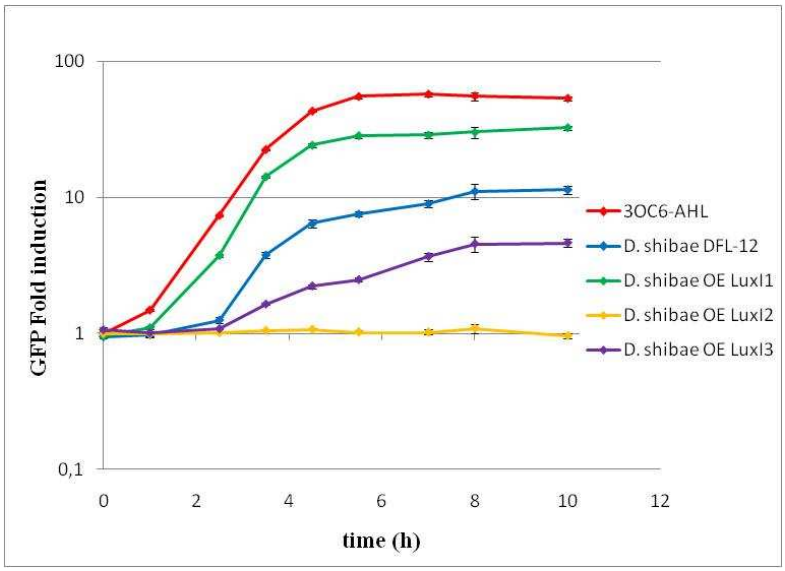

Figure 30 Detection of short-chain AHLs produced by *D. shibae* DFL-12 overexpressing (OE) LuxI$_1$, LuxI$_2$ and LuxI$_3$ during cultivation in MB.

Detection of short-chain AHLs by use of the sensor strain *E. coli* pJBA132. Presented are the mean values of three technical replicas, one biological sample.

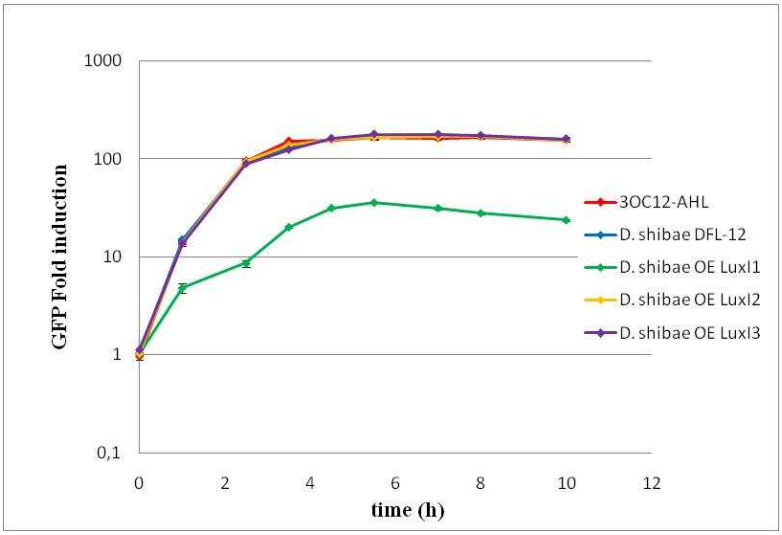

Figure 31 Detection of long-chain AHLs produced by *D. shibae* DFL-12 wild type overexpressing $LuxI_1$, $LuxI_2$ and $LuxI_3$, respectively.

Detection of long-chain AHLs by use of the sensor strain *P. putida* pKR-C12. Presented are the mean values of three technical replicas, one biological sample.

Table 14 GC-MS analyses of the AHL extracts obtained by the overexpression of *luxI*$_{1-3}$ in the wild type.

Strain /Extract	GC-MS analyses
D. shibae DFL-12	C18-en-HSL, C18-dien-HSL
D. shibae DFL-12 pBBR1MCS2::P_{Gm}-*luxI*$_1$	C18-en-HSL, C18-dien-HSL
D. shibae DFL-12 pBBR1MCS2::P_{Gm}-*luxI*$_2$	OHC14-HSL
D. shibae DFL-12 pBBR1MCS2::P_{Gm}-*luxI*$_3$	no AHLs detected

4.5 The *D. shibae* DFL-12 *luxI* mutants

4.5.1 The *luxI* genes

The *luxI*$_1$ gene (Dshi_0312) of *D. shibae* DFL-12 is located between 301.032 and 301.619 bp (+) on the chromosome. It attains a length of 588 bp and can be translated into 195 amino acids. The *luxI*$_1$ gene is flanked by the transcriptional regulator (*luxR*) and a recombination protein (*mgsA*).

The *luxI*$_2$ gene (Dshi_2851) of *D. shibae* DFL-12 is located between 3.008.719 and 3.009.339 bp (-) on the chromosome. It attains a length of 621 bp and can be translated into 206 amino acids. The *luxI*$_2$ gene is flanked by the transcriptional regulator (*luxR*) and an AAA ATPase.

The *luxI*$_3$ gene (Dshi_4152) of *D. shibae* DFL-12 is located between 84.463 and 85.098 bp (-) on the plasmid pDS86. It attains a length of 636 bp and can be translated into 211 amino acids. The *luxI*$_3$ gene is flanked by an integrase and a hypothetical protein. An adjacent LuxR-type regulator is missing.

4.5.2 LuxI gene replacement

Whole gene function is often identified through phenotypic analysis of gene deletions and complementary replacements. The replacement of wild type genes with alternate alleles (e.g. resistance cassettes) is also used *in vivo* to identify the function of specific features of genes and proteins. For this purpose the gene replacement vector pJP5603Δ*luxI*::*Gm*^{R} was constructed, which had the coding sequence of *luxI* replaced within the region of shared homology with a positive selection marker (ampicillin cassette). Double homologous recombination between the left and right arms of sequence homology on the vector and the *luxI* gene resulted in the replacement of the CDS with the ampicillin cassette and loss of the *luxI* gene. A successfull replacement of the *luxI* locus could be selected by the aquired ampicillin resistance. Cells survived antibiotic selection. Concerning *D. shibae* DFL-12, pJP5603 is a so-called suicide vector, because of its R6K origin of replication (ori). For replication of this vector, the R6K lambda *pir* gene has to be supplied *in trans*. Single homologous recombination of the targeting vector into *D. shibae* DFL-12 DNA would result in insertion of the vector into the genome, with retention of the *luxI* gene. Cells would survive the antibiotic

selection. Therefore *luxI* deletion clones were additionally verified by standard PCR techniques and sequencing.

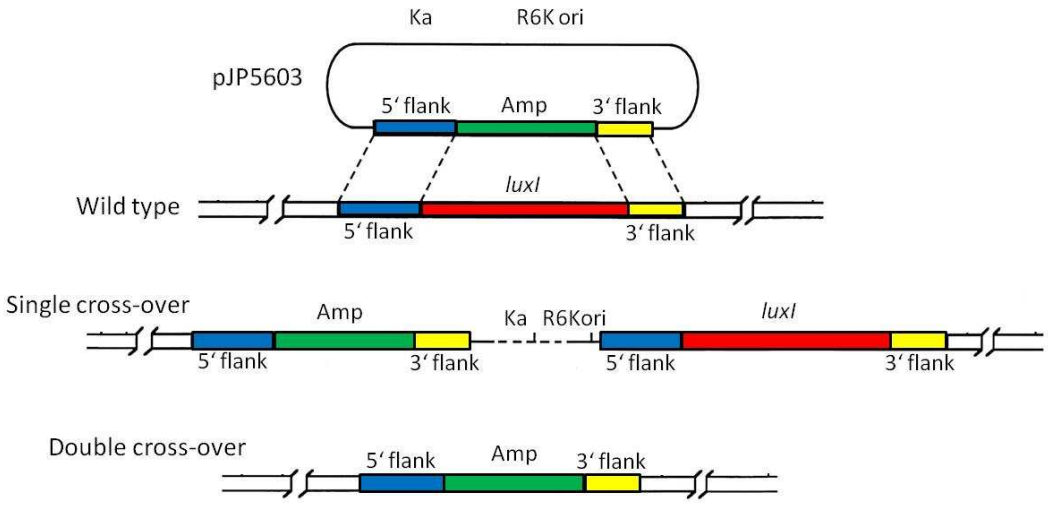

Figure 32 *luxI* gene replacement by double homologous recombination (double cross-over).

The first recombination event occurs through homologous sequences in one of the flanking region. The replacement vector is inserted into the chromosome (single cross-over). Clones are ampicillin resistant and the *luxI* gene is retained. The second recombination event occurs through homologous sequences in the second flanking region. The target gene, *luxI*, is deleted and replaced completely by the ampicillin cassette (double cross-over). Positive clones are ampicillin resistant and *luxI* can not be amplified via internal *luxI* primers using standard PCR techniques.

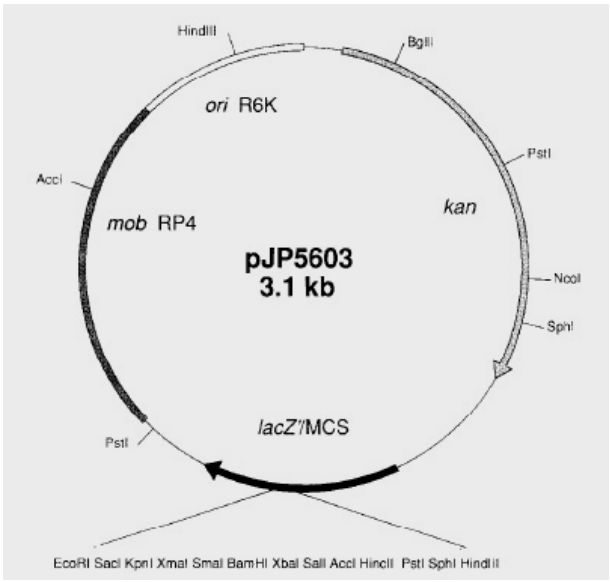

Figure 33 Map of the suicide vector pJP5603.

The R6K-based suicide vector replicates only if the R6K *pir* gene is supplied *in trans*. The vector consists of (clockwise) the R6K ori, a kanamycin resistance cassette, the pUC19 derived MCS and the RP4 mob site for plasmid mobilization. Arrows indicate the direction of transcription (Penfold and Pemberton 1992).

4.5.3 Construction of the *luxI* replacement vector

Sequences of the 5’ and 3’ flanks as well as the ampicillin cassette were amplified using *Pfu* polymerase. Afterwards 3´ A-overhangs post-amplification were added to the PCR products of the 5’ flank and the ampicillin cassette and the purified products were cloned separately into the pCR4 TOPO TA® vector from Invitrogen and transformed into *E. coli* TOP10 according to the manufacturer’s protocol. Cutting out the sequences from the pCR4 TOPO TA® vector with the required restriction enzymes, ensured a proper digestion of the sticky-ends for ligation.

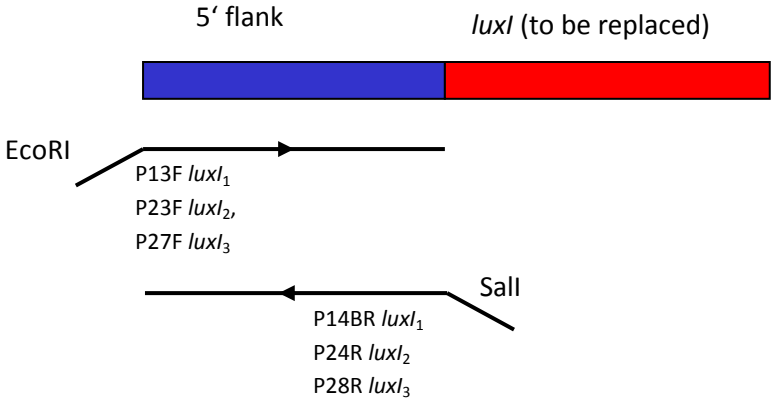

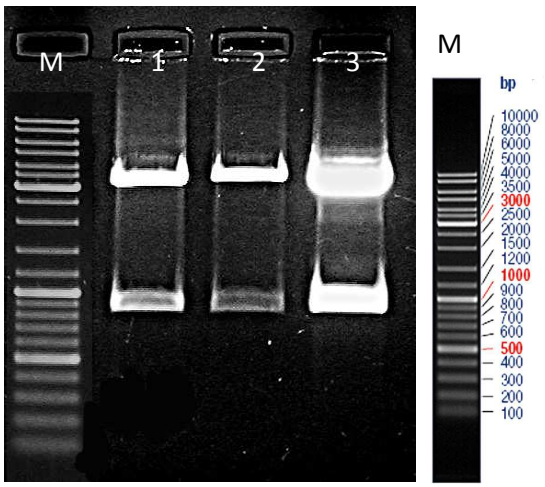

EcoRI/SalI digestion

1: pCR4 with *luxI*$_1$ 5’ flank 819 bp (26.42 ng/µl)

2: pCR4 wih *luxI*$_2$ 5’ flank 800 bp (19.35 ng/µl)

3: pCR4 with *luxI*$_3$ 5’ flank 818 bp (80.34 ng/µl)

Figure 34 Amplification of the *luxI* 5’ flank and digestion of pCR4, carrying the 5’ flank of *luxI* 1, *luxI* 2 and *luxI* 3, respectively.

The upper scheme depicts the used primer pairs (P13F/14BR, 23F/24R and 27F/28R) to amplify the 5’ flanks of *luxI* 1-3 from *D. shibae* DFL-12 wild type. The forward primer comprises an EcoRI restriction site and the reverse primer encloses the SalI restriction site. The lower image describes the EcoRI/SalI digestion of the respective 5’ flanks from the pCR4 vector. 50 µl of the digestion were mixed with 5 µl 6 x Loading dye (Fermentas) and transferred to a 1% agarose gel. Products with a size of approx. 800 bp were cutted out of the gel and purified. Values in brackets (ng/µl) are the concentrations of the digested and gel purified 5’ flanks. M: 4 µl of the GeneRuler DNA Ladder Mix (Fermentas) were used for sizing of digestion products.

The sequence of the *luxI*$_1$ 5'flank contains a natural EcoRI site 126 bp downstream of the P13F primer. As a result, the digestion with EcoRI and SalI of the pCR4 vector shortens the 5'flank to 818 bp.

Because of lacking the complete, available vector sequence, it was necessary to review the published vector data.The digestion of the vector using EcoRI or SalI (unique) resulted in the requested linearization of the vector (Figure 35, lanes EcoRI and SalI) with a size of 3.1 kb. A NheI site does not exist according to the literature. The vector was not cutted and remained circular.

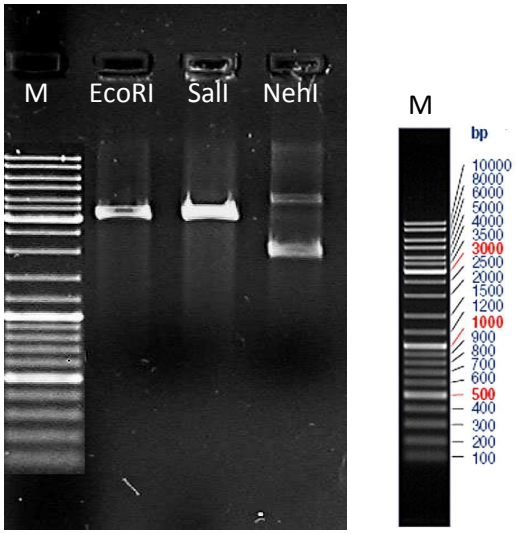

Figure 35 Control digestion of pJP5603 with EcoRI, SalI and NehI, respectively.

Restriction enzymes EcoRI and SalI should be unique and were used to linearize the vector by a single cut. The expected size of the linearized vector is 3.1 kb. The restriction site NheI does not exist according to the literature and the vector has to remain uncut and circular. 20 µl of the digestion were mixed with 5 µl 6 x Loading dye (Fermentas) and transferred to a 1% agarose gel. M: 4 µl of the GeneRuler DNA Ladder Mix (Fermentas) were used for sizing of digestion products.

The EcoRI and SalI restriction site were used to clone the 5'flank of *luxI* through directed sticky-end ligation into pJP5603.

pJP5603 is carrying a kanamycin resistance cassette. Therefore, clones grown on selective kanamycin medium were investigated. Plasmids were prepared and the correct insertion of the 5' flank into the vector was verified by PCR. Positive clones were afterwards used for the insertion of the ampicillin cassette.

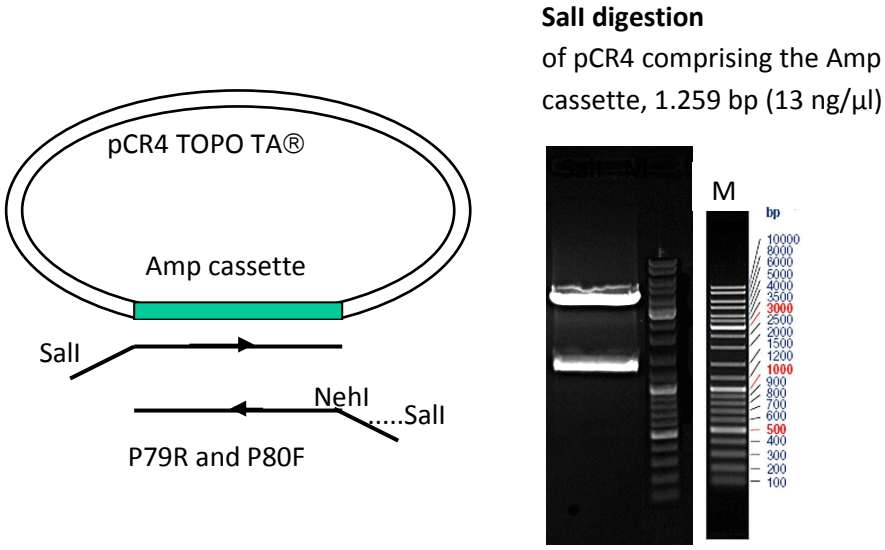

Figure 36 Amplification of the ampicillin cassette and SalI digestion of pCR4 comprising the ampicillin cassette.

The left scheme depicts the used primer pair (P79R/P80F) which was used to amplify the ampicillin cassette from vector pCR4. The forward primer comprises a SalI restriction site while the reverse primer encloses an external SalI restriction site and an internal NheI site. The PCR product was recloned into the MCS of pCR4 and recut with SalI to ensure the complete digestion of the sticky ends. The right panel shows the SalI digestion of the pCR4 vector comprising the ampicillin cassette (1.259 bp). 50 µl of the digestion were mixed with 5 µl 6 x Loading dye (Fermentas) and transferred to a 1% agarose gel. The 1.259 bp DNA band was cutted out of the gel and purified. Values in brackets (ng/µl) are the concentrations of the digested and gel purified ampicillin cassette. M: 4 µl of the GeneRuler DNA Ladder Mix (Fermentas) were used for sizing of digestion products.

The vector pJP5603::5'flank was recut with SalI and the ampicillin cassette was integrated by undirected, sticky-end ligation adjacent to the 5' flank.

In fact, the direction of the ampicillin cassette should be indifferent because it is regulated by its own constitutive promotor, but the reverse primer of the ampicillin cassette includes the NheI restriction site, which was used later on to clone the 3' flank. Therefore ampicillin resistant clones with an ampicillin cassette integrated corresponding to the natural *luxI* transcription orientation were chosen.

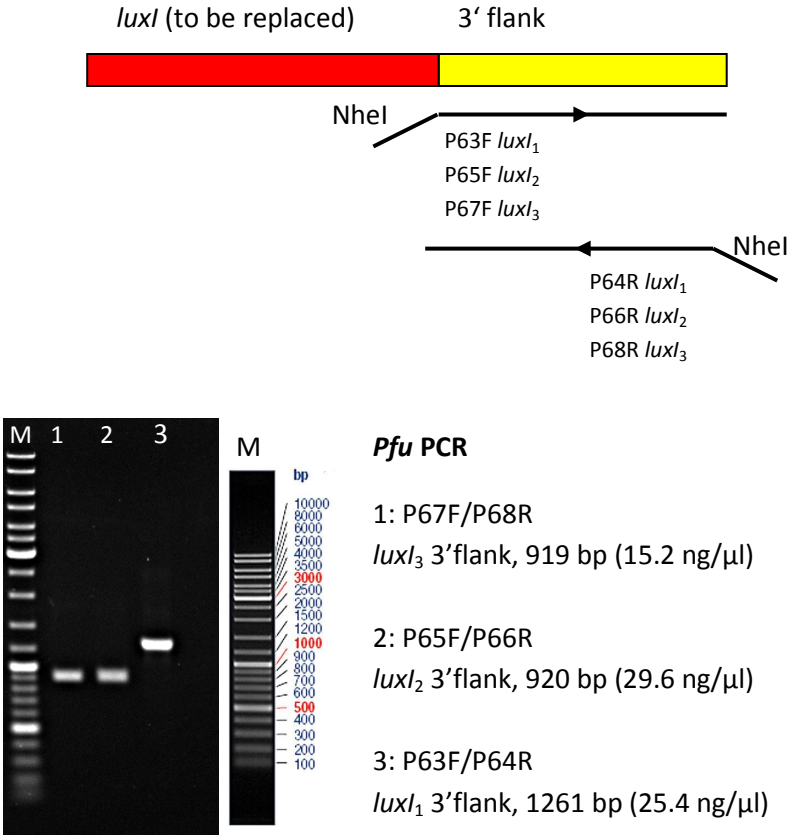

Figure 37 Amplification of the *luxI* 3’ flank using *Pfu* Polymerase.

The upper scheme depicts the used primer pairs (P63F/P64R, P65F/P66R and P67F/P68R) for amplification of the 3’flanks. Both, forward and reverse primer comprises a NheI restriction site. The lower panel shows the amplification products of the 3’flanks using *Pfu* polymerase. 4 µl of the PCR products were mixed with 2 µl 6 x Loading dye (Fermentas) and transferred to a 1% agarose gel. Values in brackets (ng/µl) are the concentrations of the purified PCR products. M: 4 µl of the GeneRuler DNA Ladder Mix (Fermentas) were used for sizing of PCR products.

The purified PCR products of the *luxI*$_2$ and *luxI*$_3$ 3’flank were digested with NheI without an additional subcloning into pCR4. Digested and purified 3’ flanks were introduced into pJP5603::5’flank-Amp^R using the generated NheI restriction site (included in primer P79R) adjacent to the ampicillin cassette.

The *Pfu* PCR product of the *luxI*$_1$ 3’flank (P63F/P64R, 1.261 bp) was digested with FspI (NsbI) using a natural FspI site which divided the PCR product into two parts with a length of 607 bp and 654 bp. After digestion, the fragments were separated through gel electrophoresis. The 654 bp fragment was gel purified and used for blunt-end ligation into pJP5603::5’flank *luxI*$_1$-Amp^R.

Therefore pJP5603::5'flank *luxI*$_1$-Amp^R was digested with NheI (sticky ends) and ends were blunted using T4 DNA Polymerase (Fermentas) according to the manufacturer's protocol. The shortened *luxI*$_1$ 3'flank was introduced adjacent to the ampicillin cassette by blunt-end ligation.

Ampicillin, which was intended for selection, looses 45 % activity at 20°C after 48 hours. In addition, activity is decreased by a factor of 10 when medium with a pH value of 8 is used (www.carlroth.com). Therefore the selection of the *luxI* knock-out clones by ampicillin was not suitable. The sequence of the ampicillin resistance was disrupted by introducing a gentamicin cassette through blunt-end ligation using a natural ScaI restriction site. The gentamicin resistance is controlled by its own constitutive promoter and was *Pfu* amplified using the primer pair P111F/P112R. It was derived from the vector pBBR1MCS-5.

Final *luxI* replacement vectors (pJP5603::5'flank-Gm^R-3'flank) were hereafter named pJP5603KO1, pJP5603KO2 and pJP5603KO3 (KO = knock-out) and their sequences were confirmed by standard PCR and sequencing.

4.5.4 Verification of the *D. shibae* DFL-12 *ΔluxI* clones

The knock-out construct pJP5603KO1-3 was transformed into the conjugation strain *E. coli* ST18 λ pir by TSS transformation and, subsequently, into *D. shibae* DFL-12 wild type by biparental mating. Exconjugants appeared after several days on selective hMB gentamicin 80 µg/ml plates and were determined by PCR analyses for correct *luxI* replacement. For high throughput verification of clones, colony PCR was carried out using primers of $luxI_1$, $luxI_2$ and $luxI_3$ as well as common 16S rRNA primers which ensure the proper disruption of the cells and the presence of DNA.

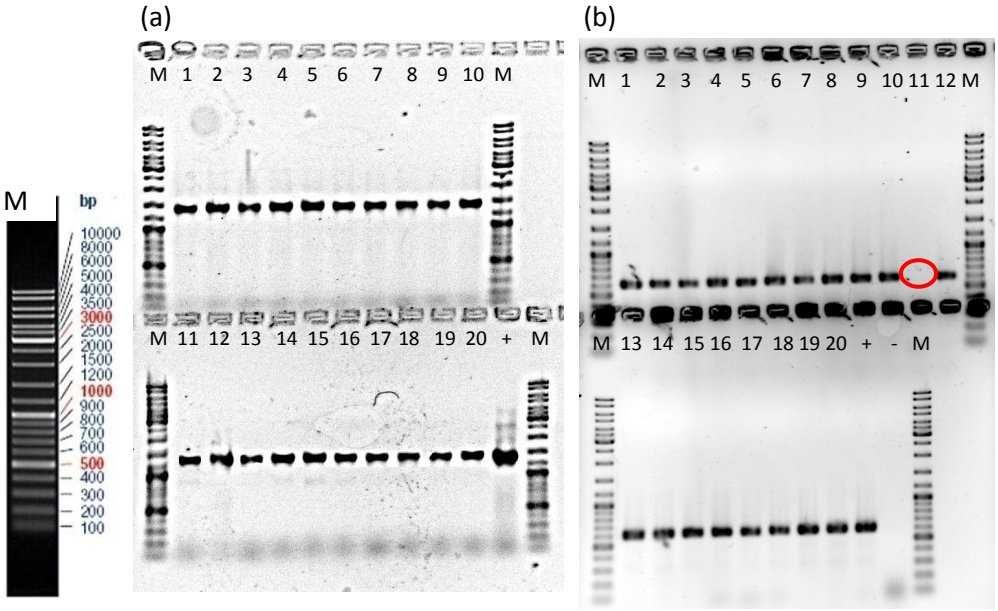

Figure 38 Amplification of the 16S rRNA and the $luxI_1$ gene by colony PCR.

(a) Amplification of the 16S rRNA of *D. shibae* DFL-12 Δ$luxI_1$ clones 1-20. The expected PCR product (size 1.542 kb) was obtained for each clone, indicating that disruption of the cells was successful. (b) Amplification of the $luxI_1$ gene (primers P37F/P38R) of *D. shibae* Δ$luxI_1$ clones 1-20. All Δ$luxI_1$ clones were positive, except for clone 11 for which no $luxI_1$ PCR product (606 bp) was obtained (red circle). As positive control (+) genomic DNA of *D. shibae* DFL-12 was used as well as water as negative control (-). 4 µl of the PCR products were mixed with 2 µl 6 x Loading dye (Fermentas) and transferred to a 1% agarose gel. M: 4 µl of the GeneRuler DNA Ladder Mix (Fermentas) were used for sizing of PCR products.

Figure 38a depicts the amplification of the 16S rRNA gene of *D. shibae* Δ$luxI_1$ clones 1 to 20 using common 16S rRNA primer. Previously cells of the clones were disrupted by heating at 98°C for 15 minutes. DNA of each clone could be

detected by 16S rRNA PCR and the same template was used to amplify the putatively replaced *luxI*$_1$ gene (Figure 38b). Despite of the selective pressure, only clones containing *luxI*$_1$ could be obtained, except for one, clone 11. Thus, clone 11 was used for further verification. Genomic DNA of the *D. shibae* Δ*luxI*$_1$ clone 11 was prepared and used for verification PCRs.

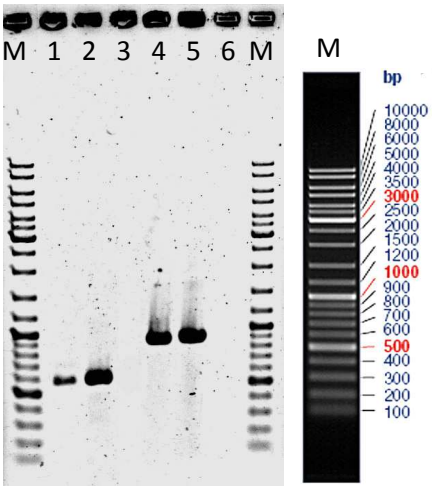

Standard PCR
Primer pair: P37F/P38R *luxI*$_1$ (606 bp)
1: Δ*luxI*$_1$ clone 11
2: *D. shibae* DFL-12 wild type
3: Water

Standard PCR
Primer pair: P111F/P112R Gm^R (897 bp)
4: Δ*luxI*$_1$ clone 11
5: pBBR1MCS-5
6: Water

Figure 39 Verification of the *D. shibae* Δ*luxI*$_1$ clone 11.

Genomic DNA of clone 11 was used to amplify the putatively replaced *luxI*$_1$ (primers P37F/P38R) and the inserted gentamicin cassette (primer P111F/P112R). Both genes, *luxI*$_1$ and the gentamicin resistance, could be amplified using the clone 11 DNA (lanes 1 and 4). Lanes 2 and 5 depict the positive, lanes 3 and 6 the negative controls. 4 µl of the PCR products were mixed with 2 µl 6 x Loading dye (Fermentas) and transferred to a 1% agarose gel. M: 4 µl of the GeneRuler DNA Ladder Mix (Fermentas) were used for sizing of PCR products.

Using genomic DNA of clone 11 resulted in the amplification of the *luxI*$_1$ gene as well as the gentamicin cassette (Figure 39). For this reason, the gentamicin concentration of the selective plates was increased up to 150 µg/ml, instead of 80 µg/ml. Afterwards clone 11 was used for inoculation of the new selective plates, to obtain subclones. Four subclones out of twenty were tested positive with respect to a successful *luxI*$_1$ replacement and named Δ*luxI*$_1$ clone 11.12, clone 11.13, clone 11.14 and clone 11.15. They were investigated by additional PCRs.

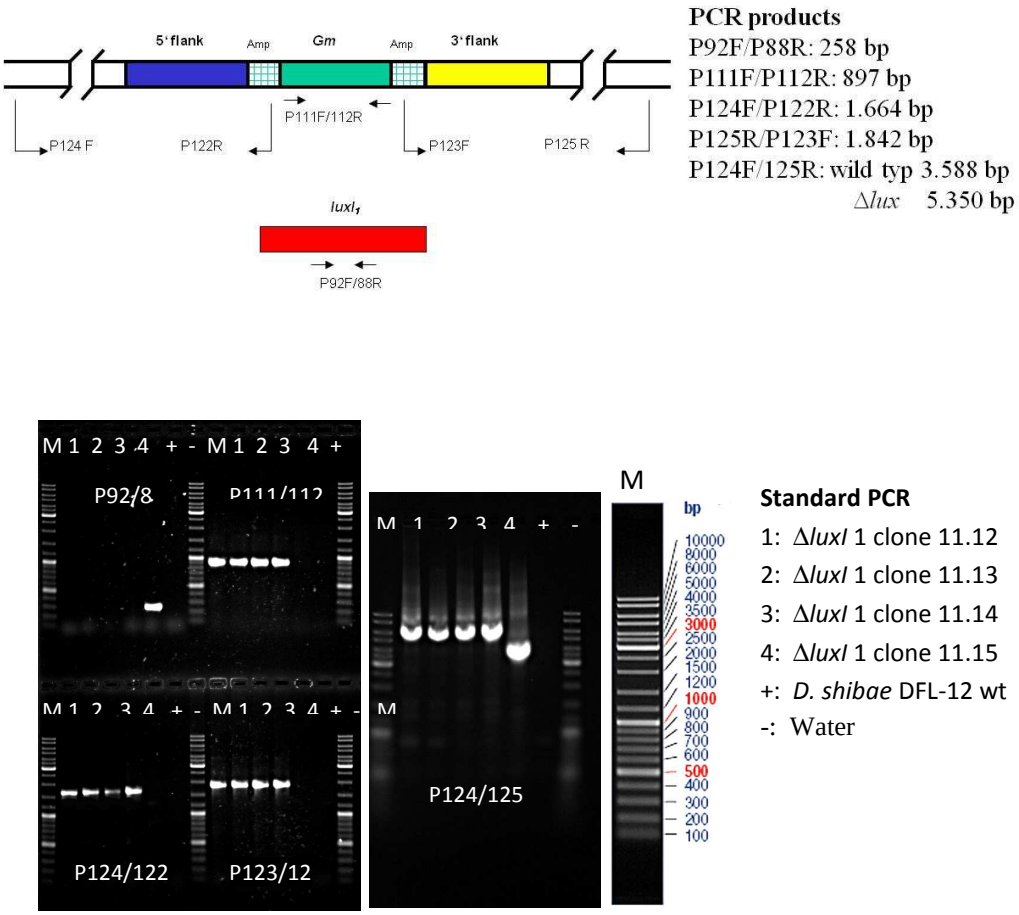

Figure 40 Verification of the *D. shibae* DFL-12 Δ*luxI*$_1$ subclones.

The upper scheme depicts the generated chromosomal region at the Δ*luxI*$_1$ locus after the *luxI* replacement. Various primer pairs are represented which were used for verification. The lower panels show the amplification of the corresponding products using genomic DNA of the four Δ*luxI*$_1$ subclones, *D. shibae* DFL-12 DNA and water. 4 µl of the PCR products were mixed with 2 µl 6 x Loading dye (Fermentas) and transferred to a 1% agarose gel. M: 4 µl of the GeneRuler DNA Ladder Mix (Fermentas) were used for sizing of PCR products.

First Δ*lux1*$_1$ subclones were tested for a successful *luxI*$_1$ replacement. Therefore internal primers of *luxI*$_1$ (P92F/P88R) were used for amplification. All four Δ*luxI*$_1$ subclones were identified to be real *luxI*$_1$ knock-outs. PCR products could not be obtained. LuxI$_1$ was exchanged against a gentamicin cassette. Thus, so primers P111F/P112R were used to prove the insertion of the antibiotic resistance cassette. In all four subclones the gentamicin cassette was present. To ensure that the double homologous recombination occurred at the correct, chromosomal position, primers were designed which were located outside of the area utilized for recombination (P124F/P125R). Expected PCR products had a size of 3.588 kb (wild type) and 5.350 kb (Δ*luxI* subclones), respectively. The

increased PCR product of the Δ*luxI* subclones is explained by the exchange of *luxI*$_1$ (606 bp) against the ampicillin-gentamicin cassette (1.762 bp).

In combination with primers located in the disrupted ampicillin resistance (P122F/P123R), the proper integration of the resistance cassette additionally was verified. In all four subclones, the expected PCR products could be obtained, confirming the exact replacement of the *luxI*$_1$ gene.

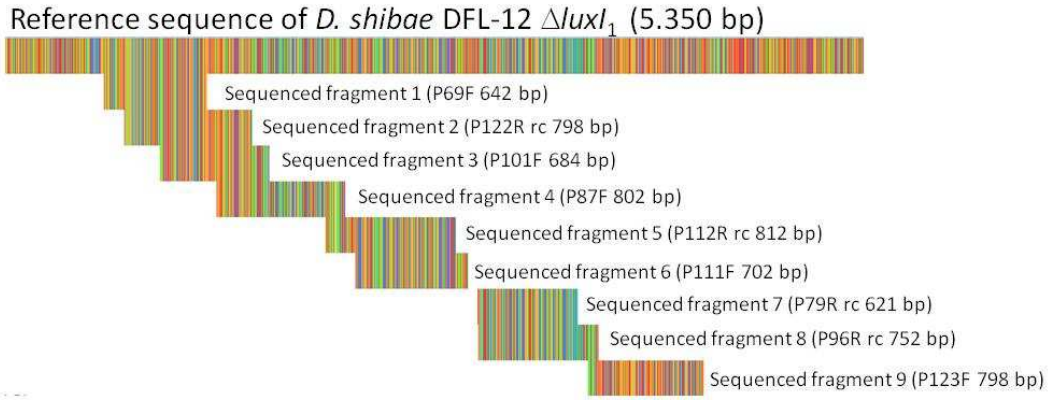

Figure 41 Alignment of nine sequenced fragments and the reference sequence of *D. shibae* Δ*luxI*$_1$.

Every single nucleotide of the sequences is figured as coloured line.

The whole sequence of the replacement affected region was amplified using the primers P124F/P125R (5.350 bp) and validated by sequencing using nine different primers. The alignment was performed by Thomas Riedel using the tools MEGA 5.0, ClustalW and Jalview 2.6.1 for illustration.

For detailed information and the completely aligned nucleotide sequences see Appendix.

For high throughput verification of Δ*luxI*$_2$ clones, colony PCR was carried out using primers of *luxI*$_2$ as well as common 16S rRNA primers which ensure the proper disruption of the cells and the presence of DNA. 16S rRNA PCR products could be obtained for the first twenty clones and the same template was used for the amplification of the *luxI*$_2$ gene using primers P39F/P40R (627 bp).

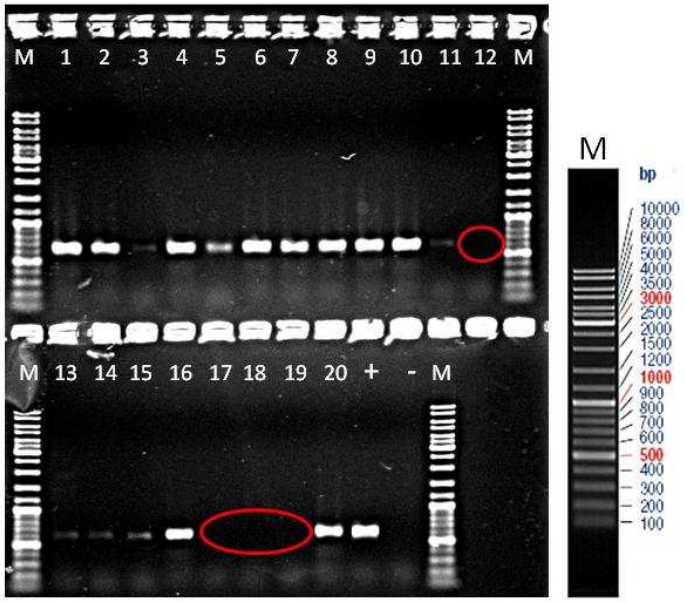

Figure 42 Amplification of the *luxI*$_2$ gene by colony PCR.

Amplification of the *luxI*$_2$ gene (primers P39F/P40R) of *D. shibae* Δ*luxI*$_2$ clones 1-20. All Δ*luxI*$_2$ clones were positive, except for clones 12, 17, 18 and 19 for which no *luxI*$_2$ PCR product (627 bp) was obtained (red circle). As positive control (+) genomic DNA of *D. shibae* DFL-12 was used as well as water as negative control (-). 4 µl of the PCR products were mixed with 2 µl 6 x Loading dye (Fermentas) and transferred to a 1% agarose gel. M: 4 µl of the GeneRuler DNA Ladder Mix (Fermentas) were used for sizing of PCR products.

Despite of the selective pressure, several clones containing *luxI*$_2$ could be obtained, except for clones 12, 17, 18 and 19. These clones were used for further verification. Genomic DNA of the *D. shibae* Δ*luxI*$_2$ clones 12, 17, 18 and 19 was prepared and used for verification PCRs.

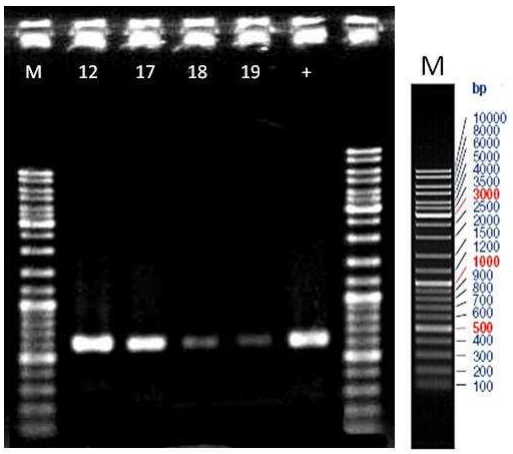

Figure 43 Amplification of the *luxI*$_2$ gene using genomic DNA of Δ*luxI*$_2$ clones 12, 17, 18 and 19.

Amplification of the *luxI*$_2$ gene (primers P39F/P40R) of *D. shibae* Δ*luxI*$_2$ clones 12, 17, 18 and 19. As positive control (+) genomic DNA of *D. shibae* DFL-12 was used. 4 µl of the PCR products were mixed with 2 µl 6 x Loading dye (Fermentas) and transferred to a 1% agarose gel. M: 4 µl of the GeneRuler DNA Ladder Mix (Fermentas) were used for sizing of PCR products.

Using genomic DNA of clones 12, 17, 18 and 19 resulted in the amplification of the *luxI*$_2$ gene. For each clone the same initial DNA concentration of 4.3 ng was used as template. Clone 12 and 17 were useless, because *luxI*$_2$ was still present, but for clones 18 and 19 just weak *luxI*$_2$ amplificates were obtained. For this reason, the gentamicin concentration of the selective plates was increased up to 150 µg/ml, instead of 80 µg/ml. Afterwards clone 18 was used for inoculation of the new selective plates, to obtain subclones. Two subclones out of ten were tested positive with respect to a successful *luxI*$_2$ replacement and named Δ*luxI*$_2$ clone 18.4 and clone 18.6. They were investigated by additional PCRs using genomic DNA.

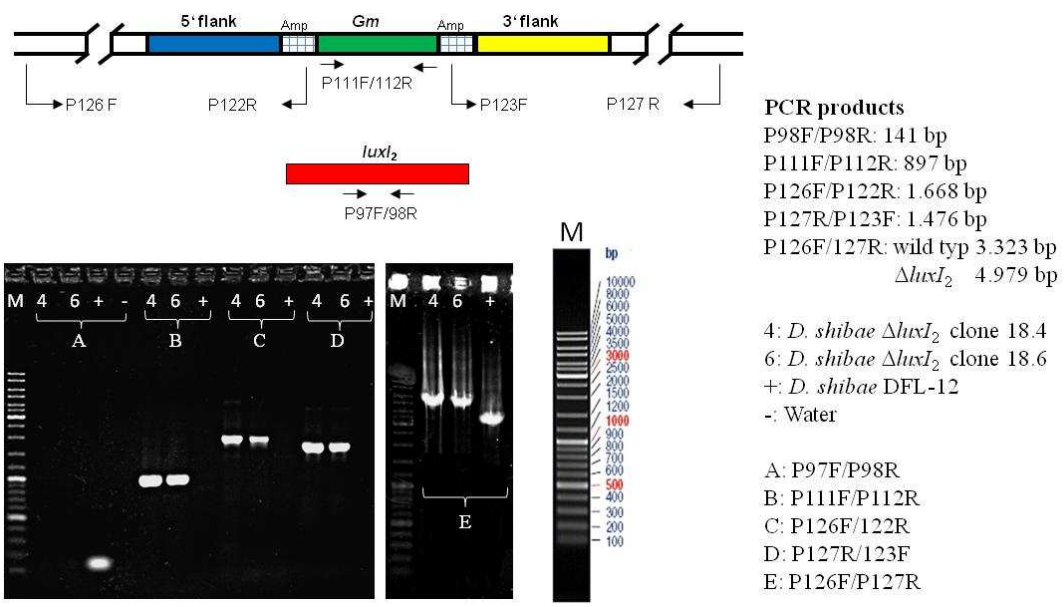

Figure 44 Verification of the *D. shibae* DFL-12 Δ*luxI*$_2$ subclones.

The upper scheme depicts the generated chromosomal region at the Δ*luxI*$_2$ locus after the *luxI* replacement. Various primer pairs are represented which were used for verification. The lower panels show the amplification of the corresponding products using genomic DNA of the two Δ*luxI*$_2$ subclones, *D. shibae* DFL-12 DNA and water. 4 µl of the PCR products were mixed with 2 µl 6 x Loading dye (Fermentas) and transferred to a 1% agarose gel. M: 4 µl of the GeneRuler DNA Ladder Mix (Fermentas) were used for sizing of PCR products.

First Δ*lux1*$_2$ subclones were tested for a successful *luxI*$_2$ replacement. Therefore internal primers of *luxI*$_2$ (P97F/P98R) were used for amplification. Both Δ*luxI*$_2$ subclones were identified to be real *luxI*$_2$ knock-outs. PCR products could not be

obtained. LuxI$_2$ was exchanged against a gentamicin cassette. Thus, so primers P111F/P112R were used to prove the insertion of the antibiotic resistance cassette. In both subclones the gentamicin cassette was present. To ensure that the double homologous recombination occurred at the correct, chromosomal position, primers were designed which were located outside of the area utilized for recombination (P126F/P127R). Expected PCR products had a size of 3.323 bp (wild type) and 4.979 bp (Δ*luxI*$_2$ subclones), respectively. The increased PCR product of the Δ*lux*$_2$ subclones is explained by the exchange of *luxI*$_2$ (627 bp) against the ampicillin-gentamicin cassette (1.762 bp). In combination with primers located in the disrupted ampicillin resistance (P122F/P123R), the proper integration of the resistance cassette additionally was verified. In both subclones, the expected PCR products could be obtained, confirming the exact replacement of the *luxI*$_2$ gene.

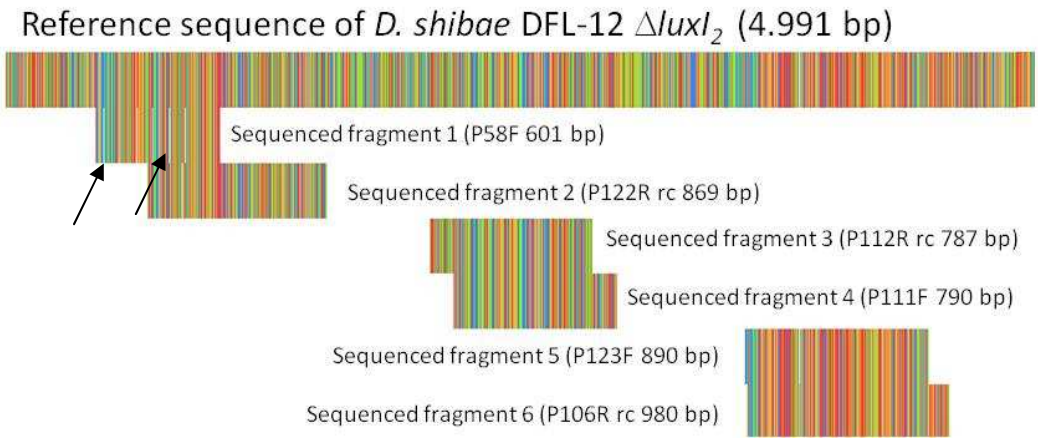

Figure 45 Alignment of six sequenced fragments and the reference sequence of *D. shibae* Δ*luxI*$_2$.

Every single nucleotide of the sequences is figured as coloured line. Nonconformity of sequenced nucleotides of fragment 1 and reference sequence is visualized as white line (black arrows).

The whole sequence of the replacement affected region was amplified using the primers P126F/P127R (4.991 bp) and validated by sequencing using six different primers.

For detailed information and the completely aligned nucleotide sequences see Appendix.

D. shibae Δ*luxI*$_3$ subclones were also verified, but the *luxI*$_3$ gene was still present as well as the introduced gentamicin cassette. Furthermore, sequencing of the Δ*luxI*$_3$ affected region revealed a mixture of wild type and knock-out sequences. *LuxI*$_3$ is located on the plasmid pDS86. The incomplete *luxI*$_3$ replacement could be due to a single cross-over by which the knock-out vector was integrated at the *luxI*$_3$ locus (see Figure 32) or a multiple copy number of plasmid pDS86 prevented a single *luxI*$_3$ knock-out event. Clones could comprise Δ*luxI*$_3$ loci as well as wild type loci. Therefore, *D. shibae* Δ*luxI*$_3$ was excluded from mutant analyses.

4.6 Analyses of the *D. shibae* DFL-12 Δ*luxI* mutants

4.6.1 Phenotype

The growth behaviour and the AHL production of the mutants compared to the wild type were investigated. Therefore all strains were cultivated in SWM with 5 mM succinate, shaking in the dark at 30°C. Growth was validated by measuring the optical density at 600 nm.

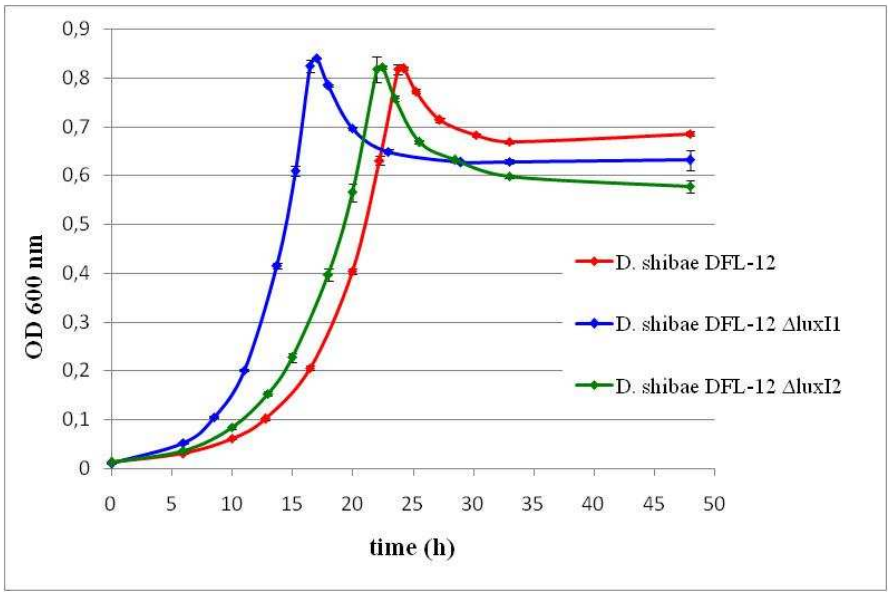

Figure 46 Growth curves of the *luxI* mutants compared to *D. shibae* DFL-12 in SWM with 5 mM succinate.

The red line depicts the growth of *D. shibae* DFL-12. The blue line shows the growth of *D. shibae* DFL-12 Δ*luxI*$_1$. The green line represents *D. shibae* DFL-12 Δ*luxI*$_2$. Presented are the mean values of three biological replicates.

The mutant strains Δ*luxI*$_1$ and Δ*luxI*$_2$ attained earlier the *log* phase compared to the wild type. The mutants grew faster until they abruptly entered the stationary phase at a final optical density of approximately 0.8. This could be due to aggregating cells in the stationary phase which distorted the values of the optical density. The generation time of *D. shibae* DFL-12 was 3.5 hours while the mutant generation times were 2.5 hours (Δ*luxI*$_1$) and 3 hours (Δ*luxI*$_2$).

To confirm, whether the AHL production was influenced by the *luxI* replacement, dichloromethane extracts were prepared and analyzed using the bioassay test.

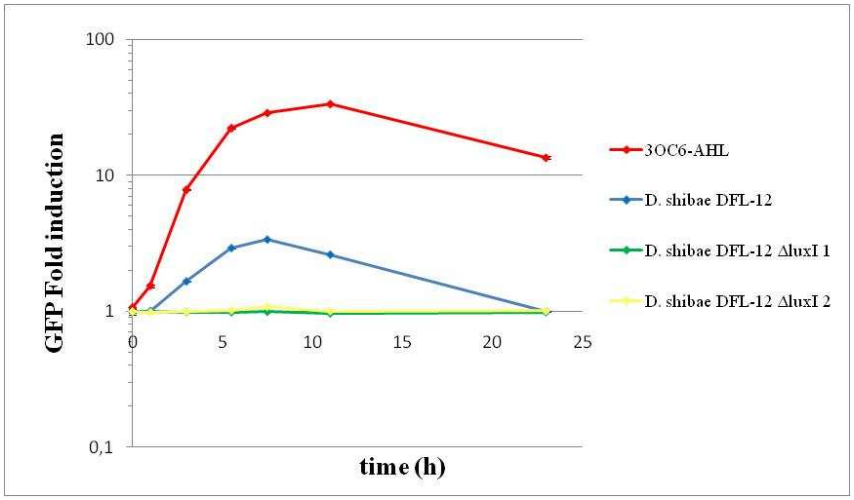

Figure 47 Detection of short-chain AHLs produced by *D. shibae* DFL-12, Δ*luxI*$_1$ and Δ*luxI*$_2$, during cultivation in SWM 50 mM succinate.

Detection of short-chain AHLs by use of the sensor strain *E. coli* pJBA132. In red, the positive control (3OC6 AHL, 0.24 µM) is depicted. The blue line displays the AHL extract of *D. shibae* DFL-12. The green line corresponds to the AHL extract of *D. shibae* DFL-12 Δ*luxI*$_1$and the yellow line to *D. shibae* DFL-12 Δ*luxI*$_2$. Presented are the mean values of three technical replicates.

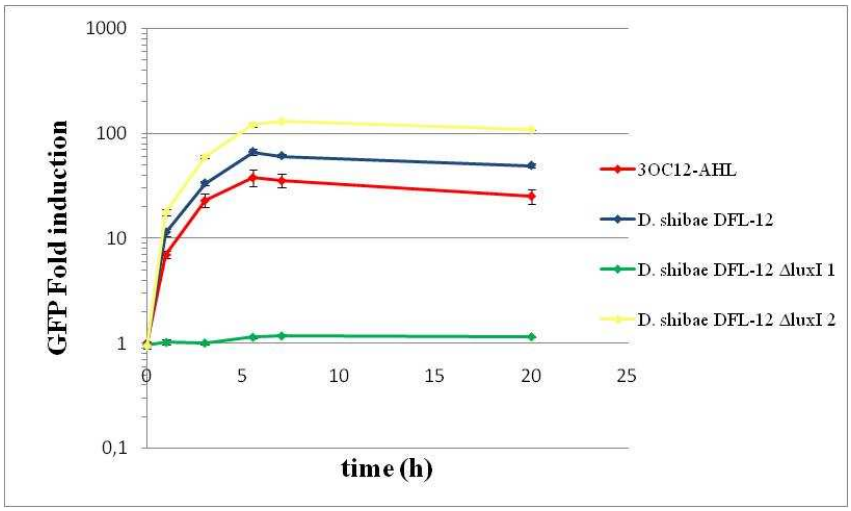

Figure 48 Detection of long-chain AHLs produced by *D. shibae* DFL-12, Δ*luxI*$_1$ and Δ*luxI*$_2$ during cultivation in SWM 50 mM succinate.

Detection of long-chain AHLs by use of the sensor strain *P. putida* pKR-C12. In red, the positive control (3OC12 AHL, 2.35 µM) is depicted. The blue line displays the AHL extract of *D. shibae* DFL-12.The green line corresponds to the AHL extract of *D. shibae* DFL-12 Δ*luxI*$_1$ and the yellow line to *D. shibae* DFL-12 Δ*luxI*$_2$. Presented are the mean values of three technical replicates.

D. shibae DFL-12 was shown to produce low amounts of short-chain and high concentrations of long-chain AHLs. Replacement of *luxI*$_1$ resulted in termination of the whole detectable AHL production. Neither short-chain nor long-chain AHLs could be detected in the *luxI*$_1$ mutant. Disruption of the *luxI*$_2$ caused the loss of short-chain AHLs, but long-chain AHL synthesis remained stable. Probably reduction of long-chain AHLs occurred, since *luxI*$_1$, *luxI*$_2$ and *luxI*$_3$ produce long-chain AHLs.

4.6.2 Expression of LuxI and LuxR genes

To support the bioassay results, qRT-PCR studies of *D. shibae* DFL-12 and mutants were performed by quantitative RT-PCR.

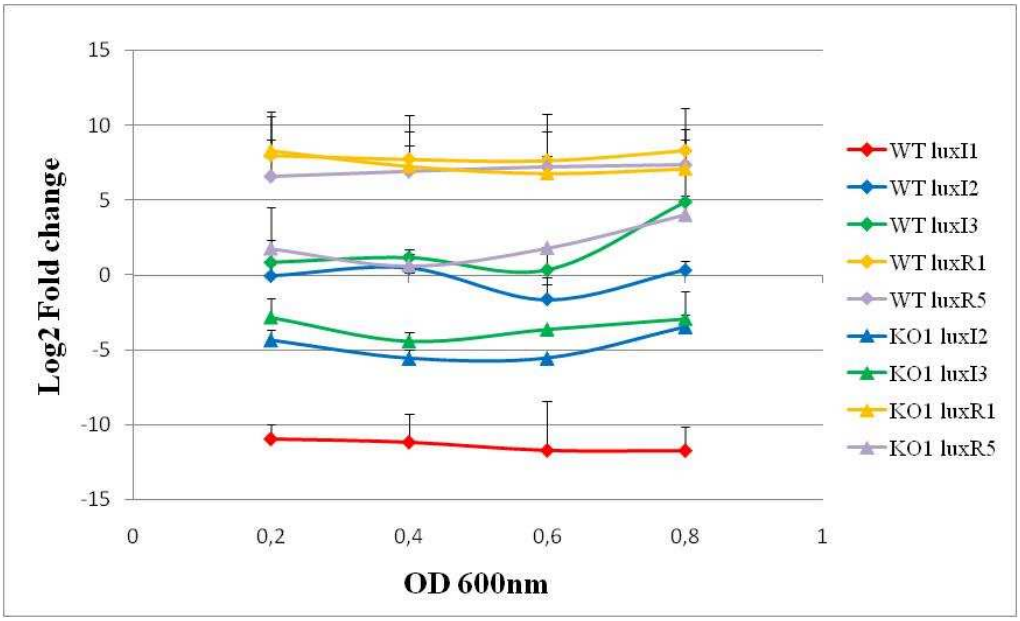

Figure 49 Expression of the *lux* genes in *D. shibae* DFL-12 Δ*luxI*$_1$ compared to the wild type.

Presented is the expression of the *lux* genes at four different optical densities in the *D. shibae* DFL-12 Δ*luxI*$_1$ compared to the wild type. Wild type (WT) gene expression is marked by rhombuses, gene expression of the mutant (KO1) by triangles. Expression of *luxI*$_1$ is depicted in red and is missing for the mutant. Blue lines show expression of *luxI*$_2$, green lines of *luxI*$_3$. The two regulators are illustrated in yellow, LuxR$_1$ and in violet, LuxR$_5$. Mean values of three technical replicates from each of two biological replicates are presented as Log2 fold change relative to the housekeeping gene *gyrA* at four different optical densities.

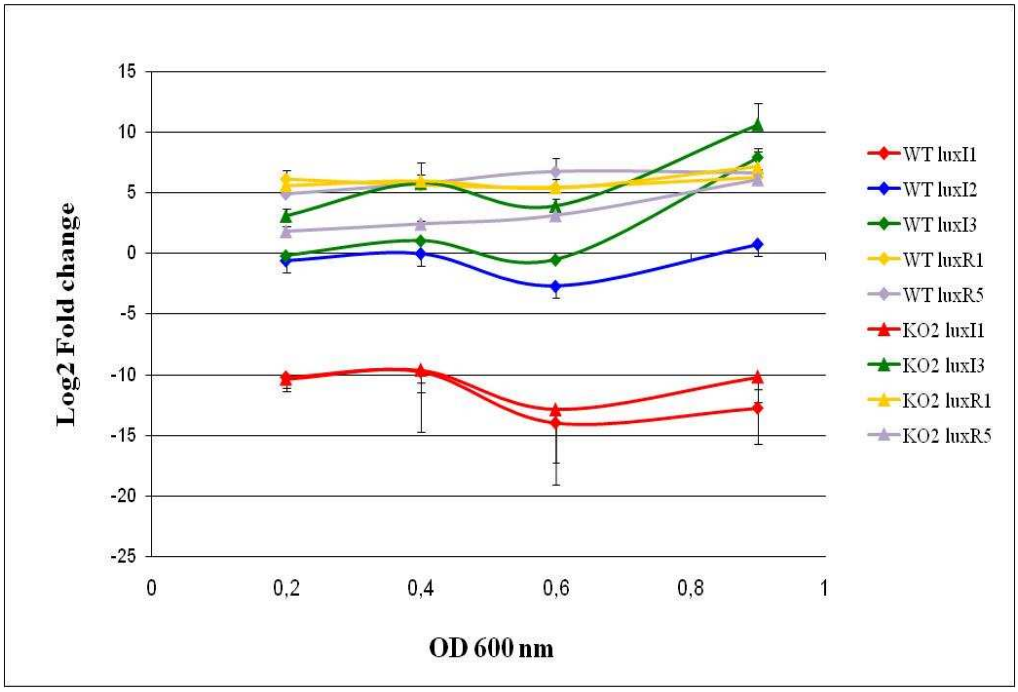

Figure 50 Expression of the *lux* genes in *D. shibae* DFL-12 Δ*luxI*$_2$ compared to the wild type.

Presented is the expression of the *lux* genes at four different optical densities in the *D. shibae* DFL-12 Δ*luxI*$_2$ compared to the wild type. Wild type (WT) gene expression is marked by rhombuses, gene expression of the mutant (KO2) by triangles. Expression of *luxI*$_1$ is depicted in red. Blue lines show the expression of *luxI*$_2$, which is missing for the mutant. Green lines correspond to *luxI*$_3$. The two regulators are illustrated in yellow, LuxR$_1$ and in violet, LuxR$_5$. Mean values of three technical replicates from one biological sample are presented as Log2 fold change relative to the housekeeping gene *gyrA* at four different optical densities.

Loss of *luxI*$_1$ resulted in a decreased expression of all *lux* genes, except for *luxR*$_1$. Transcription of the synthases *luxI*$_2$ and *luxI*$_3$ was repressed and the regulator LuxR$_5$ was more affected than LuxR$_1$ regarding to a decreased expression. At an optical density of 0.6, expression of *luxI*$_2$ and *luxI*$_3$ slightly increased. The lack of detectable AHL production in the *luxI*$_1$ mutant is in accordance with the downregulation of *luxI*$_2$ and *luxI*$_3$. Furthermore, *luxI*$_1$ could play a significant role in QS regulation of *D. shibae* DFL-12. Loss of *luxI*$_2$ resulted in a slightly increased *luxI*$_3$ expression. The regulator LuxR$_1$ was unaffected and regulator LuxR$_5$ showed a decreased transcription rate, implying a shared regulation with LuxI$_2$. Although QS genes are known to be autoregulated and their expression should increase with increasing cell density, none of the *D. shibae* DFL-12 QS genes is transcribed in a QS dependent manner.

Because of the strong transcriptional changes in *lux* gene expression and the lack of AHL production caused by the *luxI*$_1$ mutation, *luxI*$_1$ mediated autoinducer signals seem to play a key role in the QS system of *D. shibae* DFL-12.

For that reason, the priority of this thesis was to characterize the phenotypical changes caused by the *luxI*$_1$ knock-out as well as transcriptome modifications.

4.7 Genetic complementation of *D. shibae* DFL-12 Δ*luxI*$_1$ and phenotypic analysis

4.7.1 Growth

To ensure that all phenotypical changes were caused by the *luxI*$_1$ replacement and that they were not due to secondary mutations, experiments were carried out in addition with the *D. shibae* DFL-12 Comp1 complementation strain to restore the wild type phenotype. *D. shibae* DFL-12 Δ*luxI*$_1$ carrying the unmodified complementation vector Comp0 was also included, to ensure that the wild type recovery was due to *luxI*$_1$ and not to the vector. Growth was determined by measuring the optical density at 600nm. The cell number (cells/ml) was determined by flow cytometry which was performed by Hui Wang.

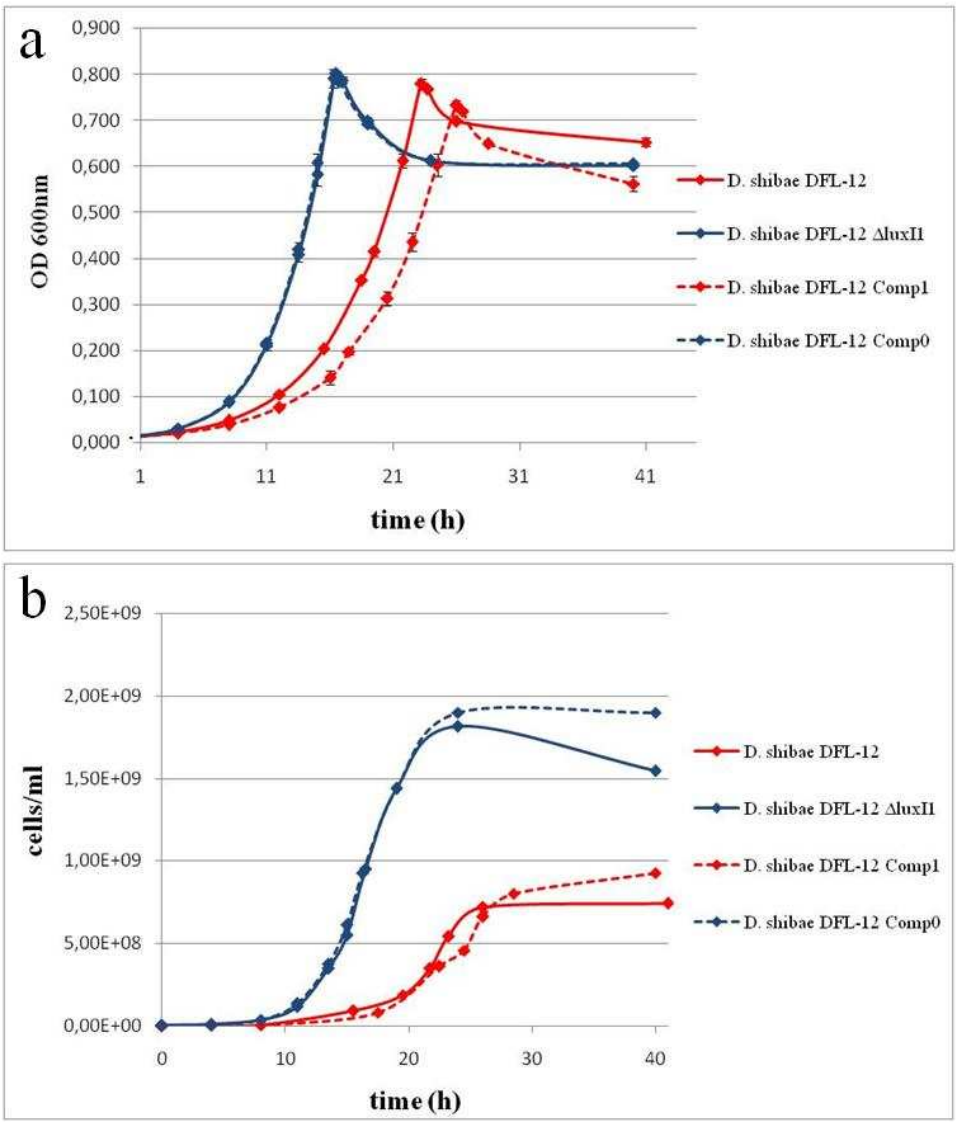

Figure 51 Growth curves and cell numbers of the Δ*luxI*$_1$ mutant and complementation strains compared to *D. shibae* DFL-12 in SWM with 5 mM succinate.

a) Growth of wild type and mutant are represented by solid lines. The wild type is depicted in red and Δ*luxI*$_1$in blue. Growth of the complementation strains is shown as dotted lines. Comp1 is depicted in red and Comp0 in blue. Presented are the mean values of three biological replicates. b) Determination of the cell numbers (cells/ml) of the wild type, mutant and complementation strains by flow cytometry.

Growth rate (μ) $$\mu = \frac{\ln X - \ln X_0}{t\text{-}t_0} = \frac{\ln \frac{X}{X_0}}{t\text{-}t_0}$$

Generation time (t_G) $$t_G = \frac{\ln 2}{\mu}$$

Division rate (g) $$g = \frac{1}{t_G}$$

Table 15 Growth rate (μ), generation time (t_G) and division rate (g) of wild type, mutant and complementation strain.

For calculation, values X and X_0 and corresponding time points of the logarithmic phase were chosen.

	X (cells/ml)	X_0 (cells/ml)	t (h)	t_0 (h)	μ (h^{-1})	t_G (h)	g (h^{-1})
D. shibae DFL-12	5.42E+08	3.48E+08	23.25	21.75	0.295	2.34	0.427
D. shibae DFL-12 ΔluxI1	9.49E+08	5.50E+08	16.5	15	0.364	1.90	0.527
D. shibae DFL-12 Comp1	6.63E+08	4.59E+08	26	24.5	0.245	2.82	0.355
D. shibae DFL-12 Comp0	9.28E+08	6.14E+08	16.25	15	0.330	2.01	0.478

The complementation vector itself had no influence on the Δ*luxI*$_1$ mutant growth behaviour. The Comp0 strain grew identical to the mutant (Figure 51, blue, dotted line). The genetic complementation with plasmid pBBR1MCS2 Comp1 resulted in recovery of growth almost identical to the wild type, except for a slightly delayed growth rate and a decreased final optical density (Figure 51a; red, dotted line).

Considering the optical density it could be expected that wild type and mutant reach the same final cell number but regarding the mutant the optical density did not correspond to the cell number. When *D. shibae* DFL-12 reached the stationary phase, also the maximum cell number was obtained ($7x10^8$ cells/ml) and remained constant. When *D. shibae* DFL-12 Δ*luxI*$_1$ reached the stationary phase according to the optical density, just half of the maximum cell number was obtained, constantly increasing to a maximum of $1.8x10^9$ cells/ml in the mid stationary phase.

Calculation of the growth parameters like the growth rate, generation time and division rate revealed that the mutant had increased growth-and division rates while the generation time was shortened from 2.34 hours to 1.90 hours compared to the wild type.

The complementation of the mutant was successful concerning the cell number. Growth rate and division rate were lower and the generation time was slightly increased compared to the wild type which reflects the delayed growth as shown in Figure 51a.

4.7.2 Cell morphology

The cell morphology of the wild type, mutant and complementation strain were investigated using light microscopy, scanning electron microscopy (SEM) and transmission electron microscopy (TEM).

Figure 52 represent SEM micrographs of cells of *D. shibae* DFL-12, *D. shibae* DFL-12 Δ*luxI*$_1$ and *D. shibae* DFL-12 Comp1 at different optical densities and various magnifications. The cell morphology of the wild type was heterogeneous and cells were extremely variable in length and width. Cells were small cocci, oval rods, bottle-shaped or elongated. After 45 hours of cultivation, in late stationary phase, the cells produced filaments (Figure 52, black arrows) to attach to the surface and were sticking to each other and formed small clusters. The mid row depicts the cell morphology of the *luxI*$_1$ mutant. Mutant cells were homogeneous, small cocci. No other type of morphology appeared during cultivation. At late stationary phase, after 47 hours of incubation, the production of exopolysaccharides in the mutant was strongly enhanced compared to the wild type. Formation of a biofilm matrix (Figure 52, black arrows) was well advanced. Mostly all mutant cells were clustering together whereas the picture of the wild type (Figure 52, 45 hours, 2.000 x magnification) illustrates even more single cells. The bottom row demonstrates the morphology of the Δ*luxI*$_1$ complementation strain Comp1. The cell morphology was recovered and cells had the same characteristics as the wild type. Also the matrix formation was similar to the wild type.

SEM micrographs of *D. shibae* DFL-12 Comp0 cells were identical to the Δ*luxI*$_1$ mutant cells (data not shown).

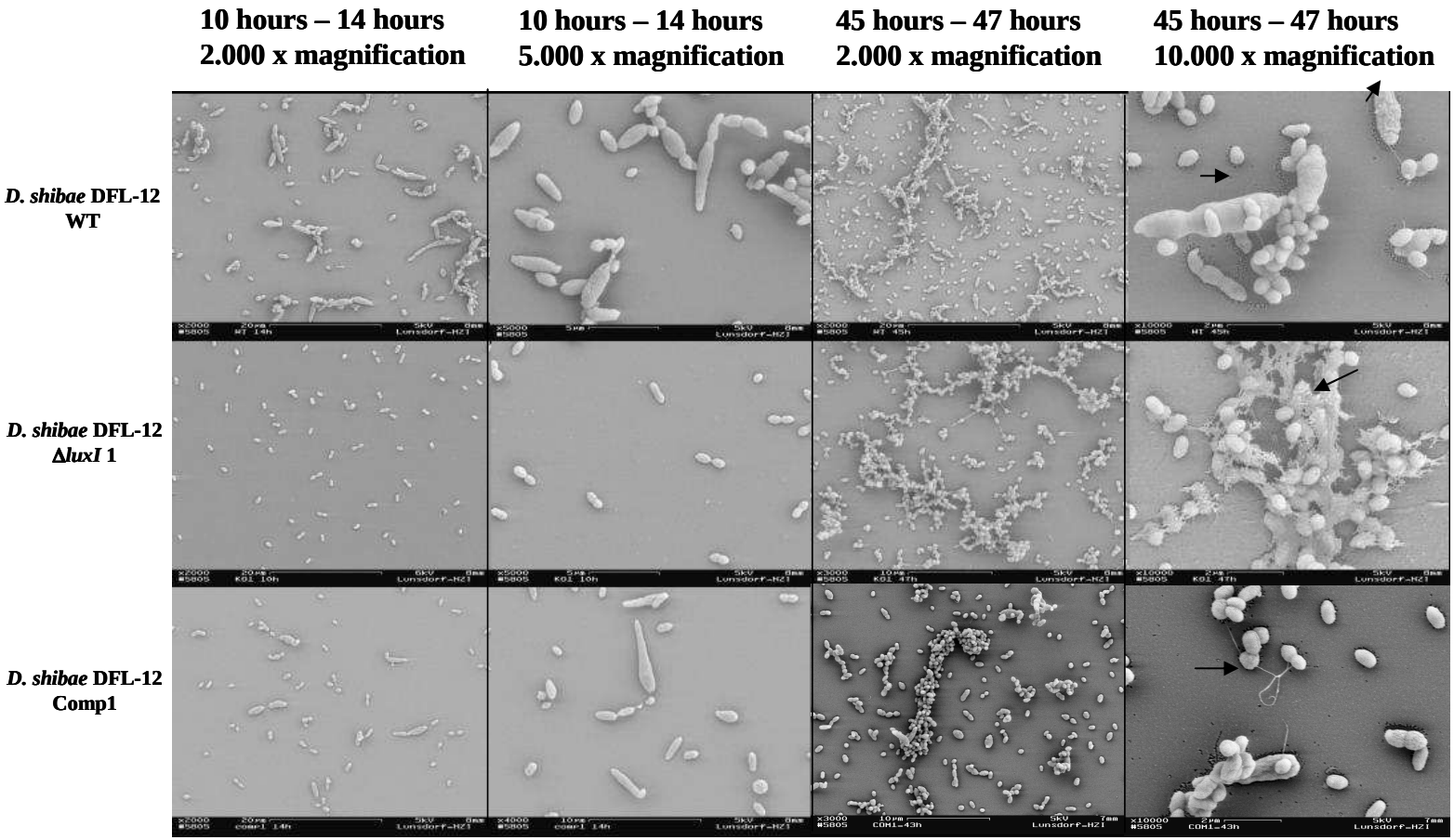

Figure 52 Scanning electron microscopy (SEM) of cells of strains *D. shibae* DFL-12, *D. shibae* DFL-12 Δ*luxI*$_1$ and *D. shibae* DFL-12 Comp1 at different time points.

2.000 to 10.000 x maginification were used to illustrate the variable cell morphology of the three strains. Black arrows indicate single exopolysacchharide filaments (wild type/Comp1) or a developing biofilm matrix (mutant).

To quantify the morphological distribution, 50.000 cells were analyzed using cell flow cytometry. Therefore *D. shibae* DFL-12, *D. shibae* DFL-12 Δ*luxI*$_1$, *D. shibae* DFL-12 Comp1 and *D. shibae* DFL-12 Comp0 were cultivated in SWM 5 mM succinate and samples were taken at OD_{600nm} 0.2, 0.4, 0.6, 0.8, S1 (early stationary phase, OD_{600nm} 0.9) and S2 (late stationary phase, OD_{600nm} 0.6). 1 ml of the samples were diluted to an optimal cell concentration of 10^{-6} cells/ml with PBS buffer and cells were stained with 10 µl of a SybrGreenI solution (100 x concentrate in DMSO). Single fluorescent cells were identified and the intensity measured by a fluorescence detector comprising a FITC-A filter. Logarithmic transformed intensities (log arbitrary units, logAU) were visualized for all four strains as density plot, where the cell size presumably correlates with the FITC-A intensity. The larger the cells were the more intense was the FITC-A signal.

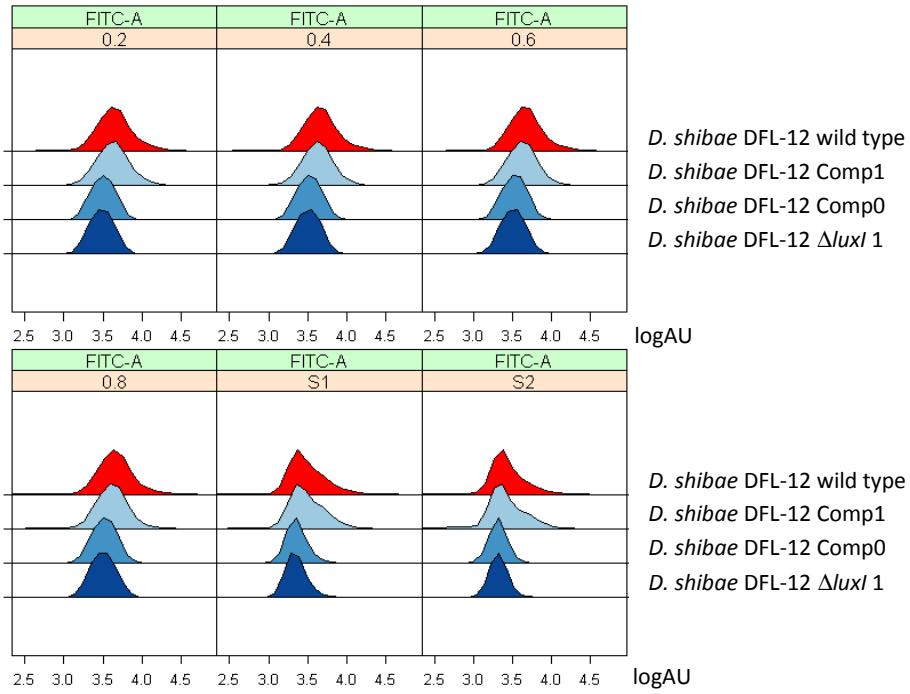

Figure 53 Density plot of *D. shibae* DFL-12 wild type, mutant and complementation strains.

The morphological distribution of 50.000 analyzed cells is presented as logarithmic transformed FITC-A intensity (logAU) resulting in an bell-shaped distribution function. The distribution of cells was analyzed at six different optical densities (OD 0.2, 0.4, 0.6, 0.8, S1 early stationary phase and S2 late stationary phase).

Values of the median, mean and variance were calculated (Table 16). The arithmetic mean is the average of all values and is highly sensitive to outliers. The median is the “middle value” in the data set. The variance describes how far the data lie from the mean (expected value). It is a quantitative measure of variability.

$$\text{Mean} = \frac{1}{n}\sum_{i=1}^{n} X_i$$

$$\text{Variance} = \frac{\sum (y - \bar{y})^2}{n-1}$$

x/y = single sample value
$\bar{y}$ = mean of all sample values
n = number of values
i = 1, …, n

$$\text{Median} = \begin{cases} \text{odd } n & X_i \quad i = \frac{n+1}{2} \\ \text{even } n & \frac{1}{2}\left(X_i + X_j\right) \quad i = \frac{n}{2}, \; j = \frac{n}{2}+1 \end{cases}$$

Table 16 Mean, median and variance values presented as log arbitrary units, logAU data.

OD02	mean	median	variance
D. shibae DFL-12 WT	*3,6115*	3,6496	0,1919
D. shibae DFL-12 Comp1	3,5753	3,6359	0,1847
D. shibae DFL-12 Comp0	3,4759	3,5097	0,0915
D. shibae DFL-12 ΔluxI 1	3,4604	3,4902	0,0899

OD04	mean	median	variance
D. shibae DFL-12 WT	3,4362	3,6493	0,6774
D. shibae DFL-12 Comp1	3,4881	3,63	0,3916
D. shibae DFL-12 Comp0	3,3848	3,5188	0,3601
D. shibae DFL-12 ΔluxI 1	3,406	3,5065	0,2933

OD06	mean	median	variance
D. shibae DFL-12 WT	3,5487	3,6669	0,4069
D. shibae DFL-12 Comp1	3,5304	3,6374	0,3029
D. shibae DFL-12 Comp0	3,4487	3,5312	0,2189
D. shibae DFL-12 ΔluxI 1	3,2976	3,4948	0,5086

OD08	mean	median	variance
D. shibae DFL-12 WT	3,4825	3,6509	0,5191
D. shibae DFL-12 Comp1	3,5478	3,6283	0,227
D. shibae DFL-12 Comp0	3,4805	3,5271	0,1255
D. shibae DFL-12 ΔluxI 1	3,4694	3,5081	0,1115

OD S1	mean	median	variance
D. shibae DFL-12 WT	3,4359	3,4006	0,2179
D. shibae DFL-12 Comp1	3,4051	3,4104	0,2596
D. shibae DFL-12 Comp0	3,3026	3,3311	0,1417
D. shibae DFL-12 ΔluxI 1	3,3264	3,3244	0,0708

OD S2	mean	median	variance
D. shibae DFL-12 WT	3,3819	3,3599	0,2169
D. shibae DFL-12 Comp1	3,3506	3,344	0,2271
D. shibae DFL-12 Comp0	3,2989	3,3112	0,0495
D. shibae DFL-12 ΔluxI 1	3,278	3,3147	0,1072

Values of mean and median which were almost similar indicating a normal (Gaussian) distribution. That was the case for the distribution of the mutant and Comp0 cells. The variance values of these two strains were relatively small in contrast to the wild type and Comp1. Cells of the wild type and Comp1 showed a skewed distribution. In these populations the amount of larger cells = enhanced FITC-A intensity was strikingly increased and the curve was skewed to the right

site. Also the variance values of wild type and Comp1 were two times to five times higher than the mutant/Comp0 variances, confirming a variable cell morphology. Furthermore, when the stationary phase was reached, the median values of all strains shift to smaller values, meaning that the cell size in general decreased.

4.7.3 Analyses of storage compounds

The $\Delta luxI_1$ strain lost the capability to form large and variable cell types. To understand the advantage of forming such kind of cells, the structure of wild type and mutant cells were investigated using nile red dye to stain lipid granules and transmission electron microscopy to clarify the intracellular organisation.

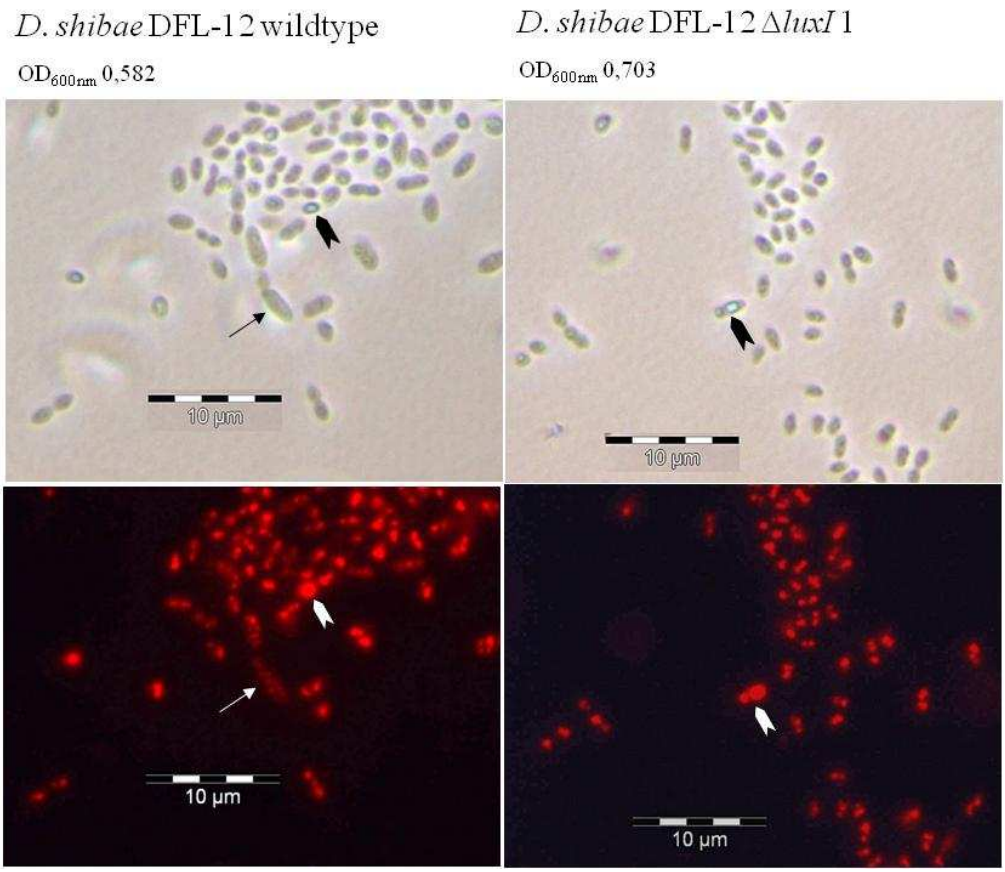

Figure 54 Analysis of lipidic inclusions using nile red fluorescent staining.

Cells of *D. shibae* DFL-12 and $\Delta luxI_1$ (log phase) were stained with nile red and investigated with a fluorescence microscope. Smaller cells of wild type and mutant predominantly comprise definite lipidic inclusions, which occur as bright red spot (arrow heads in black and white). Some cells comprise also lipid granules which are widely distributed throughout the cell without clear compartmentation and occur as diffuse signal (black and white arrows, wild type).

Using nile red staining, lipidic inclusions could be visualized inside the wild type and mutant cells. During cultivation in SWM 5 mM succinate the wild type and

mutant cells produced lots of lipidic storage compounds. The organisation of these inclusions inside the cell differed, but there was no distinction between wild type and mutant. Both strains showed various organisation patterns, regarding the concentration and compartmentation. The major part of cells comprised definite lipidic inclusions, which occurred as intense red spot, whereas some cells comprised lipidic inclusions, which were not definite and more widely distributed throughout the cell. Lipids occurred as diffuse red signal.

In the stationary phase almost all storage compounds were exhausted and could not be visualized by nile red staining. Just in a few large cells of the wild type, lipidic inclusions remained (data not shown).

To give an insight into the inner cell structure, TEM was used to investigate the wild type and mutant strain (early log phase). Additionally the Comp1 and Comp0 complementations strains were examined. Their TEM micrographs corresponded to wild type and mutant results, respectively.

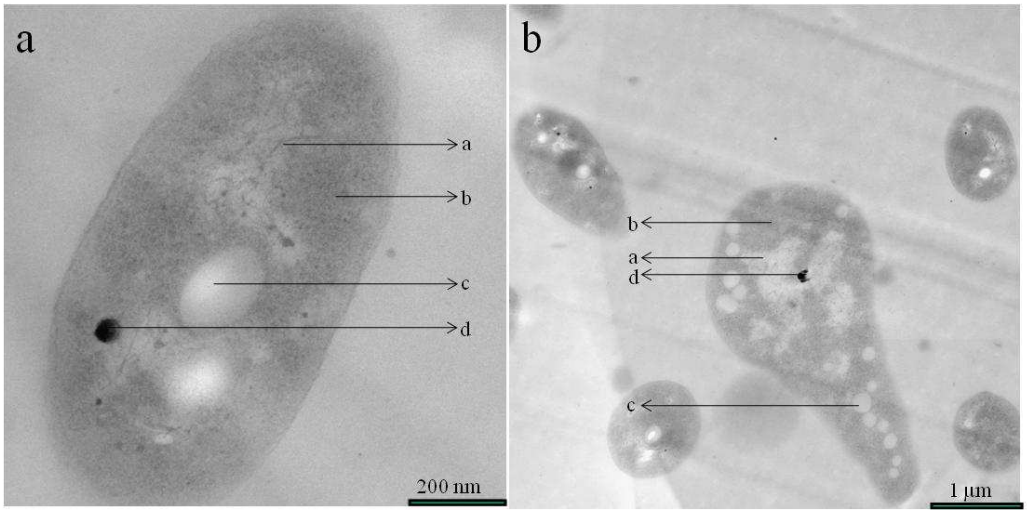

Figure 55 TEM micrographs of a) *D. shibae* DFL-12 Δ*luxI*$_1$ and b) *D. shibae* DFL-12.

Wild type and mutant cells are similar regarding the inner structure. They both are tightly packed with DNA (a) and ribosomes (b) and comprise lipidic inclusions (c) and polyphosphates (d).

There was no difference between the wild type and the Δ*luxI*$_1$ cells regarding the inner structure when they were cultivated in SWM 5mM succinate. Cells of both strains comprised high concentration of storage compounds, such as lipidic

inclusions and polyphosphates. In larger cells the concentration of lipidic storage compounds was higher. To clarify if the lipidic inclusions belong to the group of polyhydroxyalkanoats (PHAs), they would have to be extracted and analysed. Furthermore the cytoplasma was tightly packed with ribosomes and the DNA was distributed throughout the cell.

4.7.4 Motility

To investigate the motility of the Δ*luxI*$_1$ strain compared to the wild type and complementation strains, "swimming" plates were prepared using MB solidified with 0.3% agar. Strains were precultivated in SWM 5 mM succinate and 10 µl of the cell suspension were placed as single drop in the center of the plates. Afterwards the plates were incubated for 20 days (circadian rhythm) at room temperature in a humidity chamber to avoid dehydration of the agar surface.

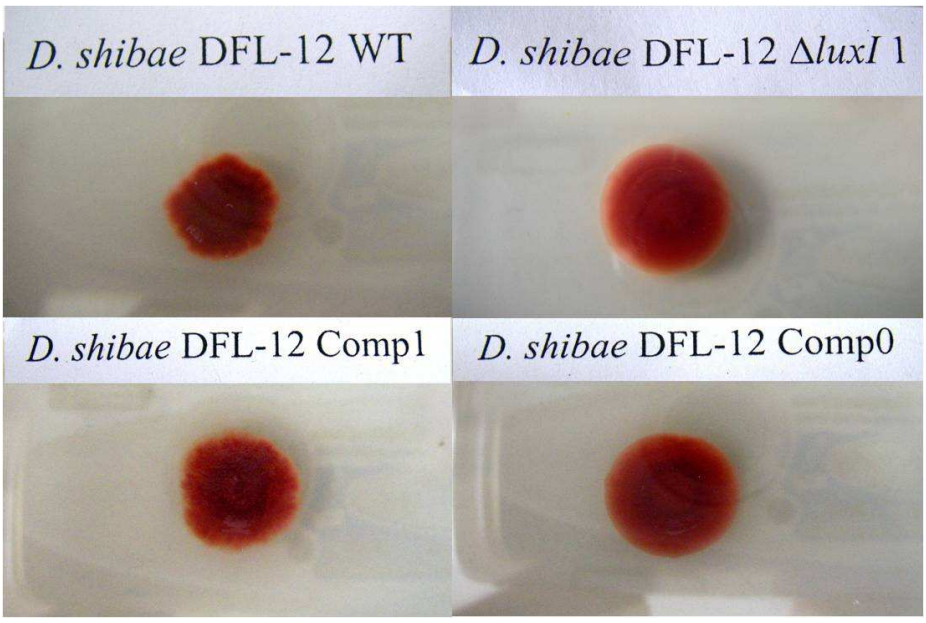

Figure 56 Motility Assay.

Motility of *D. shibae* DFL-12, Δ*luxI*$_1$ and complementation strains Comp0/Comp1 is tested using 0.3% "swimming" agar plates.

Colony shape and margin of wild type and mutant varied. The colony shape of the wild type was irregular with a frayed margin. The Δ*luxI*$_1$ mutant had a round colony shape with a smooth margin. Complementation of the *luxI*$_1$ replacement (Comp1) resulted in a restored irregular colony morphology whereas the complementation with the unmodified vector (Comp0) has no influence and colony morphology was similar to the mutant. Motility and with this flagellar assembly are known quorum sensing regulated traits. The varied colony morphology of the mutant could be an indication of flagellar gene regulation by *luxI*$_1$ mediated quorum sensing.

4.7.5 AHL production

Previous bioassay analyses of the wild type and mutant strains demonstrated that the Δ*luxI*$_1$ mutant was not able to produce detectable amounts of any AHLs. To confirm a successful complementation and restoration of the AHL production, dichloromethane extracts were prepared of wild type, mutant and complementation strain cultivated in SWM with 5 mM succinate.

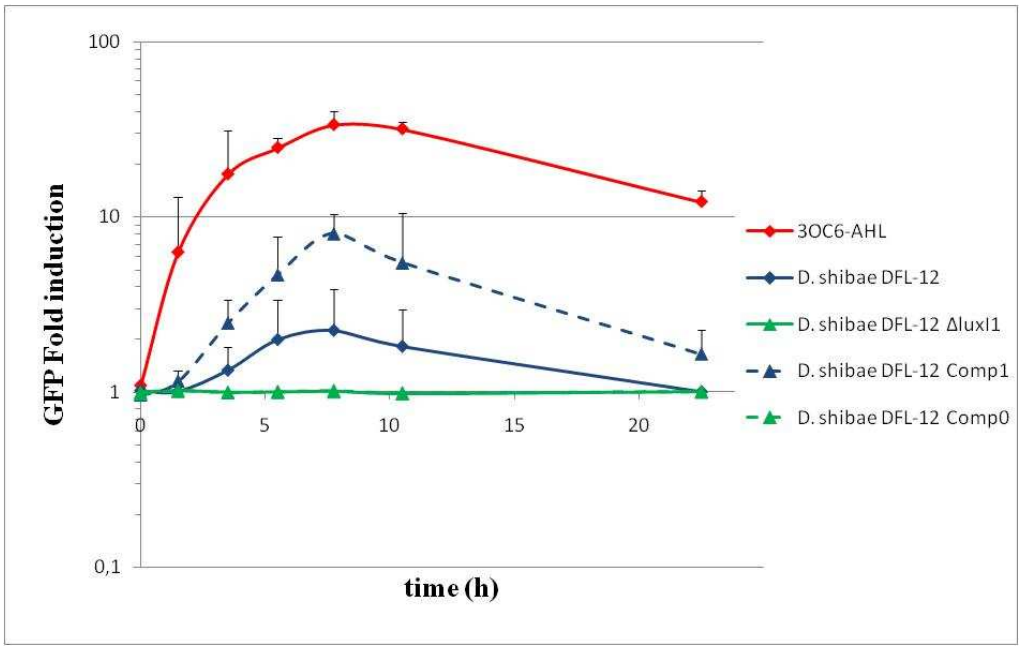

Figure 57 Detection of short-chain AHLs produced by *D. shibae* DFL-12, Δ*luxI*$_1$, Comp1 and Comp0 during cultivation in SWM with 5 mM succinate, respectively.

Detection of short-chain AHLs by use of the sensor strain *E. coli* pJBA132. In red, the positive control (3OC6 AHL, 2.4 µM) is depicted. The blue, solid line displays the AHL extract of *D. shibae* DFL-12 and the blue, dotted line of *D. shibae* DFL-12 Comp1. The green, solid line corresponds to the AHL extract of *D. shibae* DFL-12 Δ*luxI*$_1$, the green, dotted line to *D. shibae* DFL-12 Comp0. Presented are the mean values of three technical replicates from each of two biological replicates.

The production of short-chain AHLs in the mutant was restored by the genetic complementation with the vector pBBR1MCS2 Comp1. Due to the overexpression of *luxI*$_1$ caused by the constitutive gentamicin promoter, the short-chain AHL synthesis was enhanced compared to the wild type. The complementation vector on its own did not influence the mutant strain. Therefore AHL production of strain *D. shibae* DFL-12 Comp0 was still shut down.

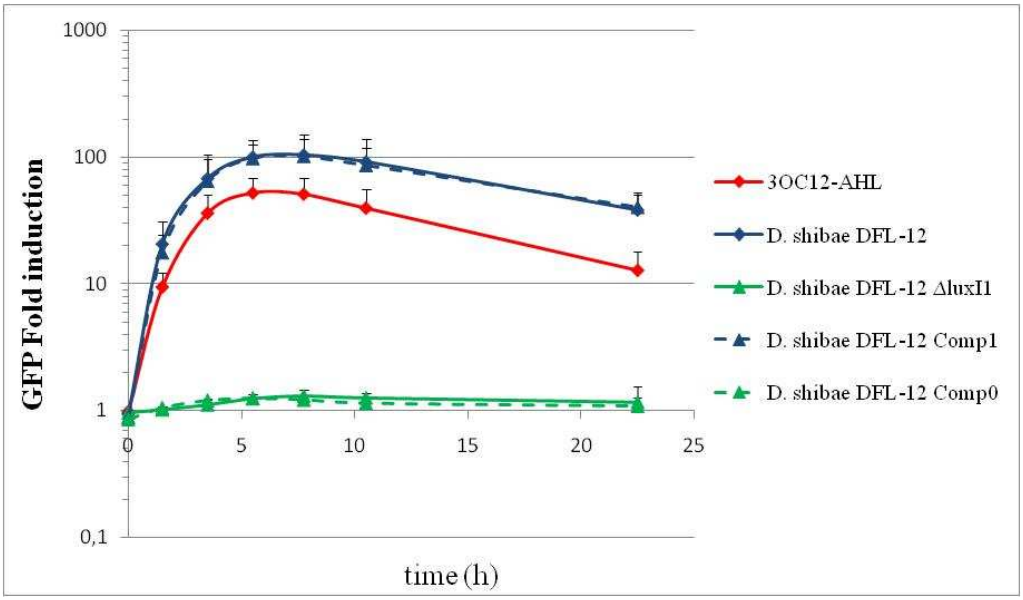

Figure 58 Detection of long-chain AHLs produced by *D. shibae* DFL-12, Δ*luxI*$_1$, Comp1 and Comp0 during cultivation in SWM with 5 mM succinate, respectively.

Detection of long-chain AHLs by use of the sensor strain *P. putida* pKR-C12. In red, the positive control (3OC12 AHL, 2.4 µM) is depicted. The blue, solid line displays the AHL extract of *D. shibae* DFL-12 and the blue, dotted line of *D. shibae* DFL-12 Comp1. The green, solid line corresponds to the AHL extract of *D. shibae* DFL-12 Δ*luxI*$_1$, the green, dotted line to *D. shibae* DFL-12 Comp0. Presented are the mean values of three technical replicates from each of two biological replicates.

Production of long-chain AHLs in the mutant was also restored by genetic complementation using vector pBBR1MCS2 Comp1. The long-chain AHL synthesis in the complentation strain was as high as the wild type synthesis. Again, vector Comp0 showed no influence and AHL production was lacking.

The *luxI*$_1$ deletion mutant was also chemically complemented by addition of 1 µg and 10 µg of C8-HSL and 1 µg and 10 µg of C18-HSL during the AHL cultivation. According to the bioassay results, the chemical complementation did not restore the lacking AHL production in the mutant (data not shown).

All extracts were additionally analysed by GC-MS. Results are presented in Table 17.

Table 17 GC-MS analyses of AHL extracts produced by *D. shibae* DFL-12 wild type, Δ*luxI* 1, Comp0 and Comp1, respectively.

AHLs in brackets present artificial AHLs which were added to chemically complement the mutant strain.

Strain	Medium	GC-MS Analysis
D. shibae DFL-12	SWM 50 mM succinate	C18-en-HSL, C18-dien-HSL
D. shibae DFL-12 Δ*luxI*$_1$	SWM 50 mM succinate	-
D. shibae DFL-12 Comp1	SWM 50 mM succinate	C16-en-HSL, C16-dien-HSL, C18-en-HSL, C18-dien-HSL
D. shibae DFL-12 Δ*luxI*$_1$ (chem. compl.)	SWM 50 mM succinate + 1 µg C8-HSL	(C8-HSL)
	SWM 50 mM succinate + 10 µg C8-HSL	(C8-HSL)
	SWM 50 mM succinate + 1 µg C18-HSL	(C18-HSL)
	SWM 50 mM succinate + 10 µg C18-HSL	C16-en-HSL, C16-dien-HSL (C18-HSL)

D. shibae DFL-12 wild type was producing C18-en-HSL and C18-dien-HSL.

In the extract of the mutant strain neither short-chain nor long-chain AHLs could be detected. In the genetic complementation of the mutant (Comp1), the production of long-chain AHLs, such as C16-en and C16-dien-HSL could be detected, as well as C18-en and C18-dien-HSL.

When Δ*luxI* 1was chemically complemented with 10 µg of C18-HSL, C16-en and C16-dien-HSL could be obtained.

In no case, the production of the expected C8-HSL could be restored by genetic or chemical complementation. Moreover, C8-HSL could not be detected in the wild type extract via bioassay and GC-MS analyses.

4.7.6 qRT-PCR of *D. shibae* DFL-12, Δ*luxI*$_1$ and Comp1

The expression of the *lux* genes in the *luxI*$_1$ mutant compared to the wild type was already presented in Figure 49. All *lux* genes were affected resulting in a decreased expression, except for the LuxR$_1$ regulator, which was not influenced by the knock-out.

To confirm the recovery of *lux* gene expression in the complementation strain Comp1, RNA was extracted at OD$_{600nm}$ 0.2, 0.4, 0.6 and 0.8, cDNA prepared and used for qRT-PCR analyses compared to the wild type and mutant.

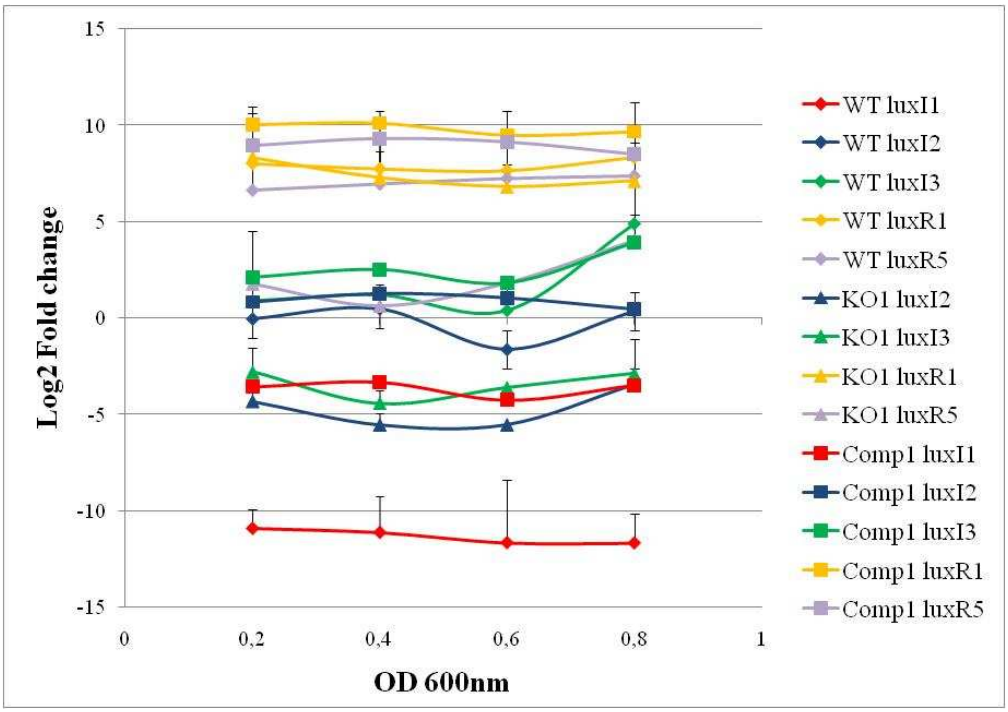

Figure 59 Expression of the *lux* genes in *D. shibae* DFL-12 Comp1 compared to the wild type and mutant.

Presented is the expression of the *lux* genes at four different optical densities in *D. shibae* DFL-12 Comp1 compared to the wild type and mutant. Wild type gene expression is visualized by rhombuses, gene expression of the mutant by triangles and the gene expression of the complementation strain is marked by squares. Presented are the mean values of three technical replicates from one biological sample (Comp1) and from each of two biological replicates (wild type and mutant).

The expression of the *lux* genes could be restored in the complementation strain Comp1. Due to the constitutive gentamicin promoter which controls the overexpression of *luxI*$_1$, the transcription rate of *luxI*$_1$ increased 10^5-fold compared to the wild type. The expression of the synthases *luxI*$_2$ and *luxI*$_3$ was also enhanced compared to the wild type level. *LuxI*$_2$ showed no QS dependent

increase of the transcription rate, but rather a constitutive expression. At OD_{600nm} 0.6, expression of *luxI*$_3$ increased. The transcription of Comp1 *luxR*$_1$ and *luxR*$_2$ was slightly enhanced compared to the wild type.

4.8 Microarray analyses of *D. shibae* DFL-12 Δ*luxI*$_1$

Quorum sensing regulated traits were identified by transcriptome profiling using eight whole genome microarrays. Using the Cy3 and Cy5 ULSTM fluorescent labeling kit, two-color-arrays were prepared by which the transcriptome of mutant and wild type at four different optical densities from two biological replicates was compared.

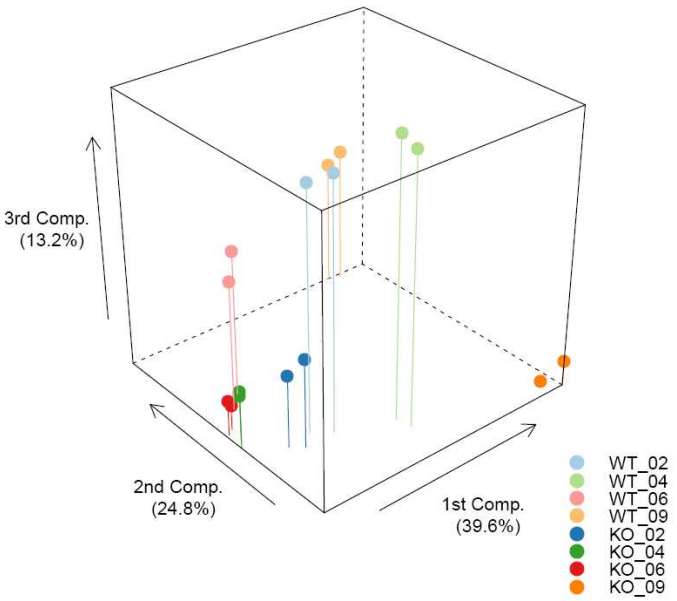

Figure 60 Principal-component analysis of the microarray samples.

The first three components, explaining 77.6% of total sample variability in gene expression, are plotted. The distance between samples on the plot is proportional to the variance between these samples by expression of genes clustered in the first three components. The samples of *D. shibae* DFL-12 are shown in a lighter color. WT, *D. shibae* DFL-12; KO, *D. shibae* DFL-12 Δ*luxI*$_1$. Units 02, 04, 06 and 09 correspond to an OD_{600nm} of 0.2, 0.4, 0.6 and 0.9.

The raw data extracted from the Agilent microarray images were processed by using the Bioconductor software packages. A principal-component analysis was performed on the expression data from all samples to highlight their variability. As shown in Figure 60, biological replicates grouped closely together which

indicates a high correlation. The data sets of OD_{600nm} 0.2 and 0.6 of the wild type were similar to the corresponding OD_{600nm} of the *luxI*$_1$ mutant, just showing 13.2% variability separated by the third component. The data sets of OD_{600nm} 0.4 of wildtype and mutant were clearly separated by the first and third component, explaining 52.8% of total variability, whereas the data sets of OD_{600nm} 0.9 of wildtype and mutant were clearly separated by the second and third component, explaining 38% of total variability. The data sets of the stationary phase (OD_{600nm} 0.9) of the mutant were distant from all other samples. The Linear Models for Microarray Analysis (LIMMA) package was used for the identification of differentially expressed genes. Comparison of the transcription profiles of the *luxI*$_1$ mutant and the wild type revealed a total of 347 genes (8.5% of the genome) that were differentially expressed (log2 fold change of = 2; p-value > 0.01). For the complete list see Appendix III. K-Means clustering was used for cluster analysis which aimed to partition the differentially expressed genes into 6 clusters in which each gene belongs to the cluster with the nearest mean.

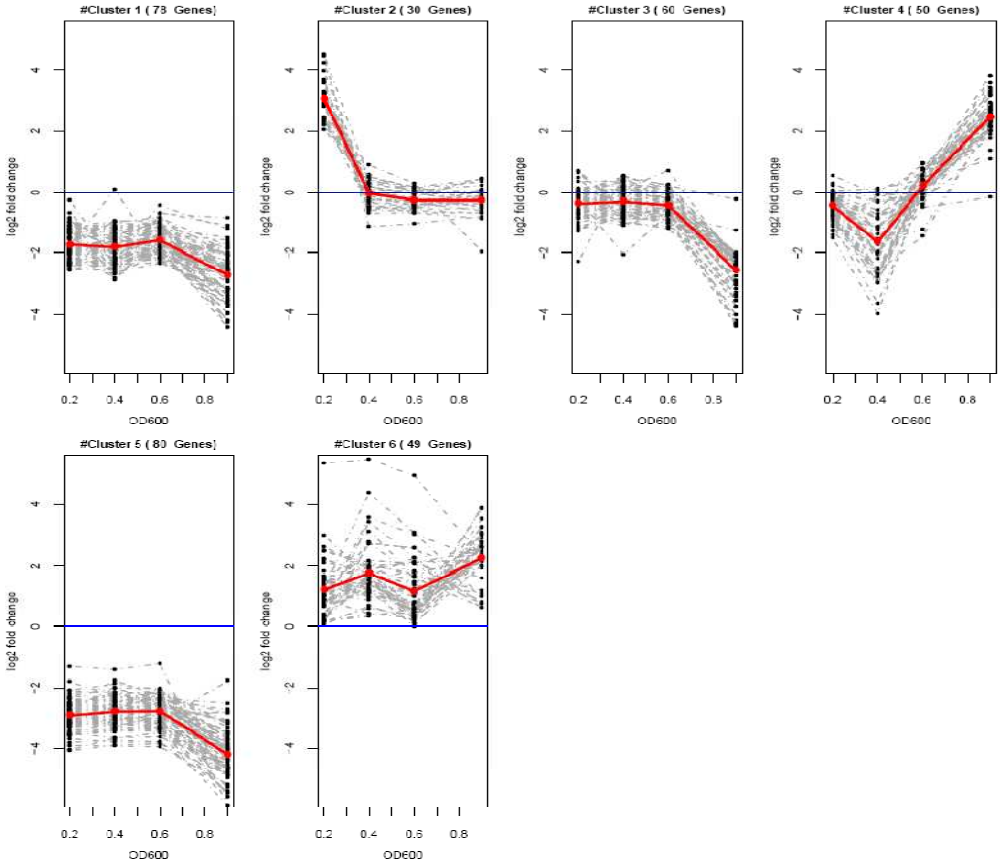

Figure 61 K-means partitioning of differentially expressed genes.

Results are presented as log2 Fold change against the optical density OD_{600nm}. Every single black dot is equivalent to one gene at OD_{600nm} 0.2, 0.4, 0.6 and 0.9, respectively. The red line depicts the mean value of the cluster.

Tendencies were visible within the six clusters. Clusters 1, 3 and 5 comprised genes which were continuously downregulated, with an enhanced downregulation in the stationary phase. Genes of cluster 2 were highly upregulated at the beginning of growth, but expression decreased to an almost unregulated level. Genes of cluster 4 were first downregulated and with increasing cell density, expression was highly upregulated. Cluster 6 comprised genes, continuously upregulated during cultivation. 138 hypothetical genes and 209 genes with known function were differentially expressed. The analytical method called Gene Set Enrichment Analysis (GSEA) was used for interpreting gene expression data. The method derives its power by focusing on gene sets, that is, groups of overrepresented genes within one cluster that share common biological functions, in this case, metabolic KEGG pathways.

Table 18 Gene Set Enrichment Analysis for KEGG pathways.

Through GSEA, regulated genes within one cluster which share common biological functions were assigned to metabolic KEGG pathways. The color code of the clusters reflects the regulation of inherent genes. Green: downregulated; red: upregulated; green-red transition: from downregulated to upregulated; red-green transition: from upregulated to downregulated.

cluster	KEGG Pathway	cluster	KEGG Pathway
1	Bacterial secretion system	5	Flagellar assembly
1	Flagellar assembly	5	Bacterial chemotaxis
1	Bacterial chemotaxis	5	Bacterial secretion system
		5	Two-component system
2	Inositol phosphate metabolism		
2	Glycine, serine and threonine metabolism	6	Valine, leucine and isoleucine degradation
		6	Sulfur metabolism
3	Nitrogen metabolism	6	Geraniol degradation
3	Vitamin B6 metabolism	6	Fatty acid metabolism
3	Propanoate metabolism		
4	Porphyrin and chlorophyll metabolism		
4	Carotenoid biosynthesis		
4	Biosynthesis of secondary metabolites		
4	One carbon pool by folate		
4	Terpenoid backbone biosynthesis		
4	Methane metabolism		

Most of the downregulated genes (cluster 1, 3, 5) are involved in biofilm formation or, more general, in the symbiotic lifestyle of *D. shibae* DFL-12.

Bacterial chemotaxis is used to “sense” possible food sources, while the flagellar assembly means cell motility. Bacterial secretion systems are important features for the establishment of the biofilm. Maybe the downregulated genes are a combination of features for *D. shibae* DFL-12 to “detect”, to “reach” and to “attach on” its algae host, which are regulated in a QS dependent manner.

4.8.1 Expression of the *lux* genes in *D. shibae* DFL-12 Δ*luxI*$_1$

Genes with a log2 fold change > 2.0 were selected for gene expression pattern discovery using K-means clustering. As shown in Figure 63, log2 fold changes of *luxI*$_1$, *luxI*$_2$ and *luxR*$_1$ were < 2.0. Therefore, genes were excluded from K-means clustering. The log2 fold change of *luxI*$_3$ and *luxR*$_5$ was > 2.0 and both genes were identified to be differentially expressed. To give an overview of the *lux* gene expression of wild type and mutant based on the microarray data, log2 intensities of both strains were presented in Figure 62.

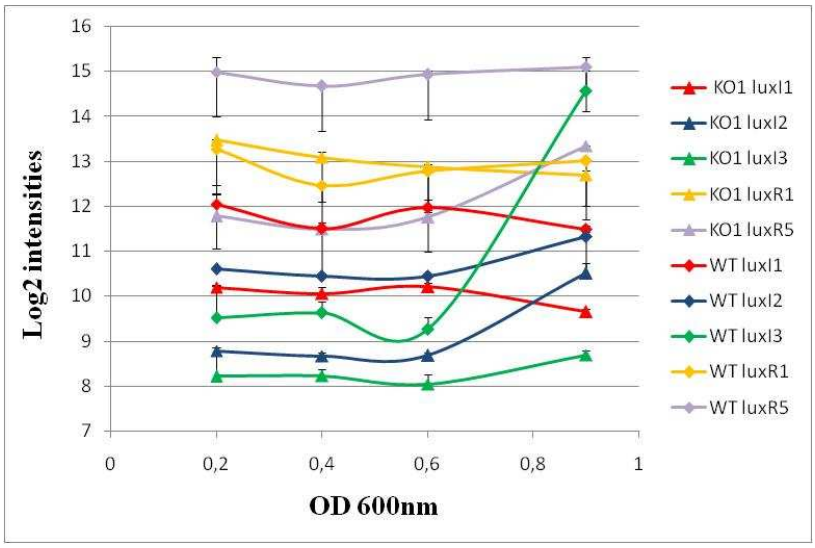

Figure 62 Expression of the *lux* genes of wild type and Δ*luxI*$_1$ mutant based on the microarray data.

Wild type (WT) gene expression is visualized by rhombuses, gene expression of the mutant (KO1) by triangles. Presented are the mean values of two biological replicates.

Log2 intensities of the *lux* gene expression were in accordance with the qRT-PCR results. All *lux* genes, except for *luxR*$_1$, were downregulated in the mutant. Based on the log2 intensities, the log2 fold changes of the *lux* genes were calculated and presented in Figure 63.

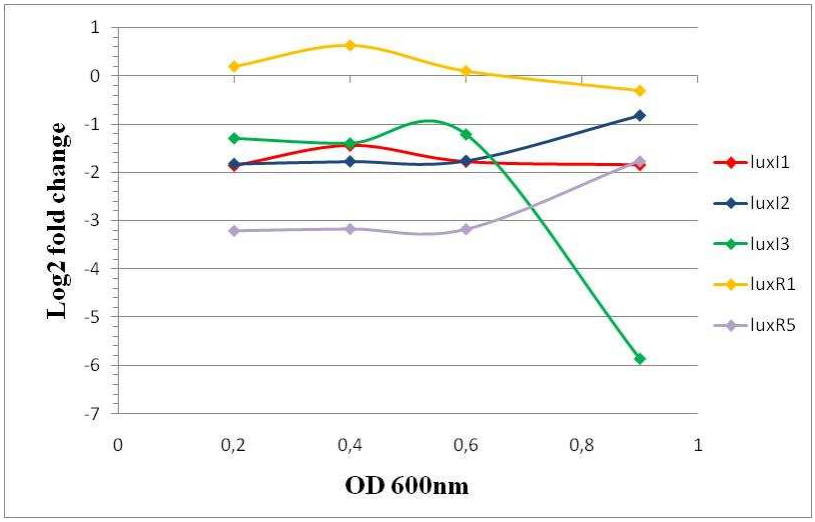

Figure 63 Differential expression of the *lux* genes in the Δ*luxI*$_1$ mutant compared to the wild type based on the microarray data.

4.8.2 Expression of *luxI*$_1$ in *D. shibae* DFL-12 Δ*luxI*$_1$

The last 188 bp of the *luxI*$_1$ coding sequence were part of the 3' flanking region which was used for homologous recombination. These nucleotides are still present in the knock-out strain. Three different probes (QS7, 8 and QS9; QS: quorum sensing) were designed for *luxI*$_1$. QS9 binds to the remaining *luxI*$_1$ base pairs in the knock-out and generates a positive signal for the *luxI*$_1$ gene (for the QS9 binding site see Appendix 9.2).

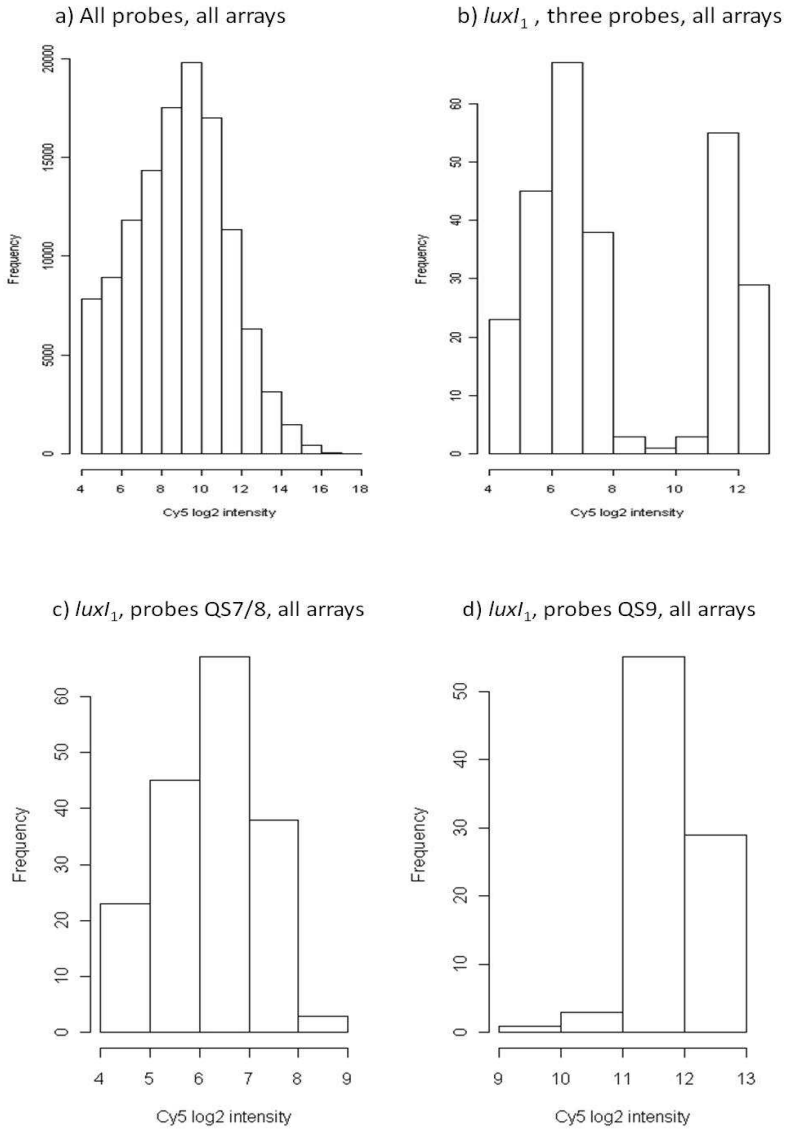

Figure 64 Comparison of probe intensities for all *luxI*$_1$ probes present on the microarray.

a) Distribution of log2 intensities of all mutant probes (Cy5) for all microarrays analysed. b) Distribution of log2 intensities for all copies of the three *luxI*$_1$ probes in the mutant (all microarays). c) and d) Seperation of b) by probes against parts of the *luxI*$_1$ sequence absent (QS7/8) or present (QS9) in the genome of *D. shibae* DFL-12 Δ*luxI*$_1$.

The log2 intensities of all probes for all microarrays analysed, ranged from 4 to 13 including the negative controls which generated signal intensities ranging from log2 = 7 to 9, although the *D. shibae* DFL-12 mRNA should not bind to these probes. The *luxI*$_1$ probes QS7 and QS8 also generated log2 intensities ranging from 4 to 9. This could be due to the propensity of non-specific binding to the glass surface or cross-hybridization. Log2 intensities of the *luxI*$_1$ probe QS9 were clearly increased (9-13). Transcription of the remaining 188 bp seemed to be highly induced by the constitutive gentamicin promoter and the mRNA could bind to the QS9 probe.

4.8.3 Expression of the orphan *luxR* in *D. shibae* DFL-12 Δ*luxI*$_1$

To indicate whether the knock-out of *luxI*$_1$ affected the orphan *luxR* expression, log2 intensities and log2 fold changes were calculated for the genes *luxR*$_2$, *luxR*$_3$ and *luxR*$_4$.

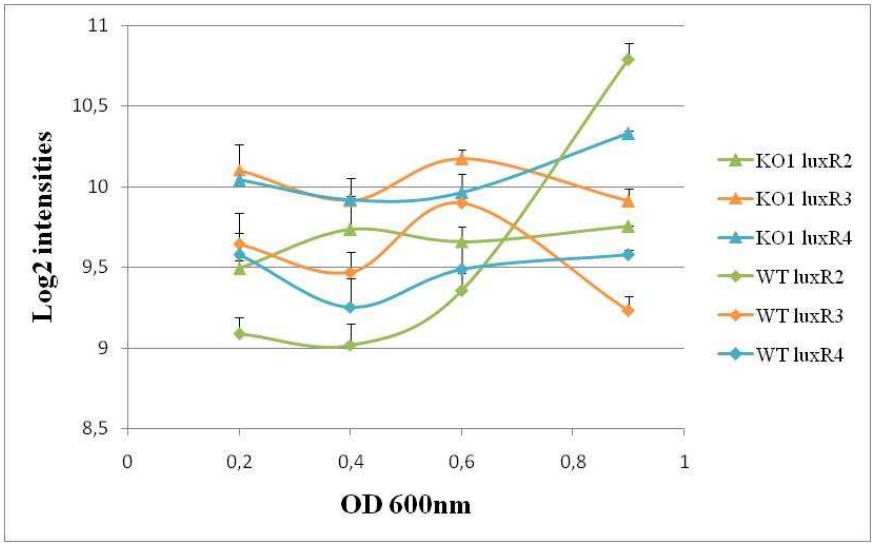

Figure 65 Expression of the orphan *luxR* of wild type and Δ*luxI*$_1$ mutant based on the microarray data.

Wild type (WT) gene expression is visualized by rhombuses, gene expression of the mutant (KO1) by triangles. Presented are the mean values of two biological replicates.

Log2 intensities of *luxR*$_3$ and *luxR*$_4$ were increased in the mutant compared to the wild type. The log2 intensity of *luxR*$_2$ in the wild type started with nine and increased in a QS dependent manner up to 10.8 while in the mutant the initial log2 intensity started with 9.5 but did not increase and remained stable.

Therefore the knock-out of *luxI*$_1$ seemed to influence also the orphan *luxR* expression, especially those of *luxR*$_2$.

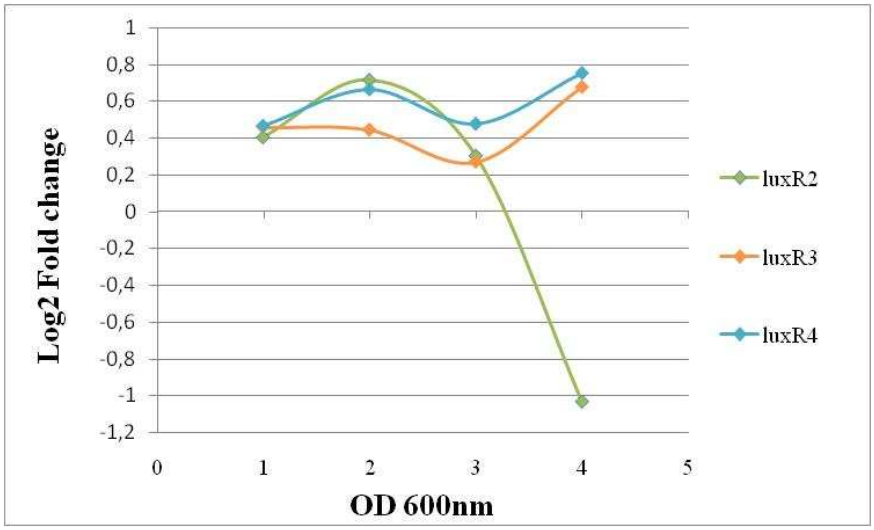

Figure 66 Differential expression of the orphan *luxR* regulators in the Δ*luxI*$_1$ mutant compared to the wild type based on the microarray data.

The orphan *luxR* genes were not considered for K-means clustering because of their log2 fold change <2.

4.8.4 Characteristics of prominent clusters

Genes of cluster 1 and 5 were continuously downregulated. Chromosomal flagellar assembly genes form a major part of both clusters. The most striking observation regarding cluster 1 and 5 was the occurrence of regulated genes in duplicates such as several virulence genes. The reason behind this is the presence of two sister plasmids in *D. shibae* DFL-12, named pDS191 and pDS126. About 80% of the sequence of the smaller replicon, including a gene cluster of 47 kb, a *vir* operon and a short inverted region, are highly conserved (Wagner-Dobler *et al.* 2010). The downregulated "sister" genes of cluster 1 and 5 are presented in the following table.

Table 19 Downregulated dublicate genes of cluster 1 and 5 derived from the sister plasmids pDS191 and pDS126.

locus tag	sister plasmid pDS191	cluster	locus tag	sister plasmid pDS126	cluster
Dshi_3628	hypothetical protein	1	Dshi_3966	hypothetical protein	5
Dshi_3636	hypothetical protein	5	Dshi_3971	hypothetical protein	1
Dshi_3637	hypothetical protein	1	Dshi_3972	hypothetical protein	1
Dshi_3638	Lytic transglycosylase catalytic	1	Dshi_3973	Lytic transglycosylase catalytic	1
Dshi_3639	hypothetical protein	1	Dshi_3974	hypothetical protein	1
Dshi_3640	type IV secretory pathway VirB3 family protein	1	Dshi_3975	type IV secretory pathway VirB3 family protein	5
Dshi_3641	CagE TrbE VirB component of type IV transporter system	1	Dshi_3976	CagE TrbE VirB component of type IV transporter system	5
Dshi_3644	hypothetical protein	5	Dshi_3977	hypothetical protein	1
Dshi_3645	VirB8 family protein	1	Dshi_3979	hypothetical protein	5
Dshi_3646	hypothetical protein	1	Dshi_3980	VirB8 family protein	1
Dshi_3647	conjugation TrbI family protein	1	Dshi_3981	hypothetical protein	1
Dshi_3648	type II secretion system protein E	1	Dshi_3982	conjugation TrbI family protein	1
Dshi_3649	hypothetical protein	1	Dshi_3983	type II secretion system protein E	1
Dshi_3656	Relaxase/mobilization nuclease family protein	1	Dshi_3989	Relaxase/mobilization nuclease family protein	1

The sequences of the sister genes are conserved but not 100% identical. Therefore probes were designed for each gene and signals could be traced back to their origins.

Furthermore, Cluster 5 comprises the highly donwregulated gene *ctrA* (Dshi_1508) which is an essential response regulator of a two component system responsible for the cell cycle progression in *D. shibae* DFL-12. CtrA is a possible candidate gene regulated by $LuxI_1$ mediated quorum sensing whose downregulation could explain the differences in mutant cell division and cell morphology. The response regulator CtrA forms together with the histidine kinase CckA (Dshi_1644) and the histidine phosphotransferase ChpT (Dshi_1470) one of several signal transduction systems of *D. shibae* DFL-12. The whole system was detected to be downregulated in the mutant. Nothing is known of cell division control in *D. shibae* DFL-12 but *Caulobacter crescentus* provides a

valuable model system to study cell cycle regulation and cellular differentiation. The master transcription factor, CtrA, is a cell fate determinant in *Caulobacter* which controls multiple events in the cell cycle, including the initiation of DNA replication, DNA methylation, cell division, and flagellar biogenesis. Furthermore, the pool of CckA phosphorylated CtrA-P determines repression of cell cycle progression (Jacobs *et al.* 1999). A homolog of CtrA is also present and essential in *S. meliloti*. The functions of CtrA in *S. meliloti* are not known but it was suggested to arrest DNA replication and cell division when bacteria differentiate (Barnett *et al.* 2001).

Cluster 4 and 6

In media with one carbon source (e.g. succinate), exponentially growing cells quickly use up the available nutrients and cease their exponential increase in biomass, thus entering a phase of culture referred to as stationary phase. The homogeneous mutant population was shown to have an increased division rate and entered faster the logarithmic growth phase. Succinate could be exhausted earlier than in the wild type culture. The lack of carbon source and entering the stationary phase led the $\Delta luxI_1$ cells to activate the stringent response. The stringent response is signaled by the alarmones guanosine pentaphosphate or tetraphosphate (p)ppGpp which decrease the synthesis of translational machinery (such as rRNA and tRNA) and increase the transcription of biosynthetic genes and catabolic operons to exploit alternative energy sources. Together with alternative sigma factors, the synthesis of phospholipids and nucleotides as well as the cell division is repressed and cells become more resistant to various stress (Navarro Llorens *et al.* 2010). The upregulation of genes involved in the methane and sulfur metabolism and the degradation of amino acids like valine, leucine and isoleucine indicate an enhanced stringent response of the mutant

The porphyrin/chlorophyll metabolism and the carotenoid biosynthesis as well as the terpenoid backbone synthesis (provides carotenoid precursors) were upregulated in the mutant when entered the stationary phase, indicating an increased production of photoactive pigments.

Cluster 6 comprised the gene with the highest log2 fold change (log2 fold change: 5.5), which was annotated as transposase IS4 family protein (Dshi_3878). It is located on the plasmid pDS153.

Insertion sequences (ISs) are small (< 2.5 kb) DNA segments able to jump, or copy themselves, into various genomic sites without no need of DNA homology, leading to genomic reshuffling and evolution. The DNA breaks and transposition are catalysed by an element encoded protein referred to as transposase. Family IS4 included 153 distinct intact elements with conservations of a DDE[1] motif and YREK[2] signature and target site duplication lengths corresponding approximately to one DNA helix turn (~ 10 bp). The transposase regions differ in sequence and length, catalytic residues, DNA end signatures and target site specifity (De Palmenaer *et al.* 2008). The insertion sequence of *Agrobacerium tumefaciens* T37, IS427 (a subgroup of the IS4-family transposases), is present at three sites in the Ti plasmid. Sequence analysis of target sites identified a DNA-binding site[3] for DNA-binding proteins like integration host factors (IHF) (De Meirsman *et al.* 1990).

BLAST results of the transposase Dshi_3878 nucleotides against the *D. shibae* DFL-12 genome revealed two additional IS4 family transposases (Dshi_3682 and Dshi_4079) whose sequences were 100% identical to Dshi_3878. Dshi_3682 is located on plasmid pDS191 while Dshi_4079 is located on plasmid pDS86. It was not possible to design probes for all three transposases due to their identical sequences. Therefore, probes for the transposase Dshi_3878 were designed, but signals could not be traced back to their origins.

[1] D, aspartate; E, glutamate

[2] E, glutamate; K, lysine; R, arginine; Y, tyrosine

[3] Consensus sequence [YANNNNTTGAT(A/T)]

Integrases are located upstream of all three transposases. Transposases together with integrases could be indicating the presence of prophages. In *Bradyrhyzobium japonicum* and *Salinibacter ruber* transposases and integrases were detected to be encoded by prophage loci (Srividhya *et al.* 2007).

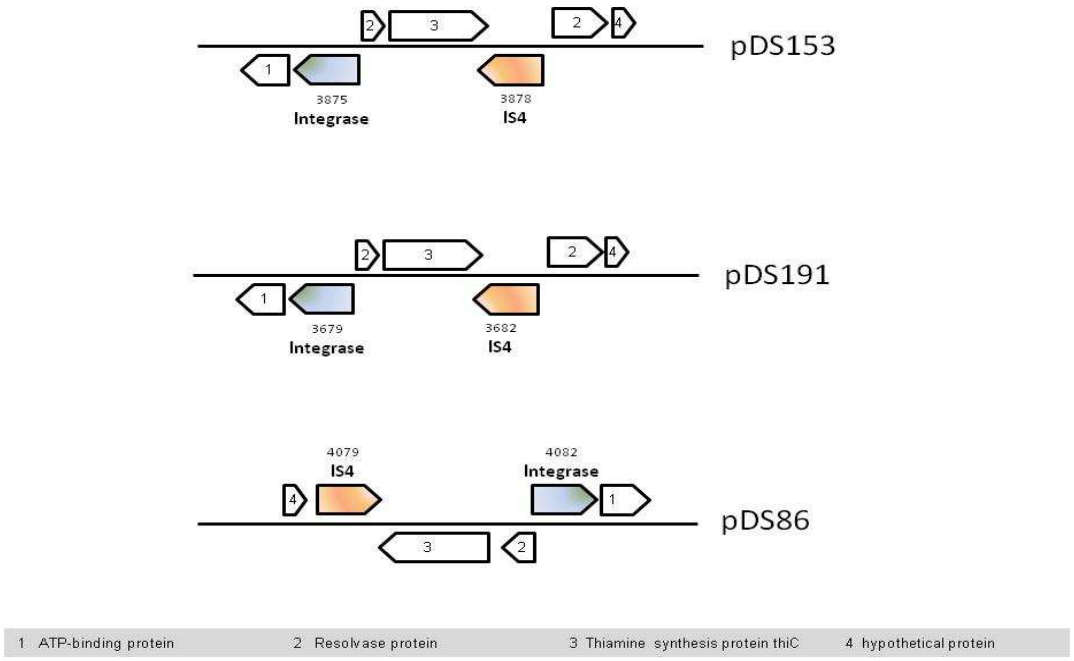

Figure 67 Neighborhood of the IS4 family transposases.

The genes of the integrase are depicted in blue. The genes of the three IS4 transposases are presented in red. Adjacent genes are numbered consecutively and corresponding product names are listed in the legend. Numbers written above the gene names match with the Dshi locus Tags.

5 Results Chapter B

Dinoroseobacter shibae DFL-12 was first isolated from *Prorocentrum lima*, a benthic dinoflagellate. The bacterium provides the grow-limiting vitamins B1 and B12 to its dinoflagellate host in exchange for essential metabolites. At present, it is technically not feasible to investigate the role of quorum sensing in *D. shibae* in its natural habitat. As a model of the natural situation, *D. shibae* DFL-12 was cocultured with the axenic (bacteria-free) dinoflagellate *P. minimum* and the axenic (bacteria-free) haptophyt *I. galbana*, respectively.

5.1 The *D. shibae* DFL-12 pKR-C12 reporter

To visualize and to quantify the AHL production *in situ* during cocultivation, a GFP-based *D. shibae* DFL-12 sensor strain was required. Because, until now, nothing is known about the promoter region and the regulation of the *luxI* synthases, an established GFP sensor plasmid was used. The conjugative sensor plasmid was extracted from a *P.putida* F117 pKR-C12 culture, purified and transformed into *D. shibae* DFL-12 via biparental mating.

Gentamicin resistant clones were investigated under the fluorescence microscope for induced GFP expression. Cultivation of a positive clone resulted in a heterogeneous subpopulation. Cells were expressing GFP in various intensities, independent of their cell size.

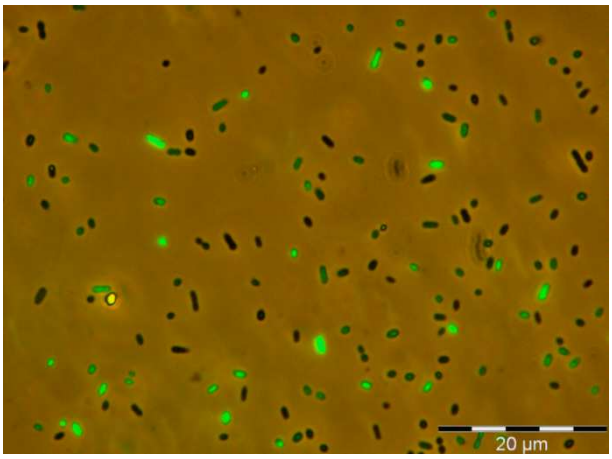

Figure 68 Heterogeneous subpopulation of *D. shibae* DFL-12 carrying pKR-C12 cultivated in hMB Gm 80 µg/ml.

Expression of the GFP is induced by the presence of long-chain AHLs. Various GFP intensities are visualized, ranging from high- through medium- to non - fluorescent. The phase-contrast is not completely hidden, to visualize cells with lacking GFP expression

In general, cell-to-cell- heterogeneity in gene expression arises from fluctuations in rate of transcription from a promoter, mRNA or protein stability and/or the rate of translation. Moreover, in plasmid-born GFP expression, the plasmid copy number and plasmid stability play a significant role. *D. shibae* DFL-12 pKR-C12 was cultivated in hMB with addition of gentamicin. Thus, GFP heterogeneity could be due to fluctuating AHL concentrations.

5.1.1 FACS analyses of heterogeneous subpopulation

To further investigate the percentage composition of the fluorescent cells, FACS was used to quantify and sort an appropriate cell number of the heterogeneous subpopulation.

First, the Forward and Side Scatter signal of 10^5 cells and particles in the sample were plotted as logarithmic (Forward Scatter) FS log data against the logarithmic (Side Scatter) SS Log data. FS Log and SS Log correlate with the cell/particel volume and surface character. The area of highest concentration (96.58% of cells) was defined as gate R1 including bacterial cells and excluding medium particles (Figure 70, left panel). Afterwards the Side Scatter signal of R1 wild type and sensor cells was analysed, using two fluorescent bandpass filter (530/30 FITC, 585/42 PE) (Figure 70, mid and right panel).

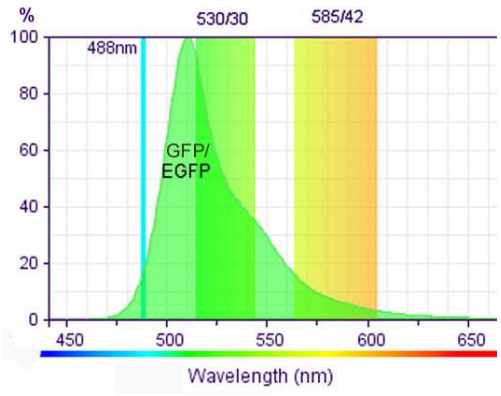

Figure 69 BD[4] Spectrum Viewer showing the GFP emission spectra and filter overlap, Courtesy of BD.

Presented is the GFP/EGFP excitation at 488 nm (blue bar) and the emission spectrum with an emission peak at 509 nm). Overlapping filters are: filter 530/30 = FITC, filter 585/44 = PE.

[4] Becton, Dickinson and Company

These filters were chosen as they were the best available filters for measuring

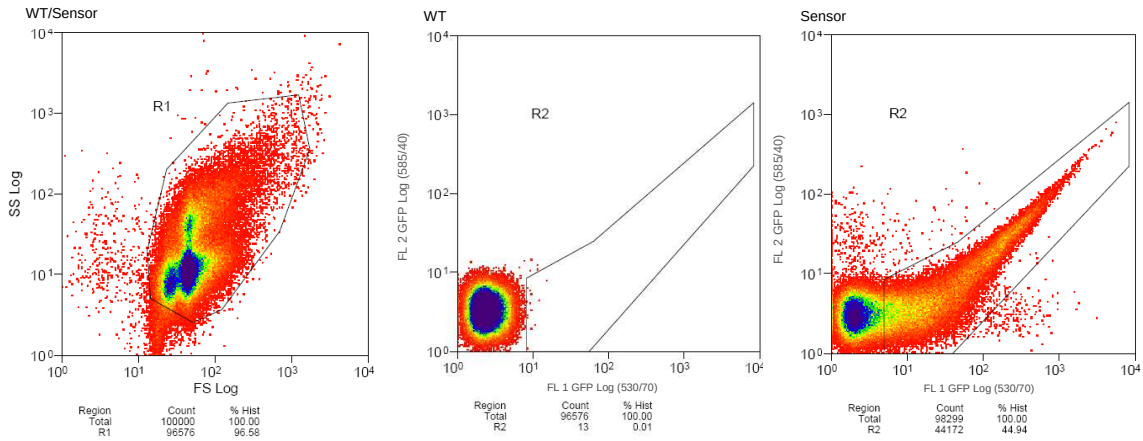

the GFP emission spectra.

Figure 70 Determination of gates R1 and R2 required for percentage composition analyses and sorting.

The left panel depicts the 2D Forward and Side Scatter plot, showing bacterial cells and medium particles. Chosen gate R1 consists of bacterial cells, used for fluorescent analyses. Mid-and right panel depict two-fluorochrome dot plots of wild type and sensor R1 cells. The fluorescent tail of sensor R1 cells was defined as gate R2 and was used for percentage composition analyses and sorting. Autofluorescent, but not GFP expressing R1 cells were excluded from gate R2 (see wild type, mid panel).

From the FACS analysis, it was shown that the sensor had 44.94% of the cell population analysed fluorescing whilst the wild type had 100% of the cell population analysed autofluorescing, not expressing any GFP. As a result, gate R2 was defined, excluding autofluorescence and comprising cells with differential expressed GFP levels.

(a)

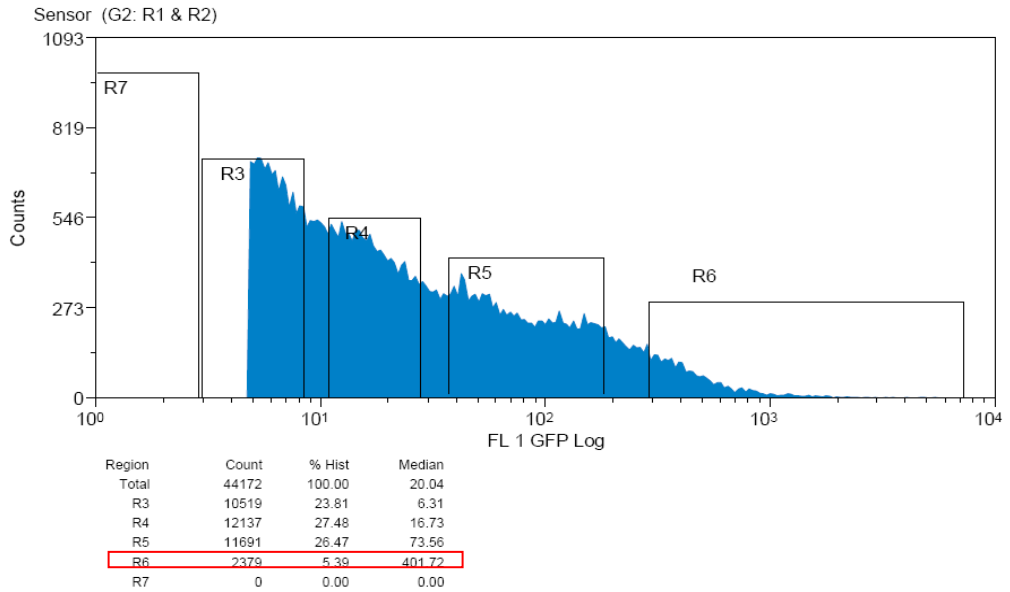

Region	Count	% Hist	Median
Total	44172	100.00	20.04
R3	10519	23.81	6.31
R4	12137	27.48	16.73
R5	11691	26.47	73.56
R6	2379	5.39	401.72
R7	0	0.00	0.00

(b)

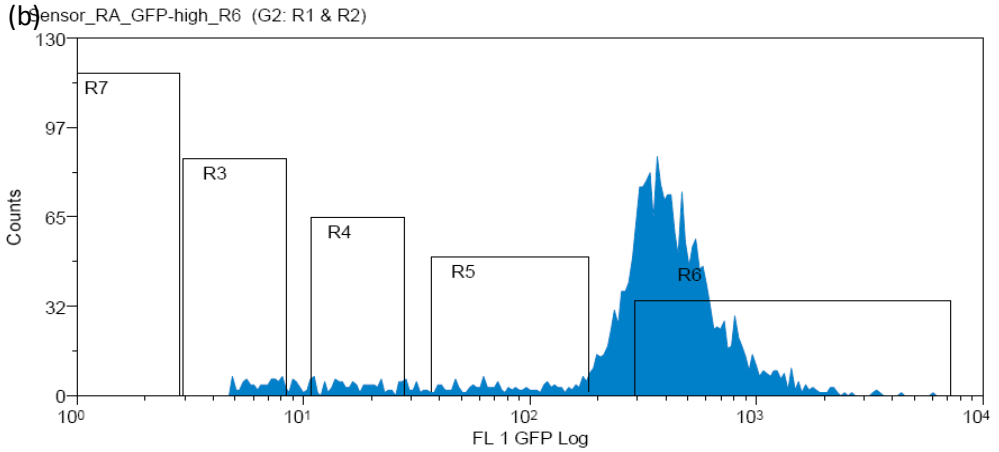

Region	Count	% Hist	Median
Total	2411	100.00	387.47
R3	71	2.94	6.54
R4	95	3.94	16.73
R5	133	5.52	81.98
R6	1796	74.49	447.69
R7	0	0.00	0.00

Figure 71 GFP intensity of sensor cells of gate R2 and re-analysis of gate R6 after sorting.

Figure 71a depicts the GFP intensity of sensor cells of gate R2, presented as cell counts against the logarithmic GFP intensity (FL 1 GFP log). Five additional gates were set (R3-R7) to partition the GFP intensity, whereas cells with the highest GFP intensity are counted among gate R6. Red box: 5.4% of cells of gate R2 are highly expressing GFP. Figure 71b depicts the re-analysis of gate R6 after sorting and the enrichment of cells, highly expressing GFP up to 74.5% (red box). For GFP measurement the bandpass filter 530/30 FITC was used. Gate R7 is the negative control and consists of non GFP expressing “dark” cells.

The GFP intensity of cells of gate R2 was partitioned into five additional gates (R3-R7), whereas cells with the highest GFP intensity were counted among gate R6. The largest fraction of cells (R3: 23.8%, R4: 27.5% and R5: 26.5%) were expressing GFP at low to medium levels, just 5.4% of the gate R2 cells could be

counted among gate R6. 16.8% of the population were not expressing GFP (gate R7). Re-analysis of gate R6 after sorting resulted in an increased number of cells highly expressing GFP (74.5%). Furthermore, single cells of gate R6 were directly spotted onto hMB Gm 80 µg/ml agar plates.

One colony derived from a single spotted gate R6 cell was used to inoculate a subculture. The subculture was cultivated in hMB Gm 80 µg/ml and hereafter was called *D. shibae* DFL-12 FACS6.

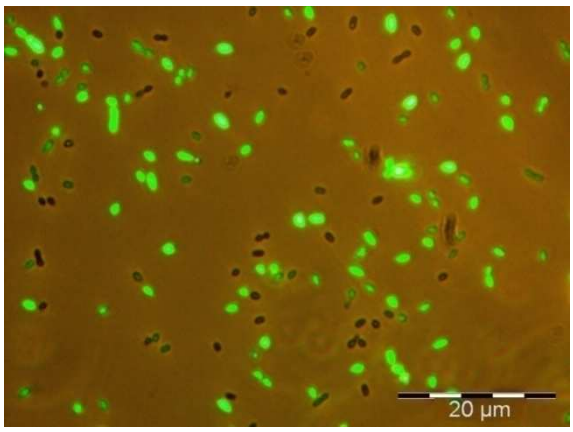

Figure 72 Heterogeneous subpopulation of *D. shibae* DFL-12 FACS6 in hMB Gm 80 µg/ml.

Expression of the GFP is induced by the presence of long-chain AHLs. Various GFP intensities are visualized, ranging from high- through medium- to non - fluorescent. The phase-contrast is not completely hidden, to visualize cells with lacking GFP expression.

The subpopulation of *D. shibae* DFL-12 FACS6 consisted of an increased number of highly GFP expressing cells. Figure 68 and Figure 72 depict heterogeneous populations at the same OD_{600nm} of 0.3, but the FACS6 subpopulation had 51% of the cells analysed highly fluorescing whilst the initial heterogeneous population had just 9% of the cells analysed highly fluorescing. The strain *D. shibae* DFL-12 FACS6 was used for cocultivation experiments with two different algae to investigate whether the presence of the algae and produced metabolites have an influence on the bacterial AHL production.

1.1.1 Plasmid stability in MB

Artificial incorporated plasmids only remain stable in the bacterial cell if they are advantageously for survival such as acquired plasmid-borne antibiotic

resistances. Therefore antibiotics are added to the medium to guarantee plasmid stability. In coculture experiments antibiotics were omitted to not affect the algae growth. For that reason, plasmid stability of the pKR-C12 plasmid maintained in the *D. shibae* DFL-12 FACS6 sensor, was tested in antibiotic free medium such as MB. A generation time of 11 hours was calculated based on the optical density for the sensor strain when cultivated in MB at 30°C.

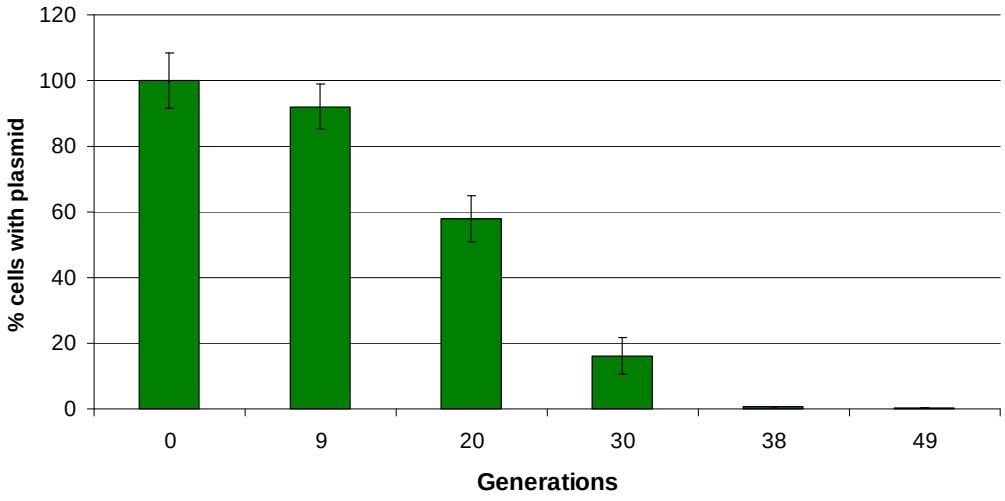

Figure 73 Plasmid stability after 49 generations (22 days) in liquid MB without antibiotic selection.

Cells were grown at 30°C in MB for 96 h, starting from this culture fresh medium was inoculated, and again incubated 96 h under the same conditions. Procedure was repeated for additional five times, which roughly matches 49 generations. The percentage of cells with plasmid is shown; values are the average of three biological replicates.

After 9 generations (4 days) in liquid MB without antibiotics, 90% of the cells were still carrying the plasmid pKR-C12. After 20 generations (9 days) without selective pressure 42% plasmid loss occurred. Cultivation in MB for 49 generations (22 days) resulted in a complete plasmid loss.

5.2 Cocultivation

For cocultivation experiments, cobalamin (vitamin B12) was omitted from the L1 medium to grow the algae under vitamin B12 limitation and forcing the

metabolic crosstalk. When cobalamin became growth limiting, cultures of three biological replicas were inoculated with *D. shibae* DFL-12 FACS6, provided with the lacking cobalamin or remained untreated (negative control). Three biological replicates of the algae culture with complete medium and without inoculation of *D. shibae* FACS6 were used as positive control to monitor normal algae growth.

D. shibae DFL-12 FACS6 was cocultivated with the axenic dinoflagellate *P. minimum* and the axenic haptophyt *I. galbana*, respectively.

5.2.1 *Isochrysis galbana* with *D. shibae* DFL-12 FACS6

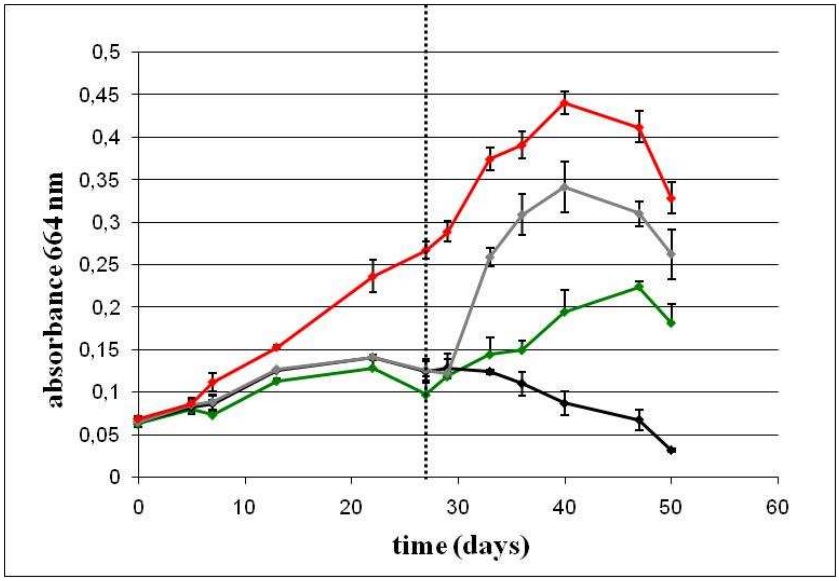

Figure 74 *D. shibae* DFL-12 FACS6 provides cobalamin (B12) to the haptophyt *I.galbana* in coculture.

Growth of the haptophyt is shown as the amount of chlorophyll *a* (absorbance 664 nm). Colored lines show cultures on L1 medium lacking cobalamin (black, grey and green) and positive control (red, complete L1 medium). On day 27 (dotted line) cultures were provided with the lacking vitamin (grey), were inoculated with *D. shibae* DFL-12 FACS6 (green) or remained untreated (black). Presented are the mean values of three biological replicates.

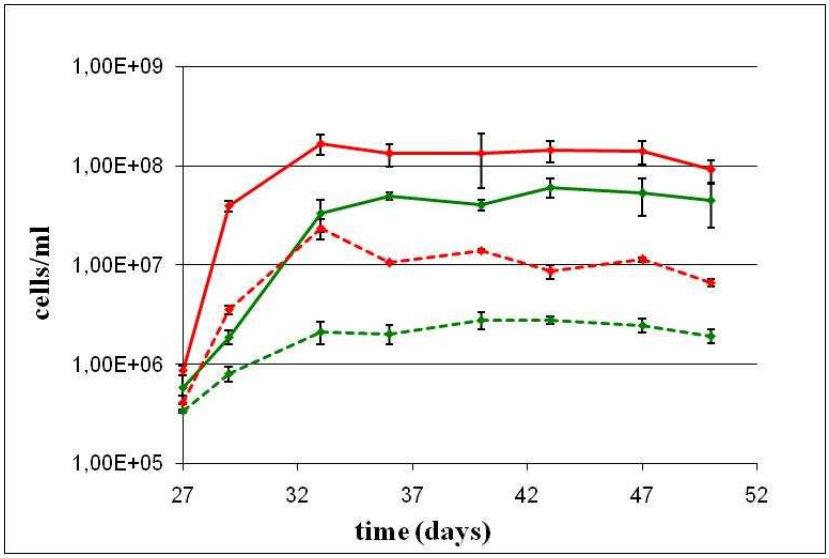

Figure 75 Bacterial growth and GFP expression of *D. shibae* DFL-12 FACS6 in coculture with *I. galbana*.

Growth of the bacterium is shown as the amount of cells (cells/ml). Red lines depict the positive control, *D. shibae* DFL-12 FACS6 without algae on L1 5 mM succinate. Green lines correspond to the coculture of *D. shibae* DFL-12 FACS6 with *I. galbana*. Solid lines reflect the total cell number, calculated by counting SybrGreen stained cells whereas dotted lines reflect the GFP expressing cells, calculated by counting unstained, fluorescing cells. Presented are the mean values of three biological replicates.

Figure 74 shows that *D. shibae* DFL-12 FACS6 stimulated the growth of *I. galbana* in the absence of cobalamin. Supplementation with pure vitamin B12 resulted in a faster and stronger recovery of the haptophyt culture compared to the inoculation with *D. shibae* DFL-12 FACS6. Furthermore the cocultivation with *I. galbana* allowed the bacterium to grow and the production of long-chain AHLs could be visualized through GFP expression as represented in Figure 75. The density of bacterial cells was determined by microscopic counts of SybrGreenI stained cells and of GFP expressing cells. From an initial density of 8.74 x 10^5 cells/ml (*D. shibae* DFL-12 FACS6 without algae in L1 5 mM succinate) and 5.81 x 10^5 cells/ml (coculture of *D. shibae* DFL-12 FACS6 with *I. galbana*) they increased to 1.67 x 10^8 cells/ml and 6.07 x 10^7 cells/ml. Approximately 10% of the cells showed GFP expression during cocultivation and in pure bacterial culture.

For calculation of the *D. shibae* DFL-12 FACS6 generation times in coculture and in pure L1 with 5 mM succinate, values X and X_0 and corresponding time points of the exponential phase were chosen.

	D. shibae FACS6 in coculture	*D. shibae* FACS6 in L1 5 mM succinate
t_0	0 d (0 h)	0 d (0 h)
t	2 d (48 h)	2 d (48 h)
X_0	5.81E+05 cells/ml	8.74E+05 cells/ml
X	1.89E+06 cells/ml	3.95E+07 cells/ml
μ	0.024 h^{-1}	0.079 h^{-1}
t_G	**29 h**	**9 h**

Growth rate (μ) $\mu = \frac{\ln X - \ln X_0}{t - t_0} = \frac{\ln \frac{X}{X_0}}{t - t_0}$ Generation time (t_G) $t_G = \frac{\ln 2}{\mu}$

5.2.2 *Prorocentrum minimum* with *D. shibae* DFL-12 FACS6

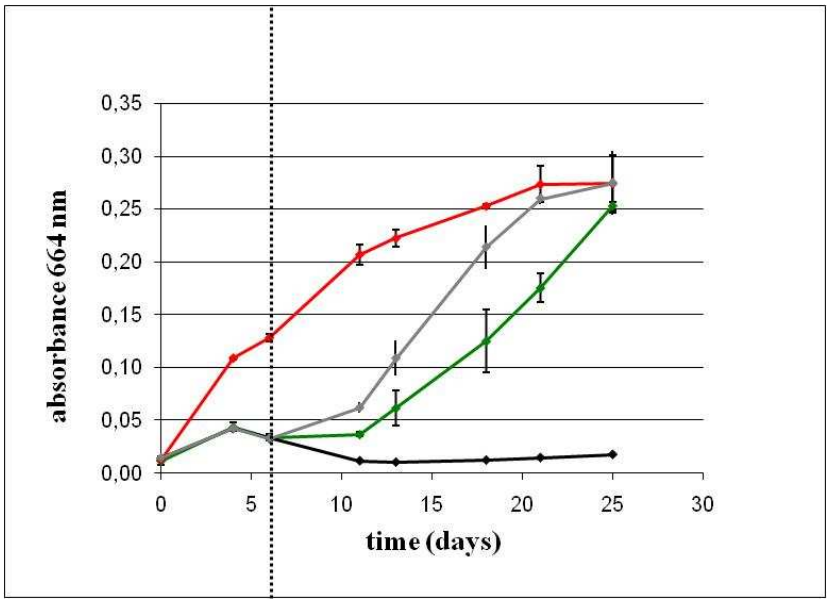

Figure 76 *D. shibae* DFL-12 FACS6 provides cobalamin (B12) to the dinoflagellate *P. minimum* in coculture.

Growth of the dinoflagellate is shown as the amount of chlorophyll a (absorbance 664 nm). Colored lines show cultures on L1 medium lacking cobalamin (black, grey and green) and positive control (red, complete L1 medium). On day 6 (dotted line) cultures were provided with the lacking vitamin (grey), were inoculated with *D. shibae* DFL-12 FACS6 (green) or remained untreated (black). Presented are the mean values of three biological replicates.

Figure 76 shows that *D. shibae* DFL-12 FACS6 stimulated the growth of *P. minimum* in the absence of cobalamin. Supplementation with pure vitamin B12 resulted in a faster recovery of the dinoflagellate culture compared to the inoculation with *D. shibae* DFL-12 FACS6. Growth of both supplemented cultures reached the equal, final chlorophyll amount of the positive control. Also the cocultivation with *P. minimum* allowed the bacterium to grow and the production of long-chain AHLs could be visualized through GFP expression

(Figure 77). The density of bacterial cells was determined by microscopic counts of SybrGreenI stained cells and of GFP expressing cells. From an initial density of 1.88 x 10^6 cells/ml (*D. shibae* DFL-12 FACS6 without algae in L1 0.5 mM succinate) and 2.48 x 10^6 cells/ml (coculture of *D. shibae* DFL-12 FACS6 with *P. minimum*) they increased to 4.19 x 10^7 cells/ml and 4.56 x 10^7 cells/ml.

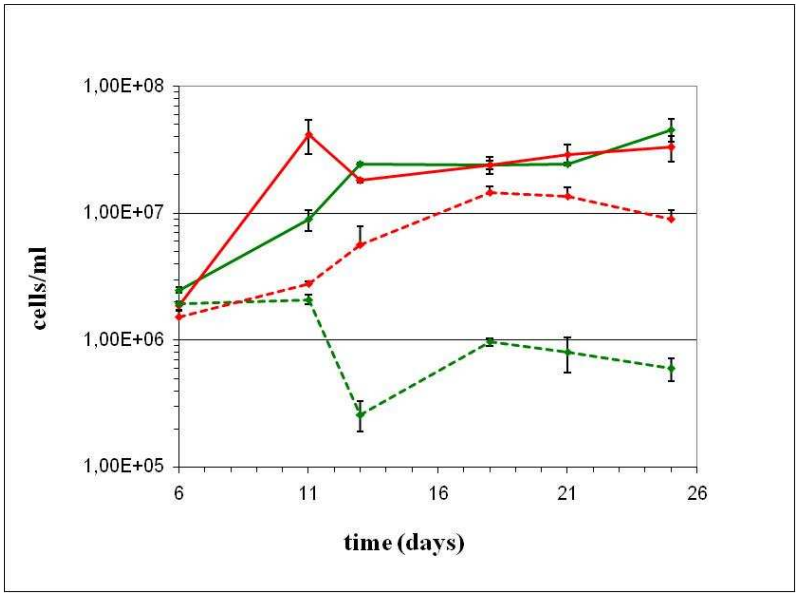

Figure 77 Bacterial growth and GFP expression of *D. shibae* DFL-12 FACS6 in coculture with *P. minimum*.

Growth of the bacterium is shown as the amount of cells (cells/ml). Red lines depict the positive control: *D. shibae* DFL-12 FACS6 without algae grown on L1 0.5 mM succinate. Green lines correspond to the coculture of *D. shibae* DFL-12 FACS6 with *P. minimum*. Solid lines reflect the total cell number, calculated by counting SybrGreen stained cells whereas dotted lines reflect the GFP expressing cells, calculated by counting unstained, fluorescing cells. Presented are the mean values of three biological replicates.

For calculation of the *D. shibae* DFL-12 FACS6 generation times in coculture and in pure L1 with 0.5 mM succinate, values X and X_0 and corresponding time points of the exponential phase were chosen.

	D. shibae FACS6 in coculture	*D. shibae* FACS6 in L1 0.5 mM succinate
t_0	8 d (192 h)	9.5 d (228 h)
t	10 d (240 h)	12 d (288 h)
X_0	6.00E+06 cells/ml	6.00E+06 cells/ml
X	2.00E+07 cells/ml	1.50E+07 cells/ml
μ	0.03 h^{-1}	0.015 h^{-1}
t_G	**23 h**	**46 h**

Growth rate (μ) $\mu = \frac{\ln X - \ln X_0}{t - t_0} = \frac{\ln \frac{X}{X_0}}{t - t_0}$ Generation time (t_G) $t_G = \frac{\ln 2}{\mu}$

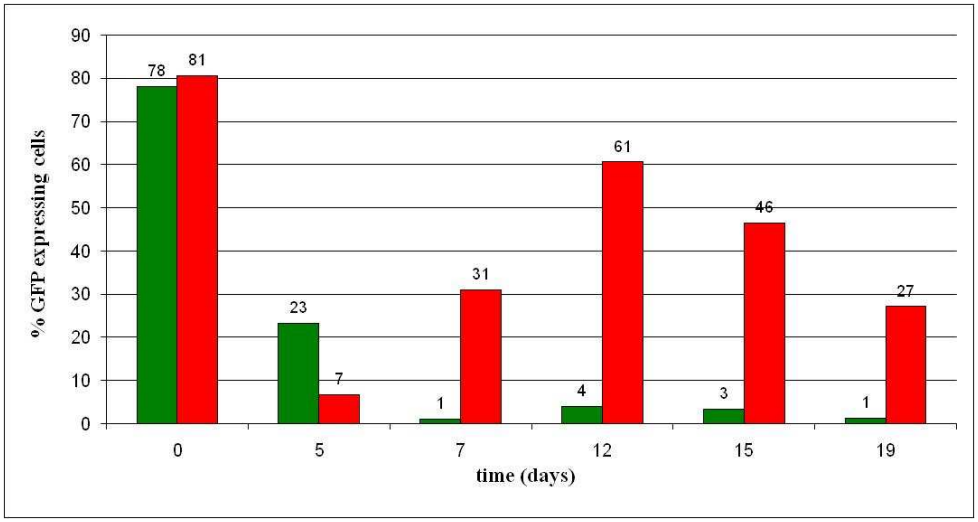

Figure 78 GFP expression of *D. shibae* DFL-12 FACS6 cells cultivated in L1 0.5 mM succinate and in coculture with *P. minimum*.

The amount of GFP expressing cells is shown as percentage. Fluorescing cells of *D. shibae* DFL-12 FACS6 in L1 0.5 mM succinate are shown in red and fluorescing cells of *D. shibae* DFL-12 FACS6 in coculture are shown in green. Fluorescing cells were calculated by direct microscopy counts as well as the total cell number, which was calculated by direct microscopy counts of SybrGreen stained cells. The total cell number was set to 100% for each time point.

Figure 78 shows the amount of GFP expressing cells of *D. shibae* DFL-12 FACS6 when it was cultivated in L1 0.5 mM succinate and grown in coculture with *P. minimum*. When *D. shibae* DFL-12 FACS6 was grown without algae in L1 0.5 mM succinate, the production of AHLs (and GFP expression) increased to maximum percentage at day 12 and decreased after 15 days of cultivation. In coculture with *P. minimum*, the GFP expression and AHL production, respectively, decreased after seven days to average 2% and did not recover until the end of cocultivation. Thus, it seems that *P. minimum* produces inhibitory compounds that repress AHL production of *D. shibae* DFL-12 in coculture. In pure bacterial culture and in coculture plasmid stability should be equal in order that differences in AHL production can not be due to partial plasmid loss in the coculture.

5.2.3 Expression of the *lux* genes and symbiosis relevant genes during cocultivation with *P. minimum*

To investigate the expression of several bacterial genes during cocultivation, the RNA from a 15 days old *D. shibae* DFL-12 FACS6 / *P. minimum* coculture was extracted as well as from an equal volume of a corresponding *P. minimum* culture and of a *D. shibae* DFL-12 FACS6 L1 0.5 mM succinate culture. The cDNA was prepared and used for qRT-PCR analyses with different primers. The transcription rates of the *lux*, alginate, fascicline genes and genes involved in the biosynthesis of thiamine and cobalamin were determined. According to the RNA extraction protocol which is designed for bacteria, small amounts of eukaryotic RNA were extracted and no results for the qRT-PCR regarding the pure dinoflagellate RNA and cDNA, respectively, were obtained. The bacterial RNA concentration of the mixed coculture was 18.75 ng/µl. For *D. shibae* DFL-12 FACS6 in L1 0.5 mM succinate 147.33 ng/µl of RNA could be obtained. 225 ng of RNA were transcribed into cDNA (20 µl) and the cDNA was diluted 1:6 for qRT-PCR experiments.

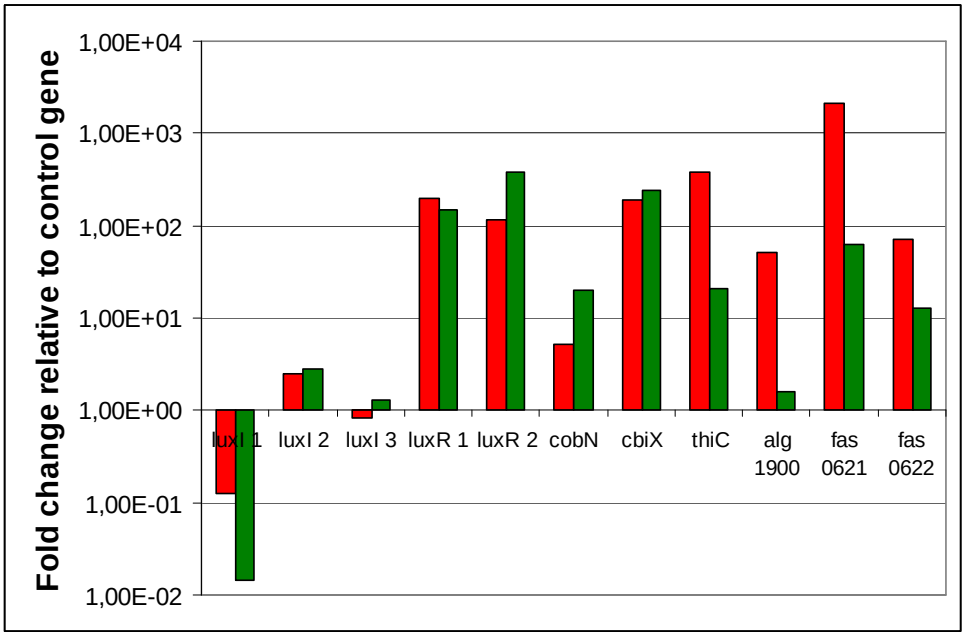

Figure 79 Bacterial gene expression determined after 15 days of cultivation in L1 0.5 mM succinate and in coculture with *P. minimum*, respectively.

Presented is the expression of the *lux* genes ($luxI_{1\text{-}3}$, $luxR_{1,2}$) and symbiotic relevant genes (*cobN, cbiX*, *thiC, alg* Dshi_1900, and *fas* Dshi_0621, 0622) after 15 days of incubation as fold change relative to the control gene *gyrA*. Gene expression of *D. shibae* DFL-12 FACS6 in L1 0.5 mM succinate is visualized in red. Gene expression of *D. shibae* DFL-12 FACS6 cocultivated with the dinoflagellate *P. minimum* is visualized in green. Presented are the mean values of three technical replicates from one biological sample.

As shown inFigure 79, the expression of *luxI*$_1$ was repressed in the cocultured *D. shibae* DFL-12 FACS6 strain compared to the pure *D. shibae* DFL-12 FACS6 culture. Expression of *luxI*$_2$ did not differ in both cultures as well as *luxI*$_3$, which was slightly upregulated in the coculture and slightly downregulated in the pure bacterial culture. The two regulators were differentially expressed. LuxR$_1$ was slightly upregulated in the pure culture whereas LuxR$_5$ was upregulated in coculture.The transcription rate of CobN, which is an ATP-dependent cobalt chelatase and responsible for cobalt insertion in the aerobic route of cobalamin synthesis, was increased in the coculture strain, indicating a higher vitamin B12 consumption by the algae. CbiX, the respective ATP-independent cobalt chelatase of the anaerobic pathway, showed no differentiated expression pattern. Thiamin, which was provided abundantly to the coculture medium, but omitted in the pure bacterial culture, was significantly higher expressed in the pure culture. Genes which are postulated to play a role in adhesion and biofilm formation, such as fascicline and alginate were clearly repressed in the coculture.

5.2.4 SEM micrographs of the *P. minimum* cocultivation

To take a look at the coculture regarding possibly attached bacterial cells on the surface of the dinoflagellate, SEM micrographs of a 20 days old coculture were made. In Figure 80 *P. minimum* appear as cushion-shaped, prickly-armoured, 15 µm sized cell. The small rod-shaped bacteria have a size of approx. 1.5-2 µm and are attached to the surface of the dinoflagellate or are stuck side by side at the polysaccharide filaments. Not every single, bacterial cell was associated with the host surface or filaments, some remained planktonic

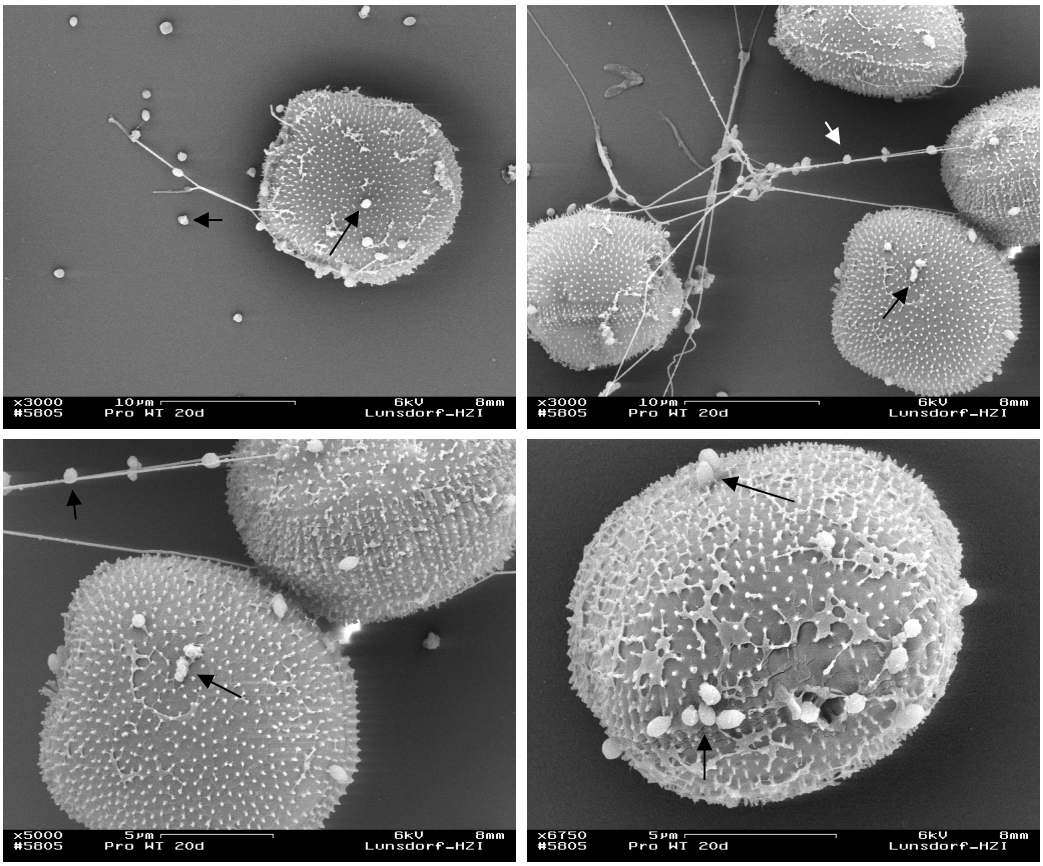

Figure 80 SEM micrographs illustrating *D. shibae* DFL-12 wild type in coculture with *P. minimum*.

3.000 to 6.750 x maginification were used to visualize the attachment of the bacteria to its dinoflagellate host *P. minimum* after 20 days of cocultivation. Bacterial cells adhere on the prickly-armoured surface of the algae or are beaded like “pearls” on a string of filaments. Arrows indicate single bacterial cells.

6 Discussion Chapter A

6.1 The functionality and specifity of the *D. shibae* DFL-12 LuxI synthases

Proteobacteria use LuxI type synthases to produce AHLs to which co-evolved members of the LuxR family of transcription factors respond. *Roseobacter* strains have usually one or two autoinducer synthases, whereas in *Rhizobia* up to four have been found. The lengths of the fatty acyl groups vary from 4 to 18 carbon atoms depending on the specific system. In *Alphaproteobacteria* some QS regulated phenotypes are known such as host invasion, virulence, biofilm formation, motility or the production of exopolysaccharides. Furthermore *R. palustris* is using a LuxI ortholog (RpaI) to produce *p*-coumaroyl-HSL which is controlling chemotaxis. One aim of this work was, to unravel the QS system of *D. shibae* DFL-12, which has three autoinducer synthases.

6.1.1 AHL production of *D. shibae* DLF-12

AHL production is clearly dependent on growth parameters, such as temperature, pH-value, growth stage, carbon source and amino acids, which can have a dramatic influence on the level of the signal molecules produced (Brelles-Marino and Bedmar 2001). Therefore, negative results have been difficult to interpret and attention should be paid to the growth conditions used and the specifity of sensor strains and GC-MS detection limits. At the beginning of this thesis the complex medium MB was used for cultivation and AHLs were extracted in methanol. Bioassay analyses revealed the presence of short-chain and long-chain AHLs, but GC-MS analyses just confirmed the occurrence of C18-en-AHL and C18-dien-AHL. C8-AHL could not be detected via GC-MS which could be due to concentrations below the detection limit. Extraction of AHLs from an increased MB culture volume (1 litre) resulted in the same AHL composition (C18-en-and C18-dien-AHL) and no C8-AHL was detected (data not shown). By the group of Decho *et al.*, it was shown that in alkaline conditions (pH > 8) relatively rapid hydrolyses occurred in AHLs having acyl-chain length less than C10 (Decho et al. 2009). Therefore, C8-AHL synthesis could be low in MB (pH > 8) and are additionally exposed to degradation. However, identification of the AHLs via GC-MS was difficult when rich complex medium was used. MB extracts

comprise high amounts of diketopiperazines which interfere with the AHL signals in GC-MS analyses. Thus, artificial seawater medium (SWM) with succinate as only carbon source was used for cultivation. Methanol extraction of AHLs derived from cultivation in SWM was not successful (data not shown). For that reason the polar solvent dichloromethane was used for extraction. The use of 50 mM succinate for cultivation influenced the concentration of AHLs. Through bioassay analyses short-chain AHLs could be identified in addition to long-chain AHLs while the use of 5 mM succinate led to the detection of long-chain AHLs. But when both extracts (5 mM and 50 mM succinate) were supplied for GC-MS analyses, just long-chain AHLs such as C18-en-AHL and C18-dien-AHL could be identified.

The bioassay reporter *E. coli* MT102 pJBA132 was used to detect short-chain AHLs. This strain is known to be sensitive to high concentrations of 3OC12-AHL. Therefore, the supposed detection of short-chain AHLs in the 50 mM succinate extract as well as in the MB extract could be due to the increased production of long-chain AHLs caused by the higher carbon concentration.

It is obvious that the media composition greatly affects the AHL production. The effect of different media (LB, NB, KingsB and M9) on the C8-AHL and C10-AHL producer *B. cepacia* was investigated by the group of X. Li *et al.*. The interference peaks of C8-and C10-AHL were observed when LB, NB and KingsB full media were used. No C8-AHL peak and a weak C10-AHL peak appeared when the bacteria were grown in M9 minimal media. Additionally, the production of C10-AHL was 40 times higher in LB than in minimal media (Li *et al.* 2006).

In summary it can be said, that carbon rich media like MB and high concentrated succinate led to an increased production of long-chain AHLs which were detected by the long-chain AHL bioassay reporter (*P. putida* F117 pKR-C12) as well as by the short-chain reporter (*E. coli* MT102 pJBA132). Reduction of the succinate (5 mM) resulted in the loss of the short-chain AHL bioassay signal. C18-en-AHL and C18-dien-AHL could be detected via GC-MS in every extract (MB, culture volume of 100 ml-1L; SWM with 5 mM – 50 mM succinate) but no C8-AHL.

Moreover, it was shown by Blosser-Middleton and Gray that multiple AHL signals of *R. leguminosarum* are synthesized in a distinct temporal pattern. *R. leguminosarum* produces the AHLs 3OC8-AHL, C8-AHL, C6-AHL and 3OHC14-en-AHL, in decreasing order of abundance. Synthesis of the chromosomally encoded 3OHC14-en-AHL was inhibited below detectable levels during growth. Production of 3OC8-AHL was strongly induced in the mid-exponential phase and was quickly shut off at the onset of stationary phase. Synthesis of C8-AHL was induced at about the same time as 3OC8-AHL but the rate was less than one-half the maximal rate. Maximal rates of C8-AHL were obtained during transition to stationary phase. C6-AHL was produced in very small amounts and synthesis increased gradually until the onset of the stationary phase (Blosser-Middleton and Gray 2001).

Individual AHLs are synthesized in different amounts in batch culture and each exhibites a unique temporal pattern of induction and subsequent shutoff.

Quorum sensing and starvation-sensing pathways are clearly interconnected (Lazazzera 2000). The production of an AHL signal molecule in *R. solanacearum* requires the alternative sigma factor σ^s that is maximally active under starvation conditions (Flavier *et al.* 1997).

Therefore, the sampling time point for AHL extraction could also play an important role. AHL extracts in this thesis always were obtained during logarithmic phase.

QRT-PCR studies of the Lux genes of *D. shibae* DFL-12 revealed that all three synthases were transcribed during cultivation in SWM 5 mM succinate. $LuxI_1$ was constantly transcribed at very low levels (log fold change of 10^{-3} to 10^{-4}) relative to the control gene *gyrA*. $LuxI_2$ and $LuxI_3$ were expressed 10^3-fold higher than $LuxI_1$. The synthases $LuxI_{1-3}$ showed no significant upregulation during grow. $LuxI_1$ was expressed constitutively as well as $LuxI_2$ and $LuxI_3$. Expression of $LuxI_3$ was additionally slightly increased at late logarithmic phase.

The AHL production in *Vibrio fischeri*, which has become the “paradigm organism” of AHL regulation, is upregulated during growth by its own AHL signal.

Thus, the AHLs of *V. fischeri* have been called autoinducers. The autoinducible loop found in *V. fischeri* is not a phenomenon specifically linked to AHL production. Several other studies have also demonstrated that AHL production may be constitutive (Bassler *et al.* 1993;Byers *et al.* 2002;Ravn *et al.* 2001;Throup *et al.* 1995). The microarray data of the wild type revealed the same constitutive expression of $LuxI_1$ and $LuxI_2$ but $LuxI_3$ was strongly upregulated in the logarithmic phase, indicating a possible autoinducible loop.

Overexpression (OE) of $LuxI_1$ in the wild type background suggested an increased short-chain AHL production compared to the wild type. $LuxI_2$ and $LuxI_3$ showed no or a reduced short-chain AHL production. The production of long-chain AHLs of all three overexpression strains was similar to the wild type. The overexpression strains were cultivated in MB and AHLs were detected via bioassay analyses. In contrast to the bioassay, only long-chain-AHLs were identified by add-on GC-MS analyses. C18-en- and C18-dien-AHLs were detected in the extract of the $LuxI_1$ OE strain while C14-OH-AHL was identified in the extract of the $LuxI_2$ OE strain. C14-OH-AHL was not detected before in the wild type by GC-MS analyses. The enhanced short-chain AHL bioassay signal could be due to increased long-chain AHLs concentrations, falsely detected as short-chain AHLs. Moreover, the *E. coli* pJBA132 sensor strain showed a differential affinity to unsaturated and saturated long-chain AHLs, because C18-en- and C18-dien-AHL (OE $LuxI_1$) induced a stronger signal than C14-OH-AHL (OE $LuxI_2$) which was not detected by the short-chain AHL reporter.

Successful GC-MS analyses of the extracts were not reproducible. Therefore, it is necessary to optimize the media, culture volumes, solvents, preparation of the extracts and GC-MS setups to obtain reliable results.

6.1.2 Heterologous expression of the LuxI synthases

To confirm the specifity of every single LuxI synthase, each coding sequence was expressed from an inducible P_{lac} promoter in *E. coli* using the protein expression vector pTrcHis-TOPO TA. Expression of the proteins was visualized using SDS-PAGE and Western-Blot and the AHL production was determined by bioassay and GC-MS analyses. Expression of $LuxI_1$ could not be visibly induced, not until the

His-tagged protein was purified and high concentrated. Using Western-Blot, small amounts of the concentrated $LuxI_1$ protein could be detected. A LuxI homolog of *M. loti*, MrlI3, was shown to be also deficient in heterologous AHL production under *in vitro* growth conditions, but was upregulated in *M. loti* bacteroids. Thereof the authors assumed that MrlI3 may be functional and required during symbiosis, but not under laboratory conditions (Yang *et al.* 2009). That could be true for $LuxI_1$. Moreover, $LuxI_1$ heterologous expressed is controlled by an inducible promoter and should be independent from QS regulatory circuits which could cause repression of the synthase in the wild type. The favored component required by $LuxI_1$ to produce its specific signal might be lacking in *E. coli*.

The successful expression of $LuxI_2$ and $LuxI_3$ in *E. coli* resulted in an unexpected production of various long-chain AHLs (C12 to C16-AHLs). It was reported that heterologous expression of LasI from *P. aeruginosa* could lead to changes in AHL composition through differences in the pools of acyl-ACP that exist in a cell at a given time point or metabolic phase. The AHLs produced by LasI expressed in *E. coli* were vastly different from the AHLs known to be produced in the wild type strain (Gould *et al.* 2006). $LuxI_2$ and $LuxI_3$ expressed in *E. coli* may deplete its favored acyl-ACP but still be able to synthesize long-chain AHLs from other acyl-ACPs.

Heterologous expression of $LuxI_{1-3}$ using the vector pBBR1MCS2::P_{Gm}-*luxI*$_{1-3}$ revealed the expression of long-chain AHLs of each single synthase detected by bioassay analyses. Expression control by the constitutive gentamicin promoter was more effective than use of the inducible lactose promoter in pTrcHis. AHLs of these extracts could not be detected via GC-MS analyses.

All three LuxI synthases, present in *D. shibae* DFL-12 were tested to be functional and producing in all likelihood long-chain AHLs like C14-OH-AHL, C18-en-AHL and C18-dien-AHL.

6.2 Elucidating the role of quorum sensing in *D. shibae* DFL-12

D. shibae DFL-12 is a member of the marine *Roseobacter* cluster. They play a crucial role in the complex global sulfur cycle because of their conversion of phytoplankton derived DMSP into DMS, which has an impact on the Earth's climate. Therefore, it is consistent that these bacteria inhabit the niche, so-called phycosphere, surrounding phytoplankton. *D. shibae* DFL-12 lives planktonically or associated with algae. The group of Hmelo and coworkers demonstrated that AHL regulated behaviors are very unlike to be active in open seawater, because of AHL levels below the analytic limit of detection (10 pmol 1^{-1}). Quorum sensing in *Proteobacteria* is generally induced at AHL levels at least of 10 nmol 1^{-1}. Thus, quorum sensing thresholds are much more likely to occur in marine biofilms (marine snow) or other microbial "hotspots", like algae blooms (Hmelo and Van Mooy 2009). This has to be taken into account when quorum sensing regulated phenotypes are discussed. Quorum sensing in *D. shibae* DFL-12 could play a role in initiating and maintaining its symbiosis with algae, because the production of AHLs during the planktonic lifestyle is unlikely to exceed the necessary threshold levels.

The first striking phenotype regarding the Δ*luxI* strains was the growth. Measuring the optical density at 600 nm revealed a shortened *lag* phase of *D. shibae* DFL-12 Δ$luxI_{1, 2}$ as well as shortened generation times (wild type: 3.5 h, Δ$luxI_1$: 2.5h and Δ$luxI_2$: 3 h) but similar final optical densities of all strains. Possible explanations for the changed growth behavior will be given in detail when regulated targets of $luxI_1$ mediated QS are discussed.

The loss of $LuxI_2$ had no influence on the production of long-chain AHLs. Short-chain AHLs could not be detected anymore. Loss of $LuxI_1$ resulted in a total breakdown of AHL production. Neither long-chain, nor short-chain AHLs were detected. Furthermore, the expression of all Lux genes, except for $LuxR_1$, was 10-fold repressed in the Δ$luxI_1$ background compared to the wild type.

6.2.1 Regulated traits of $LuxI_1$ mediated QS

Due to the fact that the $luxI_1$ appears to play a key role in the regulation of the QS cascade in *D. shibae* DFL-12, thematic priority in this work was, to

characterize the phenotypical and transcriptional changes caused by the $LuxI_1$ disruption. Additionally, *D. shibae* DFL-12 Δ*luxI*$_1$ was genetically complemented with the vector pBBR1MCS2::P_{Gm}-*luxI*$_1$ (Comp1) and with the unmodified vector pBBR1MCS2 (Comp0) which were included in every study. In every experiment, the genetic complementation of the mutant resulted in a restored wild type phenotype while the complementation strain with the unmodified vector (Comp0) retained the mutant phenotype.

The CckA/CtrA two component signal transduction system

In the bacterium *Caulobacter crescentus*, the cell cycle master regulator CtrA coordinates DNA replication, cell division and polar morphogenesis. CtrA activity varies during cell cycle progression and is modulated by CckA mediated phosphorylation, proteolysis and transcriptional control. CtrA, in a phosphorylated state, binds specific DNA sequences, regulates the expression of genes involved in cell cycle progression and silences the origin of replication. The two component signal transduction system CckA/CtrA was detected to be downregulated in the Δ*luxI*$_1$ mutant. Nothing is known of cell division control in *D. shibae* DFL-12 but *C. crescentus* provides a valuable model system to study cell cycle regulation and cellular differentiation.

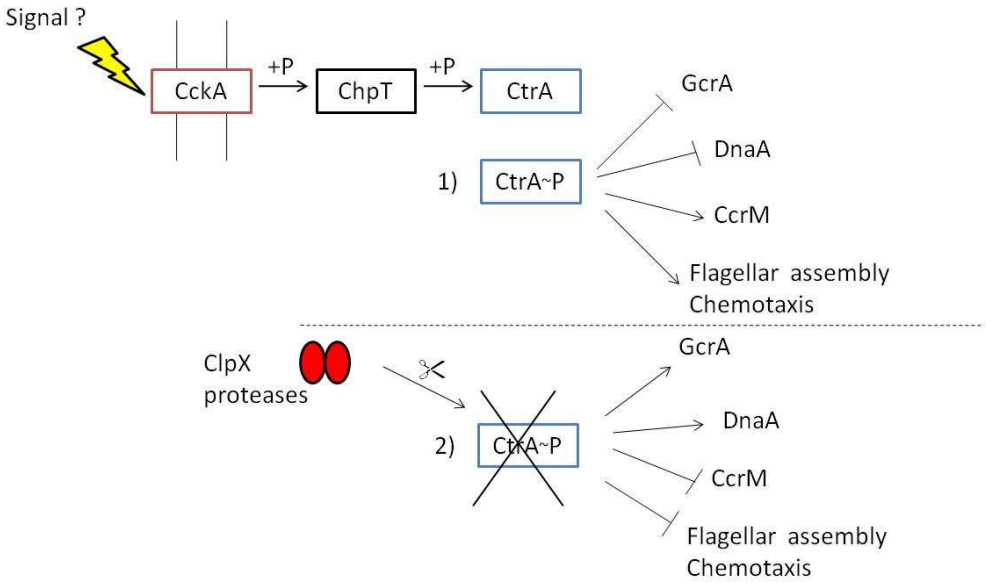

Figure 81 Scheme of the Ccka/CtrA two component system in *C. crescentus* and regulated traits.

A phospho-signaling pathway originating at the polar-localized Ccka histidine kinase controls the phosphorylation state of CtrA. 1) CtrA~P represses cell cycle progression genes (GcrA, DnaA) and activates a DNA methyltransferase (CcrM), flagellar assembly and chemotaxis genes. 2) Is CtrA~P cleared from the cell by ClpX proteases, expression of the cell cycle progression genes is activated and CcrM, flagellar assembly and chemotaxis genes are repressed.

CckA, a histidine kinase, is found around the entire cell membrane and becomes active when it is localized at the cell poles in early predivisional cells. Through the histidine phosphotransferase ChpT, CckA phosphorylates CtrA. CtrA~P activates the cascade of flagellar gene transcription, chemotaxis genes and the expression of CcrM, encoding an essential DNA methyltransferase. Initiation of the DNA replication (DnaA, GcrA) and cell division are repressed. The CtrA~P protein is preferentially cleared from the cell of late predivisional cells by ClpX proteases, allowing the initiation of cell cycle progression while DNA methylation, and flagellar assembly and chemotaxis genes are repressed (McAdams and Shapiro 2009). CckA plays a central role in the regulation of CtrA activity. Loss of CckA function corresponds in a loss of CtrA activity and lacking phosphorylation of CtrA, respectively. Loss of CtrA~P promotes cell cycle progression. Moreover, beside the cell-cycle-controlled localization which may play an important role in CckA regulation, signals responsible for CckA activation are not known (Jacobs *et al.* 2003). Maybe the CckA histidine kinase is inactive as well as CtrA~P because of the missing $LuxI_1$ autoinducer and cells could proliferate steadily in the mutant population.

That AHLs could serve as signals for histidine kinases to activate phosphorylation/dephosphorylation signal transduction cascades is well known from the *V. harveyi* quorum sensing system.

Cell cycle progression and cell differentiation were completely altered in the mutant strain. The evaluation of growth curves and cell numbers revealed that growth and division rates of the mutant were increased and the generation time was shortened. To determine the growth phases of wild type and Δ*luxI*$_1$ mutant, calculation of the cell number using cell flow cytometry was required. According to the cell numbers, both strains entered stationary phase after approximately 25 hours of incubation but with different final cell densities. Cell numbers of *D. shibae* DFL-12 Δ*luxI*$_1$ were twice as high as the final cell numbers of *D. shibae* DFL-12 when strains entered the stationary phase. In case of *D. shibae* DFL-12 Δ*luxI*$_1$ measurements of the optical density and cell numbers did not correspond. Using the optical density misrepresented the actual growth phase.

Genetical complementation of the Δ*luxI*$_1$ mutant restored the growth and division rates as well as the generation time. Environmental signals, through different mechanisms, feed into the action of transcriptional regulators and sigma factors that direct the activity of RNA polymerases towards gene expression in different growth phases. AHLs could present one of these signals influencing the different levels of regulation at the onset of growth phases.

Population heterogeneity versus homogeneity

Cells of the mutant were homogenous while the wild type population occurred extremely heterogenous in SWM with 5 mM succinate. Wild type cell morphologies varied from coccoid cells and small rods to bottle-shaped cells to sustained, giant cells. Mutant cells were uniform, small coccoids. The variability of the cell morphology was also quantified by use of flow cytometry which revealed also extensive cell heterogeneity in *D. shibae* DFL-12 and cell homogeneity in LuxI$_1$ mutant batch cultures. Loss of cell heterogeneity in the mutant population may be caused by the downegulation of CtrA(~P) which

controls not only cell cycle progression but also cell differentiation (McAdams and Shapiro 2009), but also starvation may play a significant role.

Assuming that the large cells of the wild type represent “fat-cells”, storage compound analyses were performed. Furthermore, the genome annotation of *D. shibae* DFL-12 revealed a complete pathway for the synthesis of storage compounds like polyhdyroxyalkanoates (PHAs). Nile red staining of wild type and mutant cells showed high production of lipidic storage compounds of both, wild type and mutant. Obviously the giant cells are able to store larger amounts than mutant cells, but also in the mutant cells lipidic inclusion could be visualized. Also TEM micrographs showed no differences in the cell organisation of wild type and mutant.

Loss of the $LuxI_1$ signal caused morphological changes and homogeneity. All mutant cells were smaller as the result of reductive division. Reductive division increases the surface/volume ratio, producing spherical cells which lead to an effective adaption to low nutrient concentrations. Cell heterogeneity occurred within the wild type population under same conditions. Giant cells which grew slowly and were filled with storage compounds appeared as well as small, fast growing cells comprising low amounts of storage compounds. Population heterogeneity could be an adaption to fluctuating environments and is a kind of survival strategy of the whole population (Kussell *et al.* 2005). Thus, using artificial SWM with only one carbon source could trigger population heterogeneity because of the nutrient limitation. Heterogeneity is typical for QS regulated traits. Bioluminescent heterogeneity, for example, occurs within the population of *V. harveyi* where it was found in all media and all tested temperatures. Therefore it appears unlikely that the observed heterogeneity is attributed to laboratory conditions. Furthermore, the percentage of luminescent cells of *V. harvyi* increased after addition of synthetic AI-2. These results suggested that *V. harveyi* naturally produces and/or keeps the AHL level at non-saturating concentrations which differs from cell to cell causing bistability. According to the theory of Anetzberger and coworkers, a variable cellular LuxR concentration contributes heterogeneous behaviour of the *V. harveyi* wild type

strain and these results imply that *V. harveyi* self-limits the autoinducer concentration. Thus, "dark" cells might not be quorum sensing inactive but rather the LuxR level in these cells might be below the threshold concentration to induce bioluminescence (Anetzberger *et al.* 2009).

D. shibae DFL-12 carrying pKR-C12 revealed AHL heterogeneity. Cells were producing long-chain AHLs in distinct concentrations which led to the induction of several GFP intensities. When the signal of the master synthase (presumably the *luxI*$_1$ product) was disrupted, morphological heterogeneity disappeared. There is no indication how AHL-producing and non-producing cells differ physiologically. To study this, the bacterial flow-cytometric sorting of cells and subpopulation-specific transcriptome analysis of AHL-producing and non-producing cells could be combined. Sorting would be guided by a fluorescent protein reporter controlled by a strongly QS induced promoter (Lemme *et al.* 2011).

Flagellar assembly and chemotaxis genes

Flagella and chemotaxis genes are known targets to be QS regulated. For example, chemotaxis, flagellar and motility genes as well as the production of exopolysachharides are known quorum sensing regulated traits in *Sinorhizobium meliloti* (Llamas *et al.* 2004;Marketon *et al.* 2003;Sourjik *et al.* 2000). Moreover, *S. meliloti* produces AHLs with the same chain-length (C18-HSL) as *D. shibae* DFL-12. The downregulation of flagellar assembly and chemotaxis genes could be directly caused by the loss of the LuxI$_1$ signal or could be indirectly due to the loss of CtrA~P activity. Motility tests of wild type and mutant also revealed different colony shapes and margins. The round shape and smooth margin of the mutant colony indicated the loss of flagellar motility.

Photosynthetic pigments

The porphyrin/chlorophyll metabolism and the carotenoid biosynthesis as well as the terpenoid backbone synthesis (provides carotenoid precursors) were upregulated in the Δ*luxI*$_1$ mutant when entered the stationary phase (according

to the optical density), indicating an increased production of photoactive pigments.

As mentioned before, cell numbers were strongly increased and the mutant was just apparently in stationary phase. Cell division requires the production of new photosynthetic pigments for the resulting daughter cell. Thus, genes of the photosynthetic pigments were upregulated in the Δ*luxI*$_1$ mutant due to increased growth and division rates.

IS4 family transposase

Gene Dshi_3878 was annotated as transposase IS4 family protein. It is located on the plasmid pDS153. Two additional, 100% identical transposases were found on plasmids. Expression of Dshi_3878 was highly upregulated in the mutant but signals could not be traced back to their origins. The signal intensity could be derived from the identical mRNA of three induced transposases. Moreover all three transposases are located on plasmids and we do not know anything about the copy number of each plasmid and transposase gene, respectively. Only very few IS4 elements have been studied in detail. The distribution of family IS4 in *Proteobacteria* uncovered a clear preference for single genomic copies, followed by a preference for two, three and six to eight copies per genome. (De Palmenaer *et al.* 2008). Considerable diversity was observed at the level of target site specifity. In *P. aeruginosa*, IS19999 (a subgroup of the IS4 family) was inserted into the integron-specific recombination site, *attI1*, upstream of the integron-born *bla* gene, that encodes an extended-spectrum β-lactamase (Aubert *et al.* 2006). Upregulation of the transposases could be due to the LuxI$_1$ knock-out in order to provide the necessary genome flexibility for adaption to the new genomic situation and altered phenotypes. Thus, complementation of the mutant with the plasmid-born *luxI*$_1$ synthase did not change the genomic situation of the natural *luxI*$_1$ locus and transposase activity was not restored. Remarkable secondary mutations caused by transposase activity did not occur so far and altered phenotypes of the Δ*luxI*$_1$ mutant could be restored by genomic complementation.

6.2.2 The LuxI$_1$ product and its possible role in the QS network

LuxI$_1$ may play a superior role in the QS regulation system and could be a "master synthase", controlling the expression of a QS cascade. Expression of all Lux genes, except for LuxR$_1$, was decreased and AHL production did not occur. In the related *Alphaproteobacterium*, *Rhizobium leguminosarum* bv. *viciae*, a complex cascade of QS loops was characterized. The *cinRI* locus, responsible for the production of 3OHC14-en-AHL, appears to be the master control for three other AHL-dependent QS systems, synthesizing C6-HSL and C8-HSL. The chromosomally encoded 3OHC14-en-HSL which is synthesized in very low levels during grow still appears to be required for normal production of others AHLs made by two additional synthases. The complex effects of 3OHC14-en-HSL suggests that there may be communication among different quorum sensing loci and thus a hierarchy of AHL signals within *R. leguminosarum* (Blosser-Middleton and Gray 2001).

Expression of LuxR$_2$, one of the orphan regulators, was also repressed in the mutant, indicating a possible interaction between the LuxI$_1$ product and the LuxR$_2$ regulator. It was not possible to trace back the different long-chain AHL signals to their original synthases. AHLs identified in the wild type, complementation and overexpression strains were: OHC14-AHL (OE LuxI$_2$), C16-en-AHL and C16-dien-AHL (Comp1), C18-en-AHL and C18-dien-AHL (wild type, Comp1 and OE LuxI$_1$), but the master signal could not be identified.

A hypothetical model of the quorum sensing network in *D. shibae* DFL-12 is shown in Figure 67.

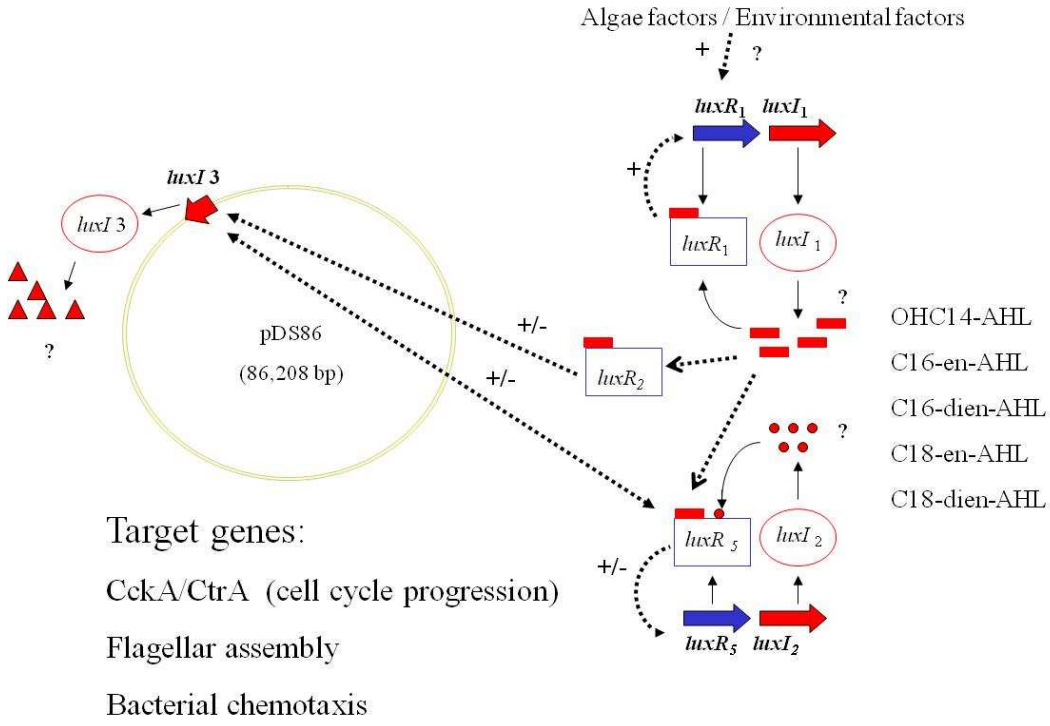

Figure 82 Hypothetical quorum sensing cascade in *D. schibae* DFL-12.

$LuxR_1$ induces *luxI*$_1$ expression allowing the production of the master signal, which together with $LuxR_1$ activates *luxI*$_1$ to form a positive feedback loop. The master signal additionally together with the orphan $LuxR_2$ influences the expression of *luxI*$_3$, an AHL autoinducer synthase located on the plasmid pDS86 and *luxI*$_2$, another QS synthase located on the chromosome. The master signal leads to the production of different AHLs. Traits controlled by this putative cascade are the CckA/CtrA two component system and chemotaxis and flagellar assembly genes. → indicates a demonstrated regulation, ⇢ indicates a putative regulation.

$LuxR_1$ is located upstream of the $LuxI_1$ synthase. Therefore, it is likely that expression of both is autoregulated by the signal molecule produced by $LuxI_1$. But $LuxR_1$ is highly and consistently expressed while the expression of $LuxI_1$ is very low during growth. Moreover, the knock-out of the $LuxI_1$ signal does not influence $LuxR_1$ expression. Thus, it is postulated that $LuxR_1$ expression is controlled by alternative signal molecules like algae or environmental factors, but actively induces or represses $LuxI_1$ expression to a minimum level allowing the production of small concentrations of a master signal. This marginal but effective dose of the master signal induces expression of the second and third autoinducer synthase which leads to the production of different long-chain AHLs. The orphan regulator $LuxR_2$ could play a role in induction of $LuxI_2$ and $LuxI_3$. A missing master signal inactivates long-chain AHL synthesis which revealed that regulation of $LuxI_2$ and $LuxI_3$ seems to be master signal dose dependent. This

indicates $LuxI_1$ to be a master synthase regulating the quorum sensing network of *D. shibae* DFL-12. Traits like the Ccka/CtrA two component system (cell cycle progression and differentiation), chemotaxis and flagellar assembly genes were shown to be controlled by this complex quorum sensing cascade.

6.3 Conclusions

The three LuxI synthases present in *D. shibae* DFL-12 and their role in AHL production were examined throughout this thesis. This was the first functional analysis of QS regulatory genes in *D. shibae* DFL-12 and results revealed that the *D. shibae* DFL-12 $LuxI_1$ synthase controls a complex QS regulatory network as possible "master" synthase. Together with a second and a third LuxI synthase ($LuxI_2$ and $LuxI_3$), each of these systems could coordinate with one another various kinds of cellular functions like cell cycle progression and differentiation, chemotaxis and flagellar assembly.

.

7 Discussion Chapter B

To force the exchange of metabolites and, if required, the attachment of *D. shibae* DFL-12 to the algal host, cobalamin (vitamin B12) was omitted from the L1 coculture medium to grow the algae under vitamin B12 limitation.

7.1 Detection of long-chain AHLs during cocultivation

The effect of cultivation parameters on the synthesis of AHLs was studied by means of the GFP-based reporter construct (pKR-C12) of Kathrin Riedel, present in *D. shibae* DFL-12 during cocultivation with axenic algae in chemically defined medium. The construct is most sensitive for 3OC12-HSL and related long-chain AHLs (Riedel *et al.* 2001). Thus, the intracellular occurrence of long-chain AHLs was monitored in *D. shibae* DFL-12 cells during algae symbiosis.

Transformation of the sensor construct into *D. shibae* DFL-12 wild type generated a heterogeneous sensor population. Cells with various GFP intensities emerged. FACS analyses of the sensor population revealed a classification into cells brightly expressing GFP, cells with a medium GFP induction and cells without any GFP expression. Disruption of GFP expression could not be due to plasmid loss, because the sensor strain was grown in medium with selective pressure through antibiotic treatment.

In general, cell-to-cell- heterogeneity in gene expression arises from fluctuations in rate of transcription from a promoter, mRNA or protein stability and/or the rate of translation. Moreover, in plasmid-born GFP expression, the plasmid copy number and plasmid stability play a significant role. Plasmid stability should be guaranteed by applying selective pressure by antibiotic treatment. Assuming, that the plasmid stability has been secured, GFP heterogeneity of the *D. shibae* DFL-12 wild type population carrying pKR-C12 has to be due to varying concentrations of AHLs from cell to cell. FACS sorting generated a population with 88% of the cells expressing GFP and cells brightly expressing GFP (fraction R6) were enriched up to 74% within this population. Growing *D. shibae* DFL-12 FACS6 in short-term experiments demonstrated a certain percentage stability of brightly GFP expressing cells, but using the strain in long-term cocultivations seemed to recover the initial population heterogeneity and AHL self-limitation,

respectively. The mechanism, how *D. shibae* DFL-12 controls self-limitation of AHLs needs further investigation such as e.g. a variable LuxR concentration. The dynamics of population heterogeneity should be elucidated by flow cytometry analyses of a *D. shibae* DFL-12 FACS6 population to clarify whether the enforced GFP heterogeneity will be stable (74% brightly GFP expressing cells) or will regress to initial conditions. Cells with distinct GFP concentrations which indicate diverse levels of AHL self-limitation could be sorted by FACS and transcriptional variances could be analysed using qRT-PCR or Microarray studies.

7.2 Quorum sensing during algae symbiosis

Axenic cultures of *P. lima*, from which *D. shibae* DFL-12 originally was isolated, are not available in culture collections. Thus, *P. minimum* the closely related dinoflagellate was used for cocultivation. Although *D. shibae* DFL-12 has also been isolated from the haptophyt *I. galbana*, cocultivation results using axenic *P. minimum* and axenic *I. galbana* varied significantly.

The axenic haptophyt *I. galbana* was not colonized by *D. shibae* DFL-12. SEM micrographs visualized that no attachment of bacteria to the haptophyt surface occurred (micrographs not shown). All bacterial cells remained planktonic. *D. shibae* DFL-12 FACS6 stimulated the growth of *I. galbana* in the absence of cobalamin. Supplementation with pure vitamin B12 resulted in a faster and stronger recovery of the haptophyt culture compared to the inoculation with *D. shibae* DFL-12 FACS6. The cocultivation with *I. galbana* allowed the bacterium to grow and the production of long-chain AHLs could be visualized through GFP expression. Nevertheless, the concentration of produced long-chain AHLs was stable, but very low in both cultures. The generation time of *D. shibae* DFL-12 FACS6 in pure SWM with 5 mM succinate was 9 hours. After ~8 days (20 generations) of cultivation 58% of the cells still comprise the plasmid but just 10% of the cells were producing long-chain AHLs. The generation time of *D. shibae* DFL-12 FACS6 in coculture with *I. galbana* was 29 hours. After ~8 days (6.4 generations) of cultivation > 92% of the cells still harboring the plasmid but just in 10% of the cells GFP expression was induced. Thus, lacking GFP induction was not due to plasmid loss but rather due to low concentrations of long-chain AHLs.

This relationship could be described as loose mutualistic relationship. Interactions do not involve close physical contact, but rely on produced metabolites. In fact, mutually required nutrients were released by both species into the surrounding habitat which agrees with the work of M. R. Droop who demonstrated that the requirement for vitamins is low. Thus, there is not a general need for direct bacterial symbiosis involving the vitamins to assure that concentrations in marine environments are usually not limiting growth (Droop 2007).

P. minimum was colonized by *D. shibae* DFL-12 FACS6. SEM micrographs clearly demonstrated that many bacterial cells were attached to the dinoflagellate surface or to filaments which linked the eukaryotic cells among each other. Furthermore, *D. shibae* DFL-12 FACS6 stimulated the growth of *P. minimum* in the absence of cobalamin as well as the addition of pure vitamin B12 resulted in recovery of the dinoflagellate culture. Growth of both supplemented cultures reached the equal, final chlorophyll amount of the positive control. Also the cocultivation with *P. minimum* allowed the bacterium to grow and the production of long-chain AHLs could be visualized through GFP expression. But, unlike in coculture with *I. galbana*, AHL production of *D. shibae* DFL-12 FACS6 differed in pure L1 medium with 0.5 mM succinate and in coculture with *P. minimum*. When *D. shibae* DFL-12 FACS6 was grown without algae in L1 0.5 mM succinate, the production of AHLs increased in a QS dependent manner. The generation time of *D. shibae* DFL-12 FACS6 in L1 with 0.5 mM succinate was 35 hours which secured plasmid stability for >92% of the cells during 13 days of cultivation. In 61% of the cells GFP expression was induced (day 12). In coculture with *P. minimum*, the GFP expression and AHL production, respectively, decreased already after seven days to average 2% and did not recover until the end of cocultivation although >92% of the cells still harbored the sensor construct (generation time *D. shibae* DFL-12 FACS6 in coculture: 23 hours). The repression of AHL production could imply a possible quorum quenching activity due to compounds made by *P. minimum*. First prepared cocultivation experiments with *P. minimum* showed that inoculation with bacterial cell numbers higher than 5 x 10^6 cells/ml resulted in the breakdown of the weakened

dinoflagellate population (data not shown). Therefore, *P. minimum* should have developed mechanism to regulate the colonization by bacteria. The repressing of relevant genes by quorum quenching signals would be one possible method to control the attachment of prokaryotes (Pan and Ren 2009). First evidence found, regarding quorum quenching activity, was the repression of the *D. shibae* AHL synthesis in coculture with *P. minimum*. To investigate the expression of some relevant genes, qRT-PCR studies were performed of a pure *D. shibae* DFL-12 FACS6 culture and a coculture. The transcription rates of the *lux*, alginate, fascicline genes and genes involved in the biosynthesis of thiamine and cobalamin were determined. Interestingly, the expression of the "master" synthase $LuxI_1$ was downregulated in the cocultured *D. shibae* DFL-12 FACS6 strain which could explain the lack of GFP induction. Furthermore, QS regulated genes which are postulated to play a role in adhesion and biofilm formation such as fascicline and alginate were clearly repressed in the coculture. The transcription rate of CobN, which is an ATP-dependent cobalt chelatase and responsible for cobalt insertion in the aerobic route of cobalamin synthesis, was increased in the coculture strain, indicating a higher vitamin B12 consumption by the algae. CbiX, the respective ATP-independent cobalt chelatase of the anaerobic pathway, showed no differentiated expression pattern. Thiamin, which was supplemented to the coculture medium, but omitted in the pure bacterial culture, was significantly higher expressed in the pure culture. The transcriptional information is just based on one single experiment at one time point, but it is likely that QS controls many bacterial behaviors that are essential for *roseobacter*-algae symbiosis including the initiation and establishment of the symbiosis. There is an obvious benefit for a bacterium to attach to an algal cell. It obtains metabolites from the algae, is in close proximity to other bacteria which permits transfer of genes and signal molecules and forming a biofilm protects the bacteria against predators such as bacteriovores (Geng and Belas 2010b).

P. minimum was shown to repress the quorum sensing system of *D. shibae* DFL-12 FACS6. Although the dinoflagellate requires vitamin B12, it may not be dependent on a symbiosis with *D. shibae* DFL-12 to obtain it. Moreover, colonization seemed to be fended and could harm the alga. *P. minimum* did not

appear as ideal symbiosis partner to study the role of QS during cocultivation because of its quorum quenching capability.

7.3 Conclusions

The insertion of a GFP-based reporter construct into *D. shibae* DFL-12 generated a heterogeneous population regarding the GFP induction and therefore the long-chain AHL concentration. These results suggested that *D. shibae* DFL-12 naturally produces and/or keeps the long-chain AHL level at non-saturating concentrations or that the ratio of different long-chain AHLs varied from cell to cell. Maybe OH14C-AHL and C16-en/dien-AHL are more specific to the sensor construct pKR-C12 than C18-en/dien-AHL and induce GFP expression.

Cocultivation with an axenic dinoflagellate as well as an axenic haptophyt revealed that *D. shibae* DFL-12 provides the algae with vitamin B12 in exchange for nutrients. *I. galbana* did not influence the long-chain AHL production of *D. shibae* DFL-12 and the bacterium did not attach. *P. minimum* with its prickly armored surface was colonized by *D. shibae* DFL-12. It seems to be that *P. minimum* is able to control bacterial attack by producing inhibitory compounds. In coculture the long-chain AHL production was reduced in *D. shibae* DFL-12 as well as genes responsible for establishment of a biofilm. Moreover, the expression of CobN, a key enzyme in the aerobic route of cobalamin synthesis, was increased in the coculture strain, indicating an enhanced algae-required vitamin B12 production. Many questions need to be unraveled. What kind of quorum quenching compound influences the long-chain AHL mediated quorum sensing system? What kind of regulatory key activates enhanced vitamin B12 expression in coculture? The association of *D. shibae* DFL-12 with algae seems to be host-specific and could be mutualistic (*I. galbana*) or possibly parasitic (*P. minimum*). Depending on the algae, the *D. shibae* DFL-12 QS system could play an important role in the establishment of symbiotic relationships between *D. shibae* DFL-12 and its host.

8 Summary

8.1 The functionality and specifity of the three LuxI synthases present in *D. shibae* DFL-12

- D *shibae* DFL-12 was shown to produce short- and long chain AHLs, using a GFP-based bioassay.
- The production of C18-en-HSL and C18-dien HSL could be verified by GC-MS but not that of C8-HSL.
- Heterologous expression of $LuxI_2$ and $LuxI_3$ in *E. coli* led to the synthesis of several long-chain AHLs, verified by GC-MS, having various chain-lengths (C12-C16) and substitutions and thus differed from the AHL molecules produced by *D. shibae* DFL-12, presumably due to a different metabolism of precursor synthesis in *E. coli*.
- Using bioassay and GC-MS analysis, no AHL could be detected by heterologous expression of $LuxI_1$ (pTrcHis) in *E. coli*.
- The amount of produced $LuxI_1$ protein in *E. coli* was very low, since only in a concentrated sample the His-tagged protein could be detected by Western Blot analysis, explaining the lack of AHL molecules in *E. coli* extracts.
- Using the bioassay analysis, long-chain AHLs could be detected by heterologous expression of $LuxI_1$ (pBBR1MCS2::P_{Gm}-*luxI*$_1$) in *E. coli*.
- Overexpression of the $LuxI_1$ gene in the *D. shibae* DFL-12 wild type background was carried out to obtain more insights about its function. Using the bioassay, extracts of the strain overexpressing $LuxI_1$ showed a significant increase in the production of short-chain molecules and a decreased synthesis of long-chain AHL molecules compared to the parental strain.
- Quantitative real-time PCR revealed that transcription of *luxI*$_1$ was much lower than the expression of *luxI*$_2$ and *luxI*$_3$. The production of different long-chain molecules (OHC14-AHL, C16-en/dien-AHL and C18-en/dien-AHL) is carried out by *luxI*$_1$, *luxI*$_2$ and *luxI*$_3$.

8.2 The role of LuxI$_1$ mediated QS in *D. shibae* DFL-12

- Deletion of the *luxI*$_1$ gene decreased the production of all signaling molecules below the detection limit of the bioassay and GC-MS. All *lux* genes, except for LuxR$_1$, were shown to be repressed in qRT-PCR analyses, indicating a possible LuxI$_1$ master synthase.
- Deletion of *luxI*$_2$ had no impact on the bioassay used for the detection of short-and long-chain AHLs.
- *D. shibae* DFL-12 Δ*luxI*$_1$ showed the loss of AHL production, a homogeneous cell morphology and increased growth-and division rates, all of which could be successfully complemented by introduction of a plasmid-born copy of *luxI*$_1$.
- Transcriptome analysis at various growth stages of *D. shibae* DFL-12 Δ*luxI*$_1$ showed dramatic changes in gene expression levels compared to the wild type.
- The two-component system CckA/CtrA was downregulated in the mutant and could be controlling cellular processes like cell cycle progression and differentiation.
- Affected traits like flagellar assembly and chemotaxis genes were downregulated in the mutant which could cause the loss of motility. Flagellar and chemotaxis genes could be influenced directly through AHL signaling or indirectly by the CckA/CtrA two component system.
- Two highly conserved *vir* operons located on the sister plasmids pDS191 and pDS126 were downregulated in the mutant. Probe signals of the microarray could be traced back to their origins.
- An IS4 family transposase was highly upregulated in *D. shibae* DFL-12 Δ*luxI*$_1$. Two additional, 100% identical transposases are present in *D. shibae* DFL-12 Δ*luxI*$_1$. Therefore, hybridization of the probe derived from the mRNA of possibly three activated transposases.

8.3 The role of QS during cocultivation with axenic algae

- Long–chain AHL production during cocultivation was visualized using the GFP-based sensor plasmid pKR-C12 (Riedel *et al.* 2001), which was introduced into *D. shibae* DFL-12 by biparental mating.
- *D. shibae* DFL-12 pKR-C12 showed a strong heterogeneity of GFP expression. Despite antibiotic pressure and thus the presence of the plasmid in all cells, GFP expression levels in individual cells of the population ranged over several orders of magnitude.
- A single cell, producing a high level of GFP was removed from the heterogeneous culture by FACS and further subcultivated. Daughter cells showed an increased GFP expression and were used to monitor AHL expression during cocultivation with different algae.
- Cocultivation with the axenic haptophyt *I. galbana* did not change the level of GFP expression, and thus production of AHL molecules, in *D. shibae* DFL-12 cells.
- GFP expression, and thus long-chain AHL production, was strongly repressed during cocultivation with the dinoflagellate *P. minimum*. Accordingly, expression of *luxI*$_1$ was significantly reduced compared to the control, using qRT-PCR.
- Microscopic analysis revealed that *D. shibae* DFL-12 was able to attach to the surface of *P. minimum*, whereas no interaction with *I. galbana* could be visualized. Transcription levels of possible symbiotic genes were determined in coculture with *P. minimum* and showed a strong downregulation for fascicline and alginate genes.
- Provision of vitamin B12 from *D. shibae* DFL-12 to both algae was shown, since inoculation with *D. shibae* DFL-12 could substitute vitamin B12 supplementation, necessary to promote the growth of both algae. Accordingly, expression of genes involved in the production of vitamin B12 were increased in *D. shibae* DFL-12 during cocultivation.

References

Alberghini,S., Polone,E., Corich,V., Carlot,M., Seno,F., Trovato,A. and Squartini,A. (2009) Consequences of relative cellular positioning on quorum sensing and bacterial cell-to-cell communication. *FEMS Microbiol. Lett.* **292**, 149-161.

Alekshun,M.N. and Levy,S.B. (2007) Molecular mechanisms of antibacterial multidrug resistance. *Cell* **128**, 1037-1050.

Allgaier,M., Uphoff,H., Felske,A. and Wagner-Dobler,I. (2003) Aerobic anoxygenic photosynthesis in Roseobacter clade bacteria from diverse marine habitats. *Applied and Environmental Microbiology* **69**, 5051-5059.

Andersen,J.B., Heydorn,A., Hentzer,M., Eberl,L., Geisenberger,O., Christensen,B.B., Molin,S. and Givskov,M. (2001) gfp-based N-acyl homoserine-lactone sensor systems for detection of bacterial communication. *Applied and Environmental Microbiology* **67**, 575-585.

Andersen,R.A. (2004) Biology and systematics of heterokont and haptophyte algae. *American Journal of Botany* **91**, 1508-1522.

Anetzberger,C., Pirch,T. and Jung,K. (2009) Heterogeneity in quorum sensing-regulated bioluminescence of Vibrio harveyi. *Mol. Microbiol.* **73**, 267-277.

Aubert,D., Naas,T., Heritier,C., Poirel,L. and Nordmann,P. (2006) Functional Characterization of IS1999, an IS4 Family Element Involved in Mobilization and Expression of {beta}-Lactam Resistance Genes. *The Journal of Bacteriology* **188**, 6506-6514.

Barnett,M.J., Hung,D.Y., Reisenauer,A., Shapiro,L. and Long,S.R. (2001) A Homolog of the CtrA Cell Cycle Regulator Is Present and Essential in Sinorhizobium meliloti. *The Journal of Bacteriology* **183**, 3204-3210.

Bassler,B.L. (1999) How bacteria talk to each other: regulation of gene expression by quorum sensing. *Curr. Opin. Microbiol.* **2**, 582-587.

Bassler,B.L., Wright,M., Showalter,R.E. and Silverman,M.R. (1993) Intercellular signalling in Vibrio harveyi: sequence and function of genes regulating expression of luminescence. *Mol. Microbiol.* **9**, 773-786.

Belas,R., Horikawa,E., Aizawa,S. and Suvanasuthi,R. (2009) Genetic determinants of Silicibacter sp. TM1040 motility. *J Bacteriol.* **191**, 4502-4512.

Benjamini,Y. and Hochberg,Y. (1995) Controlling the False Discovery Rate - a Practical and Powerful Approach to Multiple Testing. *Journal of the Royal Statistical Society Series B-Methodological* **57**, 289-300.

Biebl,H., Allgaier,M., Tindall,B.J., Koblizek,M., Lunsdorf,H., Pukall,R. and Wagner-Dobler,I. (2005) *Dinoroseobacter shibae* gen. nov., sp nov., a new

aerobic phototrophic bacterium isolated from dinoflagellates. *International Journal of Systematic and Evolutionary Microbiology* **55**, 1089-1096.

Blosser-Middleton,R.S. and Gray,K.M. (2001) Multiple N-acyl homoserine lactone signals of Rhizobium leguminosarum are synthesized in a distinct temporal pattern. *J Bacteriol.* **183**, 6771-6777.

Branda,S.S., Vik,A., Friedman,L. and Kolter,R. (2005) Biofilms: the matrix revisited. *Trends in Microbiology* **13**, 20-26.

Brelles-Marino,G. and Bedmar,E.J. (2001) Detection, purification and characterisation of quorum-sensing signal molecules in plant-associated bacteria. *J Biotechnol.* **91**, 197-209.

Brinkhoff,T., Giebel,H.A. and Simon,M. (2008) Diversity, ecology, and genomics of the Roseobacter clade: a short overview. *Arch. Microbiol.* **189**, 531-539.

Buchan,A., Gonzalez,J.M. and Moran,M.A. (2005) Overview of the marine roseobacter lineage. *Applied and Environmental Microbiology* **71**, 5665-5677.

Byers,J.T., Lucas,C., Salmond,G.P. and Welch,M. (2002) Nonenzymatic turnover of an Erwinia carotovora quorum-sensing signaling molecule. *J Bacteriol.* **184**, 1163-1171.

Cortes-Altamirano,R., Hernandez-Becerril,D.U. and Luna-Soria,R. (1995) [Red tides in Mexico: a review]. *Rev. Latinoam. Microbiol* **37**, 343-352.

Costerton,J.W., Stewart,P.S. and Greenberg,E.P. (1999) Bacterial Biofilms: A Common Cause of Persistent Infections. *Science* **284**, 1318-1322.

De Meirsman,C., Van Soom,C., Verreth,C., Van Gool,A. and Vanderleyden,J. (1990) Nucleotide sequence analysis of IS427 and its target sites inAgrobacterium tumefaciens T37. *Plasmid* **24**, 227-234.

De Palmenaer,D., Siguier,P. and Mahillon,J. (2008) IS4 family goes genomic. *BMC Evolutionary Biology* **8**, 18.

Decho,A.W., Visscher,P.T., Ferry,J., Kawaguchi,T., He,L., Przekop,K.M., Norman,R.S. and Reid,R.P. (2009) Autoinducers extracted from microbial mats reveal a surprising diversity of N-acylhomoserine lactones (AHLs) and abundance changes that may relate to diel pH. *Environ. Microbiol.* **11**, 409-420.

Defoirdt,T., Boon,N. and Bossier,P. (2010) Can bacteria evolve resistance to quorum sensing disruption? *PLoS. Pathog.* **6**, e1000989.

Defoirdt,T., Boon,N., Sorgeloos,P., Verstraete,W. and Bossier,P. (2008) Quorum sensing and quorum quenching in Vibrio harveyi: lessons learned from in vivo work. *ISME J* **2**, 19-26.

Droop,M.R. (2007) Vitamins, phytoplankton and bacteria: symbiosis or scavenging? *Journal of Plankton Research* **29**, 107-113.

Eberhard,A., Burlingame,A.L., Eberhard,C., Kenyon,G.L., Nealson,K.H. and Oppenheimer,N.J. (1981) Structural identification of autoinducer of Photobacterium fischeri luciferase. *Biochemistry* **20**, 2444-2449.

Faith,S.A. and Miller,C.A. (2000) A newly emerging toxic dinoflagellate, Pfiesteria piscicida: natural ecology and toxicosis to fish and other species. *Vet. Hum. Toxicol.* **42**, 26-29.

Flavier,A.B., Ganova-Raeva,L.M., Schell,M.A. and Denny,T.P. (1997) Hierarchical autoinduction in Ralstonia solanacearum: control of acyl-homoserine lactone production by a novel autoregulatory system responsive to 3-hydroxypalmitic acid methyl ester. *J Bacteriol.* **179**, 7089-7097.

Fuqua,C. and Greenberg,E.P. (2002) Listening in on bacteria: acyl-homoserine lactone signalling. *Nat. Rev. Mol. Cell Biol.* **3**, 685-695.

Fuqua,C., Parsek,M.R. and Greenberg,E.P. (2001) REGULATION OF GENE EXPRESSION BY CELL-TO-CELL COMMUNICATION: Acyl-Homoserine Lactone Quorum Sensing. *Annual Review of Genetics* **35**, 439-468.

Gaines, G. and Elbrächter, M. Heterotrophic nutrition. Taylor F.J.R. The biology of dinoflagellates[21]. 1987. Oxford, Blackwell Scientific Publications. Botanical Monographs.
Ref Type: Serial (Book,Monograph)

Garneau,J.E., Dupuis,M.E., Villion,M., Romero,D.A., Barrangou,R., Boyaval,P., Fremaux,C., Horvath,P., Magadan,A.H. and Moineau,S. (2010) The CRISPR/Cas bacterial immune system cleaves bacteriophage and plasmid DNA. *Nature* **468**, 67-71.

Geng,H. and Belas,R. (2010a) Expression of tropodithietic acid biosynthesis is controlled by a novel autoinducer. *J Bacteriol.* **192**, 4377-4387.

Geng,H. and Belas,R. (2010b) Molecular mechanisms underlying roseobacter-phytoplankton symbioses. *Curr. Opin. Biotechnol.* **21**, 332-338.

Gilson,L., Kuo,A. and Dunlap,P.V. (1995) AinS and a new family of autoinducer synthesis proteins. *J Bacteriol.* **177**, 6946-6951.

Giovannoni,S.J. and Stingl,U. (2005) Molecular diversity and ecology of microbial plankton. *Nature* **437**, 343-348.

Gould,T.A., Herman,J., Krank,J., Murphy,R.C. and Churchill,M.E. (2006) Specificity of acyl-homoserine lactone synthases examined by mass spectrometry. *J Bacteriol.* **188**, 773-783.

Grant,S.G., Jessee,J., Bloom,F.R. and Hanahan,D. (1990) Differential plasmid rescue from transgenic mouse DNAs into Escherichia coli methylation-restriction mutants. *Proc. Natl. Acad. Sci. U. S. A* **87**, 4645-4649.

Guillard,R.R. and RYTHER,J.H. (1962) Studies of marine planktonic diatoms. I. Cyclotella nana Hustedt, and Detonula confervacea (cleve) Gran. *Can. J Microbiol* **8**, 229-239.

He,X., Chang,W., Pierce,D.L., Seib,L.O., Wagner,J. and Fuqua,C. (2003) Quorum sensing in Rhizobium sp. strain NGR234 regulates conjugal transfer (tra) gene expression and influences growth rate. *J Bacteriol.* **185**, 809-822.

Henke,J.M. and Bassler,B.L. (2004) Bacterial social engagements. *Trends Cell Biol.* **14**, 648-656.

Hense,B.A., Kuttler,C., Muller,J., Rothballer,M., Hartmann,A. and Kreft,J.U. (2007) Does efficiency sensing unify diffusion and quorum sensing? *Nat. Rev. Microbiol.* **5**, 230-239.

Heredia-Tapia,A., Arredondo-Vega,B.O., Nunez-Vazquez,E.J., Yasumoto,T., Yasuda,M. and Ochoa,J.L. (2002) Isolation of Prorocentrum lima (Syn. Exuviaella lima) and diarrhetic shellfish poisoning (DSP) risk assessment in the Gulf of California, Mexico. *Toxicon* **40**, 1121-1127.

Herrero,M., de,L., V and Timmis,K.N. (1990) Transposon vectors containing non-antibiotic resistance selection markers for cloning and stable chromosomal insertion of foreign genes in gram-negative bacteria. *J Bacteriol.* **172**, 6557-6567.

Hmelo,L. and Van Mooy,B.A.S. (2009) Kinetic constraints on acylated homoserine lactone-based quorum sensing in marine environments. *Aquatic Microbial Ecology* **54**, 127-133.

Hoang,H.H., Gurich,N. and Gonzalez,J.E. (2008) Regulation of motility by the ExpR/Sin quorum-sensing system in Sinorhizobium meliloti. *J Bacteriol.* **190**, 861-871.

Horng,Y.T., Deng,S.C., Daykin,M., Soo,P.C., Wei,J.R., Luh,K.T., Ho,S.W., Swift,S., Lai,H.C. and Williams,P. (2002) The LuxR family protein SpnR functions as a negative regulator of N-acylhomoserine lactone-dependent quorum sensing in Serratia marcescens. *Mol. Microbiol.* **45**, 1655-1671.

Jacobs,C., Ausmees,N., Cordwell,S.J., Shapiro,L. and Laub,M.T. (2003) Functions of the CckA histidine kinase in Caulobacter cell cycle control. *Molecular Microbiology* **47**, 1279-1290.

Jacobs,C., Domian,I.J., Maddock,J.R. and Shapiro,L. (1999) Cell Cycle-Dependent Polar Localization of an Essential Bacterial Histidine Kinase that Controls DNA Replication and Cell Division. *Cell* **97**, 111-120.

Kang,I., Oh,H.M., Vergin,K.L., Giovannoni,S.J. and Cho,J.C. (2010a) Genome Sequence of the Marine Alphaproteobacterium HTCC2150, assigned to the Roseobacter clade. *J Bacteriol.*

Kang,I., Vergin,K.L., Oh,H.M., Choi,A., Giovannoni,S.J. and Cho,J.C. (2010b) Genome Sequence of strain HTCC2083, a Novel Member of the Marine Roseobacter Clade. *J Bacteriol.*

Kaplan,H.B. and Greenberg,E.P. (1985) Diffusion of autoinducer is involved in regulation of the Vibrio fischeri luminescence system. *J Bacteriol.* **163**, 1210-1214.

Kleerebezem,M., Quadri,L.E., Kuipers,O.P. and de Vos,W.M. (1997) Quorum sensing by peptide pheromones and two-component signal-transduction systems in Gram-positive bacteria. *Mol. Microbiol.* **24**, 895-904.

Kovach,M.E., Elzer,P.H., Hill,D.S., Robertson,G.T., Farris,M.A., Roop,R.M. and Peterson,K.M. (1995) Four new derivatives of the broad-host-range cloning vector pBBR1MCS, carrying different antibiotic-resistance cassettes. *Gene* **166**, 175-176.

Kussell,E., Kishony,R., Balaban,N.Q. and Leibler,S. (2005) Bacterial persistence: a model of survival in changing environments. *Genetics* **169**, 1807-1814.

Lazazzera,B.A. (2000) Quorum sensing and starvation: signals for entry into stationary phase. *Curr. Opin. Microbiol.* **3**, 177-182.

Lembi, C. A. a. W. J. R. Algae and Human Affairs. 1988. Cambridge, Cambridge University Press.
Ref Type: Serial (Book,Monograph)

Lemme,A., Grobe,L., Reck,M., Tomasch,J. and Wagner-Dobler,I. (2011) Subpopulation-Specific Transcriptome Analysis of Competence-Stimulating-Peptide-Induced Streptococcus mutans. *The Journal of Bacteriology* **193**, 1863-1877.

Li,X., Fekete,A., Englmann,M., G÷tz,C., Rothballer,M., Frommberger,M., Buddrus,K., Fekete,J., Cai,C., Schr÷der,P., Hartmann,A., Chen,G. and Schmitt-Kopplin,P. (2006) Development and application of a method for the analysis of N-acylhomoserine lactones by solid-phase extraction and ultra high pressure liquid chromatography. *Journal of Chromatography A* **1134**, 186-193.

Llamas,I., Keshavan,N. and Gonzalez,J.E. (2004) Use of Sinorhizobium meliloti as an indicator for specific detection of long-chain N-acyl homoserine lactones. *Applied and Environmental Microbiology* **70**, 3715-3723.

Lorenz,M.G. and Wackernagel,W. (1994) Bacterial gene transfer by natural genetic transformation in the environment. *Microbiol Rev.* **58**, 563-602.

Lunau,M., Lemke,A., Walther,K., Martens-Habbena,W. and Simon,M. (2005) An improved method for counting bacteria from sediments and turbid environments by epifluorescence microscopy. *Environmental Microbiology* **7**, 961-968.

Lunsdorf,H., Strompl,C., Osborn,A.M., Bennasar,A., Moore,E.R., Abraham,W.R. and Timmis,K.N. (2001) Approach to analyze interactions of microorganisms, hydrophobic substrates, and soil colloids leading to formation of composite biofilms, and to study initial events in microbiogeological processes. *Methods Enzymol.* **336**, 317-331.

Manefield,M., Rasmussen,T.B., Henzter,M., Andersen,J.B., Steinberg,P., Kjelleberg,S. and Givskov,M. (2002) Halogenated furanones inhibit quorum sensing through accelerated LuxR turnover. *Microbiology* **148**, 1119-1127.

Marketon,M.M., Glenn,S.A., Eberhard,A. and Gonzalez,J.E. (2003) Quorum sensing controls exopolysaccharide production in Sinorhizobium meliloti. *J Bacteriol.* **185**, 325-331.

Marketon,M.M., Gronquist,M.R., Eberhard,A. and Gonzalez,J.E. (2002) Characterization of the Sinorhizobium meliloti sinR/sinI locus and the production of novel N-acyl homoserine lactones. *J Bacteriol.* **184**, 5686-5695.

McAdams,H.H. and Shapiro,L. (2009) System-level design of bacterial cell cycle control. *FEBS Letters* **583**, 3984-3991.

Miyasaka,I., Nanba,K., Furuya,K., Nimura,Y. and Azuma,A. (2004) Functional roles of the transverse and longitudinal flagella in the swimming motility of Prorocentrum minimum (Dinophyceae). *Journal of Experimental Biology* **207**, 3055-3066.

Moran,M.A., Buchan,A., Gonzalez,J.M., Heidelberg,J.F., Whitman,W.B., Kiene,R.P., Henriksen,J.R., King,G.M., Belas,R., Fuqua,C., Brinkac,L., Lewis,M., Johri,S., Weaver,B., Pai,G., Eisen,J.A., Rahe,E., Sheldon,W.M., Ye,W., Miller,T.R., Carlton,J., Rasko,D.A., Paulsen,I.T., Ren,Q., Daugherty,S.C., Deboy,R.T., Dodson,R.J., Durkin,A.S., Madupu,R., Nelson,W.C., Sullivan,S.A., Rosovitz,M.J., Haft,D.H., Selengut,J. and Ward,N. (2004) Genome sequence of Silicibacter pomeroyi reveals adaptations to the marine environment. *Nature* **432**, 910-913.

Moran,N.A. (2006) Symbiosis. *Curr. Biol.* **16**, R866-R871.

Moré,M.I., Finger,L.D., Stryker,J.L., Fuqua,C., Eberhard,A. and Winans,S.C. (1996) Enzymatic synthesis of a quorum-sensing autoinducer through use of defined substrates. *Science* **272**, 1655-1658.

Navarro Llorens,J.M.a., Tormo,A. and Mart+¡nez-Garc+¡a,E. (2010) Stationary phase in gram-negative bacteria. *Fems Microbiology Reviews* **34**, 476-495.

Nealson,K.H. and Markovitz,A. (1970) Mutant analysis and enzyme subunit complementation in bacterial bioluminescence in Photobacterium fischeri. *J Bacteriol.* **104**, 300-312.

Noinaj,N., Guillier,M., Travis,J. and Buchanan,S.K. (2010) TonB-Dependent Transporters: Regulation, Structure, and Function. *Annual Review of Microbiology* **64**, 43-60.

Pan,J. and Ren,D. (2009) Quorum sensing inhibitors: a patent overview. *Expert. Opin. Ther. Pat* **19**, 1581-1601.

Parsek,M.R., Val,D.L., Hanzelka,B.L., Cronan,J.E., Jr. and Greenberg,E.P. (1999) Acyl homoserine-lactone quorum-sensing signal generation. *Proc. Natl. Acad. Sci. U. S. A* **96**, 4360-4365.

Pearson,J.P., van Delden,C. and Iglewski,B.H. (1999) Active efflux and diffusion are involved in transport of Pseudomonas aeruginosa cell-to-cell signals. *J Bacteriol.* **181**, 1203-1210.

Penfold,R.J. and Pemberton,J.M. (1992) An improved suicide vector for construction of chromosomal insertion mutations in bacteria. *Gene* **118**, 145-146.

Piekarski,T., Buchholz,I., Drepper,T., Schobert,M., Wagner-Doebler,I., Tielen,P. and Jahn,D. (2009) Genetic tools for the investigation of Roseobacter clade bacteria. *BMC. Microbiol.* **9**, 265.

Puskas,A., Greenberg,E.P., Kaplan,S. and Schaefer,A.L. (1997) A quorum-sensing system in the free-living photosynthetic bacterium Rhodobacter sphaeroides. *J Bacteriol.* **179**, 7530-7537.

Qi,B., Beaudoin,F., Fraser,T., Stobart,A.K., Napier,J.A. and Lazarus,C.M. (2002) Identification of a cDNA encoding a novel C18-[Delta]9 polyunsaturated fatty acid-specific elongating activity from the docosahexaenoic acid (DHA)-producing microalga, Isochrysis galbana. *FEBS Letters* **510**, 159-165.

Rasmussen,T.B., Manefield,M., Andersen,J.B., Eberl,L., Anthoni,U., Christophersen,C., Steinberg,P., Kjelleberg,S. and Givskov,M. (2000) How Delisea pulchra furanones affect quorum sensing and swarming motility in Serratia liquefaciens MG1. *Microbiology* **146 Pt 12**, 3237-3244.

Raven, P. H., Ray F.E and Eichorn S.E. (1999) Biology of plants. New York: W.H. Freeman and Company.

Ravn,L., Christensen,A.B., Molin,S., Givskov,M. and Gram,L. (2001) Methods for detecting acylated homoserine lactones produced by Gram-negative bacteria and their application in studies of AHL-production kinetics. *J Microbiol. Methods* **44**, 239-251.

Redfield,R.J. (2002) Is quorum sensing a side effect of diffusion sensing? *Trends Microbiol.* **10**, 365-370.

Ren,D., Sims,J.J. and Wood,T.K. (2001) Inhibition of biofilm formation and swarming of Escherichia coli by (5Z)-4-bromo-5-(bromomethylene)-3-butyl-2(5H)-furanone. *Environ. Microbiol.* **3**, 731-736.

Riedel,K., Hentzer,M., Geisenberger,O., Huber,B., Steidle,A., Wu,H., Hoiby,N., Givskov,M., Molin,S. and Eberl,L. (2001) N-acylhomoserine-lactone-mediated communication between Pseudomonas aeruginosa and Burkholderia cepacia in mixed biofilms. *Microbiology* **147**, 3249-3262.

Rizzo,P.J. (2003) Those amazing dinoflagellate chromosomes. *Cell Res.* **13**, 215-217.

Ruby,E.G. (1996) LESSONS FROM A COOPERATIVE, BACTERIAL-ANIMAL ASSOCIATION: The Vibrio fischeriΓÇôEuprymna scolopes Light Organ Symbiosis. *Annual Review of Microbiology* **50**, 591-624.

Sambrook, J. and Maniatis, T. Molecular Cloning: A Laboratory Manual. 3. 1989. Cold Spring Harbor Laboratory Press.
Ref Type: Serial (Book,Monograph)

Schaefer,A.L., Greenberg,E.P., Oliver,C.M., Oda,Y., Huang,J.J., Bittan-Banin,G., Peres,C.M., Schmidt,S., Juhaszova,K., Sufrin,J.R. and Harwood,C.S. (2008) A new class of homoserine lactone quorum-sensing signals. *Nature* **454**, 595-599.

Schaefer,A.L., Taylor,T.A., Beatty,J.T. and Greenberg,E.P. (2002) Long-chain acyl-homoserine lactone quorum-sensing regulation of Rhodobacter capsulatus gene transfer agent production. *J Bacteriol.* **184**, 6515-6521.

Schaefer,A.L., Val,D.L., Hanzelka,B.L., Cronan,J.E., Jr. and Greenberg,E.P. (1996) Generation of cell-to-cell signals in quorum sensing: acyl homoserine lactone synthase activity of a purified Vibrio fischeri LuxI protein. *Proc. Natl. Acad. Sci. U. S. A* **93**, 9505-9509.

Schuster,M., Lostroh,C.P., Ogi,T. and Greenberg,E.P. (2003) Identification, timing, and signal specificity of Pseudomonas aeruginosa quorum-controlled genes: a transcriptome analysis. *J Bacteriol.* **185**, 2066-2079.

Silbergeld,E.K., Grattan,L., Oldach,D. and Morris,J.G. (2000) Pfiesteria: Harmful Algal Blooms as Indicators of Human: Ecosystem Interactions. *Environmental Research* **82**, 97-105.

Sourjik,V., Muschler,P., Scharf,B. and Schmitt,R. (2000) VisN and VisR are global regulators of chemotaxis, flagellar, and motility genes in Sinorhizobium (Rhizobium) meliloti. *J Bacteriol.* **182**, 782-788.

Srividhya,K.V., Alaguraj,V., Poornima,G., Kumar,D., Singh,G.P., Raghavenderan,L., Katta,A.V.S.K., Mehta,P. and Krishnaswamy,S. (2007) Identification of Prophages in Bacterial Genomes by Dinucleotide Relative Abundance Difference. *PLoS ONE* **2**, e1193.

Subramanian,A., Tamayo,P., Mootha,V.K., Mukherjee,S., Ebert,B.L., Gillette,M.A., Paulovich,A., Pomeroy,S.L., Golub,T.R., Lander,E.S. and Mesirov,J.P. (2005) Gene set enrichment analysis: a knowledge-based approach for interpreting genome-wide expression profiles. *Proc. Natl. Acad. Sci. U. S. A* **102**, 15545-15550.

Thoma,S. and Schobert,M. (2009) An improved Escherichia coli donor strain for diparental mating. *FEMS Microbiology Letters* **294**, 127-132.

Thrash,J.C., Cho,J.C., Ferriera,S., Johnson,J., Vergin,K.L. and Giovannoni,S.J. (2010a) Genome sequences of Pelagibaca bermudensis HTCC2601T and Maritimibacter alkaliphilus HTCC2654T, the type strains of two marine Roseobacter genera. *J Bacteriol.* **192**, 5552-5553.

Thrash,J.C., Cho,J.C., Vergin,K.L. and Giovannoni,S.J. (2010b) Genome sequences of Oceanicola granulosus HTCC2516(T) and Oceanicola batsensis HTCC2597(TDelta). *J Bacteriol.* **192**, 3549-3550.

Throup,J.P., Camara,M., Briggs,G.S., Winson,M.K., Chhabra,S.R., Bycroft,B.W., Williams,P. and Stewart,G.S. (1995) Characterisation of the yenI/yenR locus from Yersinia enterocolitica mediating the synthesis of two N-acylhomoserine lactone signal molecules. *Mol. Microbiol.* **17**, 345-356.

Tomasch,J., Gohl,R., Bunk,B., Suarez Diez,M. and Wagner-Dobler,I. (2011) Transcriptional response of the photoheterotrophic marine bacterium *Dinoroseobacter shibae* to changing light regimes. *ISME J*.

Tu,K.C. and Bassler,B.L. (2007) Multiple small RNAs act additively to integrate sensory information and control quorum sensing in Vibrio harveyi. *Genes Dev.* **21**, 221-233.

Visick,K.L. and Ruby,E.G. (2006) Vibrio fischeri and its host: it takes two to tango. *Current Opinion in Microbiology* **9**, 632-638.

Vonshak, A. ed. *Spirulina platensis* (*Arthrospira*): Physiology, Cell-biology and Biotechnology. 1997. London, Taylor & Francis.
Ref Type: Serial (Book,Monograph)

Wagner-Dobler,I., Ballhausen,B., Berger,M., Brinkhoff,T., Buchholz,I., Bunk,B., Cypionka,H., Daniel,R., Drepper,T., Gerdts,G., Hahnke,S., Han,C., Jahn,D., Kalhoefer,D., Kiss,H., Klenk,H.P., Kyrpides,N., Liebl,W., Liesegang,H., Meincke,L., Pati,A., Petersen,J., Piekarski,T., Pommerenke,C., Pradella,S., Pukall,R., Rabus,R., Stackebrandt,E., Thole,S., Thompson,L., Tielen,P., Tomasch,J., von Jan,M., Wanphrut,N., Wichels,A., Zech,H. and Simon,M. (2010) The complete genome sequence of the algal symbiont Dinoroseobacter shibae: a hitchhiker's guide to life in the sea. *ISME J* **4**, 61-77.

Wagner-Dobler,I. and Biebl,H. (2006) Environmental biology of the marine Roseobacter lineage. *Annual Review of Microbiology* **60**, 255-280.

Wagner-Dobler,I., Thiel,V., Eberl,L., Allgaier,M., Bodor,A., Meyer,S., Ebner,S., Hennig,A., Pukall,R. and Schulz,S. (2005) Discovery of complex mixtures of novel long-chain quorum sensing signals in free-living and host-associated marine alphaproteobacteria. *Chembiochem.* **6**, 2195-2206.

Waters,C.M. and Bassler,B.L. (2005) Quorum sensing: cell-to-cell communication in bacteria. *Annu. Rev. Cell Dev. Biol.* **21**, 319-346.

Watson,W.T., Minogue,T.D., Val,D.L., von Bodman,S.B. and Churchill,M.E. (2002) Structural basis and specificity of acyl-homoserine lactone signal production in bacterial quorum sensing. *Mol. Cell* **9**, 685-694.

Wessel,D. and Flngge,U.I. (1984) A method for the quantitative recovery of protein in dilute solution in the presence of detergents and lipids. *Analytical Biochemistry* **138**, 141-143.

Wettenhall,J.M. and Smyth,G.K. (2004) limmaGUI: A graphical user interface for linear modeling of microarray data. *Bioinformatics* **20**, 3705-3706.

White,C.E. and Winans,S.C. (2007) Cell-cell communication in the plant pathogen Agrobacterium tumefaciens. *Philos. Trans. R. Soc. Lond B Biol. Sci.* **362**, 1135-1148.

Winzer,K., Hardie,K.R. and Williams,P. (2002) Bacterial cell-to-cell communication: sorry, can't talk now - gone to lunch! *Curr. Opin. Microbiol.* **5**, 216-222.

Yang,M., Sun,K., Zhou,L., Yang,R., Zhong,Z. and Zhu,J. (2009) Functional analysis of three AHL autoinducer synthase genes in Mesorhizobium loti reveals the important role of quorum sensing in symbiotic nodulation. *Can. J Microbiol.* **55**, 210-214.

9 Appendix

9.1 CDS of *luxI*$_1$ cloned into the protein expression vector pTrcHis

Appendix I
Verification of the LuxI 1 insertion into pTrcHis

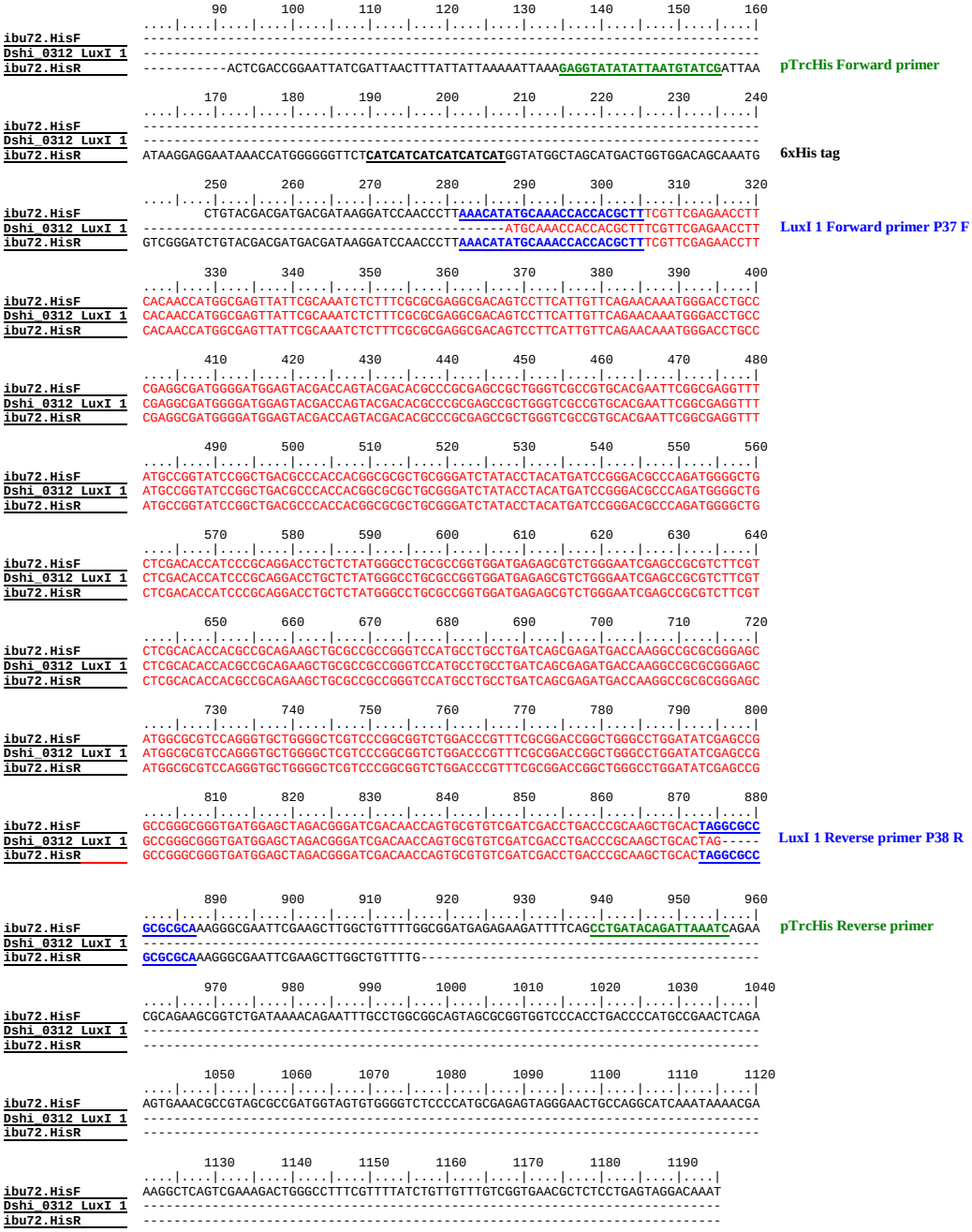

Verification of the correct integration of the *luxI 1* coding sequence into the TOPO TA protein expression vector pTrcHis.

Presented is the alignment of sequenced segments (black nucleotides) against the reference sequence of *luxI* 1 Dshi_0312 (red nucleotides). The sequenced segments ibu72. HisF and ibu72.HisR were obtained by using primers pTrcHis Forward and pTrcHis Reverse located on the vector (offered by Invitrogen). Nucleotides of the primers are marked in green and underlined. Primers which were used to amplify the coding sequence of *luxI* 1 are marked in blue and underlined. Furthermore, black underlined nucleotides show the position of 6 histidin tags located at the N-terminus of the protein.

9.2 Confirmed sequence of Δ*luxI*$_1$

First row: ΔluxI$_1$ Reference sequence; rows 2-10, sequenced fragments (different primers); arrows, primer binding site; underlined nucleotides, restriction site or start codon; bent arrows, start/end of regions; framed nucleotides, CDS of gene

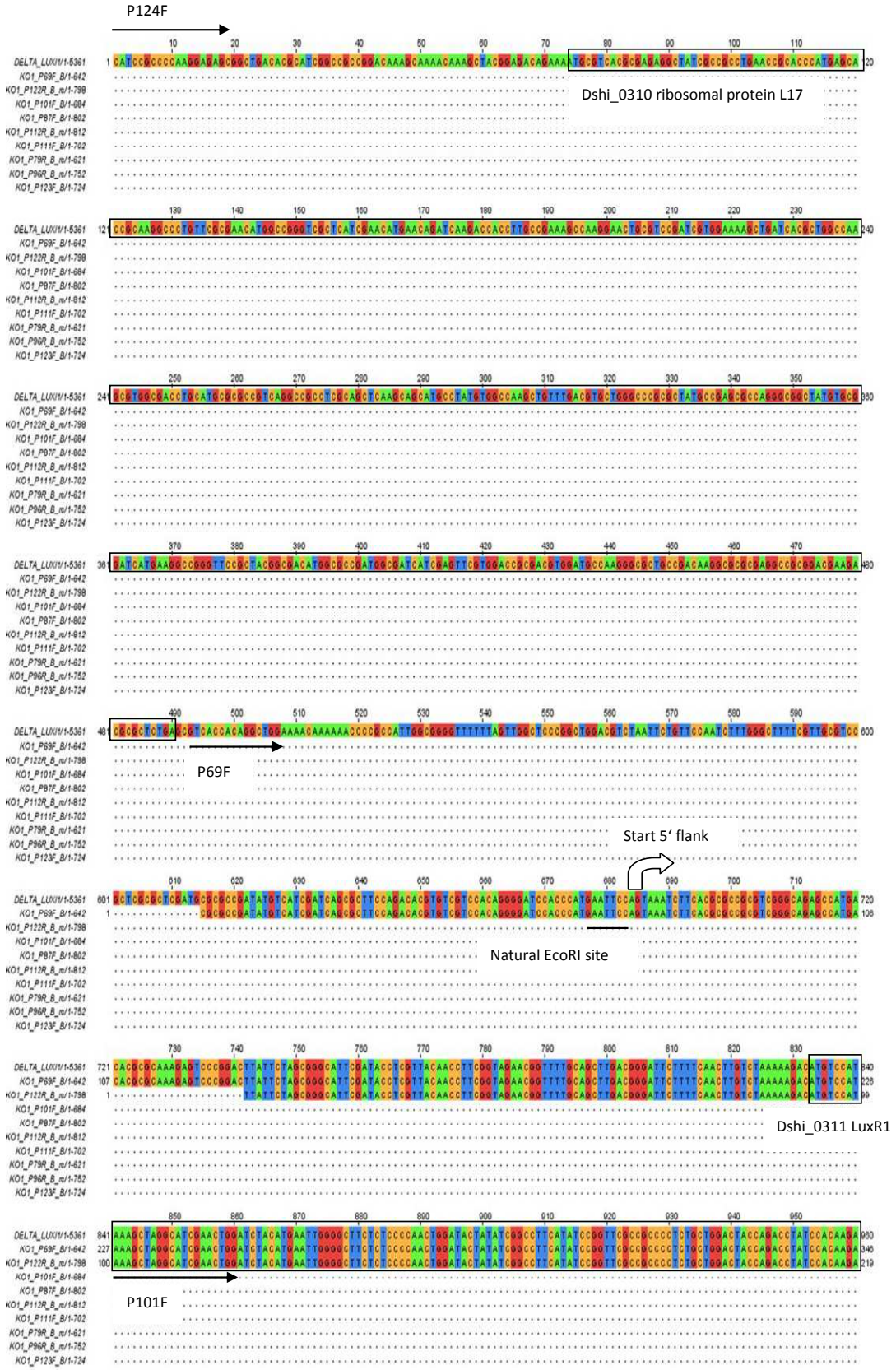

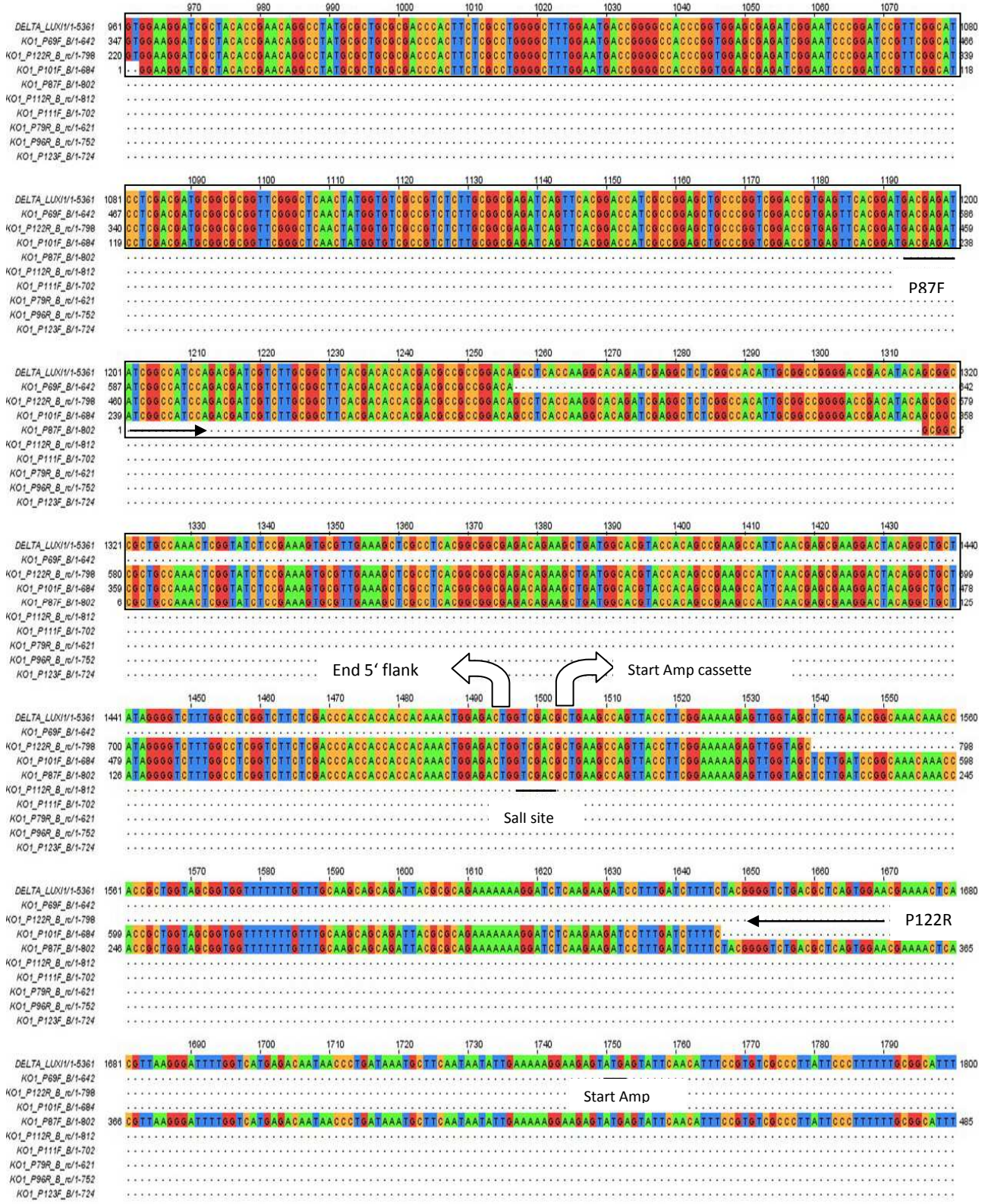
P87F
End 5' flank
Start Amp cassette
SalI site
P122R
Start Amp

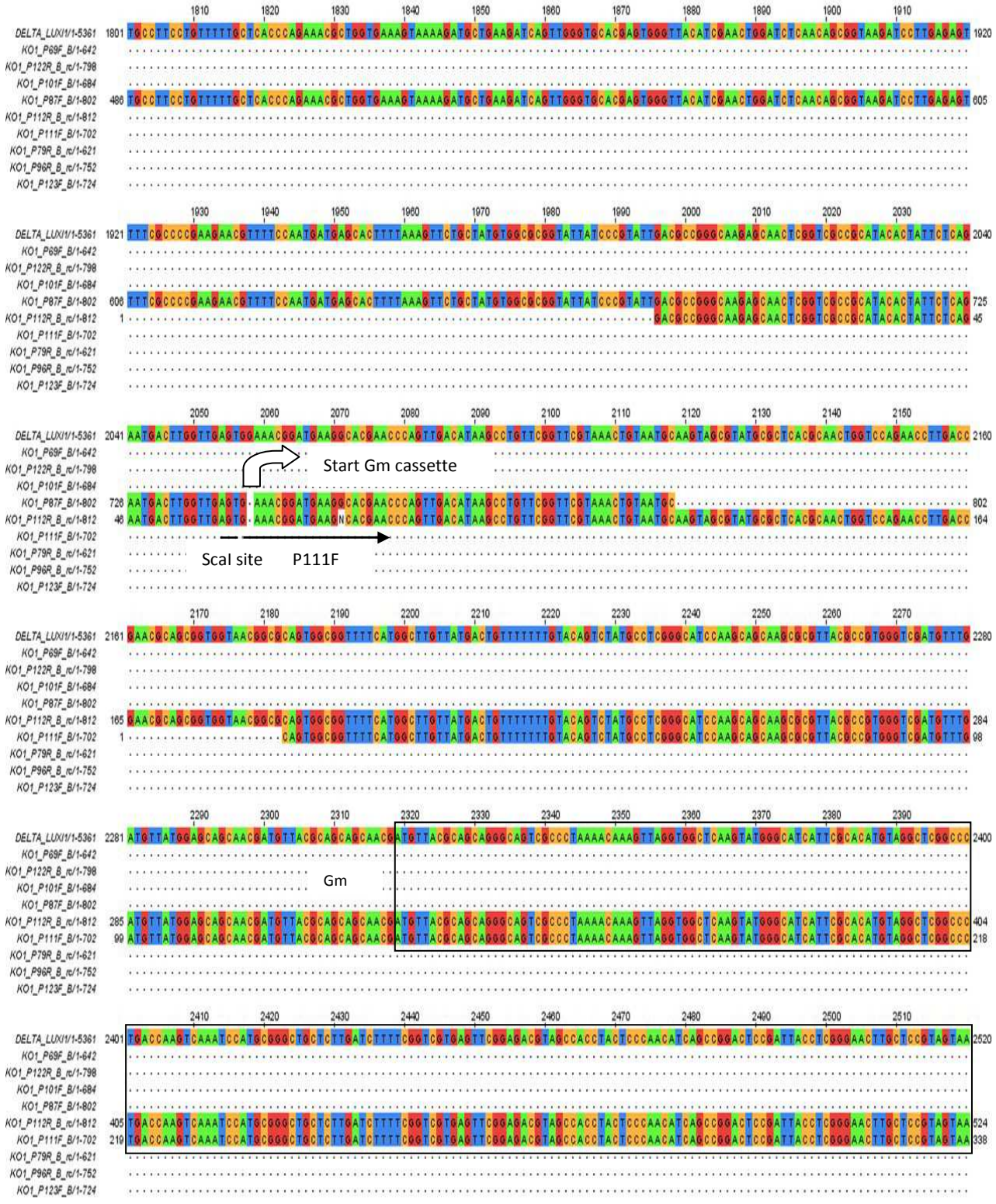
DELTA_LUXI1/1-5361
KO1_P69F_B/1-642
KO1_P122R_B_rc/1-798
KO1_P101F_B/1-684
KO1_P87F_B/1-802
KO1_P112R_B_rc/1-812
KO1_P111F_B/1-702
KO1_P79R_B_rc/1-621
KO1_P96R_B_rc/1-752
KO1_P123F_B/1-724
Start Gm cassette
ScaI site
P111F
Gm

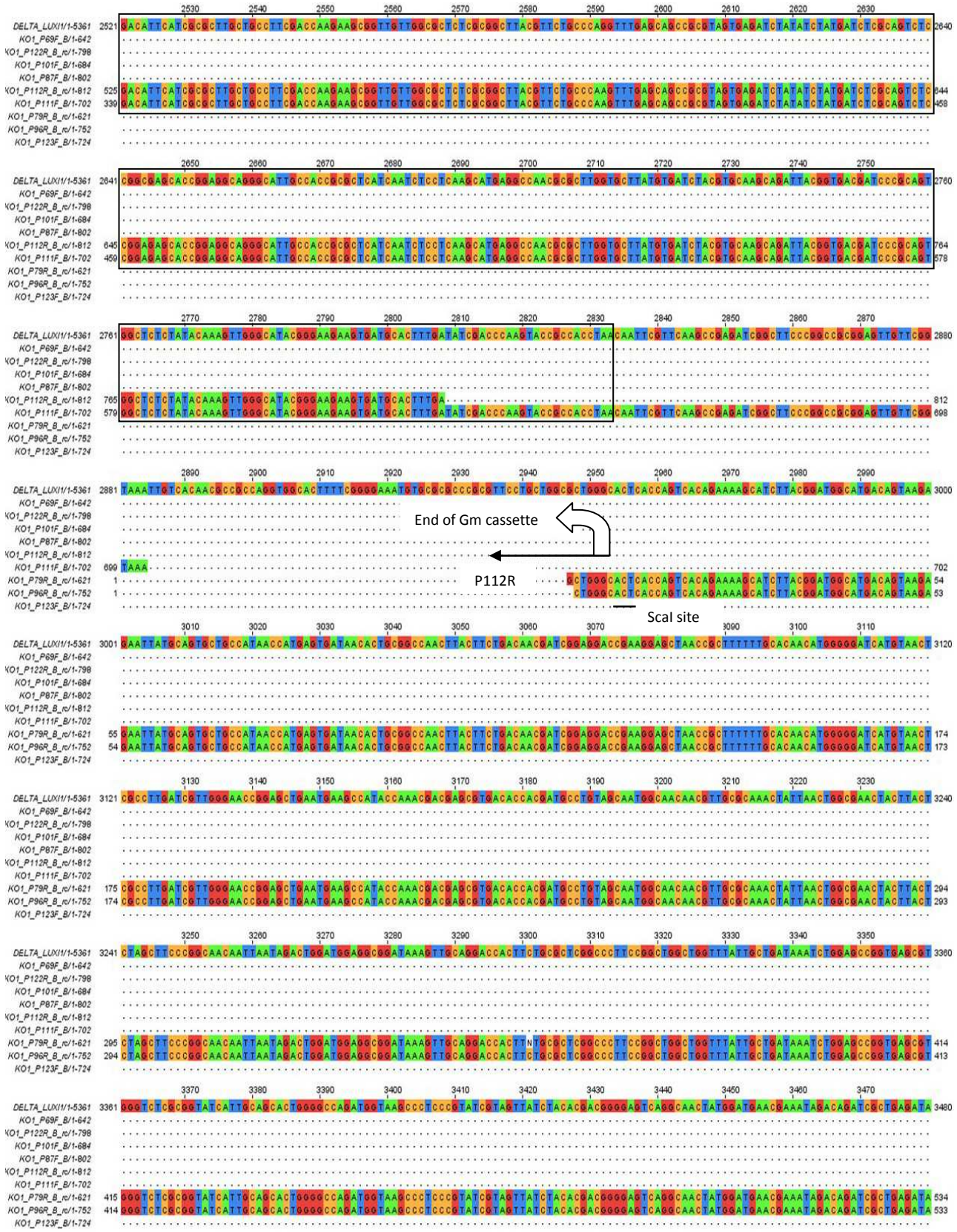
End of Gm cassette
P112R
ScaI site


P123R
End of Amp cassette
Remaining 188 bp of LuxI1
P79R
NheI blunt
P63F
QS9 probe (microarray)
Dshi_0312 AAA ATPase


End of 3‘ flank
Natural FspI site
P125 R
DELTA_LUXI1/1-5361
KO1_P69F_B/1-642
KO1_P122R_B_rc/1-798
KO1_P101F_B/1-684
KO1_P87F_B/1-802
KO1_P112R_B_rc/1-812
KO1_P111F_B/1-702
KO1_P79R_B_rc/1-621
KO1_P96R_B_rc/1-752
KO1_P123F_B/1-724

VII

9.3 Confirmed sequence of Δ*luxI*$_2$

First row: Δ*luxI*$_2$ Reference sequence; rows 2-7, sequenced fragments (different primers); arrows, primer binding site; underlined nucleotides, restriction site or start codon; bent arrows, start/end of regions; framed nucleotides, CDS of gene

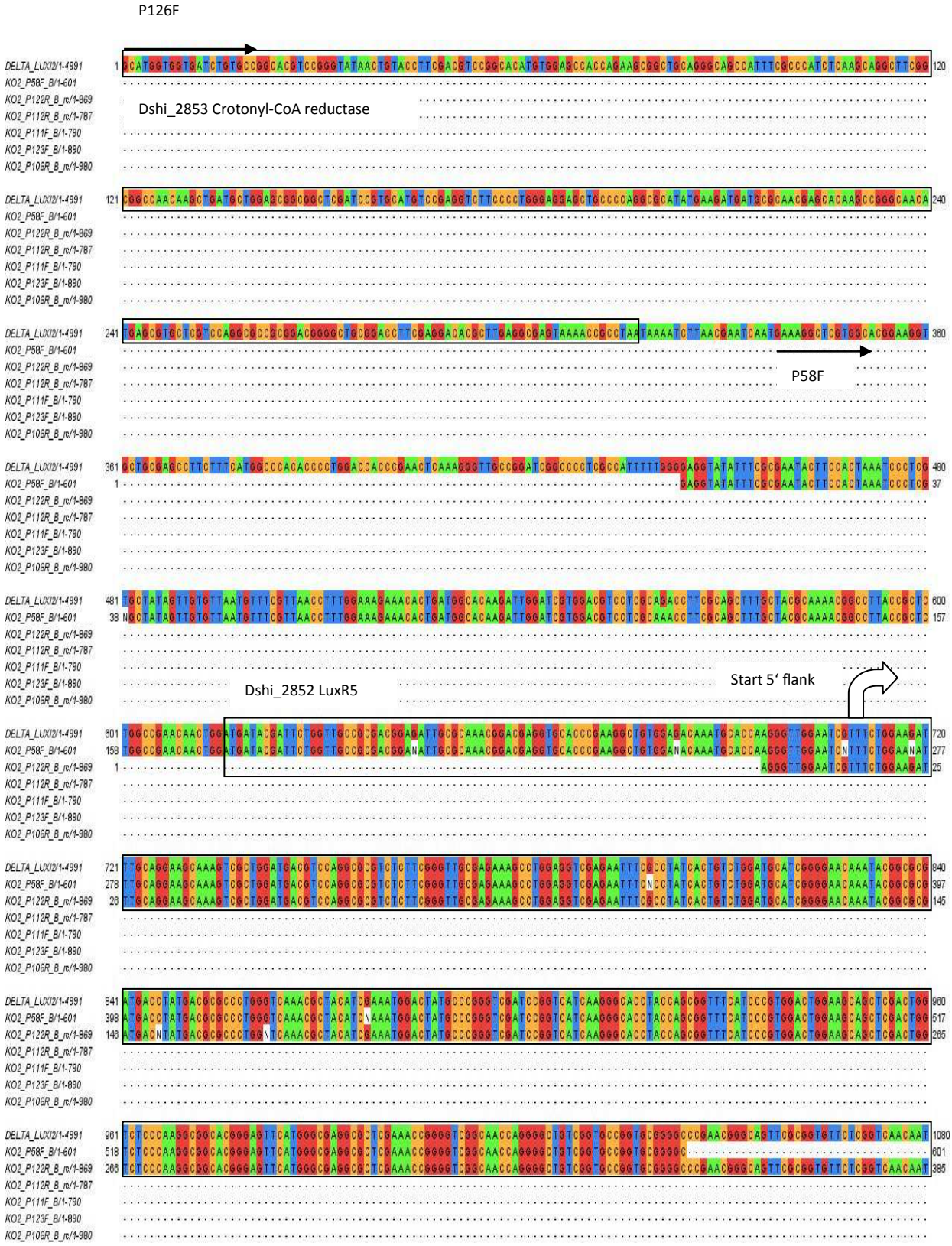

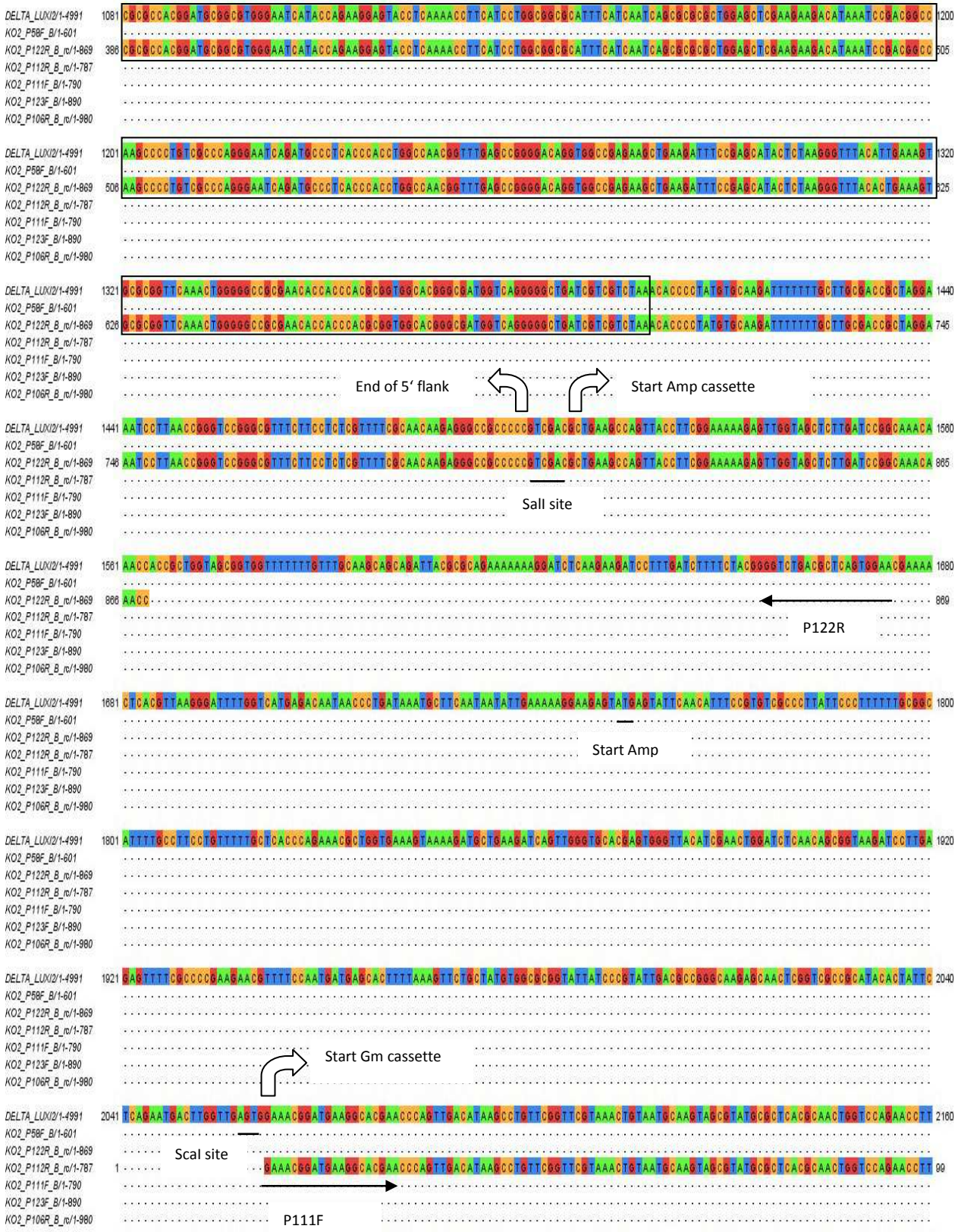
DELTA_LUXI2/1-4991
KO2_P58F_B/1-601
KO2_P122R_B_rc/1-869
KO2_P112R_B_rc/1-787
KO2_P111F_B/1-790
KO2_P123F_B/1-890
KO2_P106R_B_rc/1-980
End of 5‘ flank
Start Amp cassette
SalI site
P122R
Start Amp
Start Gm cassette
ScaI site
P111F

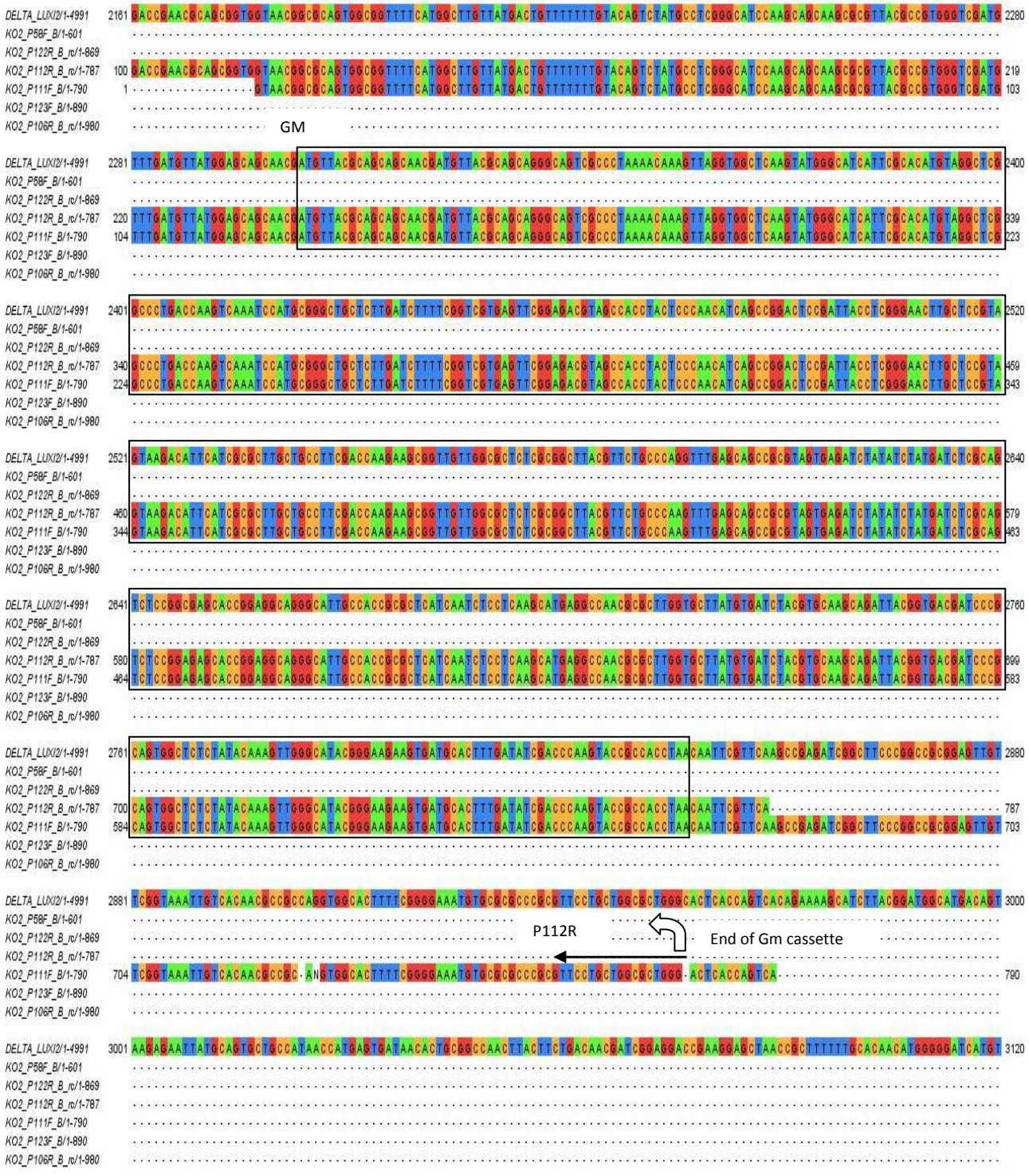

X

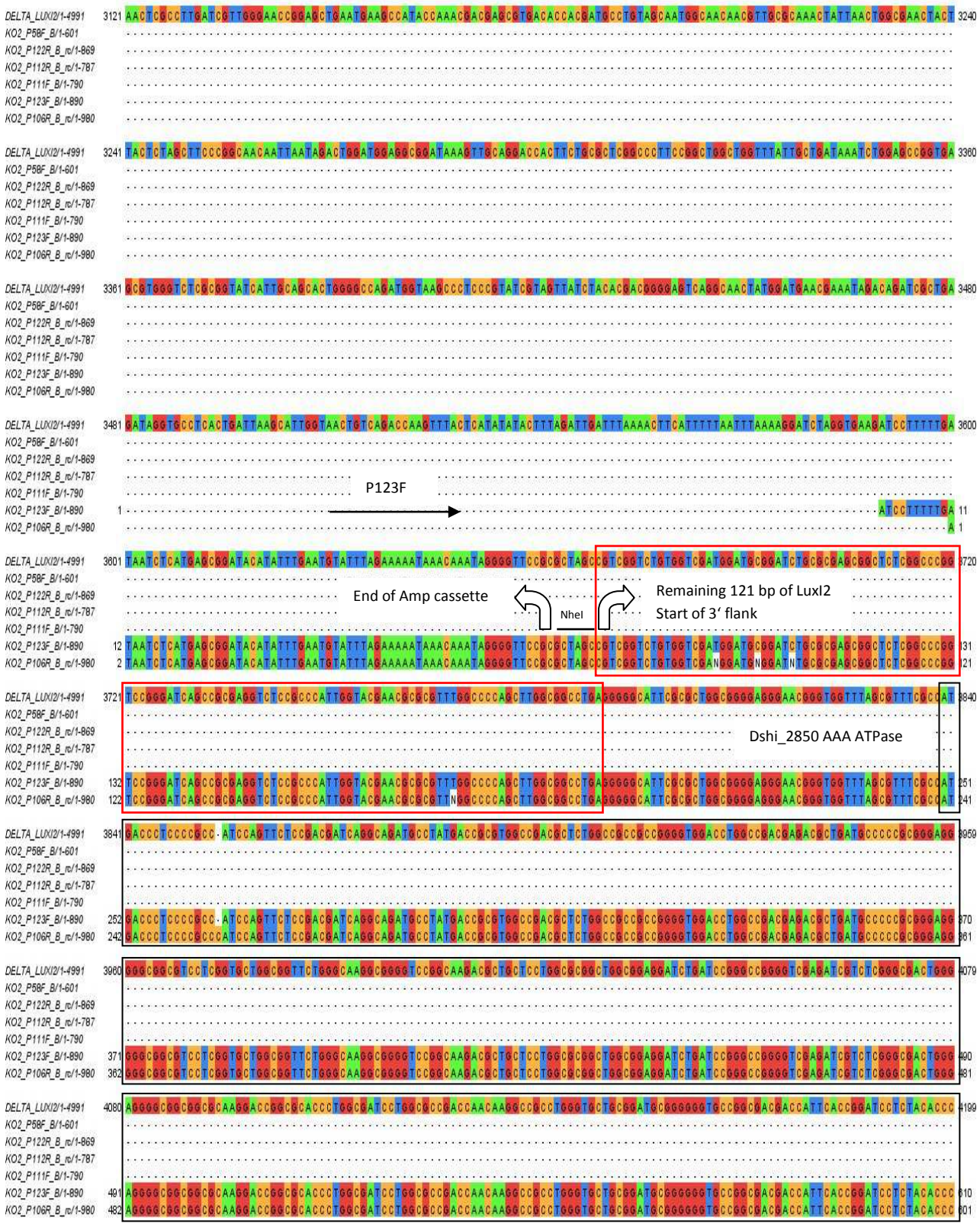
P123F
End of Amp cassette
NheI
Remaining 121 bp of LuxI2
Start of 3′ flank
Dshi_2850 AAA ATPase

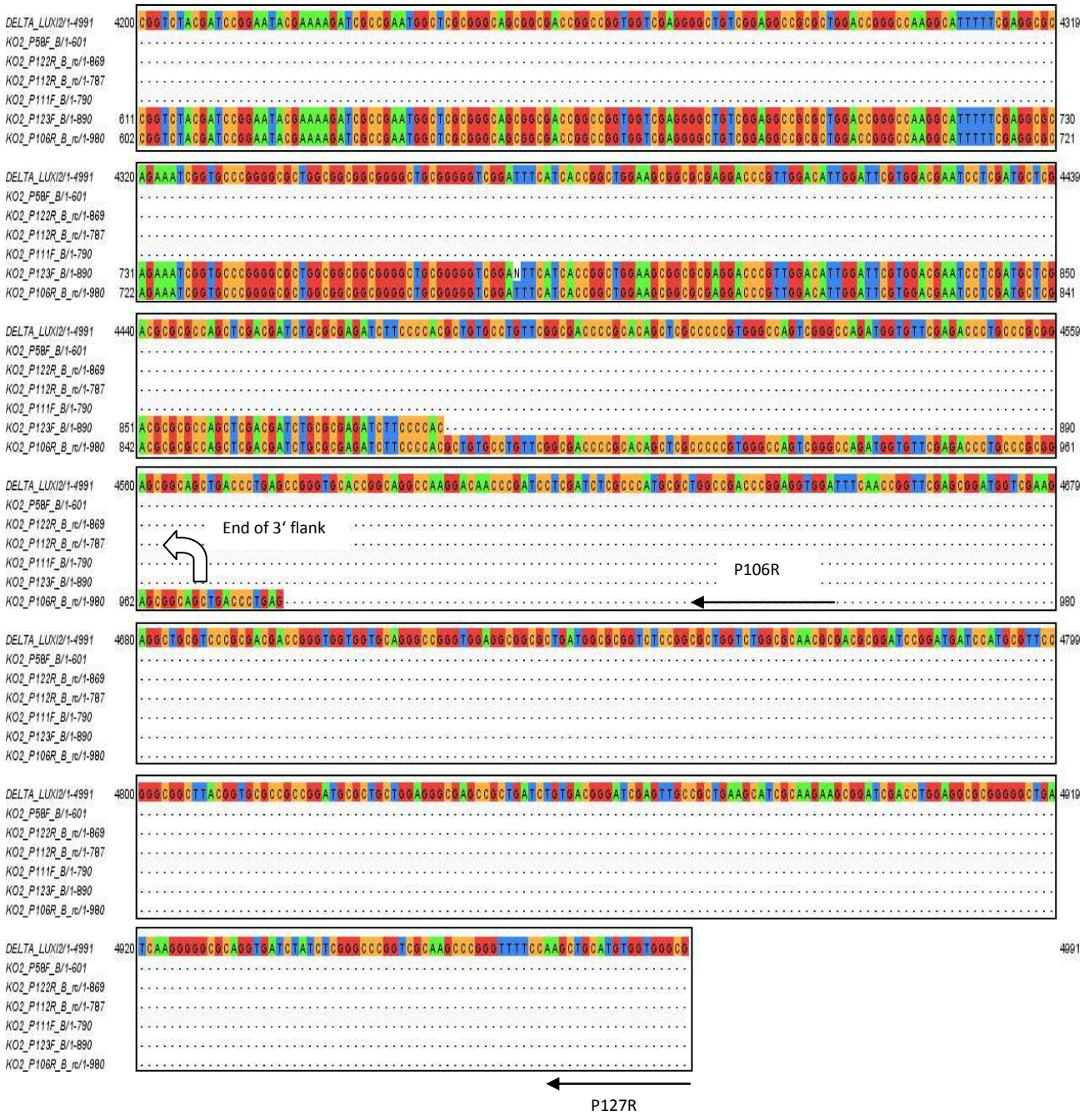
DELTA_LUXI2/1-4991
KO2_P58F_B/1-601
KO2_P122R_B_rc/1-869
KO2_P112R_B_rc/1-787
KO2_P111F_B/1-790
KO2_P123F_B/1-890
KO2_P106R_B_rc/1-980
End of 3' flank
P106R
P127R

9.4 List of differential expressed genes (Cluster 1-6)

Cluster 1

			log2 Fold change > 2			
Probe Name	LocusTag	Description	OD02	OD04	OD06	OD09
RDRS00048	Dshi_0048	putative transposase	-0,26970852	-2,33293343	-0,84351171	-1,77960692
RDRS00082	Dshi_0082	hypothetical protein	-2,29000518	-1,5456415	-1,87808725	-2,57811589
RDRS00211	Dshi_0211	integral membrane sensor signal transduction histidine kinase	-1,29977415	-1,15597179	-1,02005149	-2,58327867
RDRS00242	Dshi_0242	fatty acid hydroxylase	-1,40745336	-1,66726781	-1,70786834	-3,70985163
RDRS00243	Dshi_0243	acyltransferase 3	-1,09280331	-1,08379615	-1,25466085	-2,58852735
RDRS00328	Dshi_0329	diguanylate cyclase/phosphodiesterase	-1,50293146	-1,41602543	-1,80914194	-4,43134214
RDRS00342	Dshi_0343	aminoglycoside phosphotransferase	-1,58803449	-1,36823795	-1,51413464	-4,20154366
RDRS00376	Dshi_0377	hypothetical protein	-1,17893816	-1,82046294	-1,67996218	-2,50044941
RDRS00595	Dshi_0597	hypothetical protein	-1,22571378	-1,16067623	-1,18091525	-3,6074303
RDRS00611	Dshi_0613	band 7 protein	-1,86401767	-1,80824706	-1,56656641	-3,39473324
RDRS00612	Dshi_0614	hypothetical protein	-1,24975419	-0,97854772	-1,19395618	-2,6145018
RDRS00619	Dshi_0621	hypothetical protein	-1,01729299	-2,03742504	-0,43123439	-1,20176217
RDRS00620	Dshi_0622	hypothetical protein	-1,24004265	-2,67412938	-0,70329292	-0,84156699
RDRS00767	Dshi_0769	cold-shock DNA-binding domain protein	-0,8426984	-2,89128354	-0,66590165	-1,09305103
RDRS00815	Dshi_0817	hypothetical protein	-1,46979084	-0,99008558	-0,83039168	-2,49997175
RDRS00817	Dshi_0819	hypothetical protein	-2,04840277	-1,41480112	-0,99369955	-4,25869526
RDRS01026	Dshi_1030	hypothetical protein	-2,30933982	-1,75683614	-1,90184217	-3,2246547
RDRS01080	Dshi_1084	hypothetical protein	-1,35631022	-2,43968476	-1,04012167	-1,87077136
RDRS01082	Dshi_1086	hypothetical protein	-1,54895421	-1,23634845	-1,47916968	-2,58796968
RDRS01116	Dshi_1120	hypothetical protein	-2,35631217	-2,17379021	-2,25004047	-3,31401096
RDRS01123	Dshi_1127	response regulator receiver protein	-1,78617728	-1,96063257	-2,18176879	-3,72345435
RDRS01155	Dshi_1159	hypothetical protein	-1,99367194	-2,27210243	-2,18879522	-3,51467513
RDRS01466	Dshi_1470	hypothetical protein	-2,34097035	-2,17500293	-2,16084476	-1,66736729
RDRS01523	Dshi_1527	protein of unknown function DUF1457	-1,95803515	-1,79641167	-1,74482756	-2,00369059
RDRS01578	Dshi_1582	hypothetical protein	-1,50056966	-2,19204664	-1,98020617	-3,14491046
RDRS01617	Dshi_1621	PfkB domain protein	-0,9936292	-1,62748022	-1,64556286	-2,06254317
RDRS01618	Dshi_1622	hypothetical protein	-1,96012325	-2,64619275	-2,34083036	-3,18594262
RDRS01639	Dshi_1643	recA protein	-1,2023661	-1,09467551	-1,09242857	-2,91740201
RDRS01640	Dshi_1644	integral membrane sensor hybrid histidine kinase	-1,84865359	-1,57420193	-1,64262182	-2,37233198
RDRS01662	Dshi_1666	globin	-2,07299365	-1,80864405	-1,86634539	-3,55310913
RDRS01695	Dshi_1699	hypothetical protein	-0,67222143	-2,14605276	-1,17283228	-1,50224835
RDRS01800	Dshi_1804	ComEC/Rec2-related protein	-2,28392246	-1,82833454	-1,92469934	-2,54341632
RDRS01842	Dshi_1846	hypothetical protein	-1,36408351	-1,15936729	-1,30506925	-2,48027906
RDRS02142	Dshi_2146	hypothetical protein	-1,52663798	-1,39096618	-1,41507293	-3,40308363
RDRS02264	Dshi_2268	TadE family protein	-1,35473511	-1,71782294	-1,65511694	-3,20977707
RDRS02265	Dshi_2269	hypothetical protein	-1,78494354	-2,00701259	-2,06296873	-3,93953864
RDRS02632	Dshi_2638	hypothetical protein	-1,35013263	-1,69579734	-1,68564923	-2,86248509
RDRS02641	Dshi_2647	hypothetical protein	-1,79076917	-2,15958803	-1,93935562	-3,49397577
RDRS02774	Dshi_2780	hypothetical protein	-1,11420462	-1,20609674	-1,42090325	-3,2596328
RDRS02822	Dshi_2828	Mg chelatase, subunit ChlI	-2,57282438	-1,2282373	-1,799864	-1,83726437
RDRS02962	Dshi_2968	hypothetical protein	-0,89720483	-1,52087687	-1,37862829	-3,57698032
RDRS03188	Dshi_3194	hypothetical protein	-1,75277479	0,09562132	-2,19199872	-2,72266161
RDRS03229	Dshi_3235	hypothetical protein	-2,01222411	-1,83059121	-1,9184237	-4,2140019
RDRS03233	Dshi_3239	hypothetical protein	-1,72809451	-0,94691993	-0,94959403	-3,66687378
RDRS03240	Dshi_3246	ATPase, FliI/YscN family	-1,90711679	-1,7879975	-1,54488163	-3,17386681
RDRS03250	Dshi_3256	type III secretion exporter	-1,36709987	-1,23320408	-1,32862268	-2,45390926
RDRS03251	Dshi_3257	type III secretion system inner membrane R protein	-1,08306013	-0,9794094	-1,1499355	-2,53246691
RDRS03252	Dshi_3258	flagellar biosynthesis protein FlhA	-1,98819431	-1,79052977	-2,01615834	-3,72988854
RDRS03306	Dshi_3312	hypothetical protein	-2,29025712	-2,37631805	-2,32530767	-3,19546315
RDRS03340	Dshi_3346	multi-sensor hybrid histidine kinase	-1,89699134	-1,5000459	-1,63473254	-2,72461717
RDRS03358	Dshi_3364	hypothetical protein	-1,87546981	-1,63781344	-1,69825389	-2,96679586
RDRS03359	Dshi_3365	flagellar hook capping protein	-1,70019214	-1,66693784	-1,64169094	-3,98098599
RDRS03395	Dshi_3401	hypothetical protein	-1,08787773	-1,35833138	-0,85289175	-2,10259193
RDRS03562	Dshi_3569	DNA repair protein RadC	-2,3977023	-1,85176762	-2,11154495	-3,72302054
RDRS03621	Dshi_3628	hypothetical protein	-2,06011349	-2,81918356	-1,90667967	-2,82013194
RDRS03630	Dshi_3637	hypothetical protein	-2,18842894	-2,52511574	-1,85776096	-1,87231623
RDRS03631	Dshi_3638	Lytic transglycosylase catalytic	-2,55300894	-2,56888019	-2,09958607	-2,60011717
RDRS03632	Dshi_3639	hypothetical protein	-2,39307913	-2,29297801	-1,96176393	-3,19229353
RDRS03633	Dshi_3640	type IV secretory pathway VirB3 family protein	-2,36938796	-2,40431789	-1,9996535	-2,53815223
RDRS03635	Dshi_3642	hypothetical protein	-1,95590766	-2,37950358	-1,85570307	-1,74920037
RDRS03636	Dshi_3643	hypothetical protein	-2,19591644	-2,36393892	-1,88082865	-2,35094884
RDRS03638	Dshi_3645	VirB8 family protein	-2,52029735	-2,39141716	-1,88538932	-2,63335476
RDRS03639	Dshi_3646	hypothetical protein	-2,4026796	-2,39113654	-1,72606995	-2,65439075
RDRS03640	Dshi_3647	conjugation TrbI family protein	-1,93378303	-1,94725246	-1,49502759	-2,29009426
RDRS03641	Dshi_3648	type II secretion system protein E	-1,79696491	-1,88349234	-1,42294257	-2,10928187
RDRS03642	Dshi_3649	hypothetical protein	-1,70884975	-1,85908713	-1,36686371	-2,27527761
RDRS03649	Dshi_3656	Relaxase/mobilization nuclease family protein	-1,30950414	-1,58702637	-1,20995387	-2,09290548
RDRS03862	Dshi_3872	Hemolysin-type calcium-binding region	-0,97300299	-1,19902699	-0,97978621	-4,43482299
RDRS03961	Dshi_3971	hypothetical protein	-2,34951295	-2,69007432	-1,89580421	-2,35120999
RDRS03962	Dshi_3972	hypothetical protein	-2,13870117	-2,5099074	-1,91545485	-1,67059932
RDRS03963	Dshi_3973	Lytic transglycosylase catalytic	-1,75214421	-2,17371876	-1,73797177	-1,80901461
RDRS03964	Dshi_3974	hypothetical protein	-2,44573223	-2,11854395	-1,87333666	-2,69958884
RDRS03967	Dshi_3977	hypothetical protein	-1,74018292	-2,21244971	-1,38681281	-1,58339028
RDRS03970	Dshi_3980	VirB8 family protein	-2,31102961	-2,2205568	-1,75665863	-2,49355499
RDRS03971	Dshi_3981	hypothetical protein	-2,23268009	-2,26020938	-1,70467814	-2,22918408
RDRS03972	Dshi_3982	conjugation TrbI family protein	-1,89607568	-1,86224993	-1,45750884	-2,05037227
RDRS03973	Dshi_3983	type II secretion system protein E	-1,95315457	-2,00700388	-1,56333073	-2,00178697
RDRS03979	Dshi_3989	Relaxase/mobilization nuclease family protein	-1,28607367	-1,48745933	-1,11547882	-2,05525373

Cluster 2

			log2 Fold change > 2			
Probe Name	**LocusTag**	**Description**	**OD02**	**OD04**	**OD06**	**OD09**
RDRS01261	Dshi_1265	Inositol 2-dehydrogenase	2,80087341	0,04578272	-0,28579073	-0,12611112
RDRS01262	Dshi_1266	ketose-bisphosphate aldolase	3,18563574	0,01196969	-0,17419859	0,44327143
RDRS01263	Dshi_1267	hypothetical protein	3,13258716	-0,44854196	-0,48901091	-0,21512645
RDRS01264	Dshi_1268	PfkB domain protein	3,11412722	-0,40215016	-0,67218887	-0,67591349
RDRS01265	Dshi_1269	thiamine pyrophosphate protein central region	3,5387207	-0,69352811	-0,67605475	-0,86252689
RDRS01266	Dshi_1270	oxidoreductase domain protein	3,20218899	-0,48288979	-0,56115657	-0,52432503
RDRS01267	Dshi_1271	Xylose isomerase domain protein TIM barrel	3,21717945	-0,59357404	-0,60427292	-0,67647613
RDRS01268	Dshi_1272	oxidoreductase domain protein	3,12212042	-0,23829514	-0,31591253	-0,3773206
RDRS01269	Dshi_1273	transcriptional regulator, LacI family	3,07634272	-0,3090957	-0,41580117	-0,18190032
RDRS01270	Dshi_1274	hypothetical protein	4,43580305	-1,13649546	-1,03125736	-0,794116
RDRS01271	Dshi_1275	Monosaccharide-transporting ATPase	4,21925617	-0,13807769	-0,42037018	-0,22500184
RDRS01272	Dshi_1276	ABC transporter related	3,96090949	-0,20214855	-0,38659537	-0,41611727
RDRS01273	Dshi_1277	hypothetical protein	3,66333883	-0,54699915	-0,52802642	0,1034445
RDRS01274	Dshi_1278	Phytanoyl-CoA dioxygenase	2,89493527	-0,34031492	-0,47937273	0,0679946
RDRS01275	Dshi_1279	Myo-inositol catabolism IolB domain protein	2,43265846	-0,48903674	-0,52969226	-0,2544318
RDRS01582	Dshi_1586	trimethylamine methyltransferase	2,39737487	0,47005693	0,16603832	0,41964305
RDRS02109	Dshi_2113	Glycine hydroxymethyltransferase	2,2109449	0,17813596	-0,07690963	0,43015593
RDRS02110	Dshi_2114	Sarcosine oxidase gamma subunit	2,20336265	0,40662462	0,13014907	0,33525313
RDRS02111	Dshi_2115	sarcosine oxidase, alpha subunit family	2,3488228	0,5771525	-0,00154823	-0,18437612
RDRS02112	Dshi_2116	sarcosine oxidase, delta subunit family	2,31506086	0,32946093	0,03380489	-0,53131646
RDRS02113	Dshi_2117	sarcosine oxidase, beta subunit family	3,23196091	0,49980985	0,17152854	-0,28797853
RDRS02115	Dshi_2119	hypothetical protein	3,11471655	0,08380661	0,03198261	-0,08522026
RDRS02116	Dshi_2120	ABC transporter related	2,98266085	0,18918266	-0,05126215	-0,2786689
RDRS02117	Dshi_2121	hypothetical protein	2,38654467	0,06569045	-0,25098231	-0,47040966
RDRS02118	Dshi_2122	hypothetical protein	3,20300464	-0,06580023	-0,34255872	-0,6037077
RDRS02119	Dshi_2123	hypothetical protein	3,57009566	-0,03316497	-0,42722891	-0,22756278
RDRS02120	Dshi_2124	Creatininase	3,27122952	0,18783143	-0,05649001	-0,29779311
RDRS02122	Dshi_2126	peptidase M24	4,50623157	0,40613931	0,0470639	0,22150087
RDRS02961	Dshi_2967	FAD dependent oxidoreductase	2,04838755	0,27047481	0,05314182	0,03198248
RDRS03867	Dshi_3877	thiamine biosynthesis protein ThiC	2,46241005	0,88416557	0,29263268	-1,94991567

Cluster 3

			log2 Fold change > 2			
Probe Name	**LocusTag**	**Description**	**OD02**	**OD04**	**OD06**	**OD09**
RDRS04132	0	ISSpo6, transposase orf A	0,00313467	0,50664649	0,11452435	-2,37253167
RDRS00071	Dshi_0071	hypothetical protein	-0,15865788	0,17583809	0,15951038	-2,05614705
RDRS00126	Dshi_0126	hypothetical protein	-0,33085475	0,11660911	-0,11505708	-2,01342565
RDRS00127	Dshi_0127	hypothetical protein	-0,65134456	-0,26369083	-0,46140501	-2,92883892
RDRS00133	Dshi_0133	type I secretion target repeat protein	-1,10694949	-0,86814732	-0,90569236	-4,38671467
RDRS00139	Dshi_0139	type I secretion system ATPase	-0,07868168	-0,03050242	-0,18165108	-2,08216707
RDRS00195	Dshi_0195	hypothetical protein	-0,21173947	0,20442489	-0,06578138	-2,92573942
RDRS00196	Dshi_0196	pyridoxal phosphate biosynthetic protein PdxJ	-0,24561755	-0,06070286	-0,21096675	-2,45657797
RDRS00215	Dshi_0215	hypothetical protein	-0,83218375	-0,97529121	-1,20281551	-3,36981984
RDRS00266	Dshi_0266	ribosomal protein L7/L12	-0,2690226	0,46455179	-0,28138375	-2,5776343
RDRS00336	Dshi_0337	ATPase MipZ	-0,88600766	-0,30796339	-0,48534927	-3,29931034
RDRS00582	Dshi_0584	lipopolysaccharide biosynthesis protein	-0,79988582	-0,54050622	-0,58435003	-3,41869438
RDRS00583	Dshi_0585	ABC transporter related	-1,23707971	-0,81023817	-0,90847656	-4,02005873
RDRS00617	Dshi_0619	hypothetical protein	-1,00841807	-0,63642138	-0,64514501	-3,74446836
RDRS00721	Dshi_0723	Carbamoyl-phosphate synthase L chain ATP-binding	0,05993485	0,0073808	-0,23372284	-2,02846999
RDRS00772	Dshi_0774	hypothetical protein	-0,17598868	-2,07520061	-0,70786894	-1,255221
RDRS01295	Dshi_1299	hypothetical protein	-0,7529484	-0,76347367	-0,59217055	-2,12644969
RDRS01416	Dshi_1420	hypothetical protein	-1,15888309	-0,70274896	-1,04088214	-3,55628538
RDRS01473	Dshi_1477	Usg family protein	-0,14139319	-1,04844551	-0,69487066	-3,18270954
RDRS01602	Dshi_1606	single-strand binding protein	0,11876705	0,23252517	0,20217567	-2,04675715
RDRS01616	Dshi_1620	hypothetical protein	-0,51229706	-0,09820555	-0,65284987	-2,33242701
RDRS01663	Dshi_1667	nitrite reductase (NAD(P)H), large subunit	-0,87663317	-0,71481014	-0,80540963	-2,41616708
RDRS01675	Dshi_1679	hypothetical protein	0,04041407	0,01621379	-0,37144925	-2,6130134
RDRS01781	Dshi_1785	ribonucleoside-diphosphate reductase, adenosylcobalamin-dependent	-0,58165656	-0,59607904	-1,01084348	-2,15060456
RDRS01832	Dshi_1836	hypothetical protein	0,05047855	0,45151434	0,25558399	-2,12239643
RDRS01960	Dshi_1964	FkbH like protein	-0,32525037	-0,39971864	-0,3411741	-2,07650826
RDRS02015	Dshi_2019	putative glutamate synthase [NADPH] large chain	-0,2262713	-0,19481751	-0,37656862	-3,04931363
RDRS02080	Dshi_2084	hypothetical protein	-0,84664414	-0,54800354	-0,67707753	-2,91943098
RDRS02190	Dshi_2194	hypothetical protein	-0,43239608	-0,35658487	-0,5735428	-2,26128547
RDRS02274	Dshi_2278	hypothetical protein	0,06143863	-0,43291881	-0,94019966	-2,01927395
RDRS02392	Dshi_2396	ketol-acid reductoisomerase	-0,59167442	0,10050246	0,70896565	-2,32750289
RDRS02409	Dshi_2415	UDP-3-0-acyl N-acetylglucosamine deacetylase	-0,7286533	-1,10257429	-0,66571961	-2,12400069
RDRS02608	Dshi_2614	hypothetical protein	-0,12010919	-0,63926619	-0,75361714	-2,36890031
RDRS02680	Dshi_2686	UspA domain protein	0,66644679	-0,62910944	-0,89002484	-2,23167747
RDRS02688	Dshi_2694	hypothetical protein	0,47402598	-0,88885001	-0,77048809	-2,77498018
RDRS02790	Dshi_2796	heat shock protein Hsp20	0,62044488	-0,56354548	-0,73924525	-2,12980117
RDRS02800	Dshi_2806	hypothetical protein	0,34228694	0,36864094	-0,07824928	-2,00781228
RDRS02823	Dshi_2829	glutathione synthetase	-0,31866964	-0,02197658	-0,3296966	-2,21892157
RDRS02869	Dshi_2875	hypothetical protein	-1,28623206	-0,24348179	-0,58488146	-4,19486893
RDRS02872	Dshi_2878	succinyl-CoA synthetase, beta subunit	0,05044771	0,09469796	-0,04180674	-2,38513581
RDRS02917	Dshi_2923	5TM Receptors of the LytS-YhcK type transmembrane region	-0,58976576	-0,24048981	-0,39255296	-3,44675876
RDRS02918	Dshi_2924	Inorganic diphosphatase	-0,24380979	0,37790912	0,04898892	-2,11504206
RDRS02933	Dshi_2939	ATP-dependent Clp protease, ATP-binding subunit clpA	-0,09376394	-0,85465629	-0,43427521	-2,06223981
RDRS03061	Dshi_3067	acetoacetyl-CoA reductase	0,13366442	0,29772026	0,03606892	-2,07918535
RDRS03090	Dshi_3096	protein of unknown function DUF805	-0,67257477	-0,99480333	-1,12642403	-2,31849949
RDRS03163	Dshi_3169	hypothetical protein	-0,45645457	0,18650438	-0,35717839	-2,99725553
RDRS03205	Dshi_3211	hypothetical protein	-0,1288448	0,05694165	-0,19859848	-2,03240161
RDRS03230	Dshi_3236	Carbonate dehydratase	-0,11929586	0,14231625	-0,03652029	-2,07838381
RDRS03312	Dshi_3318	D-3-phosphoglycerate dehydrogenase	-2,29119999	0,52457701	0,21350225	-0,24491811
RDRS03400	Dshi_3406	hypothetical protein	0,02989012	-0,77755899	-0,55381985	-2,56111436
RDRS03566	Dshi_3573	ABC-2 type transporter	-0,68518816	-0,35436631	-0,3204788	-3,579928
RDRS03938	Dshi_3610	hypothetical protein	0,68947393	-0,49988108	-0,25378912	-2,15269371
RDRS03908	Dshi_3918	hypothetical protein	-0,28423879	-0,20236767	-0,24175476	-2,24866389
RDRS04057	Dshi_4071	Parallel beta-helix repeat	-0,708495	-0,3805505	-0,66476791	-4,32542045
RDRS04113	Dshi_4130	Parallel beta-helix repeat	-0,68847193	-0,44124561	-0,61915314	-4,29489328
RDRS04119	Dshi_4138	hypothetical protein	-0,4328209	-0,29360298	-0,34276947	-2,29794276
RDRS04120	Dshi_4139	GDP-mannose 4,6-dehydratase	-0,36811035	-0,31252769	-0,40896607	-2,27298067
RDRS04122	Dshi_4141	hypothetical protein	-0,74414691	-0,68662608	-0,57459635	-2,22444294
RDRS04163	Dshi_4183	hypothetical protein	-0,36223635	-0,20903494	-0,48165027	-2,37632552
RDRS04164	Dshi_4184	CsbD family protein	-0,35704692	-0,07313995	-0,34491244	-3,04345056

Cluster 4

			log2 Fold change > 2			
Probe Name	**LocusTag**	**Description**	**OD02**	**OD04**	**OD06**	**OD09**
RDRS00086	Dshi_0086	hypothetical protein	-1,14464812	-1,64266973	-1,23356566	2,16104091
RDRS00366	Dshi_0367	amine oxidase	-0,08100124	-1,13337821	0,07551616	2,57678465
RDRS01002	Dshi_1006	major facilitator superfamily MFS_1	-0,1647138	-0,71363192	0,16227465	2,16200398
RDRS01069	Dshi_1073	Methionine synthase	0,01069851	-0,31648744	-0,05916379	2,95929286
RDRS01070	Dshi_1074	homocysteine S-methyltransferase	-0,19997368	0,04139259	0,70546884	2,61744785
RDRS01206	Dshi_1210	molybdopterin dehydrogenase FAD-binding	-1,27705848	-0,01928158	-0,2029365	2,5616823
RDRS01207	Dshi_1211	(2Fe-2S)-binding domain protein	-1,40635206	-0,11013841	-0,37630313	2,38858002
RDRS01676	Dshi_1680	ferredoxin	0,27617434	-0,31111091	0,93514469	2,32588047
RDRS02026	Dshi_2030	hypothetical protein	0,5416204	-0,08388717	-0,05447523	2,12750562
RDRS02076	Dshi_2080	5,10-methylenetetrahydrofolate reductase	-0,08172431	-0,58596068	0,94385554	2,13787035
RDRS02482	Dshi_2488	transcriptional regulator, XRE family	-0,08125038	-0,31148127	-0,02693887	2,14229423
RDRS02631	Dshi_2637	magnesium-protoporphyrin IX monomethyl ester anaerobic oxidative cyclase	0,20666271	-2,68958582	0,31438341	1,08704552
RDRS02699	Dshi_2705	uroporphyrinogen decarboxylase	-0,14083666	-0,82053145	0,75742578	2,30319229
RDRS02740	Dshi_2746	hypothetical protein	-0,71770499	-2,49924479	-0,49947839	-0,16674194
RDRS02776	Dshi_2782	PAS fold-4 domain protein	-0,46860044	-1,19879687	0,48178924	3,81828913
RDRS02892	Dshi_2898	PUCC protein	-0,25986744	-1,70515098	0,25443618	2,85137252
RDRS02893	Dshi_2899	hypothetical protein	-0,97078871	-2,93402099	-0,06174345	3,1946361
RDRS02894	Dshi_2900	antenna complex alpha/beta subunit	-1,0726196	-3,65406961	-0,03920057	3,76201157
RDRS02972	Dshi_2978	RNA polymerase, sigma 32 subunit, RpoH	-0,75329757	-2,59353629	-1,46480051	2,32796419
RDRS03495	Dshi_3502	magnesium chelatase ATPase subunit I	-0,56672688	-2,00461309	-0,2238214	1,37005507
RDRS03501	Dshi_3508	Zeta-phytoene desaturase	-0,0698661	-1,56991841	0,38531225	2,56682984
RDRS03502	Dshi_3509	Squalene/phytoene synthase	-0,26774488	-1,38823839	0,18063975	2,13956572
RDRS03503	Dshi_3510	hypothetical protein	-0,21724178	-1,1738745	0,01414927	2,02285971
RDRS03505	Dshi_3512	hydroxyneurosporene synthase	-0,23804759	-0,86666275	0,07172538	2,09322983
RDRS03506	Dshi_3513	Zeta-phytoene desaturase	-0,33812943	-2,02114728	0,22128004	3,39282715
RDRS03507	Dshi_3514	Polyprenyl synthetase	-0,12072269	-1,67215263	0,21234915	2,74969984
RDRS03509	Dshi_3516	chlorophyll synthesis pathway, BchC	-0,34300976	-1,55370662	-0,0752385	2,67662558
RDRS03510	Dshi_3517	chlorophyllide reductase iron protein subunit X	-0,68279114	-2,50959642	0,27649519	3,33466913
RDRS03511	Dshi_3518	chlorophyllide reductase subunit Y	-0,77051204	-3,00531945	0,36522193	3,56703996
RDRS03512	Dshi_3519	chlorophyllide reductase subunit Z	-0,91204865	-2,67290855	0,09849753	2,80610955
RDRS03513	Dshi_3520	PufQ cytochrome subunit	-0,8098331	-2,78215045	0,16400803	2,51712691
RDRS03514	Dshi_3521	antenna complex, alpha/beta subunit	-1,52104266	-3,97949866	0,09026415	3,1790517
RDRS03515	Dshi_3522	antenna complex alpha/beta subunit	-1,25510696	-2,99912942	0,12348473	2,78923396
RDRS03516	Dshi_3523	photosynthetic reaction center L subunit	-0,76408509	-2,67089879	0,19671759	2,38511906
RDRS03517	Dshi_3524	photosynthetic reaction center, M subunit	-0,62279489	-2,17804358	0,36608617	1,97823809
RDRS03518	Dshi_3525	photosynthetic reaction centre cytochrome c subunit	-0,88283034	-2,74153885	0,27422613	2,40111956
RDRS03521	Dshi_3528	geranylgeranyl reductase	-0,29243445	-1,62885248	0,64132889	2,50109109
RDRS03522	Dshi_3529	PUCC protein	-0,09319234	-0,85161842	0,41889181	2,51325237
RDRS03523	Dshi_3530	bacteriochlorophyll/chlorophyll synthetase	-0,29060446	-1,17011478	0,63420561	2,67817104
RDRS03524	Dshi_3531	transcriptional regulator, Fis family	0,04618909	0,10982551	0,40655981	2,35608127
RDRS03525	Dshi_3532	cobalamin B12-binding domain protein	-0,14269847	-0,86789985	0,37175187	2,9198271
RDRS03526	Dshi_3533	2-vinyl bacteriochlorophyllide hydratase	-0,11781575	-1,7361306	0,76047257	3,26774542
RDRS03527	Dshi_3534	light-independent protochlorophyllide reductase, N subunit	-0,08666368	-1,68960296	0,52494275	2,73367624
RDRS03528	Dshi_3535	light-independent protochlorophyllide reductase, B subunit	-0,15471937	-1,68820013	0,72227763	2,28264879
RDRS03529	Dshi_3536	magnesium chelatase, H subunit	-0,19224814	-1,26325763	0,29519681	2,00615479
RDRS03530	Dshi_3537	light-independent protochlorophyllide reductase, iron-sulfur ATP-binding protein	-0,5878192	-2,00332712	0,75491644	2,00054628
RDRS03531	Dshi_3538	magnesium protoporphyrin O-methyltransferase	-0,50748705	-2,02550776	0,24369359	2,28424847
RDRS03533	Dshi_3540	photosynthetic reaction center H subunit	-0,79096227	-2,59552172	0,17687649	1,87999428
RDRS03534	Dshi_3541	putative photosynthetic co	-0,64353106	-2,06622027	0,18559288	1,76336873
RDRS03539	Dshi_3546	5-aminolevulinic acid synthase	-0,22523875	-1,96845047	0,71909199	2,8826005

Cluster 5

			log2 Fold change > 2			
Probe Name	**LocusTag**	**Description**	**OD02**	**OD04**	**OD06**	**OD09**
RDRS00072	Dshi_0072	putative anti-sigma regulatory factor, serine/threonine protein kinase	-3,28703836	-3,14613455	-3,14934106	-4,42704067
RDRS00073	Dshi_0073	anti-sigma-factor antagonist	-3,55666726	-3,44188975	-3,35603345	-4,67740457
RDRS00123	Dshi_0123	transcriptional regulator, LysR family	-1,80205553	-2,25339415	-2,2781684	-4,06331864
RDRS00212	Dshi_0212	two component transcriptional regulator, winged helix family	-2,37249191	-2,4614163	-2,3063598	-4,33246742
RDRS00264	Dshi_0264	hypothetical protein	-2,74812304	-2,50015102	-2,15030047	-3,32028154
RDRS00672	Dshi_0673	hypothetical protein	-2,53384064	-1,75825809	-2,25692797	-3,67779129
RDRS00763	Dshi_0765	transcriptional regulator, MarR family	-2,47583662	-2,21608919	-2,11411575	-3,69117775
RDRS00852	Dshi_0854	hypothetical protein	-3,20436594	-3,20869672	-3,29365323	-3,83348862
RDRS01120	Dshi_1124	hypothetical protein	-2,09028504	-2,13799902	-2,22521086	-4,67342617
RDRS01121	Dshi_1125	type II secretion system protein	-2,292574	-2,29360438	-2,43490568	-4,24966225
RDRS01122	Dshi_1126	type II secretion system protein E	-2,38308387	-2,44490832	-2,37952903	-4,71623155
RDRS01126	Dshi_1130	hypothetical protein	-2,52470535	-2,73864408	-2,74704929	-3,71753656
RDRS01127	Dshi_1131	hypothetical protein	-2,60253931	-2,62536421	-2,6785555	-3,73320576
RDRS01128	Dshi_1132	hypothetical protein	-2,63794927	-2,63411691	-2,83198862	-3,50963462
RDRS01134	Dshi_1138	DNA protecting protein DprA	-2,61792393	-2,20007735	-2,49853807	-3,14593528
RDRS01360	Dshi_1364	hypothetical protein	-2,51325905	-2,71599871	-2,6384013	-3,81392571
RDRS01405	Dshi_1409	hypothetical protein	-2,57819697	-2,32912714	-2,36636225	-3,86344532
RDRS01479	Dshi_1483	hypothetical protein	-2,75769914	-3,28852508	-2,95712541	-3,99406825
RDRS01503	Dshi_1507	protein of unknown function DUF1153	-3,41821573	-3,21596451	-3,32962471	-5,27043068
RDRS01504	Dshi_1508	two component transcriptional regulator, winged helix family	-3,56877352	-3,08836881	-2,89688482	-2,82129034
RDRS01580	Dshi_1584	hypothetical protein	-3,1833161	-2,89194338	-3,13956723	-3,58381643
RDRS01841	Dshi_1845	flagellar motor switch protein FliG	-3,27802962	-3,0962605	-3,09892163	-4,68682086
RDRS02143	Dshi_2147	hypothetical protein	-2,58734819	-2,1472283	-2,65226609	-4,39455312
RDRS02263	Dshi_2267	hypothetical protein	-2,65257857	-2,76953044	-2,668505	-4,65919112
RDRS02384	Dshi_2388	glycosyl transferase family 2	-2,71425619	-2,01230652	-2,38765677	-3,93999429
RDRS02625	Dshi_2631	response regulator receiver protein	-3,89533202	-3,91521887	-3,93932838	-5,18526708
RDRS02734	Dshi_2740	putative CheA signal transduction histidine kinase	-2,70612789	-2,72464345	-2,54641964	-4,18233979
RDRS02808	Dshi_2814	diguanylate cyclase	-2,72054719	-2,4992393	-2,4848831	-3,51333216
RDRS02809	Dshi_2815	Heme NO binding domain protein	-3,18418959	-3,03565912	-2,88759791	-4,62636865
RDRS02814	Dshi_2820	response regulator receiver modulated diguanylate cyclase	-3,31105981	-3,02362331	-3,03646407	-2,79199527
RDRS02824	Dshi_2830	protein of unknown function UPF0102	-2,30004781	-1,99616162	-2,0148535	-4,02419249
RDRS02846	Dshi_2852	transcriptional regulator, LuxR family	-3,21191467	-3,17389058	-3,17984755	-1,76153249
RDRS03059	Dshi_3065	diguanylate phosphodiesterase	-2,55282624	-2,59889473	-2,35355625	-4,88862693
RDRS03241	Dshi_3247	hypothetical protein	-3,31685795	-3,24341974	-3,2224855	-3,98301863
RDRS03242	Dshi_3248	flagellar basal-body rod protein FlgC	-3,03206325	-2,92698573	-2,88889294	-4,25288444
RDRS03243	Dshi_3249	hypothetical protein	-3,49163022	-3,37775645	-3,40088986	-4,89384277
RDRS03244	Dshi_3250	export protein FliQ family 3	-3,13435275	-2,94446248	-3,04556368	-4,61016409
RDRS03245	Dshi_3251	flagellar basal body rod protein	-2,57586974	-2,41365591	-2,52759055	-3,56768955
RDRS03246	Dshi_3252	flagellar basal-body rod protein FlgG	-2,9709217	-2,8282431	-2,84803211	-4,1825086
RDRS03247	Dshi_3253	hypothetical protein	-3,19536556	-3,02372665	-3,10896486	-4,59242252
RDRS03248	Dshi_3254	hypothetical protein	-3,1460684	-3,08441961	-3,19323841	-4,53151015
RDRS03249	Dshi_3255	hypothetical protein	-3,25463112	-3,17120486	-3,34223977	-4,80779305
RDRS03253	Dshi_3259	hypothetical protein	-2,78409669	-2,65167929	-2,75798137	-4,19566871
RDRS03254	Dshi_3260	hypothetical protein	-3,80447796	-3,7163702	-3,78647419	-5,38508516
RDRS03255	Dshi_3261	hypothetical protein	-3,1906302	-2,62647245	-3,25313344	-4,66675595
RDRS03256	Dshi_3262	hypothetical protein	-3,41613734	-3,35359488	-2,89013648	-4,63771346
RDRS03257	Dshi_3263	flagellar basal body-associated protein FliL	-3,20222022	-2,94696013	-3,12992387	-4,62120181
RDRS03258	Dshi_3264	hypothetical protein	-2,88299261	-2,6479546	-2,60570977	-3,44977895
RDRS03259	Dshi_3265	putative flagellar biosynthesis/type III secretory pathway protein	-3,57227468	-3,32376958	-3,34680211	-4,78788087
RDRS03260	Dshi_3266	surface presentation of antigens (SPOA) protein	-3,29429504	-3,0304338	-3,19576671	-4,76327995
RDRS03261	Dshi_3267	hypothetical protein	-3,23523093	-3,02891764	-3,35907189	-4,85872814
RDRS03309	Dshi_3315	hypothetical protein	-2,63519848	-2,4278168	-2,5920077	-4,07956527
RDRS03326	Dshi_3332	histidine kinase	-2,57790882	-2,25558261	-2,05909098	-4,31739895
RDRS03352	Dshi_3358	protein of unknown function DUF1217	-2,19319852	-2,13862875	-2,18546185	-4,63229169
RDRS03353	Dshi_3359	flagellar FlbT family protein	-3,14428433	-3,31600875	-3,37191828	-5,4344652
RDRS03354	Dshi_3360	flagellar FlaF family protein	-3,50791168	-3,63858432	-3,61355187	-4,53648427
RDRS03355	Dshi_3361	flagellin domain protein	-3,0161572	-3,05041285	-3,02061265	-3,90410033
RDRS03356	Dshi_3362	hypothetical protein	-2,75967571	-2,63400747	-2,58403037	-5,57413294
RDRS03357	Dshi_3363	flagellar protein FlgJ, putative	-3,52886089	-3,44984738	-3,45294046	-5,44883881
RDRS03370	Dshi_3376	hypothetical protein	-2,49773003	-2,28387203	-2,42455497	-3,96897424
RDRS03371	Dshi_3377	flagellar hook-associated protein FlgL family protein	-2,83174679	-2,68330326	-2,72203272	-4,39541414
RDRS03372	Dshi_3378	hypothetical protein	-3,56333844	-3,4157551	-3,28683581	-4,95066926
RDRS03373	Dshi_3379	protein of unknown function DUF1078 domain protein	-4,07502697	-3,88208178	-3,83692428	-4,87292904
RDRS03374	Dshi_3380	flagellar motor protein-like protein	-2,06967607	-1,86870555	-2,0496471	-4,14836008
RDRS03396	Dshi_3402	Serralysin	-3,67042911	-3,7933839	-3,77248465	-5,56098254
RDRS03427	Dshi_3433	hypothetical protein	-3,11595248	-2,94270484	-2,78126642	-4,0078027
RDRS03478	Dshi_3484	Hpt domain protein	-2,49920788	-2,3684127	-2,41887586	-4,0449371
RDRS03479	Dshi_3485	response regulator receiver modulated serine phosphatase	-3,17881554	-3,07739636	-3,21755797	-4,86828158
RDRS03493	Dshi_3500	competence protein F, putative	-2,89423414	-2,52751841	-2,83347183	-4,35716677
RDRS03629	Dshi_3636	hypothetical protein	-2,78134391	-3,19277135	-2,44336801	-3,45975159
RDRS03634	Dshi_3641	CagE TrbE VirB component of type IV transporter system	-2,82825383	-2,51690171	-2,07534881	-3,2022832
RDRS03637	Dshi_3644	hypothetical protein	-2,9029443	-2,64827362	-2,13198488	-3,15019299
RDRS03861	Dshi_3871	RTX toxins and related Ca2+-binding protein-like protein	-2,37811629	-2,74861306	-2,54483134	-3,48004048
RDRS03956	Dshi_3966	hypothetical protein	-2,72072682	-2,71734083	-2,22495986	-3,20698155
RDRS03965	Dshi_3975	type IV secretory pathway VirB3 family protein	-3,06951352	-2,82564786	-2,38234858	-2,73311904
RDRS03966	Dshi_3976	CagE TrbE VirB component of type IV transporter system	-3,08981872	-2,70127655	-2,2398288	-2,86037179
RDRS03969	Dshi_3979	hypothetical protein	-2,86077757	-2,76504758	-2,19179471	-3,10770556
RDRS04056	Dshi_4067	hypothetical protein	-4,05104208	-3,65099979	-3,48244999	-5,85614533
RDRS04060	Dshi_4074	transposase IS3/IS911 family protein	-3,11214621	-2,66924443	-2,35234156	-2,51622975

Cluster 6

			log2 Fold change >2			
Probe Name	**LocusTag**	**Description**	**OD02**	**OD04**	**OD06**	**OD09**
RDRS00372	Dshi_0373	Long-chain-fatty-acid--CoA ligase	0,78996351	1,46559603	0,59589105	3,07099193
RDRS00373	Dshi_0374	hypothetical protein	0,99510672	1,63120765	0,22095821	3,53130643
RDRS00374	Dshi_0375	ABC transporter related	1,0248847	1,64907153	0,33303868	3,88477215
RDRS00375	Dshi_0376	inner-membrane translocator	1,03406925	1,60241859	0,30793176	3,26651685
RDRS00378	Dshi_0379	inner-membrane translocator	1,37037834	1,75055606	0,67974959	3,06749711
RDRS00379	Dshi_0380	hypothetical protein	1,83538003	1,72259048	0,41993831	3,0203091
RDRS00380	Dshi_0381	ABC transporter related	1,6296923	1,92654188	0,56579239	2,90488516
RDRS00381	Dshi_0382	phenylacetate-CoA ligase, putative	1,12674474	1,44673884	0,45867547	2,68577804
RDRS00487	Dshi_0489	hypothetical protein	0,88083358	1,06576398	0,76401583	2,59578408
RDRS00561	Dshi_0563	hypothetical protein	0,63029087	3,5777457	3,02641897	2,20627202
RDRS00562	Dshi_0564	hypothetical protein	0,1283126	2,73096598	2,55961144	1,59258513
RDRS00563	Dshi_0565	hypothetical protein	0,34106509	2,70692958	2,57061429	0,9994712
RDRS00564	Dshi_0566	hypothetical protein	0,21134598	2,16680625	2,06800487	0,81984112
RDRS00748	Dshi_0750	hypothetical protein	1,53498466	0,97126533	1,05418273	2,12780609
RDRS01147	Dshi_1151	hypothetical protein	1,65659237	1,21177423	0,72449478	2,7515698
RDRS01148	Dshi_1152	phosphoadenosine phosphosulfate reductase	1,42099305	1,11655937	0,72433156	2,25125697
RDRS01149	Dshi_1153	nitrite/sulfite reductase hemoprotein beta-component ferrodoxin domain protein	1,59853649	1,38069486	1,17902541	2,56067274
RDRS01151	Dshi_1155	uroporphyrin-III C-methyltransferase	2,20008491	1,75053564	1,38275496	1,10702213
RDRS01201	Dshi_1205	hypothetical protein	2,46479136	1,9969557	2,0821944	2,48125121
RDRS01293	Dshi_1297	acyl-CoA dehydrogenase domain protein	0,37437262	1,38475412	0,61435252	3,84924153
RDRS01296	Dshi_1300	Propionyl-CoA carboxylase	0,83063708	1,59709386	0,54867322	2,98721749
RDRS01297	Dshi_1301	Carbamoyl-phosphate synthase L chain ATP-binding	0,8682974	1,46260778	0,41237192	2,57958016
RDRS01298	Dshi_1302	Glutathione S-transferase domain	0,88256796	1,53665225	0,35201318	2,74967889
RDRS01299	Dshi_1303	Hydroxymethylglutaryl-CoA lyase	0,99191474	1,84483262	0,46750506	3,25253564
RDRS01300	Dshi_1304	Enoyl-CoA hydratase/isomerase	0,85591428	1,12502118	0,53036871	2,27856289
RDRS01747	Dshi_1751	Enoyl-CoA hydratase/isomerase	0,23637318	1,54579225	0,2767994	2,31004407
RDRS01748	Dshi_1752	3-hydroxyisobutyrate dehydrogenase	0,3138514	1,60839755	0,09899638	2,00052783
RDRS01758	Dshi_1762	pyruvate ferredoxin/flavodoxin oxidoreductase	0,68193664	1,18375307	-0,00674442	2,58682755
RDRS01895	Dshi_1899	Multidrug resistance efflux pump-like protein	0,71258457	1,43230915	0,98866495	2,24430318
RDRS02017	Dshi_2021	hypothetical protein	1,25740554	4,39080759	3,07396271	0,98642886
RDRS02018	Dshi_2022	hypothetical protein	0,31129941	3,4376241	2,25859955	0,74044266
RDRS02047	Dshi_2051	hypothetical protein	0,28904796	1,68225222	2,23836711	0,60290289
RDRS02296	Dshi_2300	hypothetical protein	0,16538204	0,31566193	0,57784653	2,21429322
RDRS02297	Dshi_2301	hypothetical protein	0,1706303	0,37337364	0,44553962	2,37210865
RDRS02450	Dshi_2456	hypothetical protein	0,89499188	0,40797471	0,26380161	2,00047358
RDRS02454	Dshi_2460	GPW/gp25 family protein	1,09645125	0,87003034	0,80058537	2,20113488
RDRS02456	Dshi_2462	Rhs element Vgr protein	1,50917439	1,28648984	1,26980139	2,16561666
RDRS02458	Dshi_2464	conserved hypothetical phage tail protein	2,08372397	1,92630524	1,47512567	2,12781067
RDRS02459	Dshi_2465	conserved hypothetical phage tail protein	2,4888003	2,00738252	1,77004986	2,21433568
RDRS02460	Dshi_2466	hypothetical protein	2,22001487	1,66541238	1,45907875	1,92432161
RDRS02461	Dshi_2467	mucin-associated surface protein (MASP)	2,46839907	2,10246051	1,6545124	2,56713111
RDRS02472	Dshi_2478	hypothetical protein	0,0556257	0,66747967	0,18695166	2,60041271
RDRS02586	Dshi_2591	transcriptional regulator, BadM/Rrf2 family	0,15246626	0,59204874	0,35877215	2,16035141
RDRS03275	Dshi_3281	Endonuclease/exonuclease/phosphatase	2,59932002	1,89177613	2,12063987	2,1625219
RDRS03585	Dshi_3592	Cna B domain protein	2,98262867	1,59225107	1,82993448	0,75369518
RDRS03868	Dshi_3878	transposase IS4 family protein	5,36183849	5,48497623	4,9815156	2,26433722
RDRS03869	Dshi_3879	hypothetical protein	1,57526949	1,19519564	1,17113034	2,21240377
RDRS04204	Dshi_4224	hypothetical protein	1,2844902	3,1270387	1,67696867	1,20113254
RDRS04205	Dshi_4225	hypothetical protein	1,01523284	2,74916858	1,6268193	0,62740205

9.5 Ligation and microarray parameters

Parameters for construction of the fragment P_{Gm}-*luxI*

	P_{Gm}	*luxI* 1	*luxI* 2	*luxI* 3
Restriction enzymes	NdeI	NdeI	NdeI	NdeI
Purification	PCR pur.	PCR pur.	PCR pur.	PCR pur.
Concentration	21.19 ng/µl	20.38 ng/µl	19.03 ng/µl	17.57 ng/µl
Size (kb)	0.324	0.606	0.627	0.642

Ligation (ratio P_{Gm}:*luxI* = 1:1)	P_{Gm} + *luxI* 1	P_{Gm} + *luxI* 2	P_{Gm} + *luxI* 3
Vector	2.5 µl	2.5 µl	2.5 µl
Insert	2.5 µl	2.6 µl	2.8 µl
10 x T4 DNA Ligase Buffer	2 µl	2 µl	2 µl
T4 DNA Ligase (Fermentas)	1 µl	1 µl	1 µl
H_2O	12 µl	11,9 µl	1,7 µl
Total	20 µl	20 µl	20 µl

Ligation was carried out at 16°C overnight.

Parameters for blunt-end ligation of fragment P_{Gm}-*luxI* into pBBR1MCS2

Ligation 100 ng V : 200 ng I	pBBR1MCS2 Comp1	pBBR1MCS2 Comp2	pBBR1MCS2 Comp3
Vector	4 µl	4 µl	4 µl
Insert	18 µl	8 µl	8 µl
PEG 4000	4 µl	2 µl	2 µl
Tango buffer	8 µl	2 µl	2 µl
Restriction enzyme	EcoICRI 1 µl	EcoRV 1µl	EcoRV 1µl
T4 DNA Ligase (Fermentas)	1 µl	1 µl	1 µl
H_2O	-	1 µl	1 µl
ATP	4 µl	1µl	1µl
Total	40 µl	20 µl	20 µl

Ligation was carried out at 23°C for 3 hours. 10 µl of the ligation mixture were transformed into 50 µl *E. coli* DH10B Rb-Cl competent cells.

Parameters for ligation of the *luxI* 5' flank into pJP5603

	pJP5603	*luxI*$_1$ 5'flank	*luxI*$_2$ 5'flank	*luxI*$_3$ 5'flank
Previously cloned into pCR4	-	yes	yes	yes
Restriction enzymes	EcoRI/SalI	EcoRI/SalI	EcoRI/SalI	EcoRI/SalI
SAP dephosphory.	+	-	-	-
Purification	Gel purification	Gel purification	Gel purification	Gel purification
Concentration	34 ng/µl	26.42 ng/µl	19.35 ng/µl	80.34 ng/µl
Size (kb)	3.1	0.819	0.800	0.818

Ligation (ratio V:I = 1:3)	pJP5603 with *luxI*$_1$ 5'flank	pJP5603 with *luxI*$_2$ 5'flank	pJP5603 with *luxI*$_3$ 5'flank
Vector	3 µl	3 µl	3 µl
Insert	3 µl	4 µl	1 µl
10 x T4 DNA Ligase Buffer	2 µl	2 µl	2 µl
T4 DNA Ligase (Fermentas)	1 µl	1 µl	1 µl
H_2O	11 µl	10 µl	13 µl
Total	20 µl	20 µl	20 µl

Ligation was carried out at 16°C overnight. 5 µl of the ligation mixture were transformed into 50 µl *E. coli* CC118 λ pir Rb-Cl competent cells.

Parameters for ligation of the Amp cassette into pJP5603::5' flank

	pJP5603:: *luxI*$_1$ 5'flank	pJP5603:: *luxI*$_2$ 5'flank	pJP5603:: *luxI*$_3$ 5'flank	Amp^R
Previously cloned into pCR4	-	-	-	yes
Restriction enzymes	SalI	SalI	SalI	SalI
SAP dephosphory.	+	+	+	-
Purification	PCR purification	PCR purification	PCR purification	Gel purification
Concentration	12.3 ng/µl	14.0 ng/µl	18.7 ng/µl	13 ng/µl
Size (kb)	3.886	3.867	3.885	1.259

Ligation (ratio V:I = 1:3)	pJP5603::*luxI*$_1$ 5'flank with Amp^R	pJP5603::*luxI*$_2$ 5'flank with Amp^R	pJP5603:*luxI*$_3$ 5'flank with Amp^R
Vector	3 µl	3 µl	3 µl
Insert	2.8 µl	3.2 µl	2.9 µl
10 x T4 DNA Ligase Buffer	2 µl	2 µl	2 µl
T4 DNA Ligase (Fermentas)	1 µl	1 µl	1 µl
H_2O	11.2 µl	10.8 µl	11.1 µl
Total	20 µl	20 µl	20 µl

Ligation was carried out at 16°C overnight. 5 µl of the ligation mixture were transformed into 50 µl *E. coli* CC118 λ pir Rb-Cl competent cells.

Parameters for ligation of the 3' flank into pJP5603::5' flank-Amp^R

	pJP5603::5'flank *luxI*$_2$-Amp^R	pJP5603::5'flank *luxI* $_3$-Amp^R	3'flank *luxI* $_2$	3'flank *luxI* $_3$
Previously cloned into pCR4	-	-	no	no
Restriction enzymes	NehI	NehI	NehI	NehI
SAP dephosphory.	+	+	-	-
Purification	PCR purification	PCR purification	PCR purification	PCR purification
Concentration	25.5 ng/µl	12.2 ng/µl	29.6 ng/µl	15.2 ng/µl
Size (kb)	5.145	5.126	0.920	0.919

Ligation (ratio V:I = 1:3)	pJP5603::5'flank *luxI*$_2$-Amp^R with 3'flank *luxI*$_2$	pJP5603::5'flank *luxI*$_3$-Amp^R with 3'flank *luxI*$_3$
Vector	4 µl	8.2 µl
Insert	1.9 µl	3,5 µl
10 x T4 DNA Ligase Buffer	2 µl	2 µl
T4 DNA Ligase (Fermentas)	1 µl	1 µl
H_2O	11.1 µl	5.3 µl
Total	20 µl	20 µl

Ligation was carried out at 16°C overnight. 5 µl of the ligation mixture were transformed into 50 µl *E. coli* CC118 λ pir Rb-Cl competent cells.

Parameters for blunt-end ligation of the 3' flank into pJP5603::5' flank-Amp^R

	pJP5603::5'flank *luxI*$_1$-Amp^R	3' flank *luxI* $_1$
Previously cloned into pCR4	-	no
Restriction enzymes	NehI (blunted)	FspI
SAP dephosphory.	+	-
Purification	PCR purification	Gel purification
Concentration	29.74 ng/µl	19.2 ng/µl
Size (kb)	5.144	0.654

Ligation (ratio V:I = 1:3)	pJP5603::5'flank *luxI*$_1$-Amp^R with 3'flank *luxI*$_1$
Vector	3.4 µl
Insert	2 µl
PEG 4000	2 µl
10 x T4 DNA Ligase Buffer	2 µl
T4 DNA Ligase (Fermentas)	1 µl
H2O	9.6 µl
Total	20 µl

Ligation was carried out at 16°C overnight. 5 µl of the ligation mixture were transformed into 50 µl *E. coli* CC118 λ pir Rb-Cl competent cells.

Microarray setup

Two biological replicates (A and B) of *D. shibae* DFL-12 wild type and Δ*luxI* 1 were cultivated in SWM 5 mM succinate in the dark at 30°C, shaking. At an OD_{600nm} of 0.2, 0.4, 0.6 and 0.9 an appropriate volume of cells was harvested for RNA extraction. Assessment of the purity and yield of the RNA was carried out with the NanoDrop.

Using the Cy3 and Cy5 ULSTM fluorescent labelling kit it's necessary that for all RNAs OD 260/280 should be > 1.9 and OD 260/230 should be >2.1.

260/280: ratio of sample absorbance at 260 and 280 nm. If the ratio is appreciably lower than 1.9, it may indicate the presence of protein, phenol or other contaminants.

260/230: ratio of sample absorbance at 260 and 230 nm. If the ratio is appreciably lower than 2.1, it may indicate the presence of phenolate ions, thiocyanates or other organic compounds.

Table 20 Determination of purity and yield of the RNA.

Sample ID	ng/ul	260/280	260/230
D. shibae DFL-12 WT OD 0.2 A	245.69	2.07	2.25
D. shibae DFL-12 WT OD 0.2 B	325.04	2.04	1.93
D. shibae DFL-12 WT OD 0.4 A	925.25	2.1	2.19
D. shibae DFL-12 WT OD 0.4 B	884.36	2.09	2.28
D. shibae DFL-12 WT OD 0.6 A	711.22	2.11	2.36
D. shibae DFL-12 WT OD 0.6 B	809.05	2.11	2.32
D. shibae DFL-12 WT OD 0.9 A	622.94	2.11	2.33
D. shibae DFL-12 WT OD 0.9 B	436.71	2.02	2.27
D. shibae DFL-12 Δ*luxI* 1 OD 0.2 A	155.14	2.09	2.15
D. shibae DFL-12 Δ*luxI* 1 OD 0.2 B	229.53	2.05	2.19
D. shibae DFL-12 Δ*luxI* 1 OD 0.4 A	242.18	2.08	2.21
D. shibae DFL-12 Δ*luxI* 1 OD 0.4 B	938.77	2.11	2.17
D. shibae DFL-12 Δ*luxI* 1 OD 0.6 A	442.59	2.02	2.23
D. shibae DFL-12 Δ*luxI* 1 OD 0.6 B	615.41	2.11	2.31
D. shibae DFL-12 Δ*luxI* 1 OD 0.9 A	309.18	2.06	2.24
D. shibae DFL-12 Δ*luxI* 1 OD 0.9 B	793.88	2.11	2.36

For the ULS labelling 16 µl of RNA with a concentration of 2 µg were used.

RNA (2 µg) + RNAse free water	16 µl
Cy3/Cy5 ULS	2 µl
10 x labeling solution	2 µl
Total volume	20 µl

For example: 8.14 µl of *D. shibae* DFL-12 WT OD 0.2 A RNA was mixed with 7.86 µl RNAse free water to obtain 16 µl with a RNA concentration of 2 µg.

To ensure that the RNA was properly labelled and could be used for microarray hybridisation, the degree of labelling (DoL) was determined. Therefore, the labelled RNA was measured with the NanoDrop and the DoL was calculated using a web form on the manufacturer's homepage.

(http://www.kreatech.com/Portals/kreatech/downloads/labeling/27_DoL%20calculator_28082007.xls)

Table 21 Determination of the degree of labelling (DoL).

Sample ID	Dye	labelled RNA (ng/µl)	Dye Conc. (pmol/µl)	DoL (%)
D. shibae DFL-12 WT OD 0.2 A	Cy3	95.68	6.45	2.3
D. shibae DFL-12 WT OD 0.2 B	Cy3	94.6	5.42	1.9
D. shibae DFL-12 WT OD 0.4 A	Cy3	77.42	5.7	2.5
D. shibae DFL-12 WT OD 0.4 B	Cy3	102.18	7.55	2.5
D. shibae DFL-12 WT OD 0.6 A	Cy3	77.22	6.37	2.8
D. shibae DFL-12 WT OD 0.6 B	Cy3	72.68	5.57	2.6
D. shibae DFL-12 WT OD 0.9 A	Cy3	95.23	8.3	3.0
D. shibae DFL-12 WT OD 0.9 B	Cy3	150.28	9.84	2.2
D. shibae DFL-12 Δ*luxI* 1 OD 0.2 A	Cy5	89.4	5.7	2.2
D. shibae DFL-12 Δ*luxI* 1 OD 0.2 B	Cy5	93.71	6.12	2.2
D. shibae DFL-12 Δ*luxI* 1 OD 0.4 A	Cy5	120.82	7.11	2.0
D. shibae DFL-12 Δ*luxI* 1 OD 0.4 B	Cy5	73.1	5.35	2.5
D. shibae DFL-12 Δ*luxI* 1 OD 0.6 A	Cy5	153.77	8.03	1.8
D. shibae DFL-12 Δ*luxI* 1 OD 0.6 B	Cy5	97.07	6.16	2.2
D. shibae DFL-12 Δ*luxI* 1 OD 0.9 A	Cy5	99.61	5.69	1.9
D. shibae DFL-12 Δ*luxI* 1 OD 0.9 B	Cy5	89.23	6.99	2.7

The DoL should be 1.0-3.6% (indicating an average of 1.0-3.6 Cy-ULS molecules per 100 nt). DoL values lower than 1.0% may not produce enough signals, whereas DoL values higher than 3.6% might cause either high background levels or quenching signals.

One Agilent slide consists of eight microarrays. As a consequence, the arrangement of the slide resulted in the following combinations:

Array 1: wild type, replica A, OD 0.2	x	mutant, replica A, OD 0.2
Array 2: wild type, replica A, OD 0.4	x	mutant, replica A, OD 0.4
Array 3: wild type, replica A, OD 0.6	x	mutant, replica A, OD 0.6
Array 4: wild type, replica A, OD 0.9	x	mutant, replica A, OD 0.9
Array 5: wild type, replica B, OD 0.2	x	mutant, replica B, OD 0.2
Array 6: wild type, replica B, OD 0.4	x	mutant, replica B, OD 0.4
Array 7: wild type, replica B, OD 0.6	x	mutant, replica B, OD 0.6
Array 8: wild type, replica B, OD 0.9	x	mutant, replica B, OD 0.9

700 ng labelled RNA of each strain, wild type and mutant, were mixed to obtain a total concentration of 1.400 ng labelled RNA for one microarray.

<u>For example Array 1:</u>

7.4 µl of the wild type Cy3 RNA were mixed with 7.9 µl of the mutant Cy5 RNA. Afterwards 5 µl of the 10 x blocking agent, 3.7 µl of RNAse free water and 1 µl 25 x

fragmentation buffer were added. For hybridization, the mixture was supplemented with 25 µl of 2x GE hybridization buffer. Finally 40 µl were used for hybridization.

9.6 List of used primers with ID number (storage number) and sequence

Primer	ID/ Storage number	Sequence (5’ → 3’)
LuxI1_F_NdeI	37	AAA CAT ATG CAA ACC ACC ACG CTT
LuxI1_R	38	TGC GCG CGG CGC CTA
LuxI1_R_NdeI	118	AAA AAC ATA TGT GCG CGC GGC GCC TA
LuxI2_F_NdeI	39	AAA CAT ATG ATC CGT TTC GTC TAT GCC
LuxI2_R	40	TCA GGC CGC CAA GCT
LuxI2_R_NdeI	117	CAT ATG TCA GGC CGC CAA GCT
LuxI3_F_NdeI	41	AAA CAT ATG ATT ACA ATA GCA CGT GG
LuxI3_R	42	CTA GGC TGC CTT TGG
LuxI3_R_NdeI	119	AAA AAC ATA TGC TAG GCT GCC TTT GG
1ups_F_SacI	13	AAA GAG CTC CGG CTG GAC GTC TAA TTC TG
1ups_R_SalI	14B	AAA GTC GAC CAG TCT CCA GTT TGT GGT GGT
2ups_F_EcoRI	23	AAA GAA TTC TGG AAT CGT TTC TGG
2ups_R_SalI	24	AAA GTC GAC GGG GGC GGC CCT CTT
3ups_F_EcoRI	27/29	AAA GAA TTC CCC ACA TCT GAC GCG
3ups_R_SalI	28/55	AAA GTC GAC GCT GCA GTC CTT CTT
1dos_F_NheI	63	AAA AGC TAG CCT GAT CAG CGA GAT GAC CAA GG
1dos_R_NheI	64	AAA AGC TAG CCC GAT ATC CTC CAC
2dos_F_NheI	65	AAA AGC TAG CCG TCG GTC TGT GGT C
2dos_R_NheI	66	AAA AGC TAG CGC TGC CGC TCC GCG G
3dos_F_NheI	67	AAA AGC TAG CCT CTG GCC TGT TCA A
3dos_R_NheI	68	AAA AGC TAG CGA CTC TAA AGC TTC C
Amp_NheI/SalI_R	79	AAA AAA GTC GAC AAA GCT AGC GCG GAA CCC CTA TTT GTT TA
Amp_SalI_F	80	AAA AAA GTC GAC GCT GAA GCC AGT TAC CTT CG
Gm_F	111	GGA AAC GGA TGA AGG CAC GAA
Gm_R	112	GCC CAG CGC CAG CAG GAA C
Gm PromF	115	ACG GCA TGA TGA ACC TGA AT
Gm PromR_ndeI	116	CAT ATG CGT TGC TGC TCC ATA ACA TC

Characterization primers were used with Pfu proofreading polymerase.

Primer	ID/Storage number	Sequence (5’ → 3’)
16S rRNA F27	-	AGA GTT TGA TCC TGG CTC AG
16S rRNA R1492	-	GGT TAC CTT GTT ACG ACT T
pJP5603_MCS_F	74	AAC AGC TAT GAC CAT G
pJP5603_MCS_R	73	GTA AAA CGA CGG CCA GT
Gm_SF	121	TTT CGG GGA AAT GTG CGC G
Amp_SF	122	TTC CAC TGA GCG TCA GAC CC
Amp_SR	123	AAC TGT CAG ACC AAG TTT AC
I1_SF	124	CAT CCG CCC CAA GGA GAG CG
I1_SR	125	GCG CGG CTT GTC AAC TCT GC
I2_SF	126	GCA TGG TGG TGA TCT GTG CC
I2_SR	127	CGC CCA CCA CAT GCA GCT TG
I3_SF	128	GAG TTG AGC AGG GAA CCG GG
I3_SR	129	ACG GGA CCG GGT CTT GGA TG

Verification primers were used with Taq polymerase.

Primer	ID/ Storage number	Sequence (5’ → 3’)
GyrA_F	021*	GTT GGC TTG GGC TAT GTA GG
GyrA_R	022*	GTG ATC AAC CCC TTG CAA AC
I1 P1 F	81	ATG TCC ATA AAG CTA GGC ATC G
I1 P3 R	86	AGG ATG CCG AAC GGA TC
RT luxI1 F	95	ATC AGC GAG ATG ACC AAG G
RT luxI1 R	96	TTG TCG ATC CCG TCT AGC TC
RT luxI2 F	97	TCG ATA CCT ATC CCC GTC TC
RT luxI2 R	98	TCA CGT AGA TCG GGT TTT CC
RT luxI3 F	99	GTG GAT CAA TGC GGA TAC TTC
RT luxI3 R	100	AGA AAC ACA GAA GCG TGT GC
RT luxR1 F	101	AAA GCT AGG CAT CGA ACT GG
RT luxR1 R	102	TAG CGA TCC TTC CAC TCT TG
RT luxR2 F	103	GTG TTC TCG GTC AAC AAT CG
RT luxR2 R	104	GCC GTC GGA TTT ATG TCT TC
RT_thiC_F	140	CTG ATC GAA CAG GCT GAA CA
RT_thiC_R	141	GAA ACT TTC GCG GTG ATG AT
RT_alg_F	136	GGA GAT CAA CTT CCG GGT CT
RT_alg_R	137	TCA AGC GTC TCG ACA TTC AG
RT_cobN_F	*	ATC CAT TTC GGG TTG ACC AC
RT_cobN_R	*	AAC GGC CGA TCT ATC ACA AC

RT_cbiX_F	*	TGC CCT ATT TCC TGT TCA CC
RT_cbiX_R	*	GCC TTG ACG AAC TGG ATC TC
RT_fas_F Dshi_0412	134	GTG CAG GGA CTG AAG GAC AT
RT_fas_R Dshi_0412	135	CGA GAC GTG ATA GAG CAG CA
RT_fas_F Dshi_0621	130	CCA TCC TGA CCT ACC ACG TC
RT_fas_R Dshi_0621	131	AGG GCA GCA GAA CCT TGT C

Primers marked with an asterisk * were provided by Jürgen Tomasch.

All primers were used with an annealing temperature of 60°C.